THE UNIVERSITY OF HULL

INTERACTION OF STRESS-RAISING FEATURES IN AEROSTRUCTURES

being a Thesis submitted for the Degree of

Doctor of Philosophy

in the University of Hull

by

Ruth Hilary Graham, MEng (Hons)

November 2001

ABSTRACT

It is widely accepted that fatigue is responsible for 90% of all unscheduled component failures, and is therefore a key research area for the aerospace industry. The basis of successful design against fatigue relies on the accurate and consistent determination of stress concentration factors around stress-raising features. Within aerostructures, design problems often occur where two or more geometric features are placed in close proximity such that their associated stress-fields interact. It is difficult to assess potential susceptibility to fatigue failure in such situations as no universally-accepted method has been available by which a design engineer could estimate accurately the stress levels produced.

This research has focused on the development of standardised evaluation techniques by which fatigue analysts can predict the stress concentration factors associated with problems involving interacting stress-raising features. These methods have been designed as flexible and accurate predictive tools to be incorporated into the fatigue analysis process as time-efficient alternatives, or pre-cursors to the application of techniques such as finite element analysis. Fundamental research was carried out into the understanding of stress concentration factors associated with a series of commonly-occurring geometries of interacting features. The approaches employed for the development and validation of the methods have included numerical solutions (using the finite element method) and experimental studies (using photoelastic analysis and strain gauge measurements). Through these research techniques, new insights have been gained into the manner in which two or more stress raisers interact when placed in proximity. Based on these understandings, two categories of evaluation tool have been developed: (i) a generic methodology for those stress-raisers that lie on a common cross-section, and (ii) individually-tailored prediction techniques for those features of alternative alignment. In all cases, these techniques were found to provide highly accurate stress concentration predictions, as compared to appropriate analytical and numerical treatments.

These methodologies are currently being implemented as standard practice within the fatigue analysis process at BAE SYSTEMS through incorporation into the SCONES knowledge-based system (Robinson et al. 2001) and the BAE SYSTEMS Technical Standards Manual for stress concentration analysis (BAE SYSTEMS 2001 (2)).

ACKNOWLEDGEMENTS

I would like to offer my gratitude to my supervisor, Professor Ken Swift, for his advice and support during this research project. I also wish to thank BAE SYSTEMS for the industrial collaboration and financial backing for this research. Consultations with Lou Gill and Simon Walker, along with a number of other fatigue experts working within BAE SYSTEMS, have provided invaluable background information and technical specifications for the project.

I am particularly grateful for the support and help generously provided by the late Ken Sharples, whose expertise and experience in the field of photoelasticity was of very great benefit to this research.

NOMENCLATURE

σ	Applied Stress
σ_{nom}	Nominal Stress
ν	Poisson's Ratio
d	Width of Narrower Cross-Section for Filleted Models
D	Width of Wider Cross-Section for Filleted Models
E	Young's Modulus
K_t	Stress Concentration Factor
K_{tn}	Net Stress Concentration Factor
K_{tg}	Gross Stress Concentration Factor
l	Model Length
p	Positioning of Feature Relative to a Fixed Point (variously stated as p, p_a, p_b, p_x, and p_y)
r_a	Radius of Hole a in Configurations involving Two Holes
r_b	Radius of Hole b in Configurations involving Two Holes
r_c	Radius of Central Hole (in Satellite Hole Configuration)
r_f	Radius of Fillet
r_h	Radius of Hole
r_n	Radius of Notch
r_s	Radius of Radial Hole (in Satellite Hole Configuration)
s	Separation Distance Between the Centres of Adjacent Features
t	Model Thickness
w	Model Width

CONTENTS

CHAPTER 1

INTRODUCTION

Within aerostructures, design and manufacturing problems often occur where geometric stress-raising features are placed in proximity such that their associated stress fields interact. A major scientific question is therefore the accurate determination of the stress concentration levels produced, to enable the assessment of any potential susceptibility to fatigue failure. The objectives of the study are firstly to carry out fundamental research into the evaluation of the stress concentration factors associated with stress-raising features in proximity within aerospace structures, and secondly to develop a methodology which enhances the facilities provided by the knowledge-based system SCONES, under development for BAE SYSTEMS at the University of Hull. This chapter provides the scientific and industrial background to this study and outlines the structure of the thesis.

1.1 BACKGROUND

Over the past 40 years, a number of surveys have been conducted to review the fracture modes associated with failure incidents in aircraft structures (Marquet and Struzik 1998; Beaudet and Roth 1991; Cooper and Kelto 1979). The pattern over time indicates the overwhelming influence of fatigue in the unscheduled failure of components in aircraft structures (Figure 1-1). The impact of fatigue failure within aircraft design came into sharp focus in the early 1950's with a series of Comet disasters (Withey 1997), which caused the near collapse of the British civil aircraft industry. The failures were caused by high levels of stress around cut-out areas, the severity of which had been underestimated through the introduction of beneficial residual stresses in initial quasi-static testing, which masked the true behaviour of the

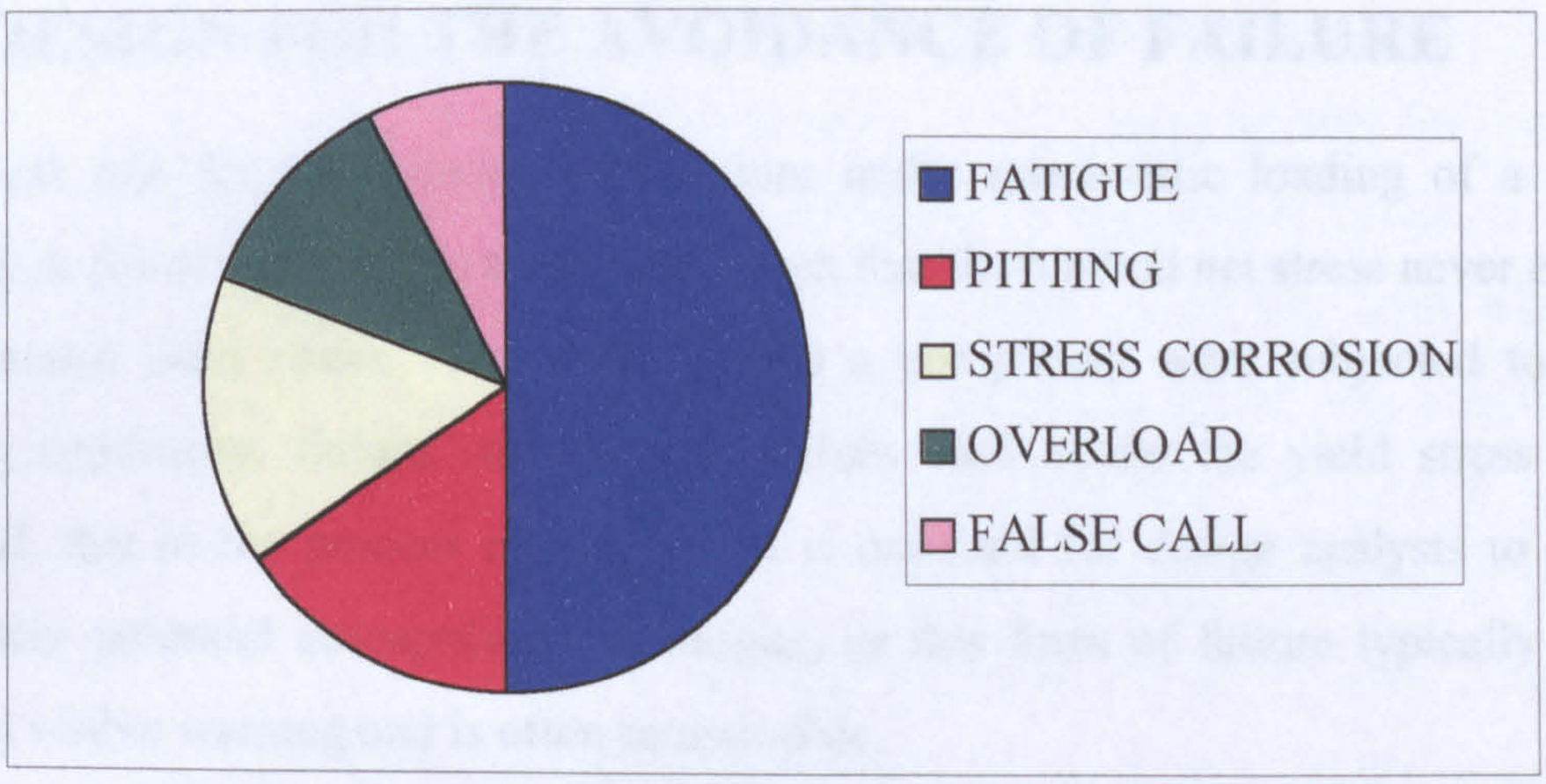

Figure 1-1. Failure mechanism for structural components in landing gear structures over a 20 year period (Beaudet and Roth 1991)

structure during the subsequent fatigue tests. Following these accidents, fatigue analysis and testing became elevated in status to a major design requirement. The role of design against fatigue is therefore of critical importance within the aerospace industry, with a constant drive for improved accuracy, consistency and standardisation. An essential prerequisite for successful fatigue analysis is the accurate determination of stress concentrations around stress-raising features (Shin et al. 1994). As one of the world's leading exporters of military and civil aircraft, BAE SYSTEMS places critical importance on the procedures involved in fatigue calculations (British Aerospace Defence Limited 1996). In this connection, BAE SYSTEMS have established a long-term partnership with the University of Hull to further knowledge in this field and to enhance and validate current stress concentration methodologies. The research described in this thesis forms one element of a larger collaborative project with BAE SYSTEMS (BAE SYSTEMS 2001 (1); Robinson et al. 2001) involved in the development of the knowledge-based system SCONES (Stress CONcentration Evaluation System). The SCONES software system has been developed as a standard tool, used throughout the design of military aircraft at BAE SYSTEMS, providing the fatigue analyst with comprehensive, validated values of stress concentration for a range of commonly-analysed single geometric features.

1.2 DESIGN FOR THE AVOIDANCE OF FAILURE

A critical rule for the avoidance of failure under quasi-static loading of a ductile material is for components to be designed such that the applied net stress never exceeds the material yield stress. However, if such a component were subjected to cyclic loading conditions, failure can occur at values well below the yield stress of the material, due to the process of fatigue. It is essential for design analysts to predict accurately potential susceptibility to fatigue, as this form of failure typically occurs without visible warning and is often catastrophic.

The process of fatigue comprises three basic stages: crack initiation (from micro-structural damage), crack propagation (through localised plastic deformation at the crack tip) and finally unstable rapid failure. Based on the detailed understanding of this process, current techniques for the prediction of fatigue damage fall into three categories:

1. 'Fail-Safe' design – the structure is designed to contain a series of secondary members such that, should fatigue failure occur in major structural elements, catastrophic failure does not occur. This technique is typically used in the design of civil aircraft, but the required structural redundancies are considered inappropriate to be used in the military sector, where competition for light-weight aircraft is very high.

2. 'Safe-Life' design – assuming there to be no initial cracks in the material, this method prescribes a safe fatigue life of the material to a pre-defined point in the fatigue process. This point is usually specified by the final customer, and can range from no detectable cracks to final failure, although it is typically defined as the development of a given length of crack (British Aerospace Defence Limited 1996). After this 'safe-life' has been reached, the component is automatically retired from service. Most European military aircraft are designed to safe-life requirements.

3. 'Damage Tolerance' – this technique assumes microscopic cracks to be inherent to all structures, and predicts the fatigue life based on the propagation of the crack to a critical crack length. Most military aircraft produced for and by the US Airforce are designed using damage tolerant principles.

There has been much recent debate (Bristow 2000; Everett and Elber 2000; Marquet and Struzik 1998) over which of these techniques is to be more suitable for economic, reliable and safe design, particularly with reference to widespread fatigue in ageing aircraft (Finch 1997; Pitt and Jones 1997). This conflict can be seen even within the United States military design, where the US Navy conforms to fail-safe requirements and the US Airforces has adopted damage tolerant principles. In general, military aircraft designed within Europe conform to the safe-life approach (Ministry of Defence 1999), while civil aircraft adopt the fail-safe approach (Joint Aviation Authorities 2000). Military aircraft are typically designed to a life of 6 000 – 14 000 hours, with more variability in the stress levels and a greater requirement for reduced weight than those expected from civil aircraft. The military sector therefore defines the fatigue life of these structures to be that of crack initiation only, with components withdrawn from service before any propagation occurs (McDonnell Douglas Aerospace 1993).

Although safe-life and damage tolerance methodologies differ in application, the same basic parameters affect the rate of fatigue development, namely:

(i) Material (material type, grain direction etc.),

(ii) Usage (loading spectrum: frequency of high tension or compression loads, order of loading etc.),

(iii) Material processes (surface coatings, life improvement techniques such as shot peening etc.), and

(iv) Geometry (stress concentrations and stress gradients).

The final of these four parameters has a crucial effect on any fatigue life predictions. Understanding of the stress gradient at points of high stress provides insights into the crack propagation rates from this point (Taylor et al. 2000; Shin et al. 1994). Calculations of stress concentration allow for identification of the critical areas where the potential for fatigue failure is high, and also provide the fatigue analyst with accurate determinations of the stress levels produced at these regions. Precise understanding of stress concentration values is therefore of critical importance within the fatigue analysis process, and is the focus of this research.

1.3 STRESS CONCENTRATIONS

If a uniform flat plate were placed in simple tension or compression, the stress distribution produced would be uniform throughout the cross-section. However, if there were any local changes in the cross-section, such as holes or notches, an irregular stress distribution would be produced. The points of peak stress which occur around these geometric discontinuities are known as stress concentrations, and are identified as the areas where fatigue cracking is most likely to occur.

The stress concentration factor (K_t) is a measure of the degree to which the stress increases at the geometric discontinuity, and is represented in two forms, the net stress concentration factor (K_{tn}) and the gross stress concentration factor (K_{tg}). The definitions of K_{tn} and K_{tg} are given below:

net stress concentration factor : $$K_{tn} = \frac{\sigma_{\max}}{\sigma_{nom}}$$

gross stress concentration factor : $$K_{tg} = \frac{\sigma_{\max}}{\sigma}$$

Definitions of the nominal stress (σ_{nom}) and the applied stress (σ) are given in Figure 1-2, using the example of a hole (radius r_h) in a finite-width plate under tension.

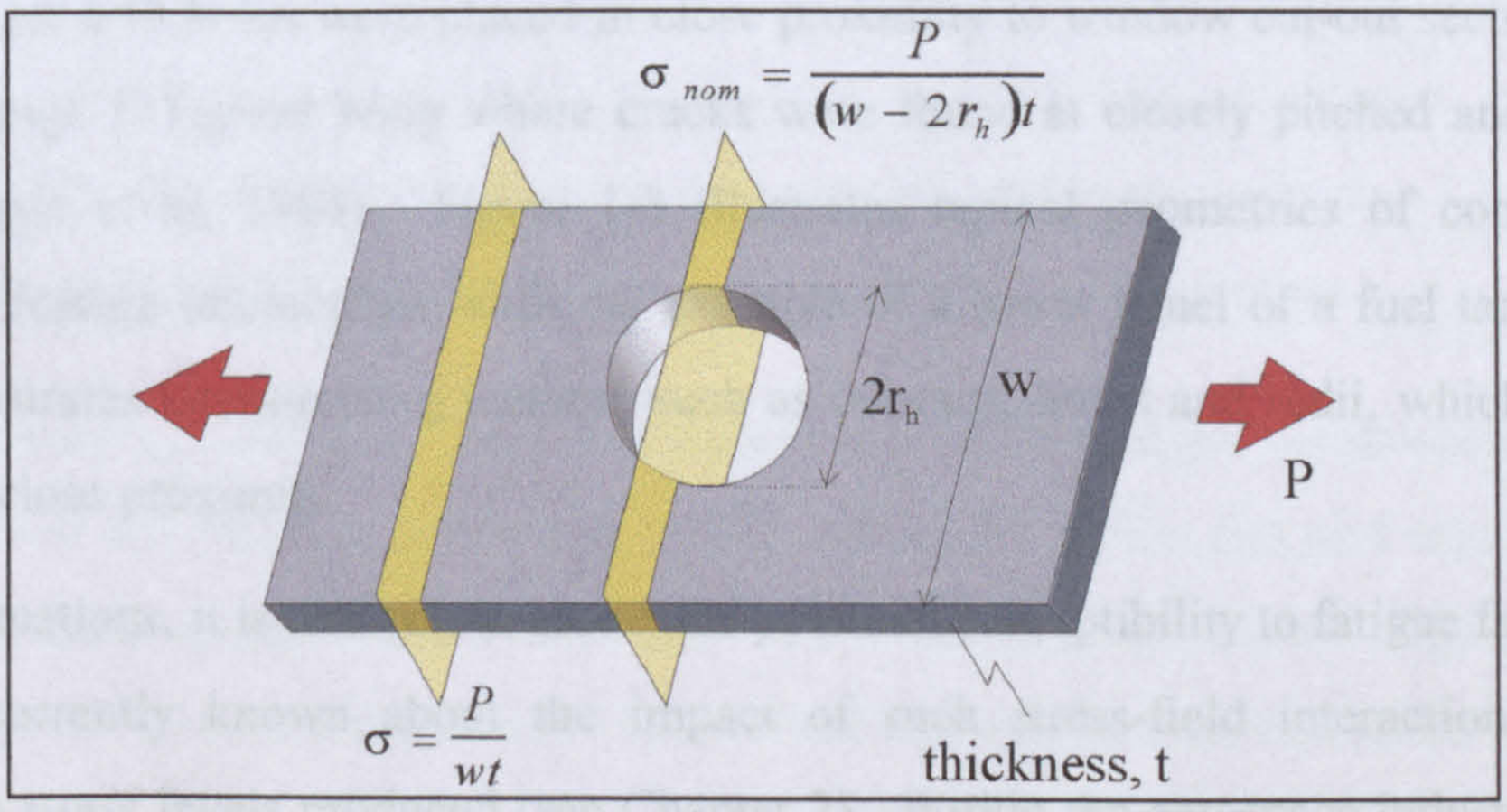

Figure 1-2. Illustration of *net* and *gross* cross-sections, using the example of a hole in a finite-width plate under tension

Stress concentration factors are theoretical elastic values which are dependent only on geometry and type of loading. In practice, a number of additional factors will influence the overall stress concentration such as surface finish, porosity, microdefects or life improvement techniques. These factors are usually incorporated into the safe-life

methodology through adjusting the stress concentration value using appropriate correction factors (British Aerospace Military Aircraft & Aerostructures 1997; McDonnell Douglas Aerospace 1993). The resulting stress concentration values are then used to evaluate fatigue life using a life prediction routine such as the Local Strain-Life or Stress-Life routines (Suresh 1998).

1.4 INTERACTION OF GEOMETRIC DISCONTINUITIES

Standard data sources (Young 1989; ESDU 1985 (1); Peterson 1974) provide the fatigue analyst with accurate values of stress concentration for a variety of single geometric features. These published values of stress concentration are based on fundamental analytical solutions (Ling 1967; Isida 1953; Howland 1929) and rigorous experimental studies, typically photoelastic (Frocht 1935; Coker and Filon 1931) and strain gauge work (Kikukawa 1962). However, within aerostructure design, situations arise where two or more features are placed in close proximity, such that their associated stress fields may interact and potentially impact significantly on the overall stress concentration produced. This is a particular issue when considering manufacturing concessions, and during certain circumstances in structural repair. Typical aerostructure case studies of this problem include the classic Comet disaster (Withey 1997), where bolt holes were placed in close proximity to window cut-out sections and in the Mirage II Fighter wing where cracks were found at closely pitched anchor-nut holes (Mann et al. 1984). Figure 1-3 illustrates typical geometries of commonly-occurring feature interactions, with the example of a lower panel of a fuel tank. The figure illustrates stress-raising features such as cut-outs, holes and radii, which are all placed in close proximity.

In such situations, it is difficult to assess the potential susceptibility to fatigue failure, as little is currently known about the impact of such stress-field interaction on the maximum stress levels produced (see Chapter 2). Within the aerospace industry, there currently exists no universally-accepted method for the analysis of these types of problem (Trevelyan et al. 2001). Further, the research base for the development of a universally-accepted method is limited, with a dearth of published data providing relevant stress concentration values (Collins 1993). Research investigating the effect of stress-raising features placed in proximity is therefore of high scientific and operational importance to the aerospace industry.

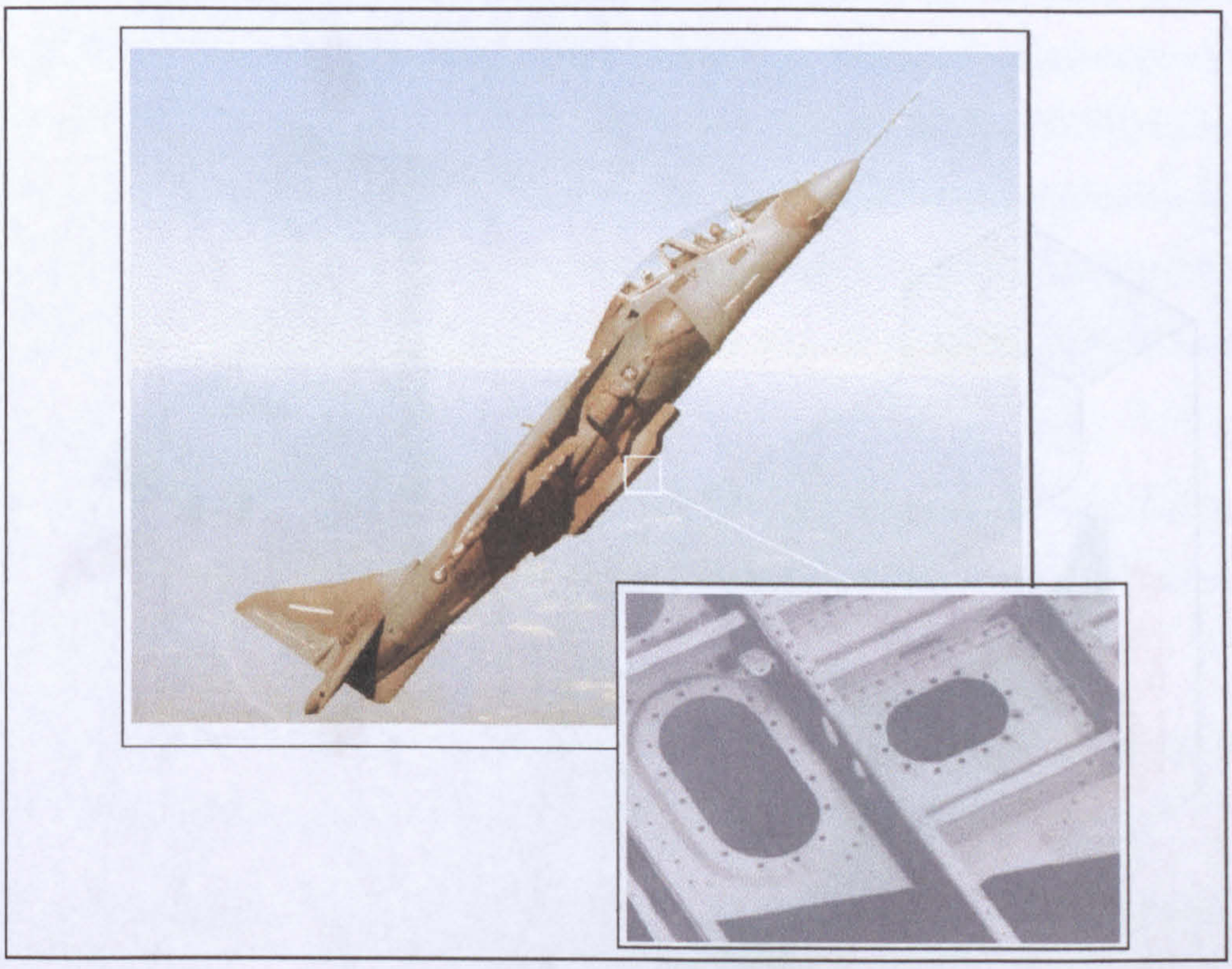

Figure 1-3. Illustration of a typical example of interacting stress features, found in the lower panel of a fuel tank on a Harrier

The assessment of problems involving interacting discontinuities is non-trivial. For single features, only a limited number of geometrical parameters affect the stress concentration values produced. However, for the case of features in proximity, the number of factors affecting the stress distribution formed is vastly increased. A typical example of a situation involving features in proximity is given in Figure 1-4, for the case of a transverse hole in close proximity to a welded shoulder section.

The right-hand portion of Figure 1-4 illustrates the localised stress distribution formed between these two interacting features. The areas shaded in blue and pink represent the unaffected stress decays formed from each individual feature. Shown in green is the resultant stress distribution produced when these two features are combined and their associated stress fields are interacting. Clearly, there are many factors which affect the form of this combined stress distribution including the feature types involved, their geometry, the direction and type of loading and the feature separation distance.

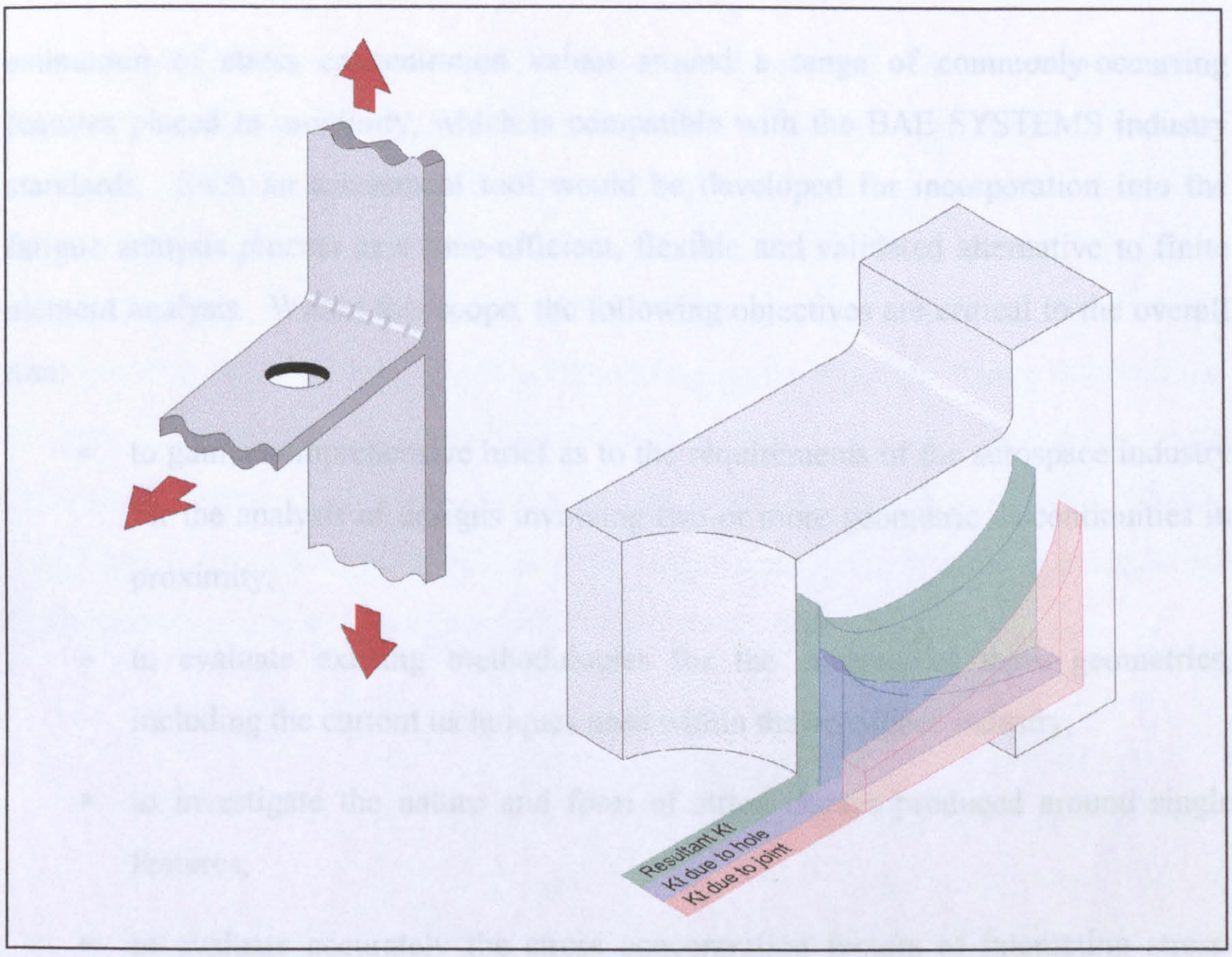

Figure 1-4. Illustration of the principle of interacting features

1.5 THE RESEARCH PROJECT AND ITS OBJECTIVES

As earlier sections have demonstrated, this research project has its background in the unresolved scientific issues relating to interacting stress-raising features as well as the requirements of the aerospace industry, and in particular BAE SYSTEMS, for an efficient method of calculating stress concentration factors in these situations. The BAE SYSTEMS standard for stress concentration determination is through the use of the knowledge-based system SCONES (BAE SYSTEMS 2001 (2)), developed at the University of Hull. The scope of this system does not extend to geometries involving multiple features. However, the designer is often required to analyse a series of alternative design configurations involving features in proximity in order to identify the optimal geometry for fatigue prevention, particularly in the early stages of design (Trevelyan and Wang 2001). Commercial finite element codes typically do not offer the flexibility required for such conceptual design optimisation, and an alternative, more time-efficient approach is required.

The primary aim of this research project is to undertake the numerical, experimental and analytical investigations necessary to develop a reliable and flexible tool for the

estimation of stress concentration values around a range of commonly-occurring features placed in proximity, which is compatible with the BAE SYSTEMS industry standards. Such an assessment tool would be developed for incorporation into the fatigue analysis process as a time-efficient, flexible and validated alternative to finite element analysis. Within this scope, the following objectives are critical to the overall aim:

- to gain a comprehensive brief as to the requirements of the aerospace industry for the analysis of designs involving two or more geometric discontinuities in proximity,
- to evaluate existing methodologies for the analysis of these geometries, including the current techniques used within the aerospace industry,
- to investigate the nature and form of stress decays produced around single features,
- to evaluate accurately the stress concentration factors of interacting stress-raising features in aerospace structures, and to determine the influence of the orientation and position of multiple interacting stress concentration features upon the stress fields and the resulting stress concentration factor,
- to translate these measures into a technique suitable for incorporation within an efficient fatigue methodology process and into the knowledge-based system SCONES, so as to enhance the efficient design of fatigue sensitive structures, and
- to validate the technique through application to 'real life' design situations. In this connection, the partnership with BAE SYSTEMS enables access to expert knowledge in the field and facilitate the investigation of case studies involving features in proximity.

1.6 CONTENTS OF THESIS

The thesis is divided into eight chapters in total. The main body of the text begins with Chapter 2. This provides a critical review of existing methodologies for the evaluation of geometric discontinuities placed in proximity, looking at foregoing analytical, experimental and numerical studies, along with an overview of those techniques

currently used within the aerospace industry. Chapter 3 discusses the research methodology adopted for this programme of work. Finite element considerations are discussed in Chapter 4, with an overview of the techniques adopted and a number of sample results. Chapter 5 describes the experimental aspects of the research, discussing the photoelastic and strain gauge work conducted. In Chapter 6, the overall experimental, numerical and analytical results are drawn together. Using these results, Chapter 7 then describes the generation of an accurate and flexible methodology for the analysis of features placed in proximity for use within the aerospace industry. Finally, in Chapter 8, the overall development of the research project is discussed, and areas are identified where further research could usefully be directed.

CHAPTER 2

LITERATURE REVIEW

The research is concerned with the development of a tool by which a stress engineer can optimise design against fatigue through the prediction of stress concentration values around stress-raising features in proximity, and with the implementation of this methodology into the expert system SCONES. This chapter provides a review of the literature in the field of feature interactions, along with an evaluation of current alternative methodologies available for stress concentration prediction under these circumstances. The chapter is divided into five sections to cover the major topic areas for this review. Sections 2.2, 2.3 and 2.4 cover the state of the art for the evaluation of feature interactions using analytical, numerical and experimental techniques respectively. Section 2.5 deals with approximation methods proposed in the literature and currently adopted in the aerospace industry for the analysis of these problems. Finally, Section 2.6 provides an overview of the key evaluation techniques highlighted in this literature review.

2.1 INTRODUCTION

Within the aerospace industry, there are currently no universally-accepted techniques by which a fatigue analyst can efficiently analyse and compare a series of alternative geometries of feature interaction in order to optimise the design of a component. For the accurate and consistent analysis of situations involving features in proximity, a series of finite element analyses would need to be conducted for each geometric configuration to determine the potential impact of the associated stress concentration level. However, when a variety of alternative geometries are under consideration during the early design stages, or where the consequences of manufacturing concessions are being assessed, a less time-consuming alternative is required. In these situations, the

expertise of the individual analyst is heavily relied upon and often approximation methods (British Aerospace Military Aircraft & Aerostructures 1997; McDonnell Douglas Aerospace 1993) are employed. These techniques typically involve rather simplistic manipulations of individual stress concentration values (British Aerospace Military Aircraft & Aerostructures 1997; ESDU 1985 (2); ESDU 1975 (1)), and often produce very diverse results. From investigation of the approximation methods currently utilised by the design engineer for the analysis of features in proximity, it was clear that they are insufficiently accurate and flexible for a rigorous fatigue analysis. The first stage of this research, therefore, was to investigate the relevant published data and alternative evaluation techniques available.

A literature search and review has been conducted into the general issue of stress-raising features placed in close proximity. This review revealed a wide range of investigative tools which had been used to analyse the problem of feature interaction. These techniques can be categorised into three main groups:

(i) **Analytical solutions** – the solutions of specific geometries of feature interaction using analytical techniques,

(ii) **Numerical techniques** – analysis of interacting geometries utilising numerical techniques such as finite element analysis, and

(iii) **Experimental studies** – experimental investigations using techniques such as strain gauge and photoelastic methods.

Sections 2.2, 2.3 and 2.4 address the knowledge gained from these three topic areas, in each case looking initially at investigations involving single features and then moving on to discuss work that has been conducted in the area of multiple features in proximity.

Also investigated as part of this research were approximation methods and 'rules of thumb' that have been proposed in the literature for the analysis of features in proximity. Analysis of these techniques will provide an understanding of the flexibility and accuracy of the tools currently employed in fatigue analysis within the aerospace industry. A review of this work will form Section 2.5 of this chapter.

Finally, in Section 2.6, an overview is provided of the key methodologies identified for the evaluation of interacting features.

2.2 ANALYTICAL SOLUTIONS

In this section, an overview is given of the foregoing analytical treatments of problems involving single and multiple geometric features. Due to the highly complex nature of the mathematics, the analytical solutions of multiple features are almost exclusively focused on configurations involving circular holes under quasi-static tension. For this reason, the discussion of analytical treatments of single geometric features (Section 2.2.1) will be confined to problems involving single holes in tension.

2.2.1 Single Features

Extensive stress concentration data are available for cases of single geometric features, contained within standard tests such as ESDU (1969; 1964), Peterson (1974) and Young (1989). In a large number of such cases for simple geometries of single features, these data are based on analytical solutions, particularly for those geometries where the feature is contained within an infinite body. Much of the early work in this field was focused on problems involving holes.

The first prominent solution to problems involving stress-raisers was published by Kirsch (1898), who used the stress function approach to analyse the geometry of a single circular hole in a thin infinite plate under uniform tension. The solution to the problem in polar co-ordinates (r, θ) provides values of stress at any point about the hole of radius a:

$$\sigma_{rr} = \sigma_{xx}\left(1-\frac{a^2}{r^2}\right)+\frac{\sigma_{xx}}{2}\left(1-\frac{4a^2}{r^2}+\frac{3a^4}{r^4}\right)\cos 2\theta$$

$$\sigma_{\theta\theta} = \frac{\sigma_{xx}}{2}\left(1+\frac{a^2}{r^2}\right)-\frac{\sigma_{xx}}{2}\left(1+\frac{3a^4}{r^4}\right)\cos 2\theta$$

$$\tau_{r\theta} = \frac{\sigma_{xx}}{2}(1+2a^2/r^2-3a^4/r^4)\sin 2\theta$$

It can be seen that these equations fulfil the boundary conditions at $r=a$, $r=\infty$ and $\theta=0$. Furthermore, the peak stress, which occurs at $r=a$, and $\theta=\pi/2$, is equal to $3\sigma_{xx}$ (i.e., the maximum stress concentration is three).

In 1913, Inglis used a closed form solution to derive the following equation for the maximum stress concentration factor at the end of the major axis of an elliptical hole in an infinite plate under tension (Inglis 1913):

$$k_t = 1 + 2\sqrt{\frac{a}{\rho}}$$ **Equation 2-1**

where, $2a$ = ellipse width over major axis
ρ = radius of curvature

The problem of a central circular hole in a finite-width plate was later solved by Howland (1929). As part of the literature review for this doctoral research, further work was conducted on this analytical solution. Howland's treatment was used to create a three-dimensional map of the stress distribution around the hole through the use of the software *Mathcad*, as illustrated in Figure 2-1.

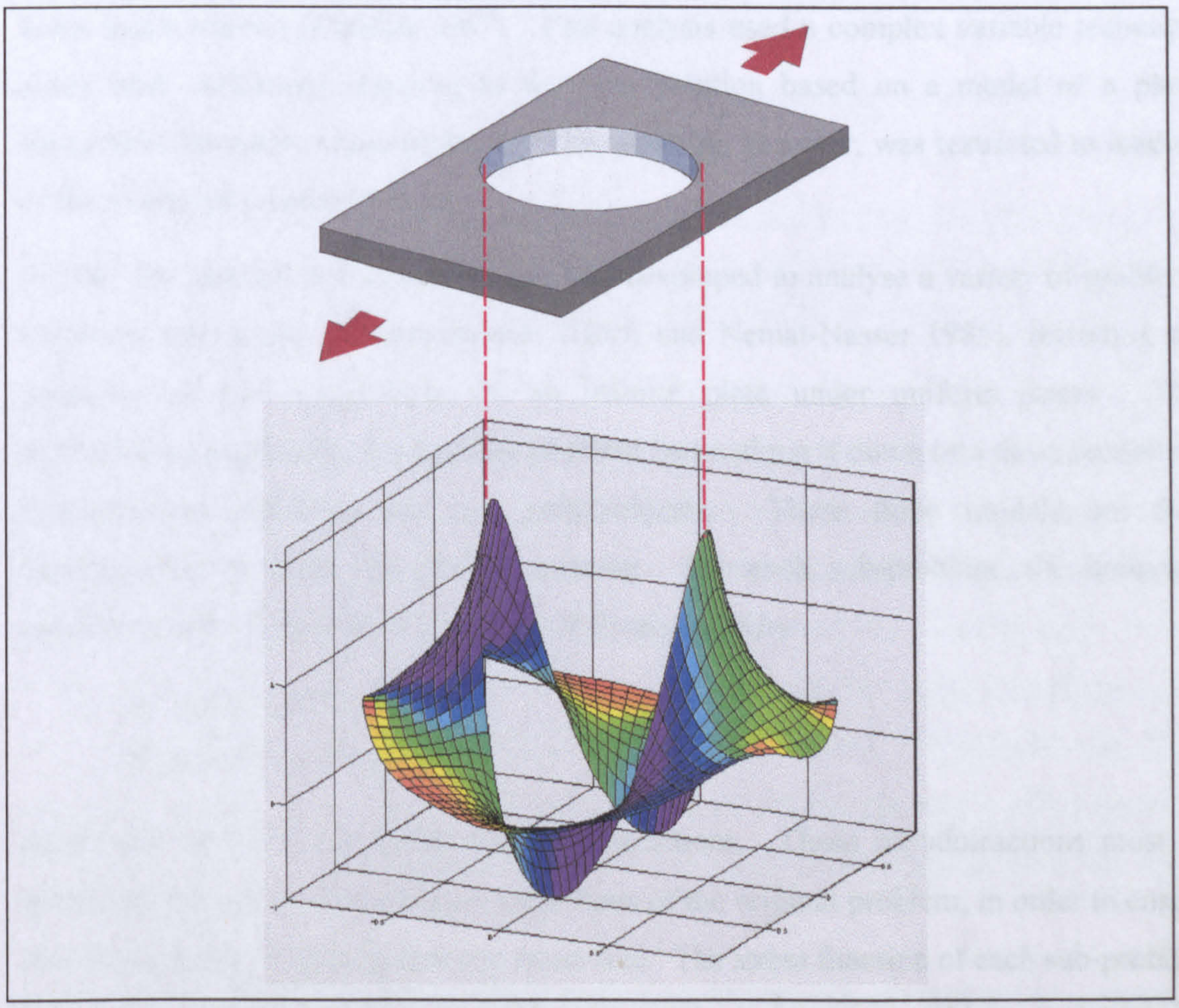

Figure 2-1. Three-dimensional map of the stress distribution around a central hole in a finite-width plate under tension, generated during this doctoral research, based on a foregoing analytical solution (Howland 1929)

This work of Howland was then extended by Isida (1953; 1952) to cover the cases of an eccentrically-placed hole under tension and bending.

In 1953, the Muskhelishvili method of complex potentials was developed (Muskhelishvili 1953) providing a versatile technique for the solution of more complex problems. Utilising this complex potential method, Savin (1961) conducted a series of

investigations into stress concentrations around a variety of problems involving non-circular holes.

2.2.2 Interacting Features

In 1948, Ling developed a solution for two equal holes in an infinite plate under tension (Ling 1948). This solution utilised a bi-planar co-ordinate system, which had been developed earlier by Mindlin (Mindlin 1948). Due to the co-ordinate system adopted, however, the model was limited to geometries displaying double symmetry. Later, Haddon developed a series solution which allowed for the consideration of unequal holes under tension (Haddon 1967). This analysis used a complex variable technique along with conformal mapping to derive a solution based on a model of a plane elastostatic boundary value problem. This solution, however, was restricted to loading of the model only under tension.

In 1985 the Method of Pseudotractions was developed to analyse a variety of problems involving interacting inhomogeneities (Horii and Nemat-Nasser 1985), including the geometry of two equal holes in an infinite plate under uniform stress. This methodology approaches a particular problem by breaking it down into three sections: a homogeneous problem, and two sub-problems. These three models are then superimposed to form the overall solution. For each sub-problem, the boundary conditions around the hole (C^j, where j=1,2) are given by:

$$\sigma^{j}{}_{r+}\sigma^{\infty j}{}_{r} + \sigma^{Pj}{}_{r} = 0$$
$$\tau^{j}{}_{r\theta} + \tau^{\infty j}{}_{r\theta} + \tau^{Pj}{}_{r\theta} = 0$$

where σ_r^{pj} and $\tau_r\theta^{pj}$ are called the pseudotractions. These pseudotractions must be determined to satisfy the boundary conditions of the original problem, in order to ensure that the surfaces of each feature are stress free. The stress function of each sub-problem is found using Muskhelishvili's complex potentials, and traction problems are expanded using a Fourier series. The graph in Figure 2-2 indicates a close similarity between the results from the Method of Pseudotractions and Haddon's analytical results for two equal holes in an infinite plate under normal tension.

In 1992, an analytical method was published (Meguid and Shen 1992) for the solution of problems involving two interacting holes. The method was primarily developed to tackle the issue of defence holes (strategically placed holes which reduce the severity of localised stress concentrations) in the aerospace industry. The boundary value problem

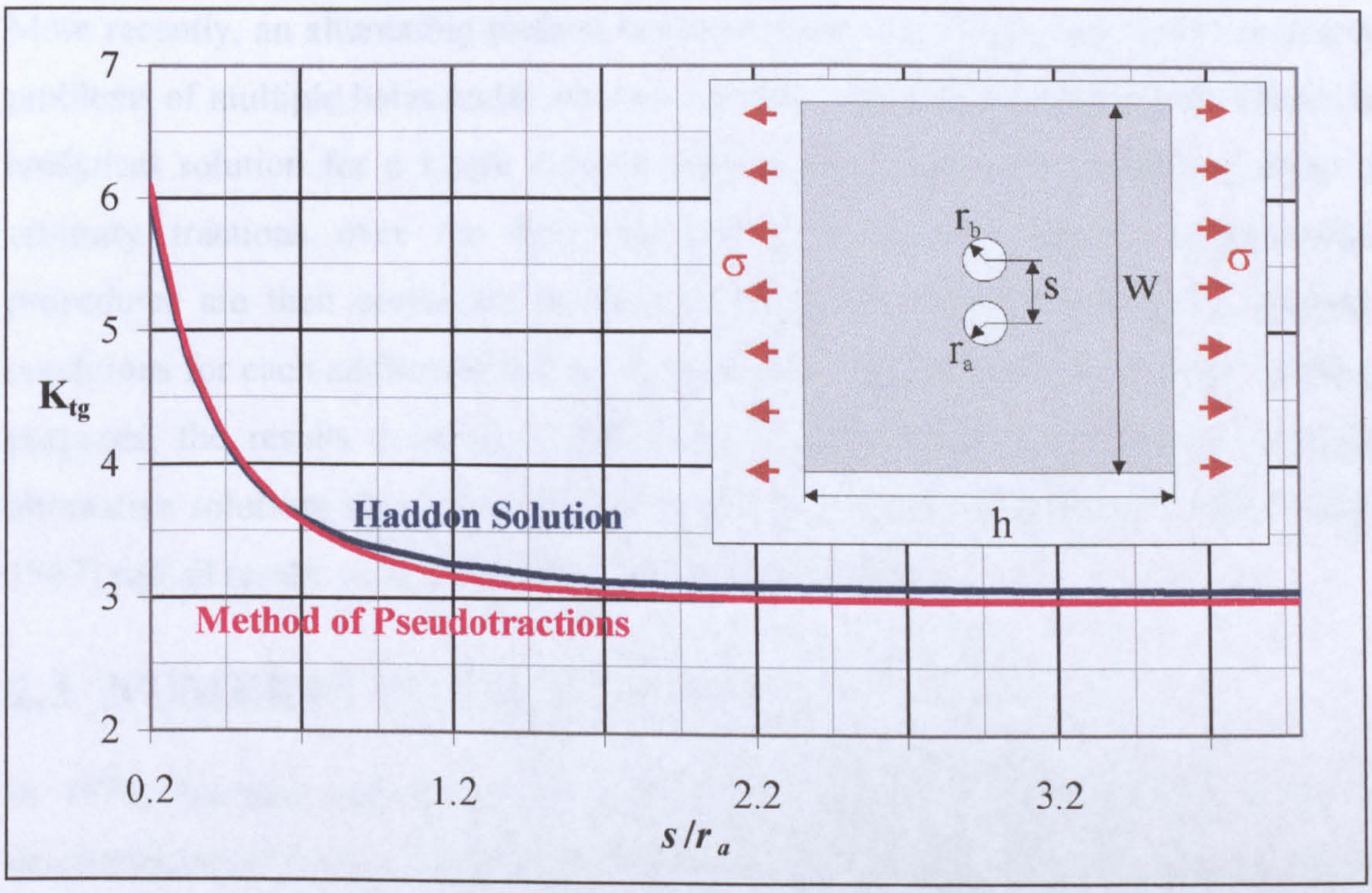

Figure 2-2. Comparison between analytical results (Haddon 1967) with those from the Method of Pseudotractions (Horii and Nemat-Nasser 1985), for $r_a=r_b$

of interacting holes was solved by using the complex potentials of Muskhelishvili (Muskhelishvili 1953) together with an appropriate superposition technique and the Laurent series expansion. The expression proposed by Meguid for the solution of the problem of two interacting holes provides a closed form expression for the tangential stress concentration around the main hole, which is derived to its fourth order. In the following year, the accuracy of the results generated from this analytical solution was investigated (Meguid and Gong 1993) by comparisons with photoelastic and finite element models. It was found that the analytical results showed a 5% maximum discrepancy with the photo-elastic results, and a 10% discrepancy with the finite element results.

As discussed earlier in this section, analytical treatments of interacting geometric features are predominantly focused on geometries involving circular holes. One of the few exceptions to this was the development of a closed-form solution for two elliptical holes in an infinite plate subject to in-plane loading (Ukadgaonker et al. 1995). This solution utilised the Kolosoff-Muskhelishvili complex functions along with the Schwarz's Alternating Method to evaluate the stress concentration factors under these geometries. Comparisons with finite element models show this solution to be in close agreement.

More recently, an alternating method has been generated (Ting et al. 1999) to analyse problems of multiple holes under arbitrary loading. The methodology firstly obtains an analytical solution for a single circular hole in an infinite body which is subject to arbitrary tractions over the hole boundary. Successive iterative superposition procedures are then conducted on these solutions in order to satisfy the boundary conditions for each additional hole in the problem under consideration. For validation purposes, the results from this method were compared with those three principal alternative solutions (Meguid and Shen 1992; Horii and Nemat-Nasser 1985; Haddon 1967) and all results were shown to be in good agreement.

2.3 NUMERICAL TECHNIQUES

In 1974, Peterson published what is widely regarded as the standard text for the determination of stress concentrations (Peterson 1974). The data presented within this reference text are predominantly sourced from analytical and/or experimental investigations of stress concentration problems. After this time, however, numerical techniques became an integral part of the stress analysis process (Zienkiewicz 1989) and have been widely used to enhance and validate stress concentration data (ESDU 1994; Pilkey 1994). This section describes the development and application of numerical techniques to the field of stress concentration evaluation for both single and combined features.

In general, there are two alternative numerical tools that are adopted for the analysis of stress concentration problems: the boundary element method (Trevelyan 1994) and the finite element method (Bathe 1996). As reflected in this literature review, finite element analysis is the more widely used technique in this application (Mackerie 1997).

2.3.1 Single Features

As discussed above, prior to the widespread use of numerical tools and computer modelling techniques, much experimental and analytical work had been compiled describing stress concentration values associated with single geometric features (Peterson 1974; ESDU 1964). For this reason, the purpose of numerical analyses of stress concentration at single features tends to be the enhancement and extension of previous knowledge, rather than the primary analyses of new features. For example, in 1984 a numerical investigation was undertaken (Chong and Pinter 1984) into the effect of large holes (hole diameter/plate width>0.8) in finite-width plates under tension,

through increasing the hole diameters to values beyond that which had been previously studied through photoelastic (Wahl and Beewkes 1943) and analytical (Howland 1929) investigations. Other examples include finite element investigations into the effect of plate thickness on the stresses in plates containing simple notches (Zhenhuan et al. 2000) and the finite element and boundary element studies of the influence of the angle of inclination and orientation of oblique holes subjected to tension and bending (Tafreshi and Thorpe 1995).

2.3.2 Interacting Features

This section looks at two aspects of numerical treatments: firstly the generation of stress concentration data through the analysis of multiple features using conventional numerical techniques (Section 2.3.2.1) and secondly the development of numerical tools specifically designed for the analysis of feature interactions (Section 2.3.2.2).

2.3.2.1 Numerical Data

Over the last two decades a major focus for numerical investigation has been analysis of defence hole systems. The introduction of defence holes is an important design tool in aircraft design as it allows not only for a decrease in component weight, but also can significantly reduce stress concentration levels (Meguid and Gong 1993). In 1983, Jindal used finite element modelling to investigate the influence of the introduction of auxiliary holes on either side of a central hole on the overall stress concentration (Jindal 1983). In this study, auxiliary holes were placed both in-line and normal to the direction of loading at a variety of distances from the central hole. Jindal also investigated the effect of allowing these features to intersect such that the overall geometry becomes that of an oblique hole. The research concludes that the optimal design modification, from those geometries investigated, was to allow the auxiliary holes to join the central hole, forming one overall oblong feature. This particular geometry was found to benefit the potential fatigue resistance of the component by not only reducing the stress concentration by up to 22%, but also through not introducing any additional regions of high stress in the form of extra features. In 1986, Meguid used finite element analysis to investigate the impact of the location and orientation of defence holes (Meguid 1986). This work was later extended as part of a larger analytical, experimental and finite element study (Meguid and Gong 1993) investigating stress concentrations associated with interacting main holes and defence holes. This

research illustrated how defence holes can be used to reduce the maximum stress concentration in critical regions of the component.

In 1998 finite element results were obtained (Ukadgaonker and Kale 1998) for patterns of large numbers of holes in a square pitch. Using the commercial code ANSYS, the research validated those theoretical solutions for this geometry (Bailey et al. 1960 cited in Ukadgaonker and Kale 1998) within 3% accuracy.

In the following year, finite element results were published (Sloan et al. 1999) of stress concentration data for the geometry of a large hole in proximity to a smaller satellite hole placed normal to the direction of tensile loading. The results of this study showed that, for large ratios of D (diameter of the main hole) to d (diameter of the satellite hole) the stress concentration factor was only dependent on the ligament distance between the holes divided by D.

2.3.2.2 Tailored Numerical Tools

Much of the numerical analysis techniques developed for the investigation of interacting features have been focused specifically on configurations of holes in close proximity. One of the earliest numerical techniques developed to deal with the issue of features in proximity was the *Body Force Method* (Nisitani 1967) which uses a boundary element approach to analyse the stresses at geometries for which there is no analytical solution. The underlying principle of this approach is the treatment of each stress-raiser as an infinite number of point forces acting on a plane flat plate (Figure 2-3).

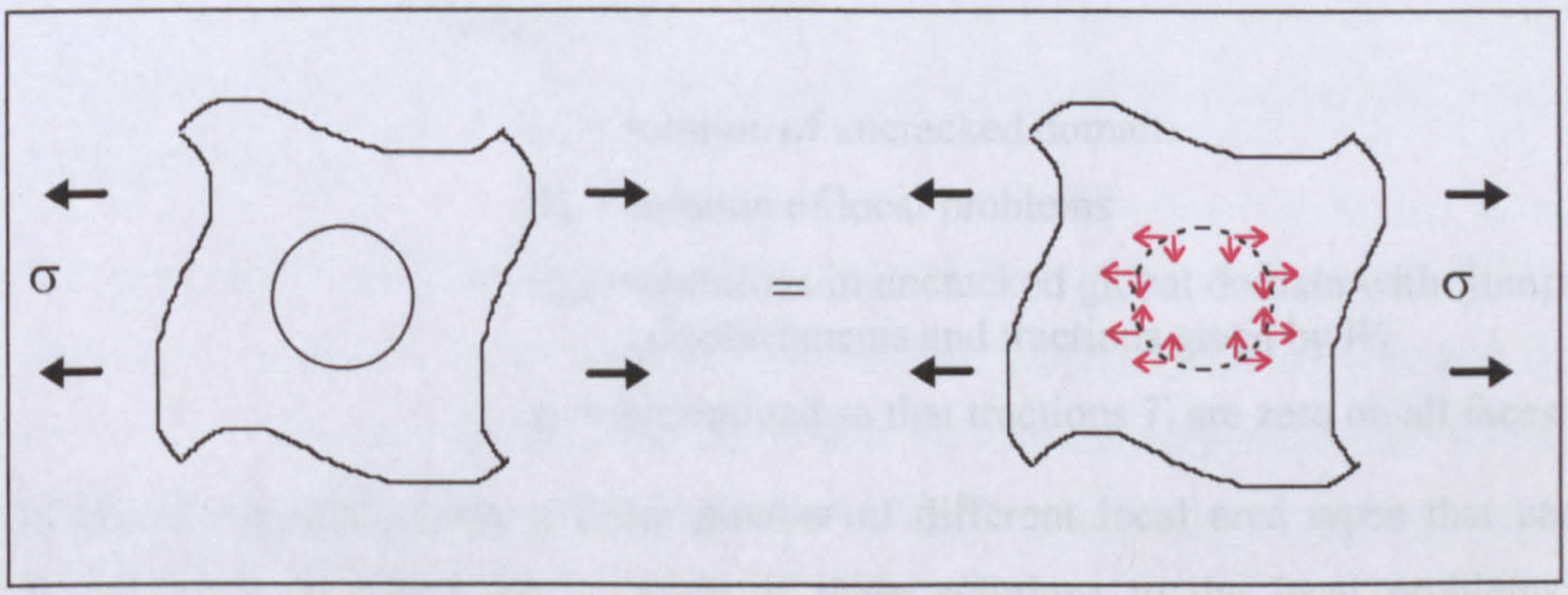

Figure 2-3. Nisitani's Body Force Method for the case of a hole in an infinite plate, illustrated as point forces acting on a unnotched plate

These infinite point forces are then approximated to a finite set of forces and the boundary conditions of the particular geometry are satisfied by adjusting the density of the point forces. The stresses at a certain desired point may then be determined by finding the influence of the body forces from each interval of the feature. This

technique was later developed for use with a digital computer (Fraga and Hewitt 1983) for the analysis of a hole near a circular-edge notch.

A 'global-local' method (Babuska and Andersson 1997) for solving three-dimensional multi-site damage problems is currently under development at the Aeronautical Research Institute, Sweden (FFA). Although this solution has been derived for general fracture mechanics problems, it has also been applied to the analysis of multiple major structural damage problems (Babuska and Andersson 1998), where battle damage may produce geometries of interacting features such as holes.

This FFA solution is based on a number of finite element analyses. The model is separated into three sub-problems:

(i) *a global problem with no damage,*

(ii) *local cracked sections (i.e. local areas each containing a feature), and*

(iii) *a global model which compensates for tractions (this is the component of the model which ensures that there are zero stresses on the crack faces).*

Each of these separate local and global areas is then analysed using the *h-p* version of finite element analysis. The overall solution is then found by appropriate superposition of the local and global problems, as given in the equation below:

$$u = U_1 + \sum_{k=0}^{m} a_k W_k - \sum_{k=0}^{m} a_k U_{2,k}$$

where,

U_1 = solution of uncracked domain

W_k = solution of local problems

$U_{2,k}$ = solutions in uncracked global domain with 'jumps' in displacements and tractions given by W_k

a_k = determined so that tractions T_i are zero on all faces

There are essentially only a finite number of different local area types that can be considered (hole, notch etc.). Each of these solutions to the local problems has therefore been created in advance and stored in a data library. This means that, for every new problem encountered, only the global area need actually be solved, thereby vastly reducing the solution time.

An example of an application of this method is shown in Figure 2-4 with the analysis of a thick plate under tension containing three interacting holes.

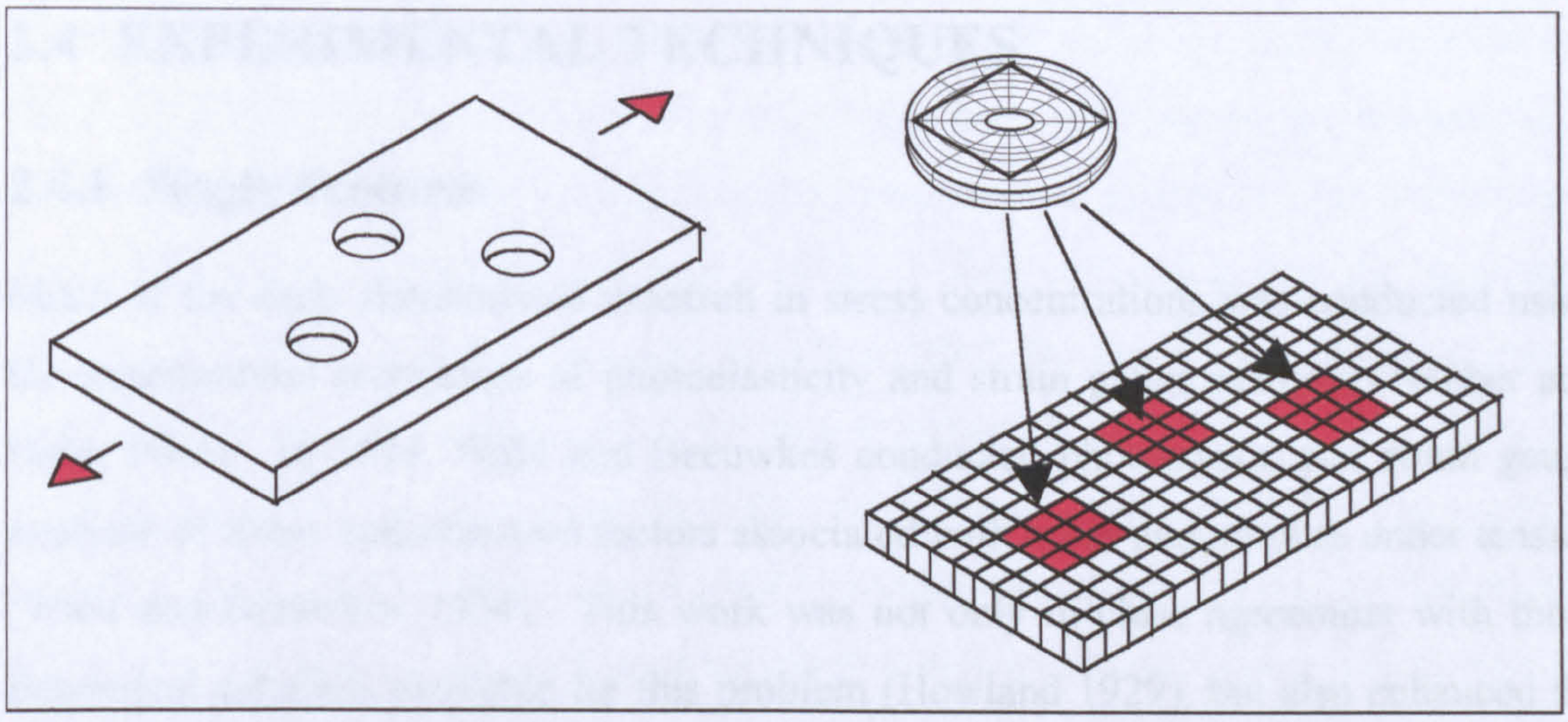

Figure 2-4. Diagram illustrating the division into global and local areas for the analysis of three holes in a thick plate under tension

Figure 2-4 illustrates how a relatively coarse mesh is used in the global area, with a finer mesh around each hole in order to produce an accurate estimation of the stresses at the hole boundaries. As this method is still under development, details such as the level of accuracy of the resulting stress concentrations are yet to be published.

More recently, a boundary element alternating method has been developed for the investigation of two-dimensional models containing configurations of discontinuities in perforated plates (Chen et al. 2000). The method uses an iterative superposition technique between the boundary element solution of the bounded geometry without holes and the analytical solution of an infinite plate containing a hole subjected to arbitrary normal and shear loading. This technique allows an extensive number and orientation of hole configurations to be analysed with limited iterations and number of boundary elements.

Currently under development at the University of Durham (Trevelyan et al. 2001) is a prototype boundary element based system entitled CODA (Concept Oriented Design Analysis). This methodology was developed for implementation into the conceptual design stage, and combines the interface of a simple sketching tool with an automated boundary element method. The system allows for user-defined design optimisation through the automatic re-analysis of the model to account for any geometric alterations. During prototype tests, this system has been applied to a number of geometries of feature interaction. However, as no validation process has yet been conducted, the accuracy of the results can not be determined.

2.4 EXPERIMENTAL TECHNIQUES

2.4.1 Single Features

Much of the early fundamental research in stress concentrations was conducted using the experimental techniques of photoelasticity and strain gauge analysis (Neuber and Hahn 1966). In 1934, Wahl and Beeuwkes conducted photoelastic and strain gauge analyses of stress concentration factors associated with holes and notches under tension (Wahl and Beeuwkes 1934). This work was not only in close agreement with those theoretical solutions available for this problem (Howland 1929), but also enhanced the scope of knowledge to a more comprehensive range of geometries. In the following year, Frocht further extended this work through the photoelastic examination of notches and fillets in both tension and compression (Frocht 1935). Over the next fifty years a wealth of photoelastic research was conducted investigating stress concentration values with particular focus on configurations of holes (Coker and Filon 1931), notches (Cole and Brown 1958) and shoulder fillets (Wilson and White 1973). The data collected from these studies have been compiled in reference texts such as Peterson (1974) and Savin (1961).

In more recent years, alternative experimental techniques have been developed to study the effect of stress concentrations in composite materials. In 2000, laser Raman microscopy was used to determine stress concentration values at a hole in Kevlar 49 fibre/epoxy under tension (Arjyal 2000). This technique detects the microscopic changes in inter-atomic forces and vibrational frequencies of the material caused by a change in the atomic separation due to the applied stress. The results from these experiments were found to be in close correlation with those predicted by theory (Muskhelishvili 1953).

2.4.2 Interacting Features

Due to its flexibility, photoelasticity is the most widely-used of all experimental techniques in the analysis of interacting geometric features. In general, experimental investigations in this field are focused on two main areas; firstly the interaction of configurations of holes and secondly the effect of the physical intersection of two geometric features. Each of these two topics will be discussed in this section.

Heywood first introduced the concept of 'defence' holes (Heywood 1952) through photoelastic investigations of uni-axial holes placed either side of a central hole in order

to reduce its associated stress concentration (see Section 2.3.2.1). Later, Erickson and Riley developed this concept through using photoelasticity to investigate the geometric parameters which affect this change in stress concentration, in terms of the defence hole size and location (Erickson and Riley 1978). They concluded that the maximum reduction in stress concentration was observed when the auxiliary holes were placed along the direction of loading and in the closest proximity to the main hole. Later, this work was extended to investigate the effect of a free boundary placed in proximity to geometries of defence holes (Rubayi 1984). Rubayi conducted a series of photoelastic experiments to investigate stress concentration levels for defence holes placed near the edge of finite-width plates under tension. As discussed in Section 2.3.2.1, the problem of defence holes was further investigated through finite element and photoelastic investigations by Jindal (Jindal 1983) and Meguid (Meguid and Gong 1993; Meguid 1986).

Throughout this period, additional studies were underway investigating alternative configurations of interacting holes. In 1965, North conducted a photoelastic study of the interaction between two holes in proximity under tension (North 1965). Solutions to this problem had previously been assessed analytically by Ling (Ling 1948), for two holes under longitudinal tension (acting parallel to the line of the holes), transverse tension (acting perpendicular to the line of the holes) and equal bi-axial tension. The study by North aimed to investigate these conditions experimentally, and to extend the results to cover the compressive stress concentrations surrounding the holes. On comparison with the theoretical solution by Ling, the results from this experimental study showed good correlation (<5%) as illustrated in the example given in Figure 2-5.

More recently, automated photoelasticity has been used to optimise the design of a row of holes in structural members (Umezaki 2000). The method identified the optimal position for the holes photoelastically through identifying the isotropic points[1] in the structure. Through the use of finite element analysis, the research verified that the placing of the holes at these points produced a minimal stress concentration, as compared to any alternative positions.

---

[1] Isotropic points are regions in where the principal stresses are equal, and can be identified using photoelasticity under white light as black spots.

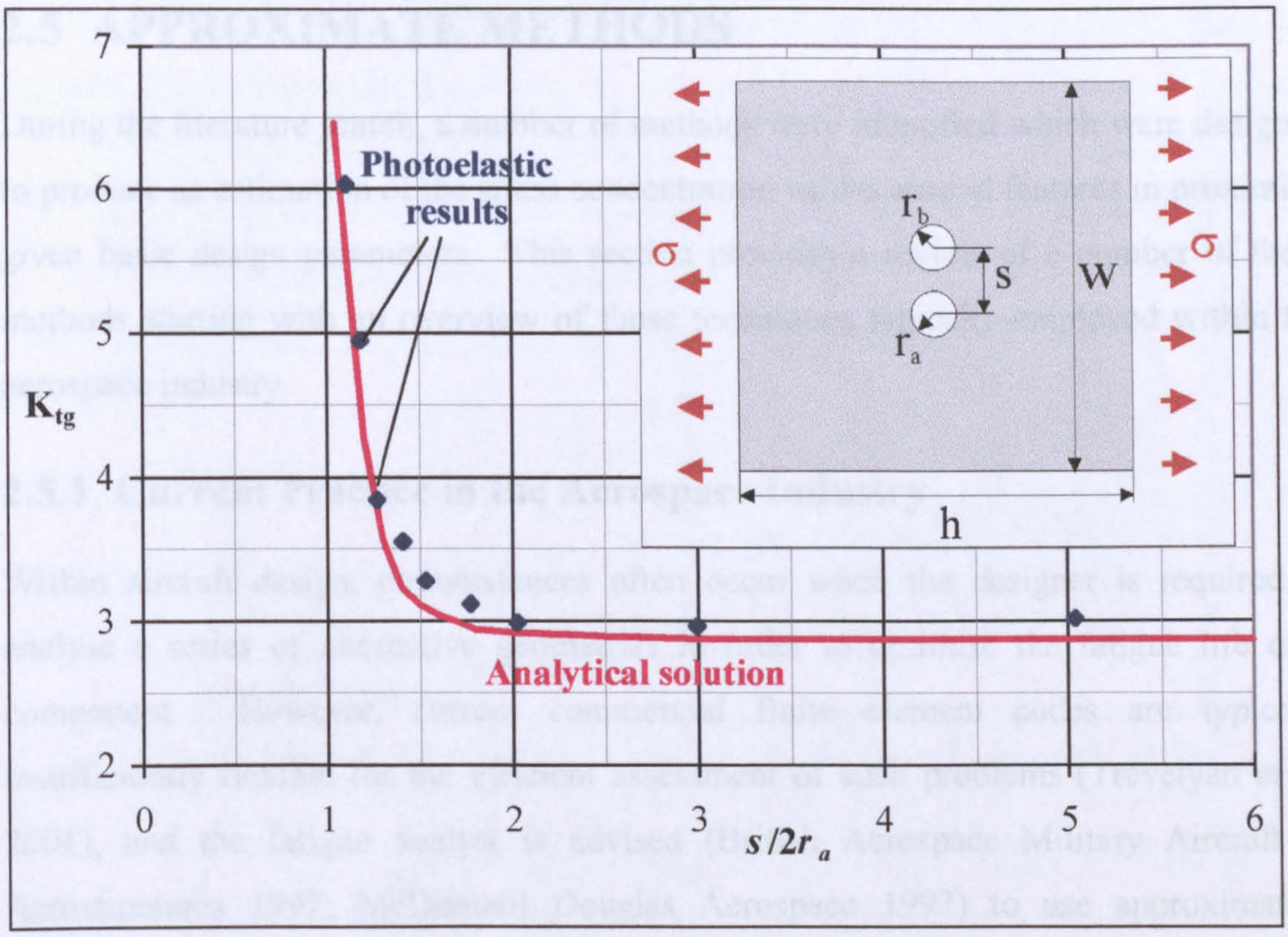

Figure 2-5. Correlation between the photoelastic results (North 1965) and the theoretical solution (Ling 1948) for the maximum stress concentration for two holes under transverse tension

A number of investigations have also been undertaken into the problem of intersecting features. In 1961, Frank and Faucett undertook a study to investigate the hypothesis that the overall maximum stress concentration at two features which are intersecting (such that they intersect at a point of maximum stress of one feature) is simply the product of each individual stress concentration (Frank and Faucett 1961). The hypothesis was proposed by Mowbray following a series of strain gauge tests on intersecting fillets and grooves (Mowbray 1953). Using photoelasticity, Frank and Faucett investigated the effect of superimposing two sets of notches on a specimen under bending, alongside a series of parallel tests for each notch individually. The results from this research indicated that, for the limited geometries investigated, a reasonably close correlation existed (around 10%) between the experimental stress concentration for the interacting features and the product of the individual experimental stress concentration. During the same year, a parallel photoelastic study was conducted looking into stress concentrations associated with intersecting notches and slots (Poe 1961) where broadly similar results were found.

2.5 APPROXIMATE METHODS

During the literature search, a number of methods were identified which were designed to produce an estimation of the stress concentration values around features in proximity, given basic design parameters. This section provides a review of a number of these methods starting with an overview of those techniques typically employed within the aerospace industry.

2.5.1 Current Practice in the Aerospace Industry

Within aircraft design, circumstances often occur when the designer is required to analyse a series of alternative geometries in order to optimise the fatigue life of a component. However, current commercial finite element codes are typically insufficiently flexible for the efficient assessment of such problems (Trevelyan et al. 2001), and the fatigue analyst is advised (British Aerospace Military Aircraft & Aerostructures 1997; McDonnell Douglas Aerospace 1993) to use approximation methods to estimate the stress levels produced. A variety of differing methodologies have been proposed (Schijve 2001; Kurajian and Na 1980; Doughtie and Vallance 1964), but in general, two approximation methods are used within the aerospace industry. These are shown below for the calculation of the overall gross stress concentration (K_t) for two interacting geometric features of individual gross stress concentration K_{t1} and K_{t2} respectively:

Method 1 (Eccles 1996)

$$K_t = K_{t1}\sqrt{K_{t2}} \qquad \text{(where } K_{t1}>K_{t2}\text{)} \qquad \textbf{Equation 2-2}$$

Method 2 (Basic 1999, Juvinall 1967)

$$K_t = K_{t1}.K_{t2} \qquad \textbf{Equation 2-3}$$

The fatigue analyst would use their judgement to determine the critical feature separation distance within which such methods should be employed.

Clearly, these approximations are very simplistic measures of what is a series of highly complex relationships. As part of this research, the relative accuracy of these methods was analysed through applying each to the standard solution of two equal holes in an infinite plate under normal tension, and the results compared to the theoretical solution developed by Haddon (Haddon 1967). The results of this comparison are shown in

Figure 2-6, where s is the ligament distance between the hole centres and r_a and r_b are the radii of each hole (where $r_a = r_b$).

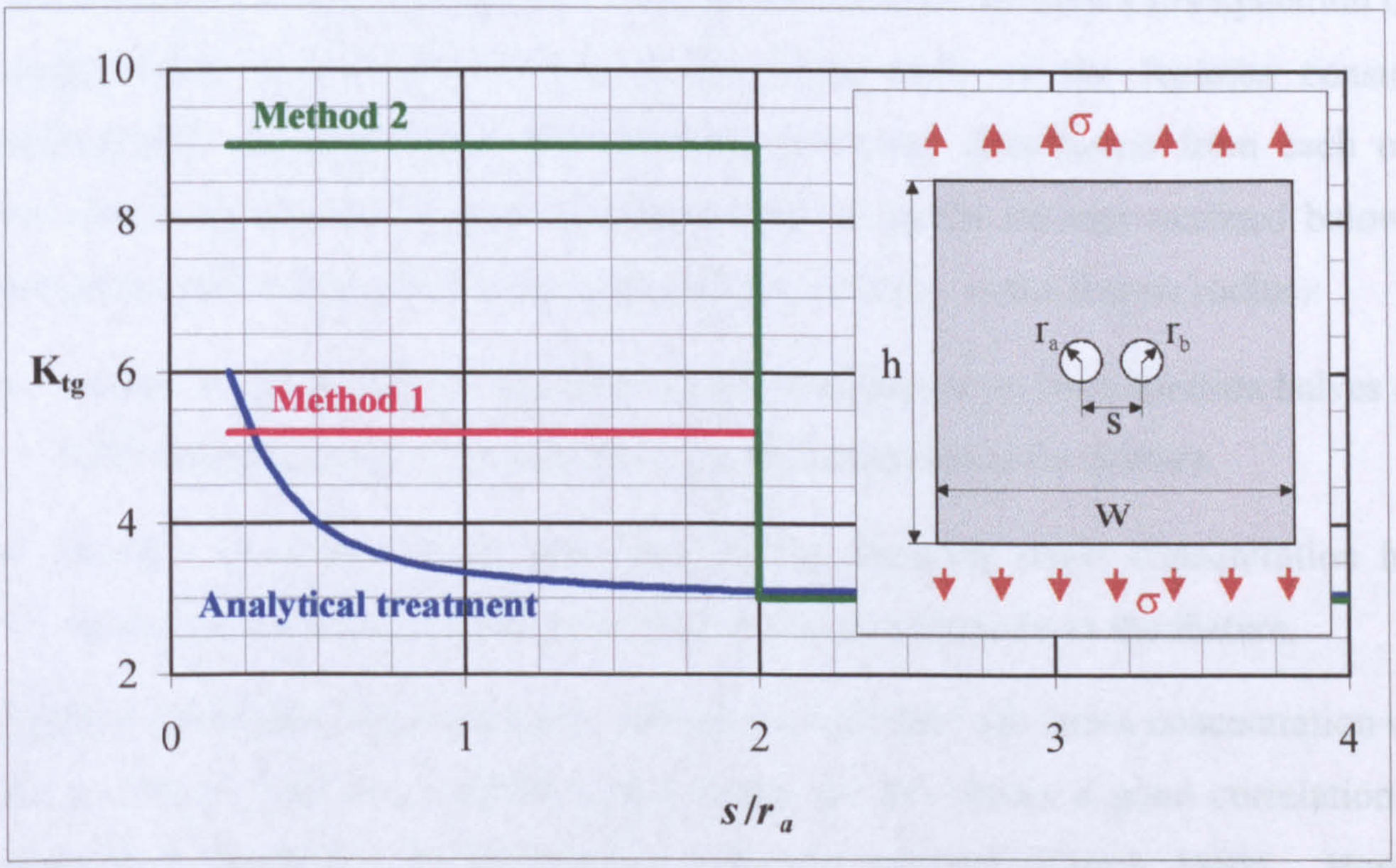

Figure 2-6. Comparison between the results of techniques typically employed in the aerospace industry, *Method 1* and *Method 2*, and the analytical treatment for the equivalent geometry (Haddon 1967)

Figure 2-6 clearly shows the inaccuracies associated with approximate methods of this type. For given feature combination types, each of the approximation methods only produces two distinct stress concentration values, which are each otherwise independent of the actual feature geometries. Both of the methods vastly overestimate the true stress concentration, particularly in the region where $s/r_a<2$.

One alternative technique which is sometimes used for the estimation of stress concentration values that lie along a line perpendicular to the applied stress, uses the known stress concentration for one of the features individually, and then adjusts this value based on the cross-sectional reduction generated from the introduction of the second feature. This 'rule of thumb', however, is considered to produce an underestimate of the actual stress concentrations present, as it only considers the material lost due to the additional feature, and does not account for any stress interaction effects between the two.

2.5.2 Approximation Techniques Proposed in the Literature

Stress concentration data for a limited number of feature interaction geometries are provided in standard ESDU texts (ESDU 1967; ESDU 1969). For cases involving

feature interactions that are not covered by these standard geometries, two alternative methods are proposed (ESDU 1985 (2); ESDU 1975 (1)) for approximating the stress concentrations around the features. Both of the methods involve a manipulation of the approximated stress concentration decays from each of the features considered individually. In either case, the stress concentration distribution from each of the features is approximated to an exponential decay in the manner outlined below, for decays *normal* and *parallel* to the applied stress (where r is the feature radius):

- *normal to applied stress*: the value of the decaying stress concentration halves every $0.25r$ from the point of maximum stress concentration at the feature.
- *parallel to applied stress*: the value of the decaying stress concentration halves every $0.5r$ from the point of maximum stress concentration at the feature.

Application of this approximation technique to estimate the stress concentration decay for a circular hole in an infinite plate under tension shows a good correlation with equivalent results for an appropriate analytical solution (Kirsch 1898). However, comparisons between the results from this technique and analytical treatments of alternative single features, such as shoulders or notches, showed very poor correlations.

Using this exponential decay, the two methods then use slightly different techniques to approximate the overall maximum stress concentration, as outlined below.

ESDU 1

The first method (ESDU 1975 (1)) involves using the exponential decay to approximate the unaffected stress distributions generated by each of the features, in order to establish the stress concentration influence of the features at the critical location under analysis, which typically occurs at the edge of one of the features. The overall maximum stress concentration is then predicted by multiplying these two values.

ESDU 2

The second method (ESDU 1985 (2)) uses a very similar principle to that of *Method 1*, but rather than of extrapolating the decayed stress from an individual feature to the edge of the second feature, this method considers the average decayed stress over the width of the second feature. Again, these two individual stress concentrations are multiplied together to generate a prediction of the overall maximum stress concentration.

The accuracy of these two methods can be gauged by again using the Haddon solution (Haddon 1967) as a benchmark against which to compare the results for the case of two

equal holes in an infinite plate under tension. The graph in Figure 2-7 shows a reasonably close correlation between the results from the two ESDU methods and the appropriate analytical solution for this problem involving circular holes. However, further investigation of these methods for different combinations of feature interactions revealed much less consistent and accurate results.

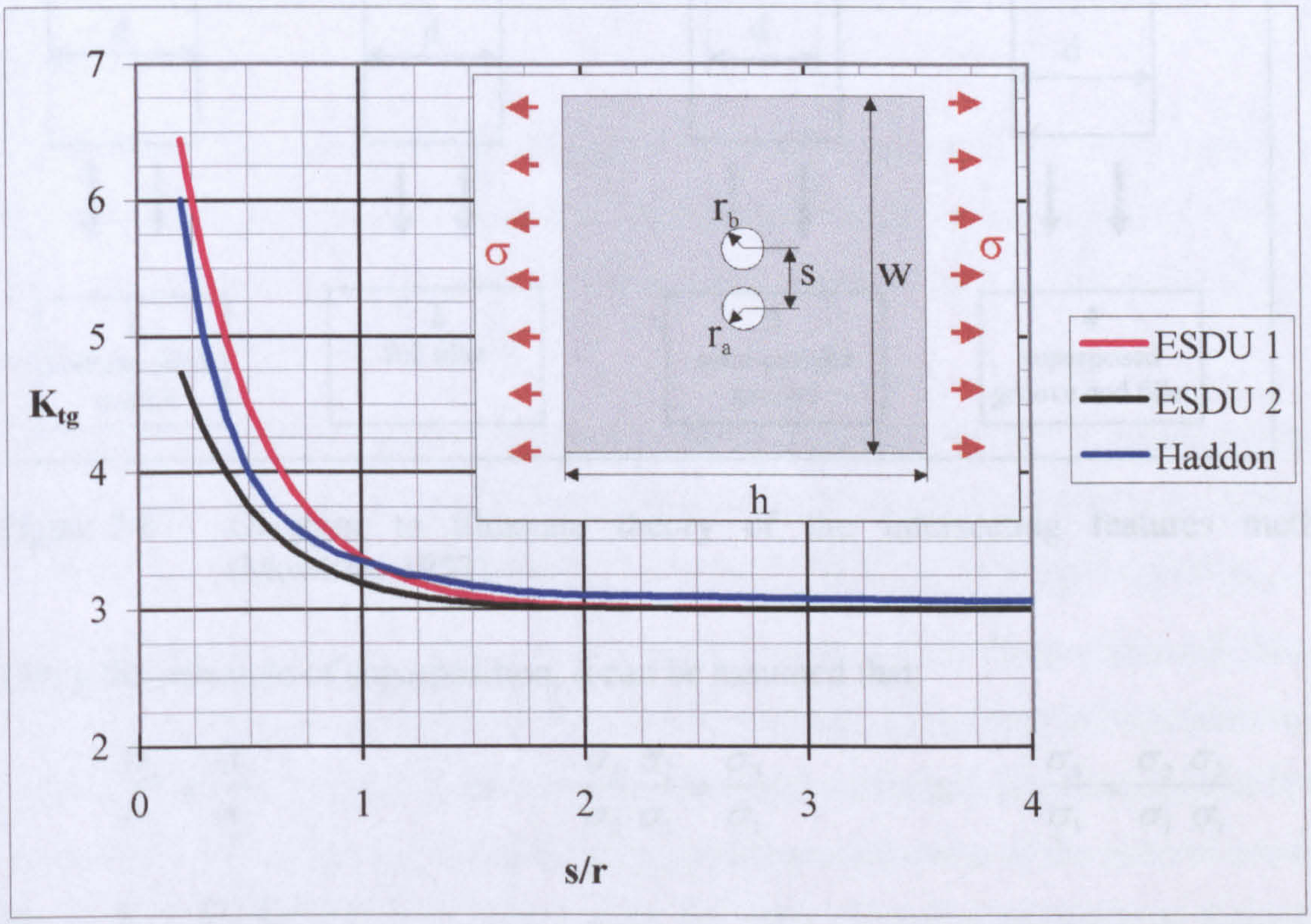

Figure 2-7. Graph to compare the results for the two methods developed by ESDU with the appropriate analytical results (Haddon 1967)

An alternative simple method of analysis was proposed by Mowbray (Schijve 2001; Mowbray 1953) for the approximation of maximum stress concentration for the specific geometry of two intersecting features, as limited data were available for these commonly-encountered problems. The method proposed simply predicted the overall maximum stress concentration using the product of the maximum stress concentration factors of the two individual features. The theory of this method is given below.

From Figure 2-8, components 1, 2, 3 and 4 have equal thickness, and equal minimum width (d) with equal applied stress σ_1. The maximum stresses in plates 1, 2, 3 and 4 are σ_1, σ_2, σ_3 and σ_4 respectively, with the stress concentration factors:

$$K_{t2} = \frac{\sigma_2}{\sigma_1} \qquad K_{t3} = \frac{\sigma_3}{\sigma_1} \qquad K_{t4} = \frac{\sigma_4}{\sigma_1}$$

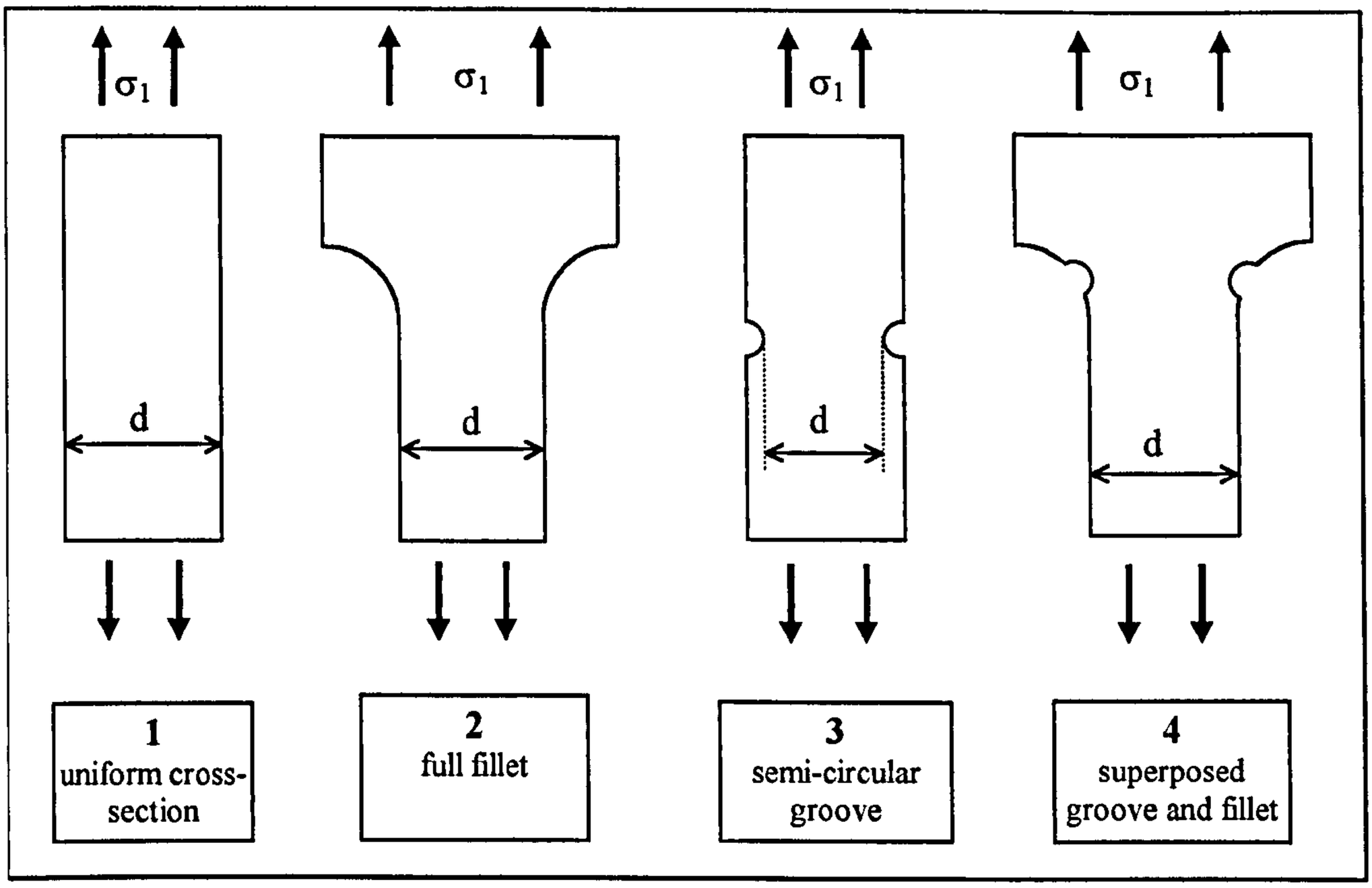

Figure 2-8. Diagram to illustrate theory of the intersecting features method (Mowbray 1953)

Using the principle of superposition, it can be assumed that:

$$\frac{\sigma_4}{\sigma_2} = \frac{\sigma_3}{\sigma_1} \quad \Rightarrow \quad \frac{\sigma_4}{\sigma_2}\frac{\sigma_1}{\sigma_1} = \frac{\sigma_3}{\sigma_1} \quad \therefore \quad \frac{\sigma_4}{\sigma_1} = \frac{\sigma_3}{\sigma_1}\frac{\sigma_2}{\sigma_1}$$

$$\Rightarrow \quad K_4 = K_3 . K_2$$

i.e. it is proposed that, using the principle of superposition, the overall stress concentration factor for intersecting features is the product of the maximum stress concentration associated with each feature individually. A number of experimental techniques have been used to validate this simple equation (James 1950; Mowbray 1953; Frank and Faucett 1961) which are described in more detail in Section 2.1. Although these results show a good correlation with Mowbray's approximation, the method is limited in application to cases where two features are intersecting in the same plane and subject to uniform tension.

2.6 DISCUSSION

The aerospace industry requires an accurate technique for the evaluation of stress concentration values around multiple features which is time-efficient, accurate and flexible. From the literature search and review described in this chapter, it is clear that there exists no data source or technique currently available which fulfils these criteria.

Although each of the analytical solutions outlined in this chapter produced highly accurate results, they are very limited in their application. Another major drawback in the use of analytical solutions in this particular application is their vast difficulty in application to problems of multiple features not involving configurations of circular holes in infinite bodies. These solutions could therefore not be considered as a suitable basis of a flexible technique for stress concentration prediction in problems of multiple features.

The review of the numerical and experimental studies revealed that a limited amount of data have been generated for the stress concentration in the region of multiple features. However, in most cases, the published data were piecemeal, and tended to focus, again, on geometries of interacting holes.

The review of alternative approximation methods indicated very low levels of accuracy, as well as an inflexibility for application to a range of alternative geometries. This was particularly true of those techniques currently used within the aerospace industry.

Throughout this chapter, many of techniques discussed have been evaluated through their employment to the simple geometry of two equal holes in an infinite plate under tension, and these results compared to an appropriate analytical solution (Haddon 1967). In each case, the results of this analysis provided an indication of the general accuracy of each of the techniques. The results for each of the approximation techniques considered, and in particular those methods typically used in the aerospace industry, showed particularly large discrepancies with the analytical solutions. These results, however, generally produced overestimates of the 'actual' stress concentrations present, and could therefore be considered simply to incorporate a very large factor of safety. For those tailored numerical methods evaluated, although the similarities with the analytical solution were typically of an acceptable level (± 10%), the flexibility and ease of application were insufficiently beneficial to provide a workable alternative to finite element analysis. Using these comparisons, it can be concluded that none of the methods available meets the aerospace industry's need for an easy and straight-forward method of producing an accurate approximation of the stress concentration for a wide range of combined features. To this end, further work will involve photoelastic, finite element and theoretical investigations of feature interactions for the development of new evaluation methodologies.

CHAPTER 3

RESEARCH METHODOLOGY

This chapter outlines the method of approach adopted in this research for the development of techniques for the prediction of stress concentrations associated with geometries of feature interaction. Details are provided of the two- and three-dimensional configurations of feature interaction considered in this research, along with the analysis tools that have been adopted to investigate them. This extensive programme of work has comprised numerical solutions (using the finite element method), experimental studies (using photoelastic analysis and automated strain gauge measurements) and the application of analytical treatments (using the complex variable method). Through a thorough data analysis process, new methodologies were then developed for the analysis of feature interaction problems.

3.1 INTRODUCTION

The overall ultimate objective of the work was to develop techniques that will enable the designer to (a) obtain an accurate, and in some cases rapid, assessment of the stress concentration resulting from features in close proximity, and (b) optimise the design so as to minimise the resulting stress concentration. The method would primarily be employed as a more time-efficient alternative or pre-cursor to analysis techniques such as finite element analysis and therefore must provide significant business benefits in terms of time, accuracy and ease of use. The final methodologies will be in a form suitable for incorporation into the expert system SCONES (Robinson et al. 2001), and fully documented as a fatigue analysis tool within the BAE SYSTEMS Technical Standards Manual (BAE SYSTEMS 2001 (2)); a document developed by the author.

In order to achieve the above set objectives, two alternative approaches were considered:

(i) carry out optimised numerical, analytical and experimental studies of the different geometries considered, and employ the resulting data to obtain a data-base for future use in a knowledge-based system, or

(ii) make use of the numerical, experimental and analytical results to generate a straight-forward predictive tool for the evaluation of features in close proximity.

The application of the latter option was contingent on establishing clear correlations between the geometric parameters for each feature combination and the resulting stress concentration value. Due to the inherent complexity of the analytical derivations of even the simplest of single geometric features, it was not clear whether any such straight-forward correlations would exist for multiple features. Therefore, the strategy adopted was, in the first instance, to conduct comprehensive numerical, experimental and analytical studies into the feature combinations under consideration, and then analyse the resulting data to establish which, if any, correlations existed. Based on this knowledge, a decision could then be made on whether the final design tool would generate stress concentration values from manipulations of the geometric parameters (approach (ii)) or whether it would simply be based on accessing an extensive bank of stored data (approach (i)).

3.2 GEOMETRIES CONSIDERED

A total of six two-dimensional and three three-dimensional geometries of feature interaction were considered during the course of this research, as illustrated in Figure 3-1 and Figure 3-2 respectively. Each of these geometries has been identified specifically by fatigue experts at BAE SYSTEMS as being those critical categories of feature interaction that occur most frequently, and for which time-consuming finite element optimisation routines are often required. Typical applications of the two-dimensional problems illustrated in Figure 3-1 within an aircraft design would include: integral machined sections containing misplaced holes such as those found in the wing skin (Diagrams (i), (ii) and (iv)), bolted joints which appear throughout the aircraft (Diagram (iii)) and hydraulic pipe fastenings, access holes and equipment fastenings (Diagrams (v) and (vi)). For the case of the three-dimensional problems, those geometries considered in Figure 3-2 occur in such designs as joint attachments (Diagram (i)), attachments for wing spars (Diagram (ii)) and grease holes (Diagram (iii)).

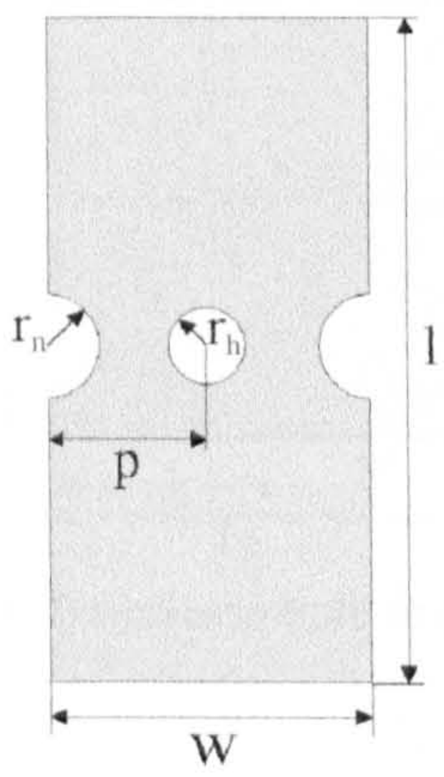

(i) Hole placed between double-edged semi-circular notches

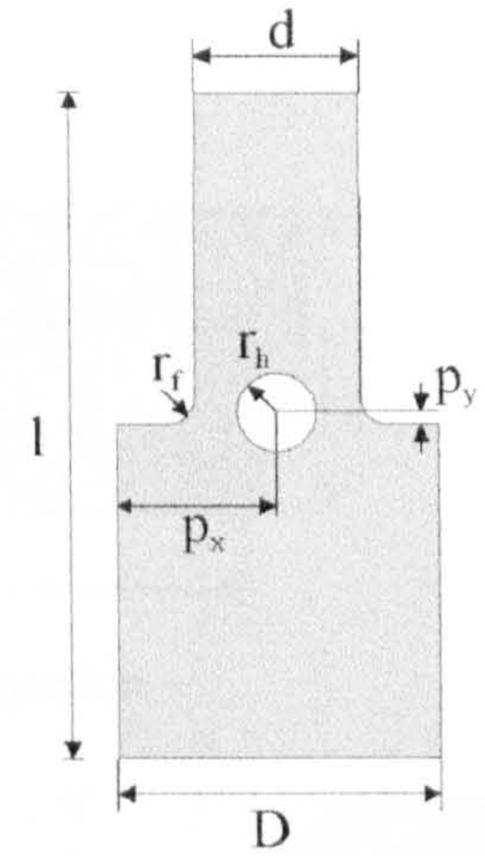

(ii) Hole placed between shoulder fillets

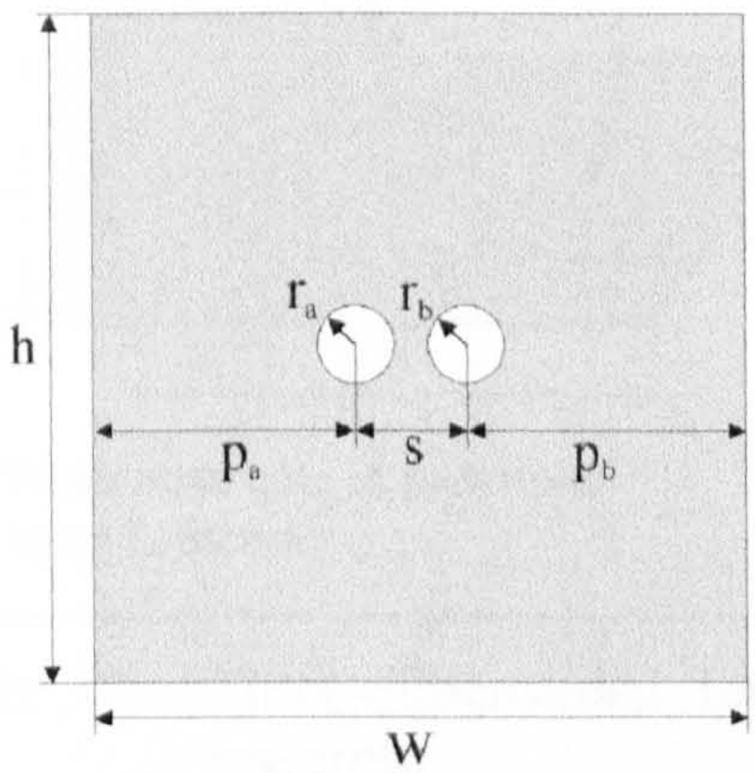

(iii) Two unequal circular holes

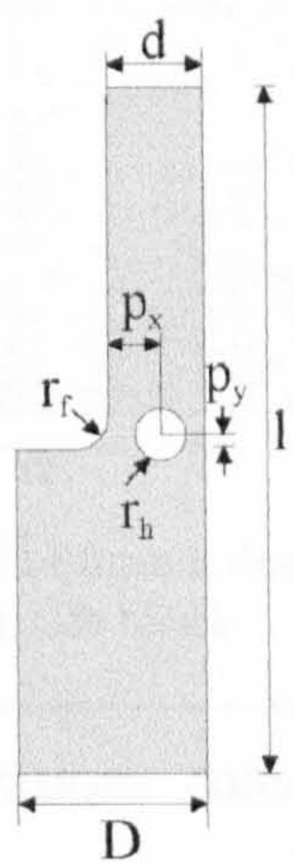

(iv) Hole placed in proximity to a shoulder fillet

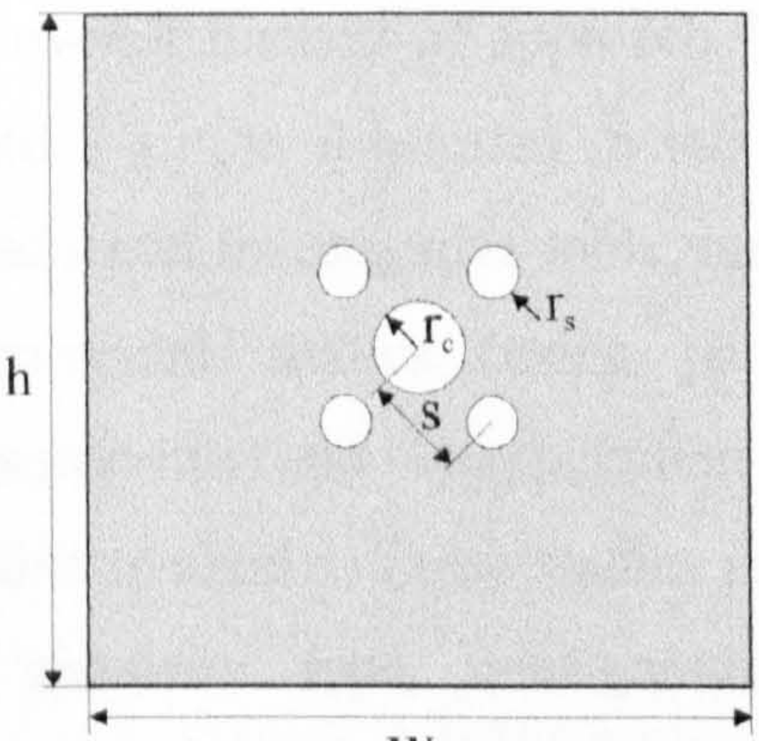

(v) Central hole surrounded by four radial holes

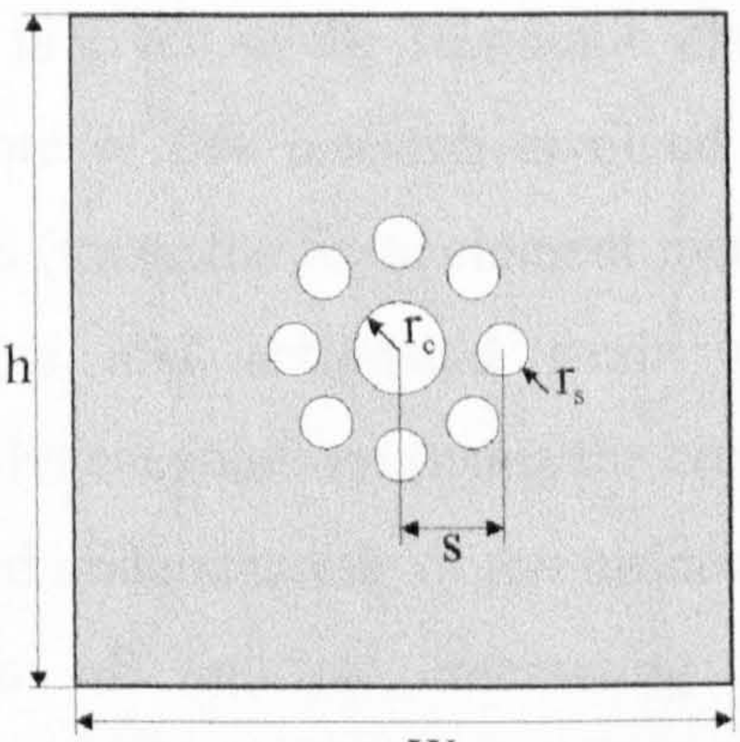

(vi) Central hole surrounded by eight radial holes

Figure 3-1. Two-dimensional feature interaction configurations considered in this research

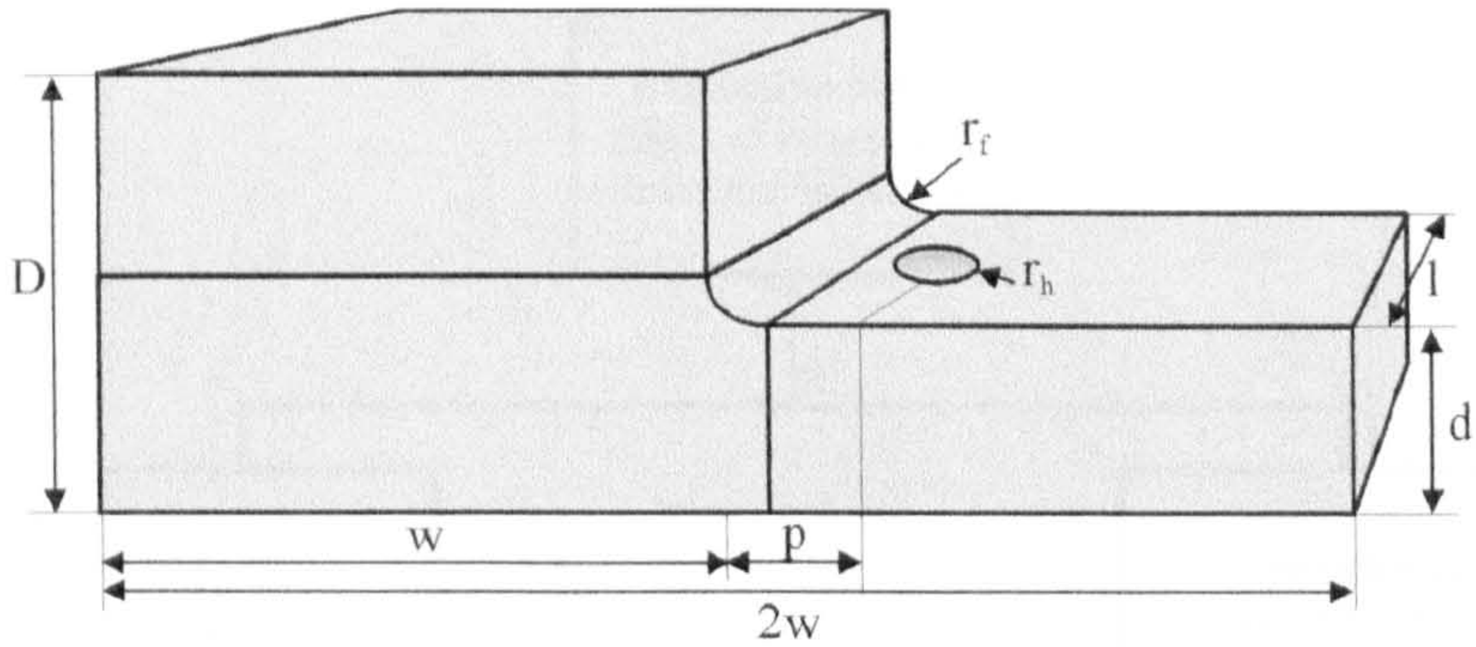

(i) Transverse hole in proximity to a radiused fillet section

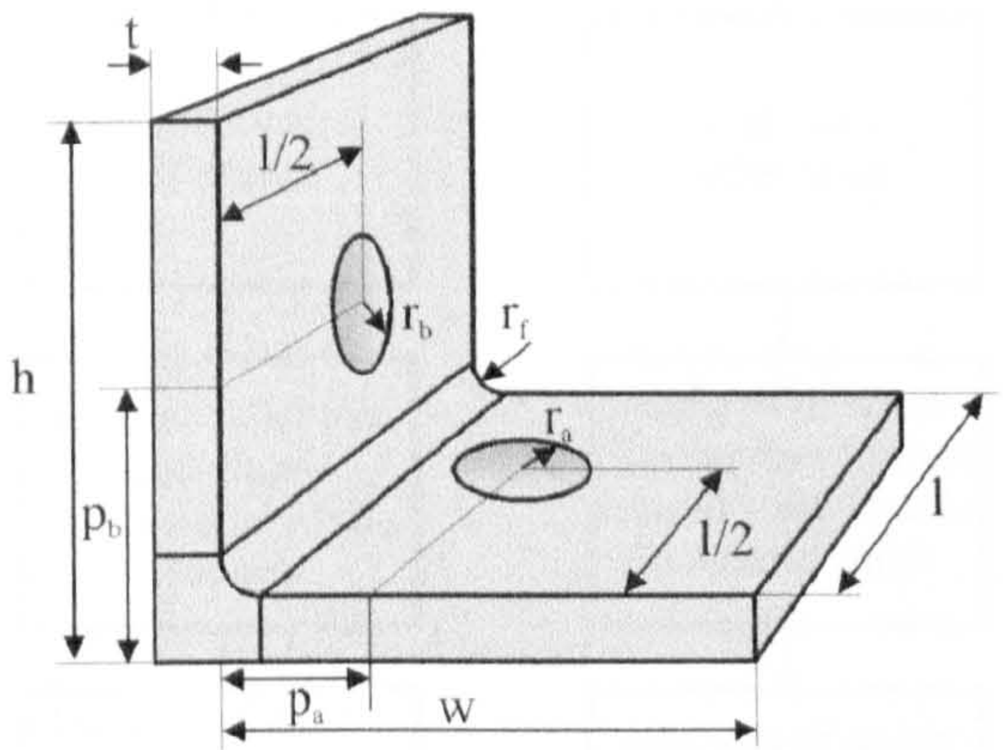

(ii) Transverse hole in proximity to an L-section

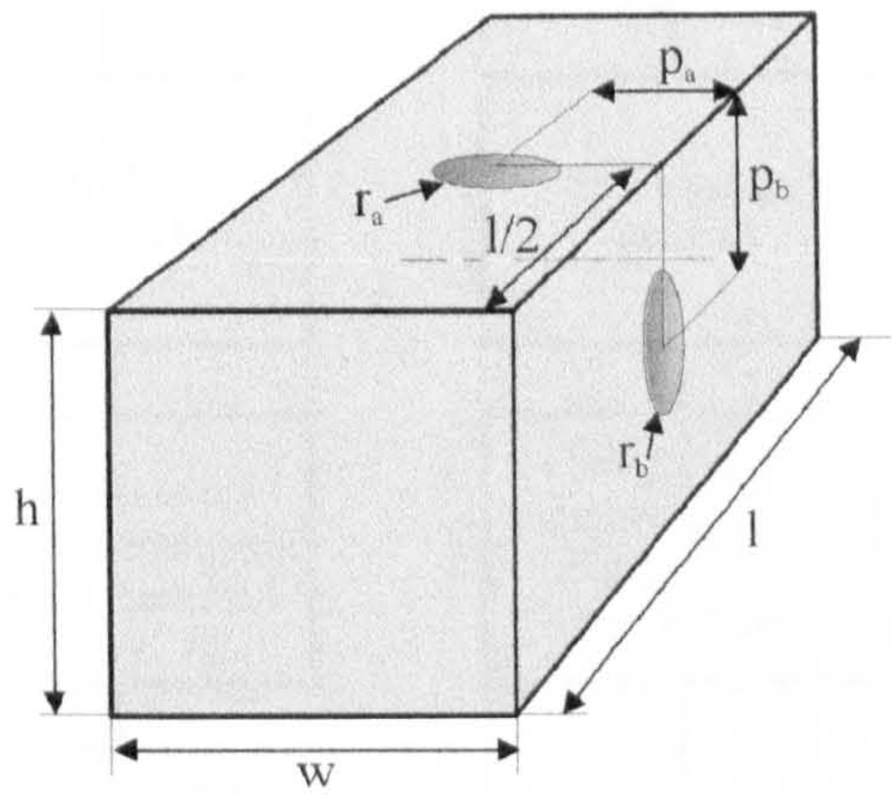

(iii) Cross-wise bore holes in a semi-infinite block

Figure 3-2. Three-dimensional feature interaction configurations considered in this research

3.3 METHOD OF APPROACH

The overall method of approach for this research is given in the schematic chart in Figure 3-3. As illustrated in this diagram, the core of this research involved three fundamental investigative tools; numerical solutions (using the finite element method), experimental studies (using photoelastic analysis and automated strain gauge measurements) and the application of foregoing analytical solutions (using the complex variable method). These studies provided a detailed understanding of the influence of the geometry type, configuration and position of multiple interacting stress concentration features upon the stress fields and the resulting stress concentration factor.

In each case, the research activities began with an analysis of the stress distributions formed around single geometric features in both two and three dimensions, achieved through the generation and investigation of numerical, theoretical and experimental

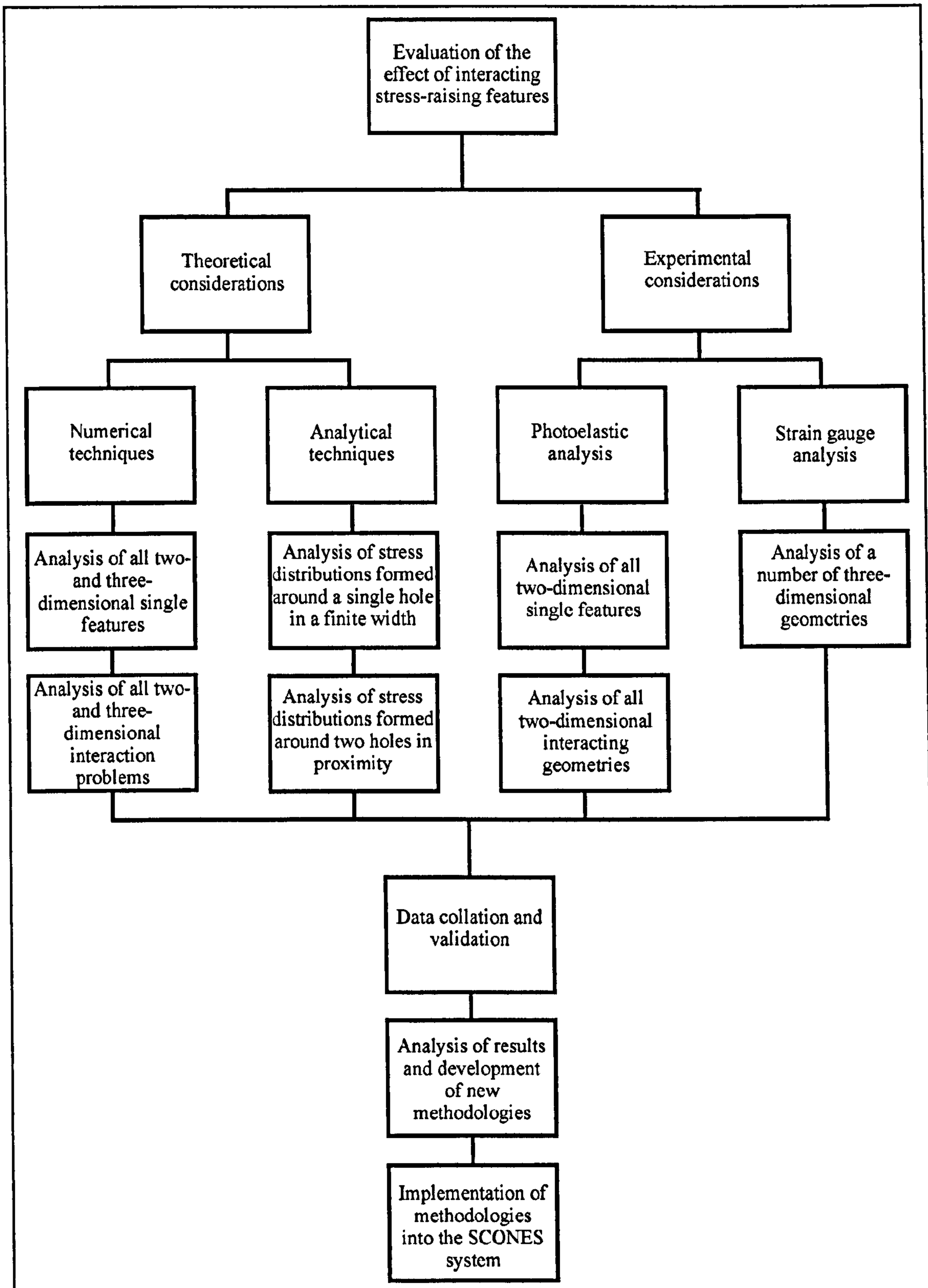

Figure 3-3. Schematic chart to illustrate the method of approach adopted in this research

analyses. Through the detailed description of the form of these individual stress decays, a more precise understanding was formed of the influence of the introduction of additional stress fields.

The primary stage of this work was to conduct comprehensive finite element studies of all single feature geometries, and each of the two- and three-dimensional interaction geometries under consideration (Figure 3-1 and Figure 3-2). For each configuration investigated, every geometric parameter was incrementally varied to create a full picture of the manner in which each of these factors affects the overall stress concentration value. The results from this finite element study allowed for the specification of the critical geometries identified for further experimental investigation and validation.

Due to the inherent complexities in the derivation of analytical solutions to problems involving stress-raising features, it was not possible to develop new treatments of these geometries for validation purposes. However, through the application and understanding of established solutions, it was possible to generate accurate stress distribution data for the single feature of a hole in a finite width plate (Howland 1929), and the multiple feature geometry of two holes in an infinite plate (Meguid and Gong 1993). These data were then used for validation of both the numerical and experimental results.

The experimental investigations comprised photoelastic techniques for the two-dimensional models, and strain gauge techniques for the three-dimensional problems. For each of the six two-dimensional problems addressed, between eight and fourteen photoelastic models were produced for full static manual photoelastic analysis. For each of the three-dimensional geometries, a number of mechanical models were produced and a series of strain gauges were attached for mechanical testing.

The combination of each of these investigative techniques provided comprehensive analysis and validation of each of the geometries considered. In each case, data were collected not only for the value of the maximum stress concentration for that geometry, but also for the position and direction of that stress concentration, as well as plots of the ligament stress concentration between adjacent features. All of these data provided a very detailed picture of the overall stress concentration distribution and its relationship with each of the geometric parameters.

After this data were collated and validated, the next stage in the research project was to identify whether any correlations existed between the geometric parameters in each case, and the resulting stress concentration factor. Based on the insights gained from this data analysis process, methodologies for the evaluation of each of the problems under consideration in this research of feature interaction were developed, validated and implemented as standard practice within BAE SYSTEMS.

CHAPTER 4

FINITE ELEMENT CONSIDERATIONS

This chapter deals with the finite element approach used in this research for the investigation of the stress concentrations associated with stress-raising features in proximity. The chapter firstly discusses the approaches adopted for two-dimensional problems, and then moves on to look at the three-dimensional geometries, in each case drawing on case-study examples for illustration. All finite element calculations were operated using the commercial code ANSYS.

4.1 INTRODUCTION

Due to their inherent complexity, generalised and unified closed form expressions describing interacting effects are complex to develop. Only in special cases, when the features are circular in nature, is it feasible to obtain approximate analytical closed form expressions. It was therefore decided that finite element models, accounting for different complexities in the geometry, would be considered in the analysis of the stress concentration resulting from the presence of interacting stress concentration features in these geometries.

This chapter is therefore devoted to an overview of the finite element method, details of the geometries considered, element selection and their convergence and sample results. Both two-dimensional and three-dimensional analyses were considered and the loads were restricted to quasi-static uni-axial loading. In the case of circular holes, the analytical model developed by Meguid and his collaborators (Meguid and Gong 1993) was considered to validate the model. In all other cases, both photoelasticity and strain gauge results were used to validate the work. Throughout this analysis, the commercial code ANSYS was used for the finite element calculations.

4.2 FUNDAMENTAL PRINCIPLE OF FINITE ELEMENT ANALYSIS

The basis of the finite element method is the approximation of a continuous variable distributed within a body through subdividing the section into a number of discrete elements. Within each of these elements, the distribution of the field variable is approximated by an interpolation function. The interpolation functions are defined by the values of the field variable at the interconnection points between the elements, called the nodal points. Each of the equations describing the discrete behaviour of each element is then assembled to form an expression for the continuous behaviour of the entire body, with the field variables at each nodal point as the unknowns.

In general there are six basic stages in the generation and solution of a stress problem using finite element analysis:

1. *Simplification of the structure* Simplification of the model will allow for more convenient divisions of the body into elements. Approximations which can be made for structural simplification include the consideration of the problem as a two-dimensional model or confining the analysis to only the repeating region of a body which displays symmetry.

2. *Discretisation of the model* The body is divided into a number of finite elements. The particular size and type of elements selected are dependent on factors such as the model size and geometry, the applied loads and the required accuracy.

3. *Ascribing the interpolation function* The interpolation function defines the distribution of the field variable through each element. Typically, this function takes the form of a polynomial. Using these functions, a stiffness matrix can be derived for each element, which is defined in terms of the applied load and the displacement at the nodal points.

4. *Assembly of the elements* The global stiffness matrix is generated through the assembly of the individual stiffness matrices of each element. The boundary conditions of the entire body are also combined into this governing equation.

5. *Solution of the global equations* The global equations which approximate the distribution of the field variable throughout the entire body are expressed in the form:

$$[K]\{U\}=\{F\} \qquad \textbf{(Equation 4-1)}$$

where, K is the stiffness matrix
U is the nodal displacements
F is the nodal applied loads

Solutions to this problem will provide values of the nodal displacements.

6 *Post-processing* For stress analysis problems, the post-processor stage will involve calculation of the local stresses and strains from the nodal displacements.

4.3 TWO DIMENSIONAL INVESTIGATIONS

A total of six two-dimensional problems involving stress concentration features under uni-axial quasi-static loading were considered: (i) a hole placed between double-edged semi-circular notches in a semi-infinite plate, (ii) a hole placed between shoulder fillets in a semi-infinite plate, (iii) two unequal holes in a finite-width plate, (iv) a hole in proximity to a single shoulder fillet in a semi-infinite plate, (v) a central hole surrounded by eight radial holes in an infinite plate, and (vi) a central hole surrounded by four radial holes in an infinite plate. The details of these geometries are illustrated in Figure 4-1. In order to provide an overview of the application of the finite element method to two-dimensional stress concentration problems, this section begins with a discussion of the finite element modelling of a single stress-raising feature (Section 4.3.1). Section 4.3.2 then moves on to look at problems involving multiple features, taking one of the problems illustrated in Figure 4-1 as a worked example. Throughout this work, the commercial finite element package ANSYS was used.

4.3.1 Single Feature

For the purposes of validating the accuracy of the numerical procedures adopted for this work, the initial geometry considered was the simple case of a single hole in an infinite plate under tension (Figure 4-2). Comparisons between the maximum stress concentration factor determined for this geometry numerically, and the analytical results (Kirsch 1898) validated the accuracy of the procedure. As illustrated in Figure 4-2, due to the symmetrical nature of the geometry under analysis, it was only necessary to model one quarter section of the plate.

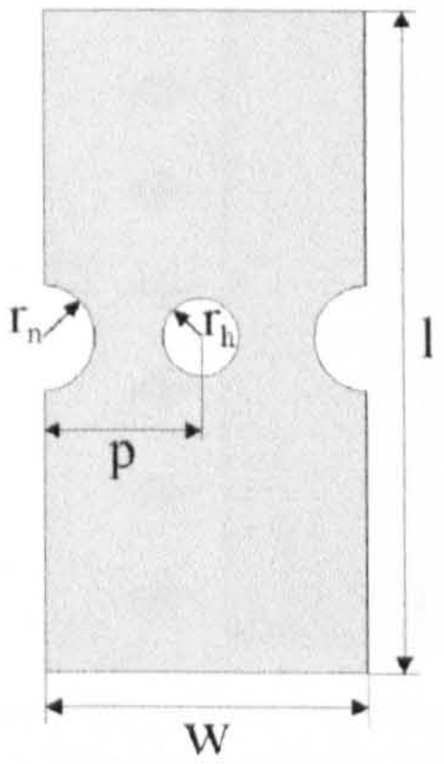

(i) Hole placed between double-edged semi-circular notches

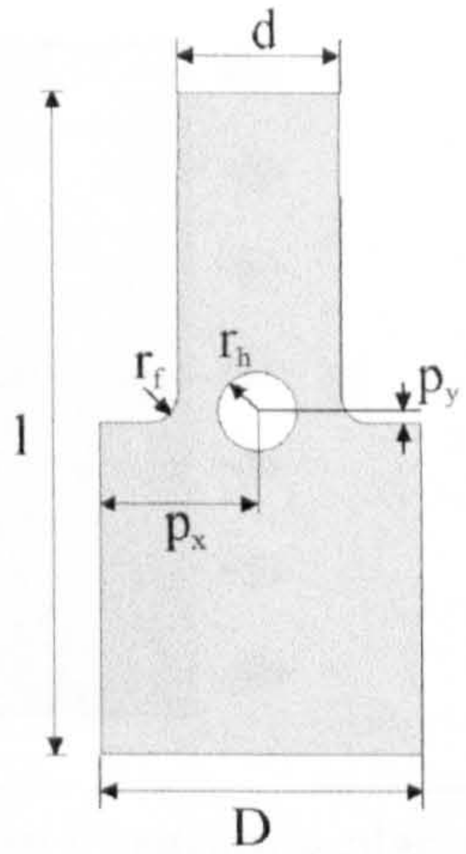

(ii) Hole placed between shoulder fillets

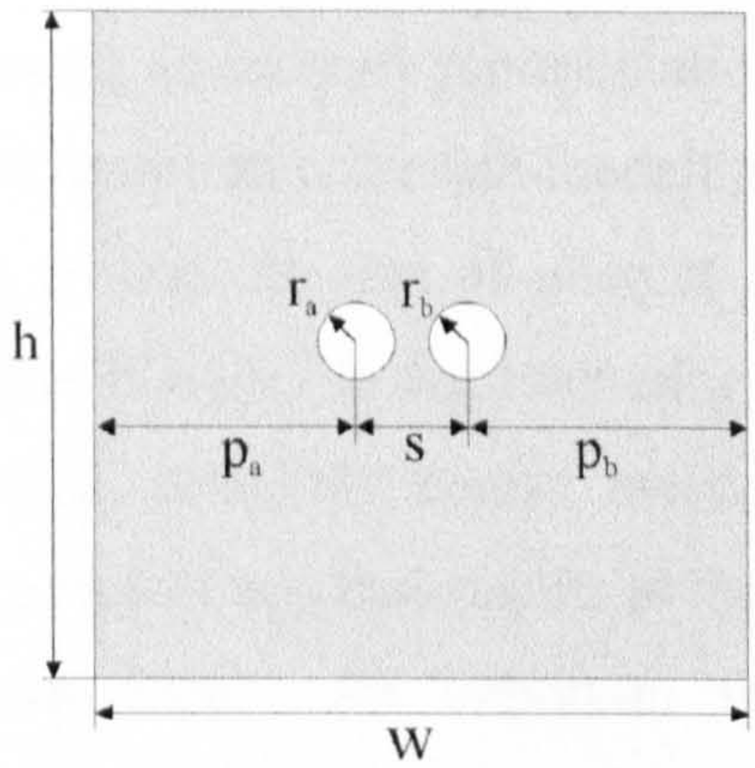

(iii) Two unequal circular holes

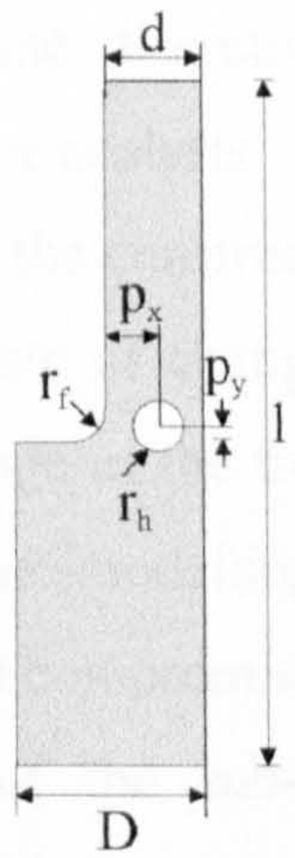

(iv) Hole placed in proximity to a shoulder fillet

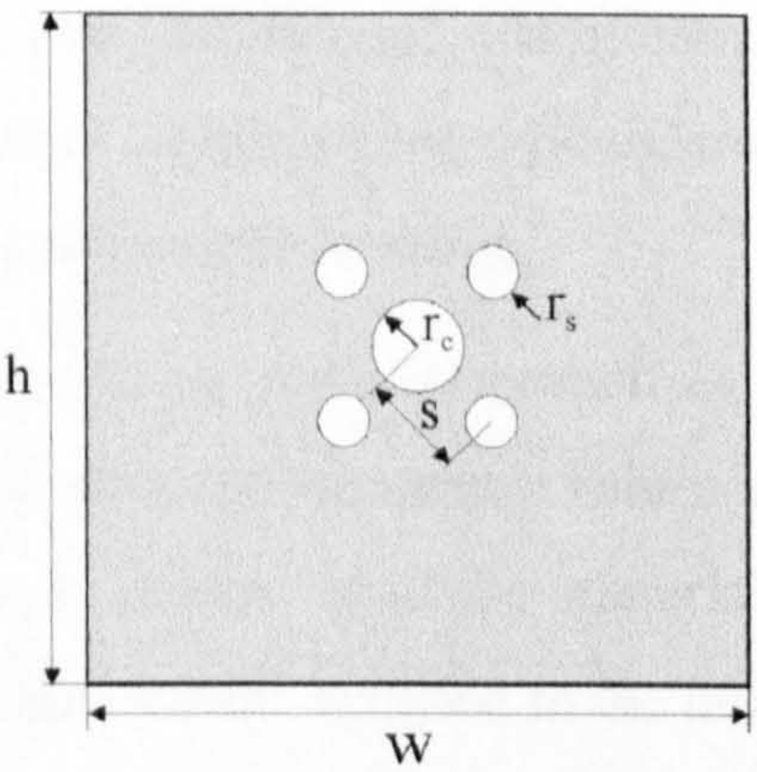

(v) Central hole surrounded by four radial holes

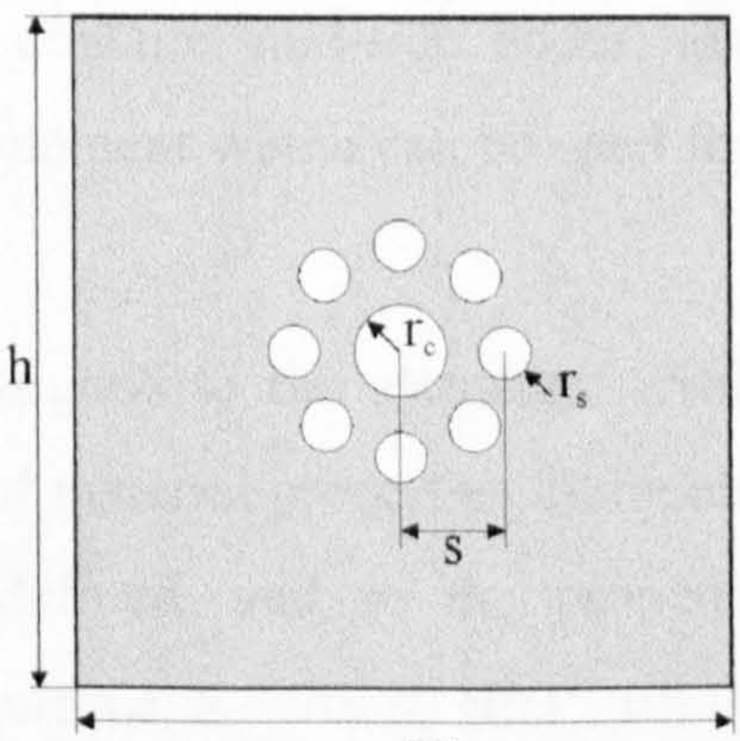

(vi) Central hole surrounded by eight radial holes

Figure 4-1. Illustration of the two-dimensional problems to be analysed using finite element modelling

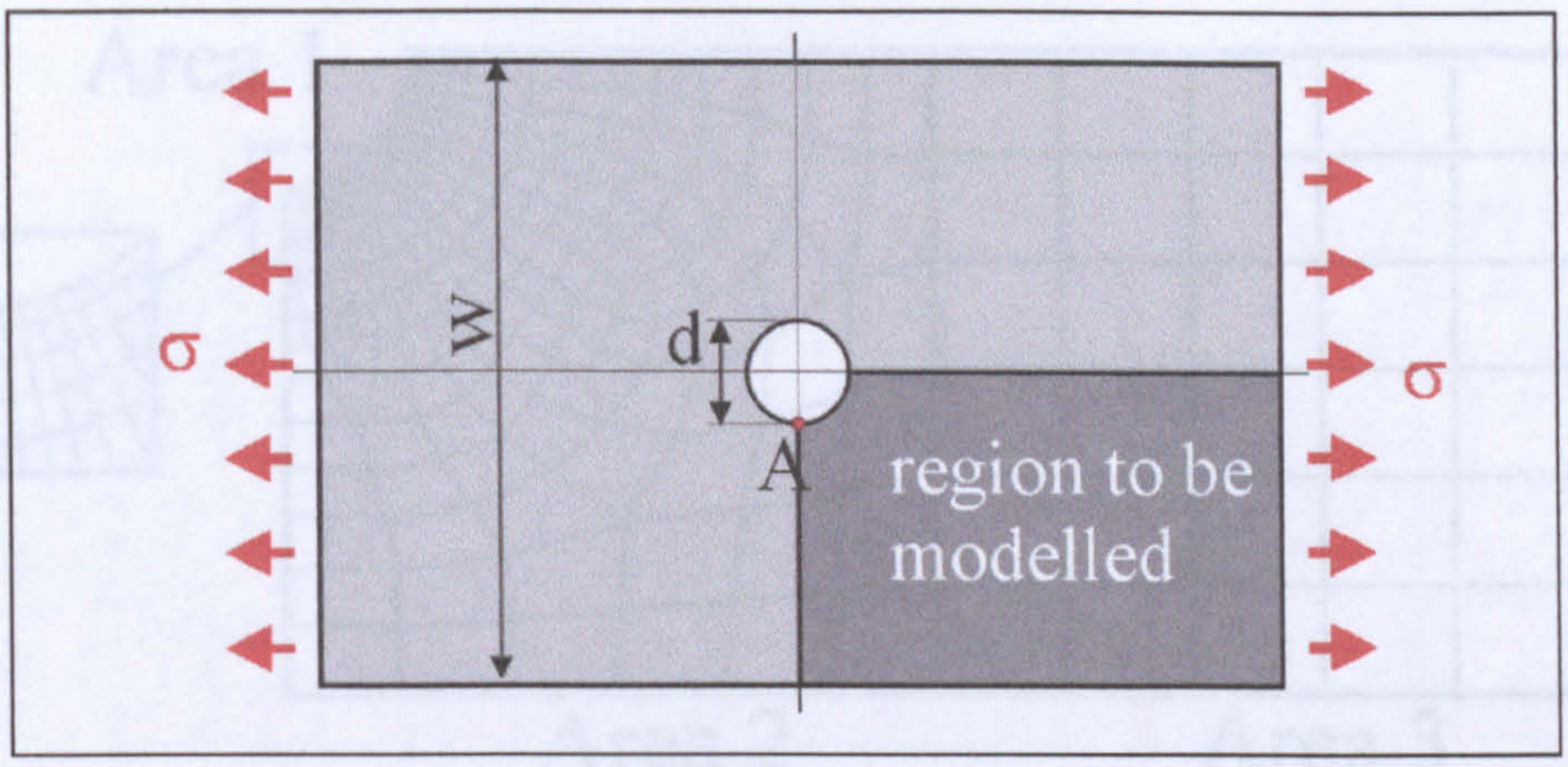

Figure 4-2. Single hole in an infinite plate under tension illustrating planar symmetry

4.3.1.1 Discretisation of the Model

The principle of the finite element procedure relies on the discretisation process producing an accurate representation of the field variable under analysis. The first stage of discretisation is the sub-modelling of the body to allow for the construction of a finer mesh around the area of interest, or in regions where the rate of change of the field variable is high. In the remaining regions, where little change in the field variable is observed, relatively coarse meshes can be employed. Sub-modelling enables the production of accurate results in the critical locations, without compromising the overall analysis time. An important factor in the definition of the sub-model is the compatibility with the element types to be used for the body. As the case of a hole in an infinite plate is relatively simple, only one element type was used throughout the body, and the *Plane 82* element was considered as the most appropriate for this application. This two-dimensional quadrilateral shell element contains mid-side nodes, and can therefore adapt to curved boundaries. It is also an element which can be used for both free and mapped meshing.

At this stage, material properties must also be assigned to the elements. Although elastic stress concentration values are independent of material properties, finite element systems require that the material attributes be defined, and so the properties of aluminium were assigned to the model (constant, isotropic, $E = 70e10$ N/m^2, $\nu = 0.33$).

For the case involving a hole in an infinite plate, it is known that the maximum stress occurs at point *A* (Figure 4-2). Therefore, three separate sub-models were defined which allowed for progressively finer meshes to be created towards this point of maximum stress (Figure 4-3).

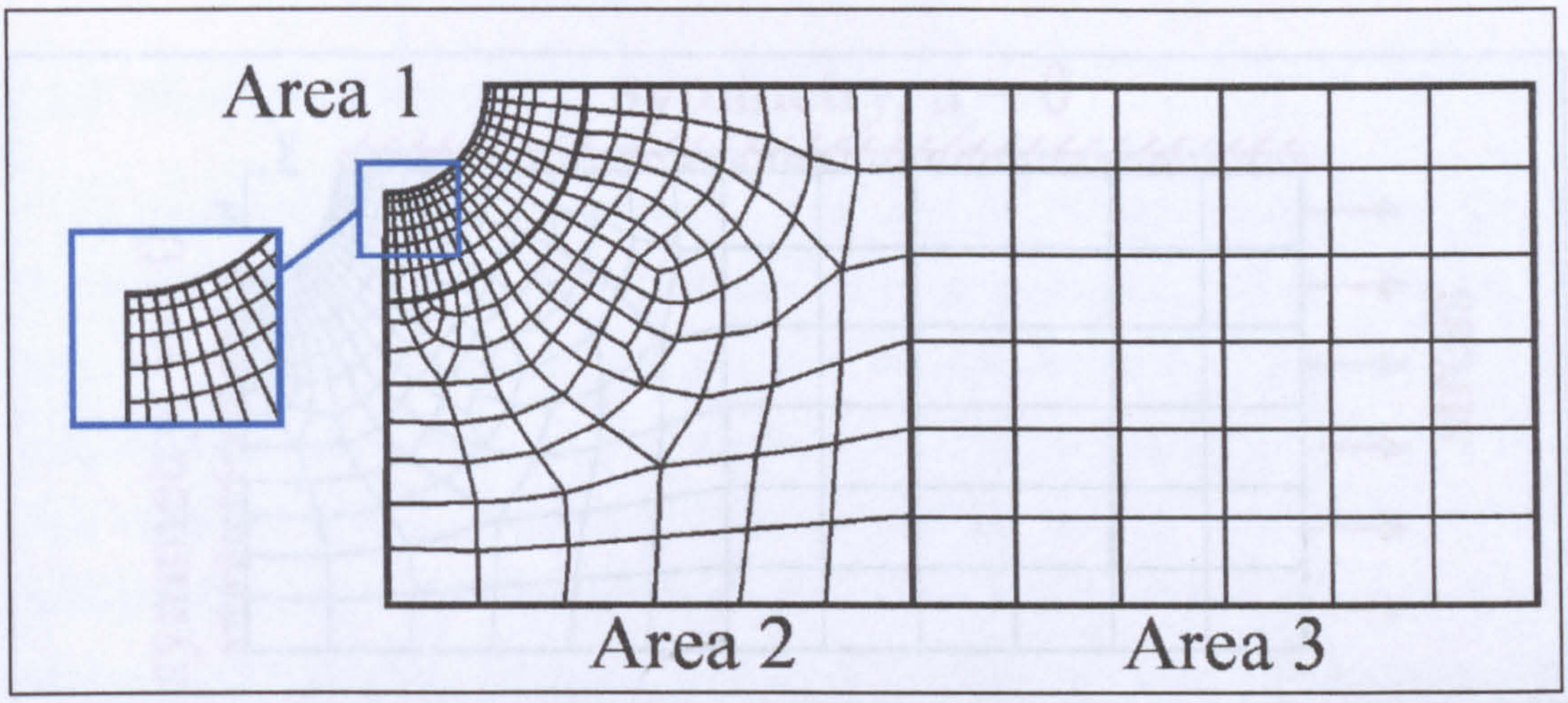

Figure 4-3. Discretisation of the model by sub-modelling and free and mapped meshing

Within each of these sub-models, a combination of free and mapped mashing was used to create the most accurate and efficient approximation to the system under analysis. The formation of a mapped mesh requires a regular mesh volume with pre-defined nodal and element points. Free meshing, on the other hand, is generated automatically by the system to create elements of a defined size within an irregular shape. As illustrated in Figure 4-3, *Area 3*, which is remote from the region of interest, was discretised using a relatively coarse mapped mesh. Due to its irregular nature, *Area 2*, requires free meshing. Finally, *Area 1* was meshed using fine mapped meshes, which was graduated towards the point of maximum stress. The most accurate form of quadrilateral elements are those which are mapped meshed to a relatively small size, have sides of equal length (aspect ratio equal to unity), meeting at 90° at the corners, and which are surrounded by elements of a similar size and shape. As illustrated in Figure 4-3, elements such as these were focused around the region of particular interest.

4.3.1.2 Loads and Constraints

As only one quarter section of the plate has been used for creation of the model, the appropriate boundaries were constrained for simulation of the symmetrical boundary conditions. As illustrated in Figure 4-4, these conditions constrain the x-direction deflections for symmetry about the y-axis, and constrain y-direction deflections for symmetry about the x-axis. For simulation of quasi-static loading, a unit pressure was applied to the far boundary.

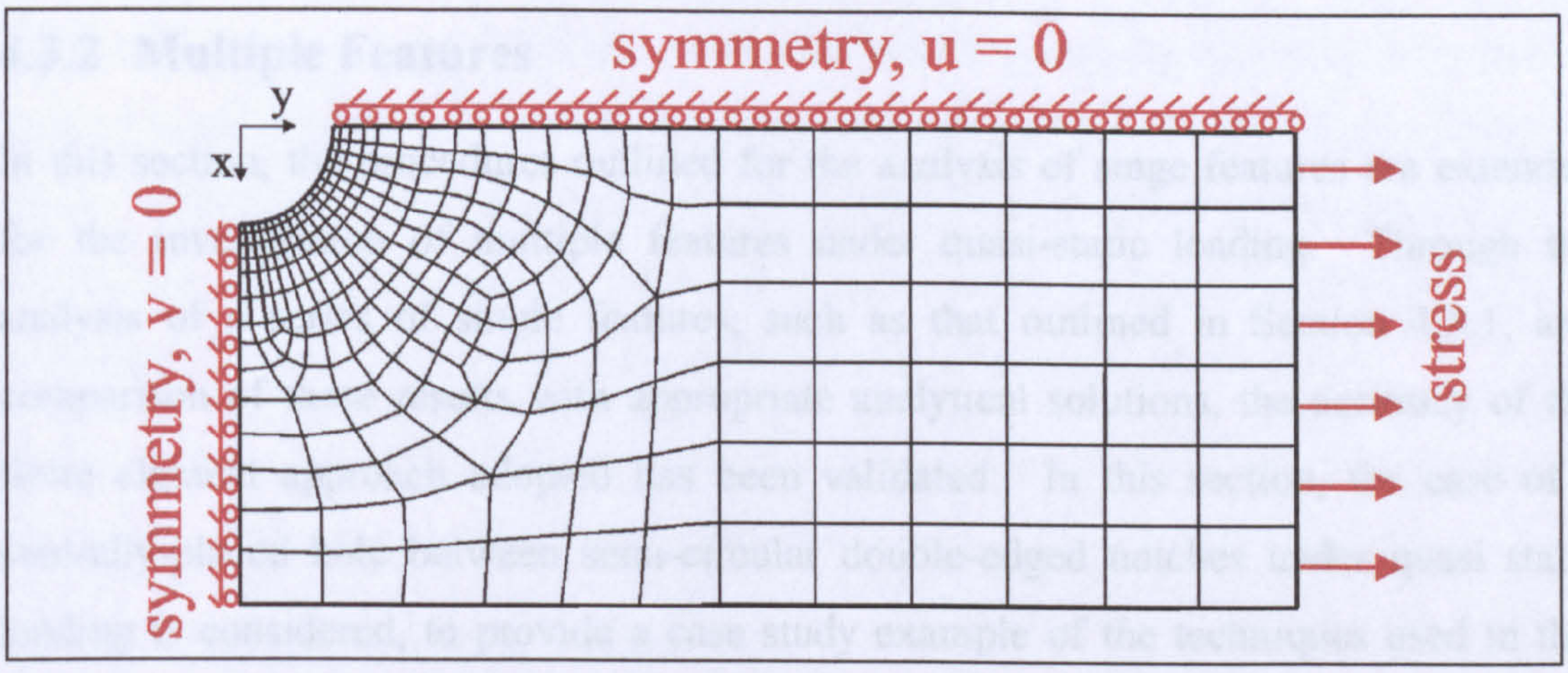

Figure 4-4. Applied loads and constraints

4.3.1.3 Mesh Convergence

A very important aspect of the finite element process is the selection of the appropriate mesh density for the model. Mesh refinement is essentially a compromise between accuracy of results and the computing capabilities available together with cost. In order to optimise the mesh density of the model under consideration, the problem can be re-analysed with a two-fold increase in the number of elements. The results of these two solutions are compared, and, if significant discrepancies exist, a further increase in mesh density is required. This process of mesh refinement continues until the reduction in element size no longer produces a significant effect on the model solution. For the case of the hole in the infinite plate, five separate mesh refinement sequences were conducted until convergence was reached for the stress concentration value at point *A* (Figure 4-2).

4.3.1.4 Accuracy of Results

Finite element analysis is an approximation method whose accuracy is dependent on how closely the discretised model represents the distribution of the field variable in the actual body and how successfully the model converges. There are a number of factors that particularly affect the accuracy of this representation. These include geometry, element properties, applied loads and constraints. For the case of the single hole in an infinite plate under tension, the accuracy of the model solution can be assessed through comparisons to the analytical treatment (Kirsch 1898) which establishes the stress concentration value to be 3 at point *A* (Figure 4-2). After mesh refinement, the finite element solution provided a stress concentration value of 2.97 at point A, which is very much within the acceptable error range for this analysis.

4.3.2 Multiple Features

In this section, the procedures outlined for the analysis of singe features are extended for the investigation of multiple features under quasi-static loading. Through the analysis of a series of single features, such as that outlined in Section 4.3.1, and comparison of these results with appropriate analytical solutions, the accuracy of the finite element approach adopted has been validated. In this section, the case of a centrally-placed hole between semi-circular double-edged notches under quasi static loading is considered, to provide a case study example of the techniques used in this research for the analysis of multiple two-dimensional features.

4.3.2.1 Geometry Considered

The model geometry illustrated in Figure 4-5 was analysed, with hole radius r_h, notch radius r_n, plate width w and the hole positioning p. The model length, l, was carefully selected to ensure that the end boundaries had no influence over the features under analysis. As the particular geometry where the hole is centrally-placed between the notches exhibits two-way symmetry, only one quarter section needed to be considered, as illustrated in Figure 4-5.

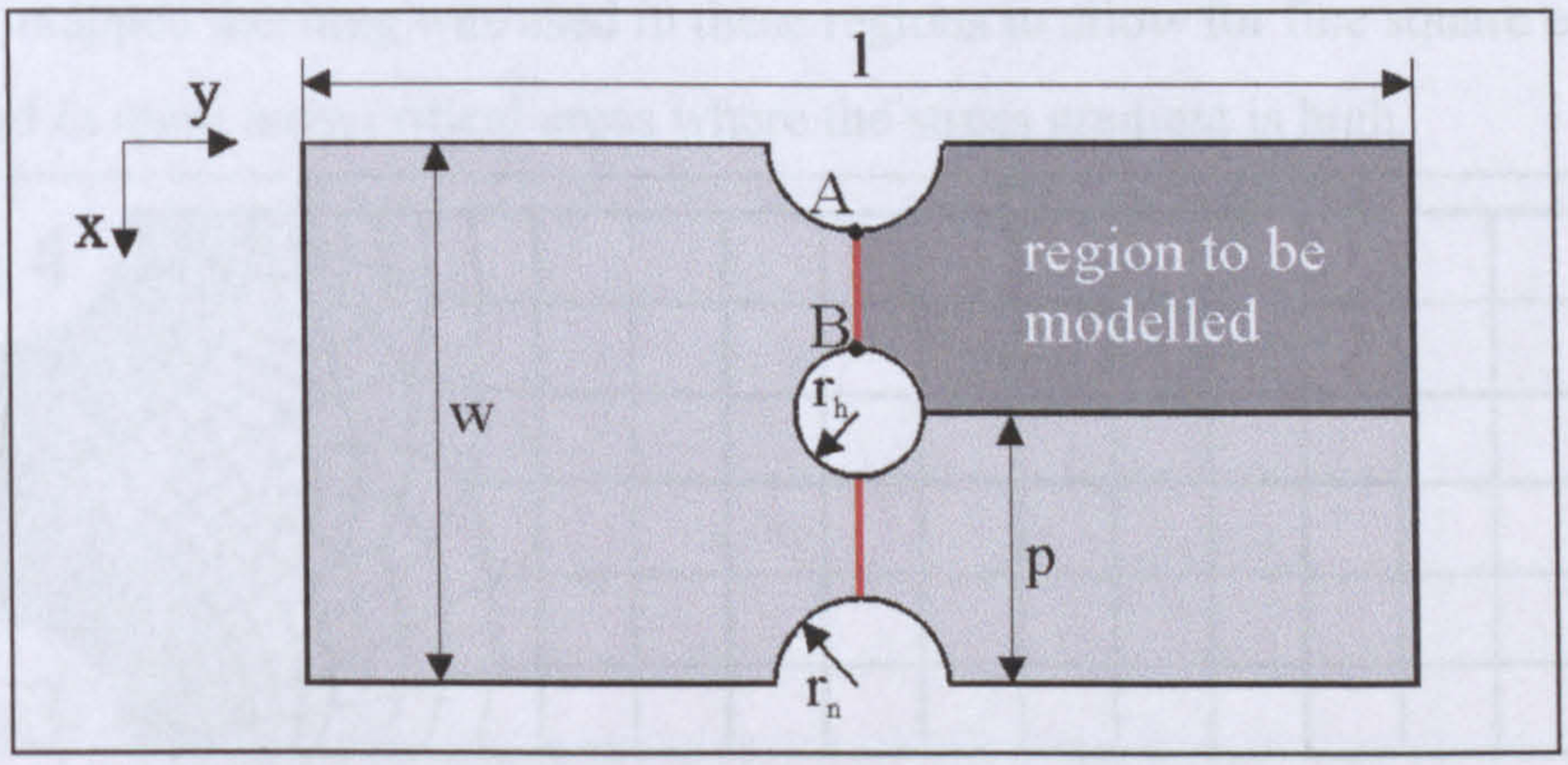

Figure 4-5. Centrally-placed hole between double-edged notches, $p=w/2$

For this geometry, finite element results were required over a range of values for r_h, p and w (with r_n held as constant). A series of analyses was conducted for values of hole radii ranging from $r_h/r_n=8/75$ to $r_h/r_n=75/8$, over a range of plate widths varying from $w/r_n=4$ to $w/r_n=24$. In addition, nine geometries of hole positioning (p) were considered, initially starting with the case of a centrally-placed hole, where $p=w/2$ (as illustrated in Figure 4-5). The consideration of each of these geometries required a total of over nine hundred separate analyses. In each case the magnitude and position of the maximum stress concentration were determined, and a ligament plot of the y-direction

nodal stress was generated for the stress distribution along the nominal cross-section marked in red (Figure 4-5). To facilitate the efficient analysis of such a large number of geometric configurations, the finite element model was generated parametrically. The parametric log file (or analysis file) contained a series of loops which allowed the variables, r_h, p and w to vary incrementally on each re-analysis of the model.

In this section, the analysis of one particular geometry is described as an illustration of the overall approached taken; the geometry where $r_n = r_h$, $w = 4\ r_h$ and p=w/2.

4.3.2.2 Discretisation of the Model

As described in Section 4.3.1.1, the two stages of the discretisation process involve firstly creating the sub-model and then, secondly, dividing these regions into elements using free or mapped meshing. Figure 4-6 illustrates the four sub-models which were created within the model. Again, the rectangular area remote from the point of interest (*Area 1*) can be discretised using coarse mapped meshing. *Area 2* requires free meshing, due to its irregular shape. Finally, two quarter-circular regions were created around the hole and notch (*Area 3 and Area 4*), which allowed for progressively finer elements to be created towards the points of maximum stress (Points *A* and *B* Figure 4-5). Again, mapped meshing was used in these regions to allow for fine square elements to be created in these most critical areas where the stress gradient is high.

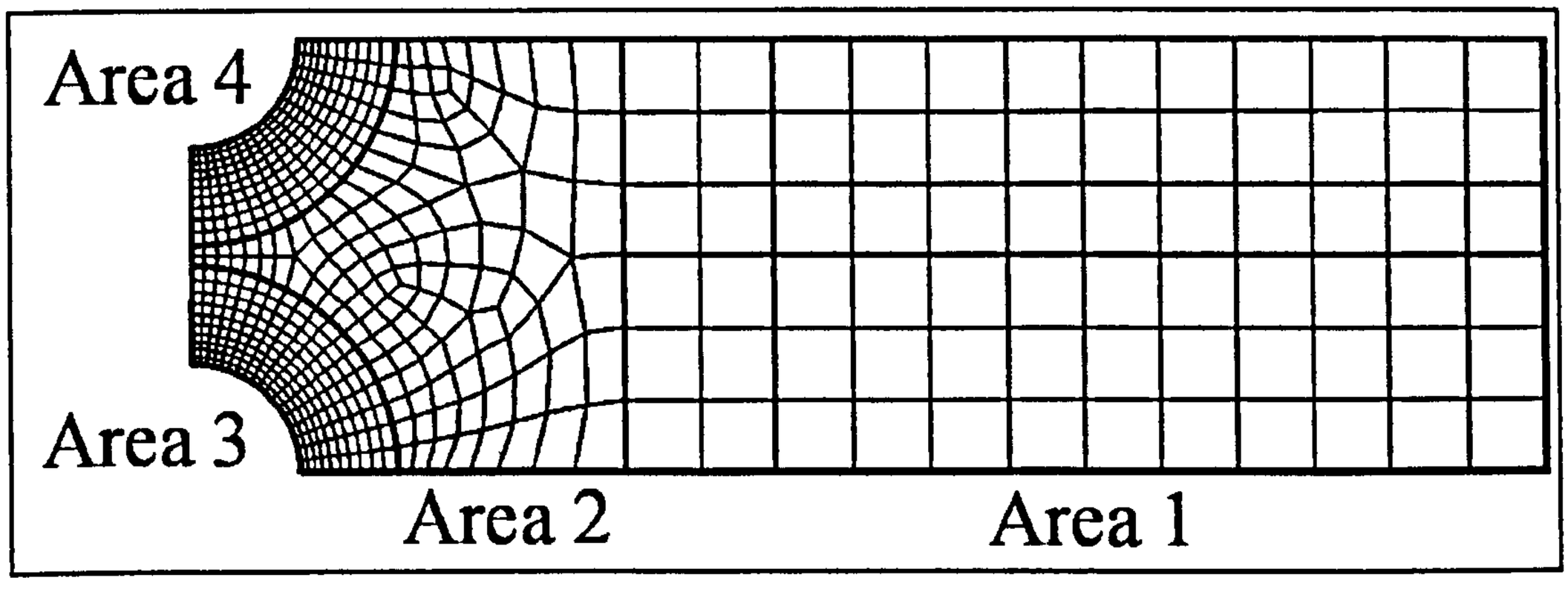

Figure 4-6. Discretisation of the model

4.3.2.3 Loads and Constraints

Loads and constraints were applied to the model as illustrated in Figure 4-7, with the appropriate displacement constraints applied to simulate symmetrical conditions and an applied unit boundary stress.

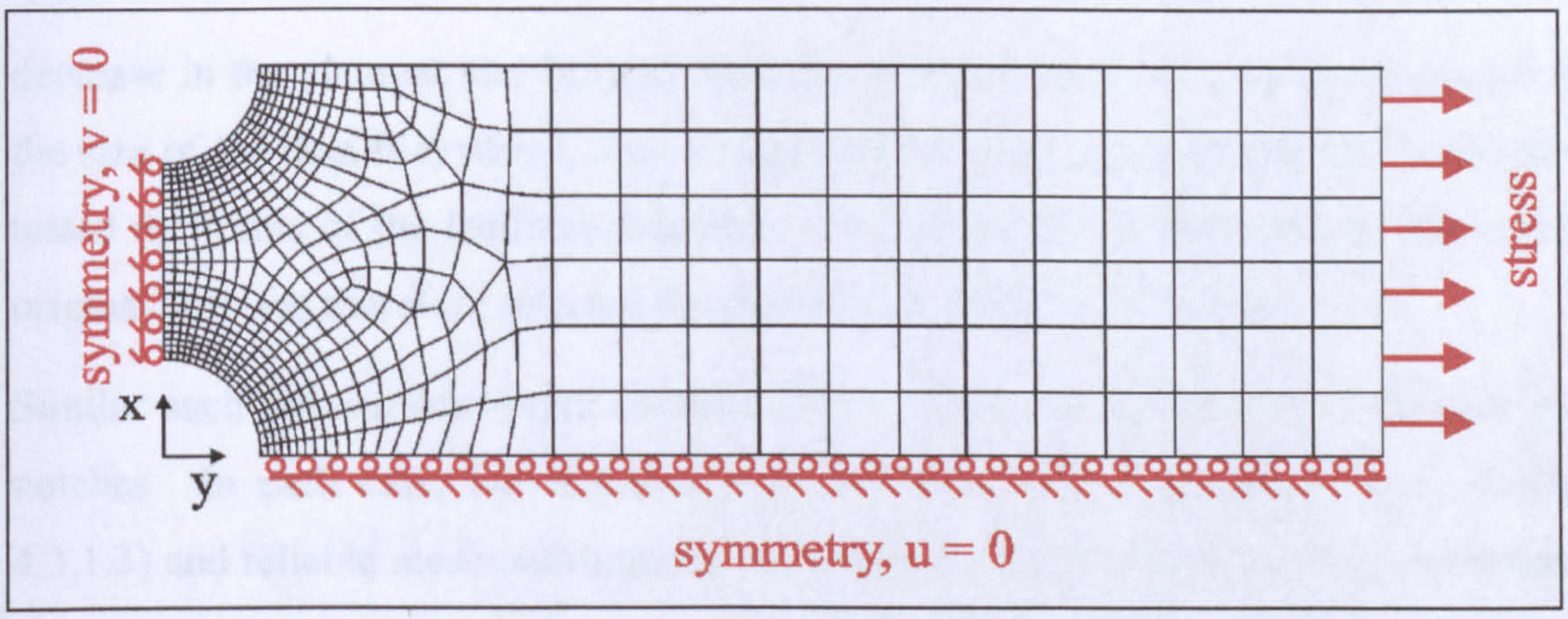

Figure 4-7. Applied loads and constraints to the model

4.3.2.4 Mesh Convergence

The creation of the parametric log file allowed for the rapid analysis of a variety of element sizes and configurations. A series of analyses was conducted for the refinement of the element size in terms of the accuracy of results and the computing capability.

As the log file was created using a loop, a large series of data files was generated over a relatively short period of time. For this analysis it was therefore particularly important to ensure that the optimum element sensitivity was created not only for converging accurate results, but also to minimise the size of the data files produced. Shown in the table in Figure 4-8 is the effect of incremental decreases in the element size, starting with a basic element size *x*, on the overall maximum stress concentration (occurring in this case at point *B* from Figure 4-5) and the size of the data file created.

Element size	**K_t**	**File size**
x	3.120	3MHz
0.5*x*	3.201	4MHz
0.25*x*	3.256	7MHz
0.125*x*	3.258	29MHz
0.0625*x*	3.259	74MHz

Figure 4-8. Table illustrating model convergence with corresponding file size for each analysis

From this comparison it was clear that no further accuracy could be attained after the element sizes are reduced to one quarter of their original dimensions. At this element sensitivity, the data file size was approximately 7MHz, which was within the acceptable limits for the computing facilities available. As illustrated in Figure 4-8, any further

decrease in the element size beyond this point would have had a significant impact on the size of the data file, which, after a large number of successive analysis, would have tested the limits of the facilities available. This element sensitivity of one quarter the original size was therefore selected for the analysis of this model (Figure 4-6).

Similar such comparisons were conducted for various configurations of the hole and notches. In each case, the elements produced were of optimal dimensions (Section 4.3.1.3) and reliable mesh convergence was reached. It can therefore be assumed that a good level of accuracy has been attained for the analysis of these models.

The finite element solution for the y-direction nodal stress for the configuration under examination is given in Figure 4-9.

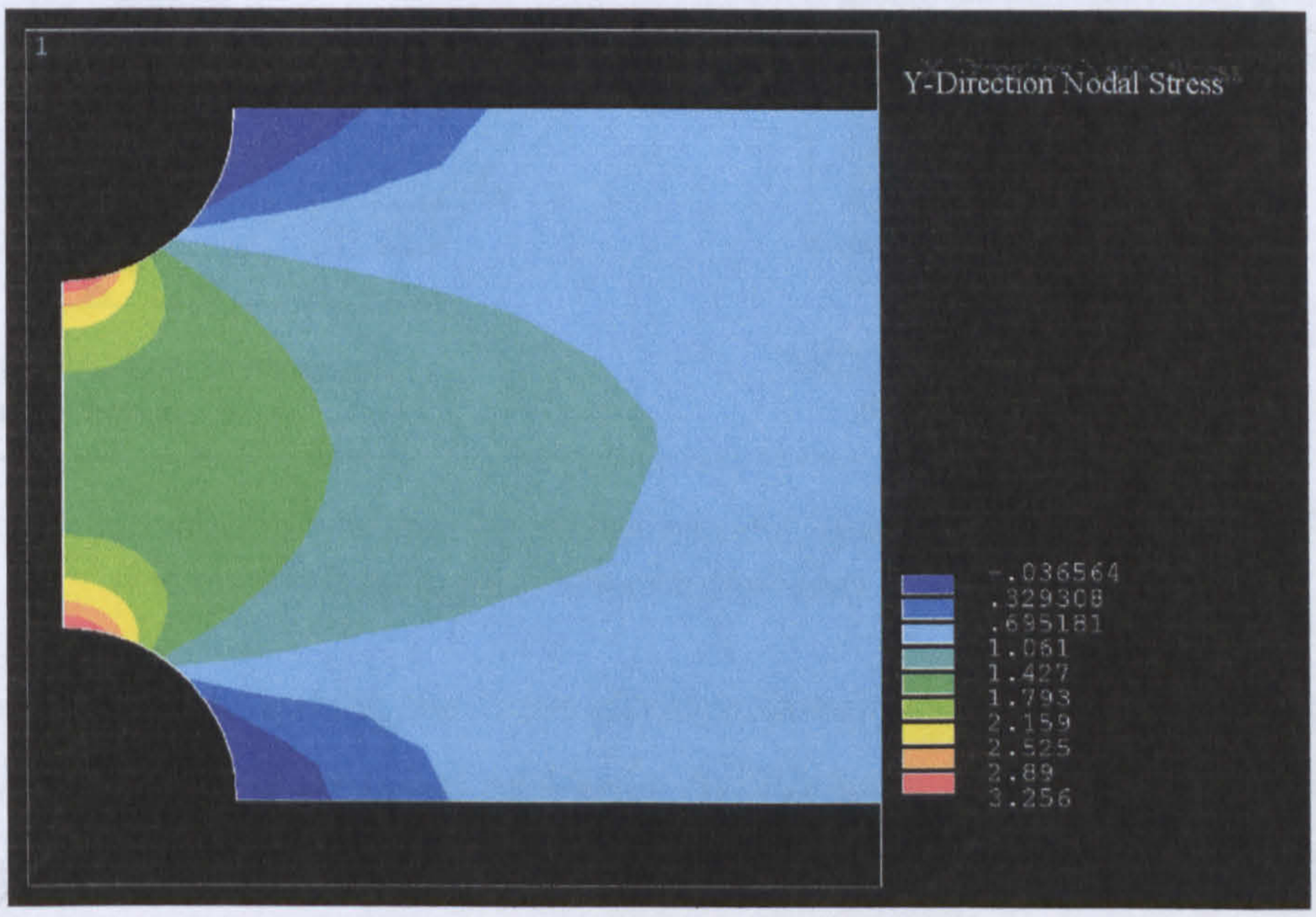

Figure 4-9. Finite element solution for the problem of a circular central hole placed between semi-circular double-edged notches under uni-axial tension

4.4 THREE DIMENSIONAL INVESTIGATIONS

In addition to the problems described in Section 4.3, three three-dimensional configurations of interacting stress concentration features were also considered, as depicted in Figure 4-10.

The geometries considered were: (i) a transverse hole in proximity to a filleted section, (ii) transverse holes in proximity to an radiused L-section, and (iii) cross-wise bore-holes in a semi-infinite block. In each case the loading conditions were uni-axial and quasi-static, and were applied to the models as illustrated in Figure 4-11, with the loads applied to the faces depicted in red in a direction normal to these surfaces.

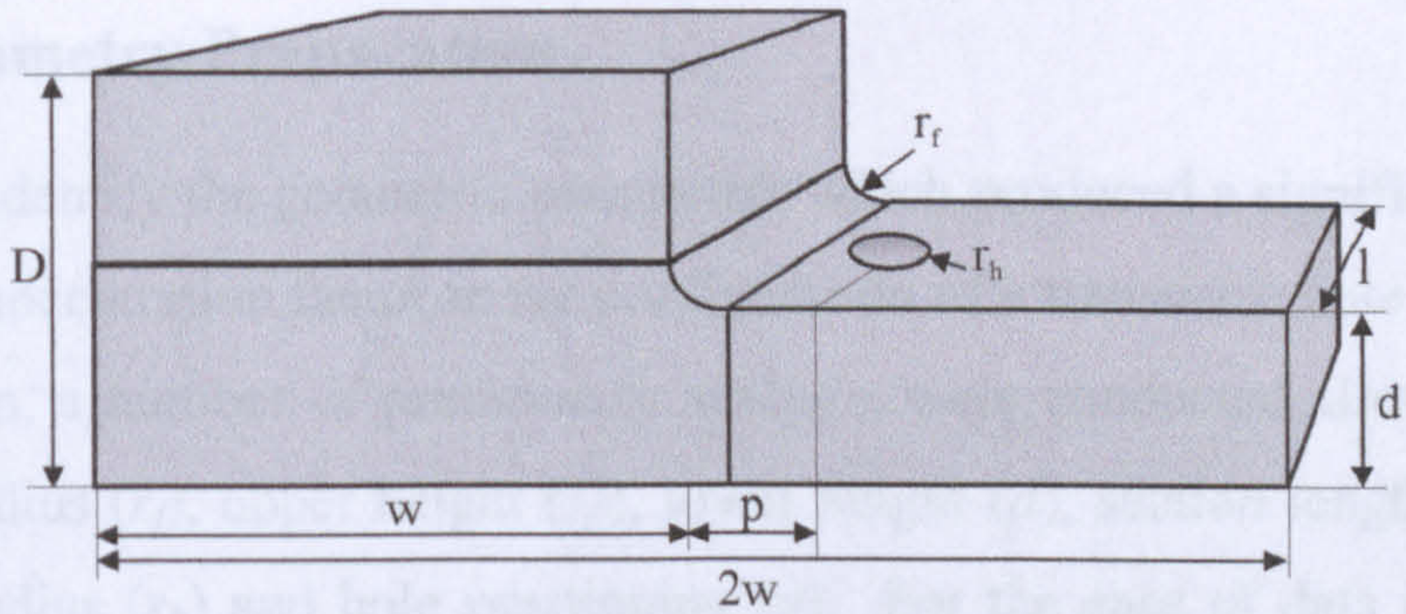

(i) Transverse hole in proximity to a radiused fillet section

(ii) Transverse hole in proximity to an L-section

(iii) Cross-wise bore holes in a semi-infinite block

Figure 4-10. Illustration of the three-dimensional geometric problems investigated in this research using numerical techniques

For the purpose of describing the finite element techniques adopted in this research for the analysis of three-dimensional problems, the illustrative examples of the transverse hole in proximity to a radiused fillet section (see Diagram (i) in Figure 4-10) and transverse holes in proximity to an L-section (Diagram (ii) in Figure 4-10) are given. This section will be devoted to a description of the modelling, discretisation and analysis of the transverse hole in proximity to a fillet section followed by an illustration of the finite element solution for the transverse hole in proximity to an L-section.

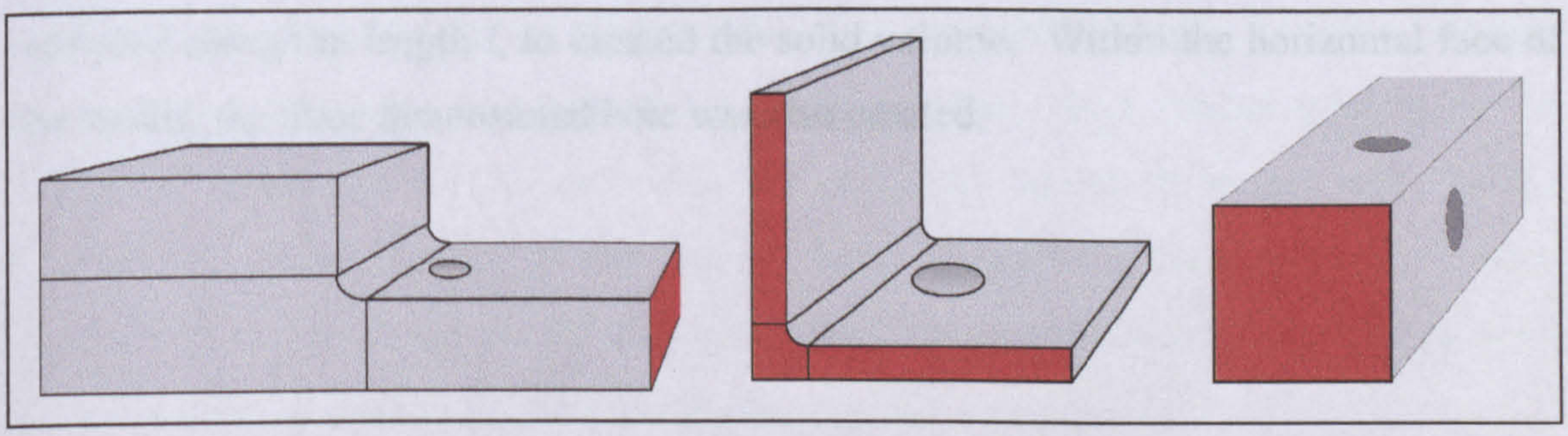

Figure 4-11. Illustration of the loading conditions of each of the three-dimensional geometries under investigation

4.4.1 Geometry Preparation

In order to identify the geometric parameters which produced a significant influence on the stress concentration factor in the configuration of a transverse hole in proximity to a fillet section, a number of preliminary analyses were conducted allowing variation in the fillet radius (r_f), upper height (D), lower height (d), section length (l), plate width (w), hole radius (r_h) and hole positioning (p). For the ease of data interpretation, all geometric parameters were normalised using the lower fillet height (d) which was kept constant throughout the analysis. Investigations were then conducted for configurations where the hole was introduced to the geometries, with variables r_f, r_h, p and D. For each given geometry of r_f, r_h and D, finite element solutions were developed for a series of incremental values of hole position (p) in the range p=-3d/2 to +3d/2.

For this illustrative example, the hole was positioned with p= 0.6d, r_f=0.1d *and* r_h=0.2d. In this case the length (l) and width (w) of the model were carefully adjusted in order that the section could be considered as semi-infinite.

4.4.2 Construction of the Model

In commercial codes such as ANSYS, the generation of a three-dimensional finite element solid model can be achieved through two basic techniques. Either models can be created from the 'top down' using fully-defined geometric primitives (which can be defined within the finite element system or transferred from an external system such as a CAD package) or they can be generated from the 'bottom up' by the user, starting with definition of the keypoints, then the lines, areas and finally volumes. For the cases considered here, bottom up construction was used, starting with the creation of the nine key-points illustrated in Figure 4-12.

From these defined key-points, three areas were constructed, each of which was extruded along the length l, to created the solid volume. Within the horizontal face of the model, the three dimensional hole was also created.

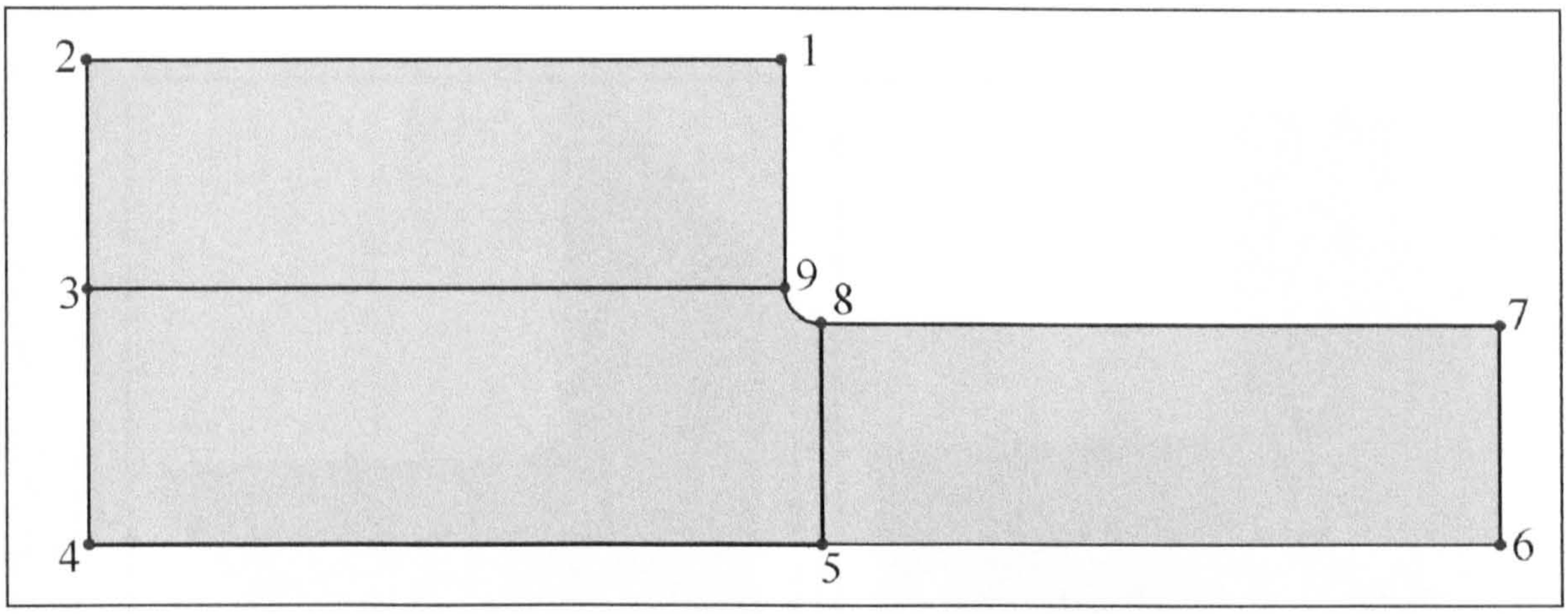

Figure 4-12. 'Bottom up' construction of the solid model

4.4.3 Discretisation and Convergence of the Model

The model was divided into a number of sub-volumes for ease of further discretisation, including a semi-cylindrical volume created around the hole to facilitate the generation of fine meshing systems in this area. For the discretisation of this solid model, two different elements were selected; *Solid 95* and *Solid 92*. *Solid 95* is a hexahedral element containing 20 nodes and is the higher order version of *Solid 45*. This element was selected for its suitability for creating mapped meshed in areas with curved boundaries, such as the volume surrounding the hole. *Solid 92* is a 10 noded tetrahedral structural element which adapts well to the free meshing of irregular shapes and is also compatible for model creation with *Solid 95*.

The cuboidal volume defined in cross-section by the keypoints 1, 2, 3 and 9 (Figure 4-12) and the sub-volume surrounding the hole were both mapped-meshed using *Solid 95* elements. The remaining regions were free meshed using *Solid 92* elements.

A number of convergence runs were conducted over a range of element sizes. Due to the large number of elements contained within such a three-dimensional geometry, a compromise had to be reached between the solution accuracy and the maximum number of elements which the commercial code will support. In a similar method to that described in Section 4.3.2.4, determination of the optimal mesh density was reached, through conducting a series of convergence runs. Variation in the number of elements in each subsection of the model also allowed for the identification of the critical areas where the mesh density could be increased.

Provided in Figure 4-13 is an illustration of the final mesh volume alongside the nodal solution for the stress for the example of a transverse hole in proximity to an L-section.

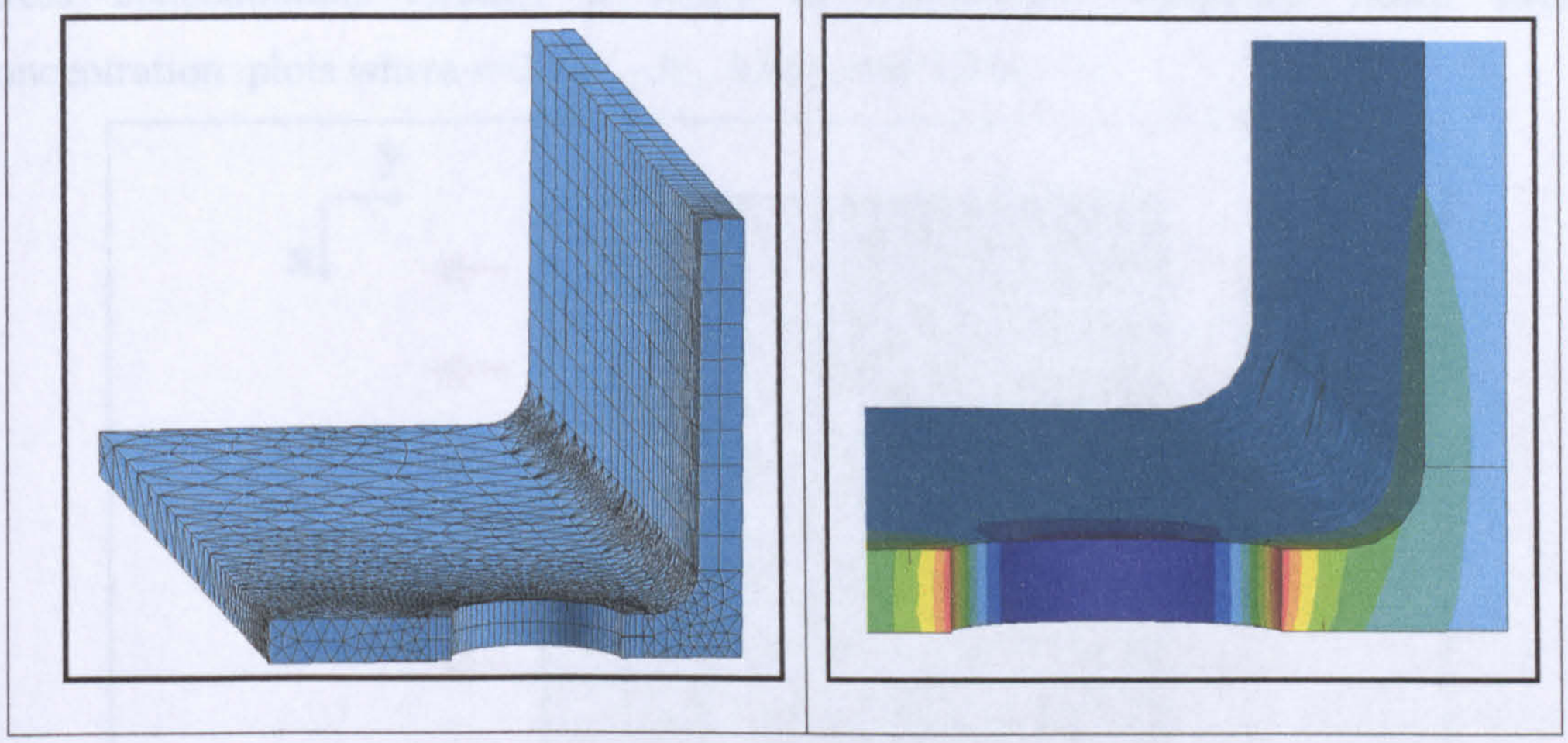

Figure 4-13. Discretised model and finite element solution for stress distribution at hole in proximity to radius section

4.5 CASE STUDIES

In addition to the determination of the magnitude of the maximum stress concentration, each geometry and configuration of multiple features was also analysed to determine the location and the direction of the maximum stress concentration and a plot of the ligament stress concentration distribution produced between the interacting features, where appropriate. Two case studies have been selected to illustrate the data generated for each of these categories.

4.5.1 Location of the Maximum Stress Concentration

For many of the geometries investigated, the maximum stress concentration values produced at each of the features under analysis were of a comparable magnitude to one another. In a number of these cases, small geometric modifications would result in a transfer in the location of the overall maximum stress concentration from one point to another. One example of this movement in the point of maximum stress occurs under the geometry of a central hole surrounded by eight radial holes, as illustrated in Figure 4-14.

This geometry was discretised, loaded and converged in a similar fashion to that described in Section 4.3.2. In one particular case, where r_s/r_c=0.5, it was observed that, as the separation distance, s, was reduced, the point of maximum stress moved from Point *B* to Point *A*. Figure 4-15 illustrates this movement in the point of maximum

stress concentration through a series of normalised y-direction nodal stress concentration plots where s=2.75r_c, 2r_c, 1.85r_c and 1.75r_c.

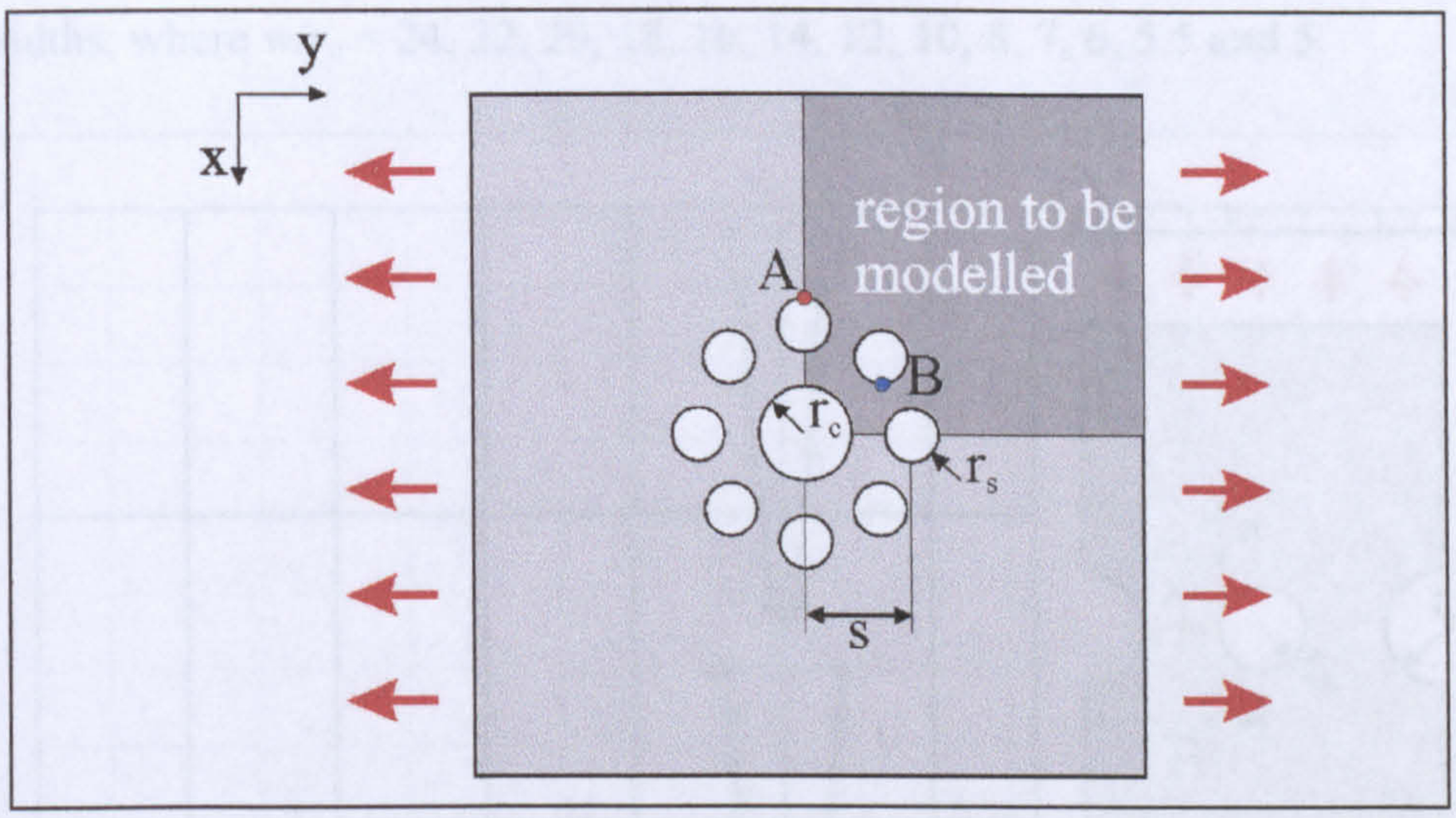

Figure 4-14. Eight radial holes surrounding a centrally-placed hole in an infinite plate under uni-axial tension

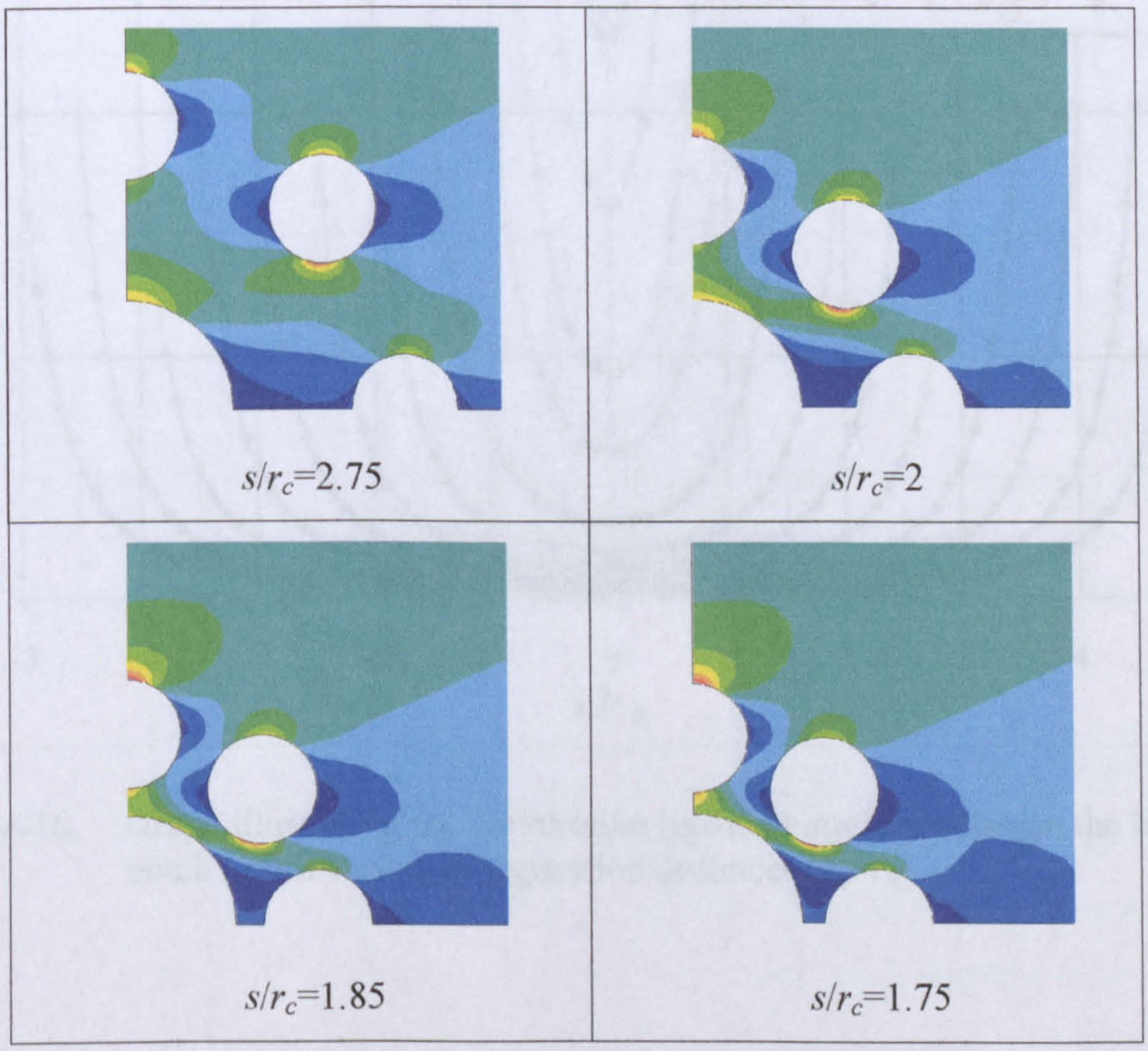

Figure 4-15. Finite element stress contours for eight satellite holes with decreasing distance (s) to the central hole, where r_s/r_c=0.5

4.5.2 Ligament Stress Plots

For the case discussed in Section 4.3.2.1, of a single circular hole between semi-circular double-edged notches, ligament plots were also created of the y-direction stress

concentrations between point *A* and point *B* (Figure 4-5). Shown in Figure 4-16 is a selection of sample results for this geometry in the case where r_h=r_n under a variety of plate widths, where w/r_n = 24, 22, 20, 18, 16, 14, 12, 10, 8, 7, 6, 5.5 and 5.

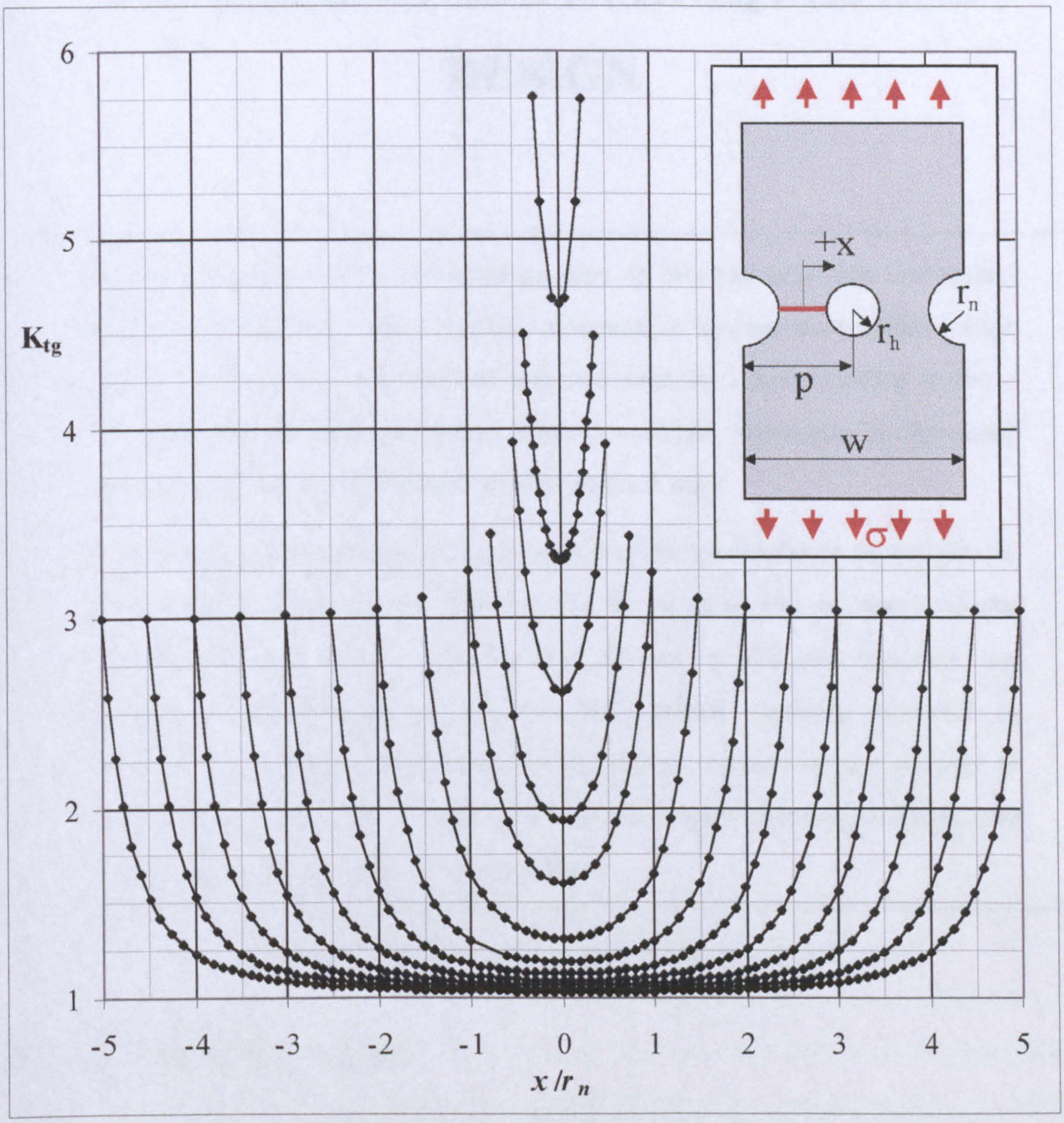

Figure 4-16. Graph illustrating the variation in ligament stresses between the hole and notch over a variety of separation distances (r_n=r_h)

CHAPTER 5

EXPERIMENTAL TECHNIQUES AND DESIGN

The experimental work conducted as part of this research has comprised extensive photoelastic investigation, alongside complimentary strain gauge analysis. This chapter is divided into two sections corresponding to these two experimental methodologies, dealing with the technique background, experimental details and sample results in each case.

As part of the development and evaluation of the photoelastic investigation, a programme of work was carried out to validate the accuracy of the experimental procedure. During the course of this investigation, an interesting phenomenon was discovered, which initially resulted in unacceptable errors in the results produced. A section of this chapter is therefore devoted to the identification of the origin of these problems and the techniques adopted to overcome them.

5.1 INTRODUCTION

There are a number of different techniques used in the analysis of stress distributions in engineering components, including finite element analysis, mathematical treatments, photoelastic analysis and strain gauge investigations. Each of these approaches offers its own advantages and limitations. This research called for a detailed examination of the stress levels produced around two geometric features placed in proximity through experimental investigation of various geometries of feature combinations. For this analysis, the main body of the experimental work has been focused on the photoelastic investigations. Due to the limitations of the experimental equipment available, the photoelastic studies were confined to two-dimensional problems of feature interaction. Strain gauge techniques were used for the investigation of three-dimensional problems,

along with additional validation of the two-dimensional cases. This chapter is divided into two sections, the first dealing with the photoelastic experimentation (Section 5.2) and the second looking at the strain gauge investigations (Section 5.3). In each section, appropriate case study examples are used to illustrate the use of each analysis technique in this application.

5.2 PHOTOELASTIC EXPERIMENTATION

5.2.1 Introduction

The origins of photoelasticity were formed in 1815 (Brewster 1815), with the discovery that coloured stress patterns were produced when polarised light was passed through sections of loaded glass. However, it was not until almost a century later that the potential engineering applications of photoelasticity were appreciated. Shortly after this time, significant advances (Coker 1920) were made, both with improved techniques and equipment, and also through the replacement of glass with materials such as celluloid. Progress made during the 1920's and 1930's (Oppel 1937; Filon and Harris 1923) allowed stresses to be 'frozen' into the material. This technique was of particular benefit when investigating three-dimensional components, as, after loading, the models could subsequently be cut into sections for individual analysis. During the 1980's, with the increased speed and availability of computers, the use of photoelasticity was largely replaced by finite element systems (Zienkiewicz 1989). However, in recent years there has been a resurgence in the use of photoelastic techniques in stress analysis applications, in particular for the analysis of large aircraft structures during the early design stages (O'Brien 1995). Comparisons between such large scale photoelastic models and the behaviour of real-life structures have shown good correlations (Albich 1994). There is, however, a current dearth in the working knowledge of the precise procedures and techniques for rigorous and accurate photoelastic analysis. A large portion of this research was therefore devoted to the understanding and refinement of the photoelastic procedures required for the work, as reflected in this chapter.

Section 5.2.2 provides a general overview of the photoelastic technique through introducing the theoretical background behind photoelasticity. For the reader not familiar with the photoelastic technique and associated equipment, a detailed description of this analysis tool is provided in a standard reference text (Hendry 1966).

During the photoelastic investigations conducted in this research, strict experimental procedures were adhered to (Hendry 1966; Heywood 1952; Frocht 1941) in order to optimise the accuracy of the results produced. The provisional specification of the equipment and experimental arrangements used in the initial investigations is given in *Section 5.2.3*. A series of experiments was conducted to validate the accuracy of the procedures adopted, which is presented in *Section 5.2.4*. Through an evaluation of the accuracy of the resulting data, these studies revealed fundamental problems with the procedures adopted, and additional investigations were recommended for detailed refinements of these techniques. In *Section 5.2.5*, the problems detected with the currently accepted procedures are discussed and details are provided of a number of alterations which vastly improved the accuracy of the results produced by this technique. *Section 5.2.6* provides an overview of the final experimental methodology adopted. Finally, a number of case studies of sample results are presented in *Section 5.2.7*.

5.2.2 The Photoelastic Technique

5.2.2.1 Fundamentals of Photoelasticity

Photoelasticity is widely accepted as a technique which can produce experimental results to a high degree of accuracy (±2%). However, in order to achieve and correctly interpret such results, a understanding of the theory, equipment and procedures is required.

The basic property on which photoelasticity is based is that when polarised light passes through a suitable transparent material (such as epoxy resin), it is split up into two beams of light, such that:

(i) the emerging beams are polarised in the direction of the principal stresses in the material (note: these two beams are therefore perpendicular to one another), and

(ii) each beam travels through the material with a velocity proportional to the magnitude of either principal stress, and therefore produces a phase difference between the emergent beams corresponding to the difference in principal stresses. The difference in stresses at each point in the material can then be calculated through analysis of the interference patterns formed by these two beams. The form of these interference patterns is shown in Figure 5-1.

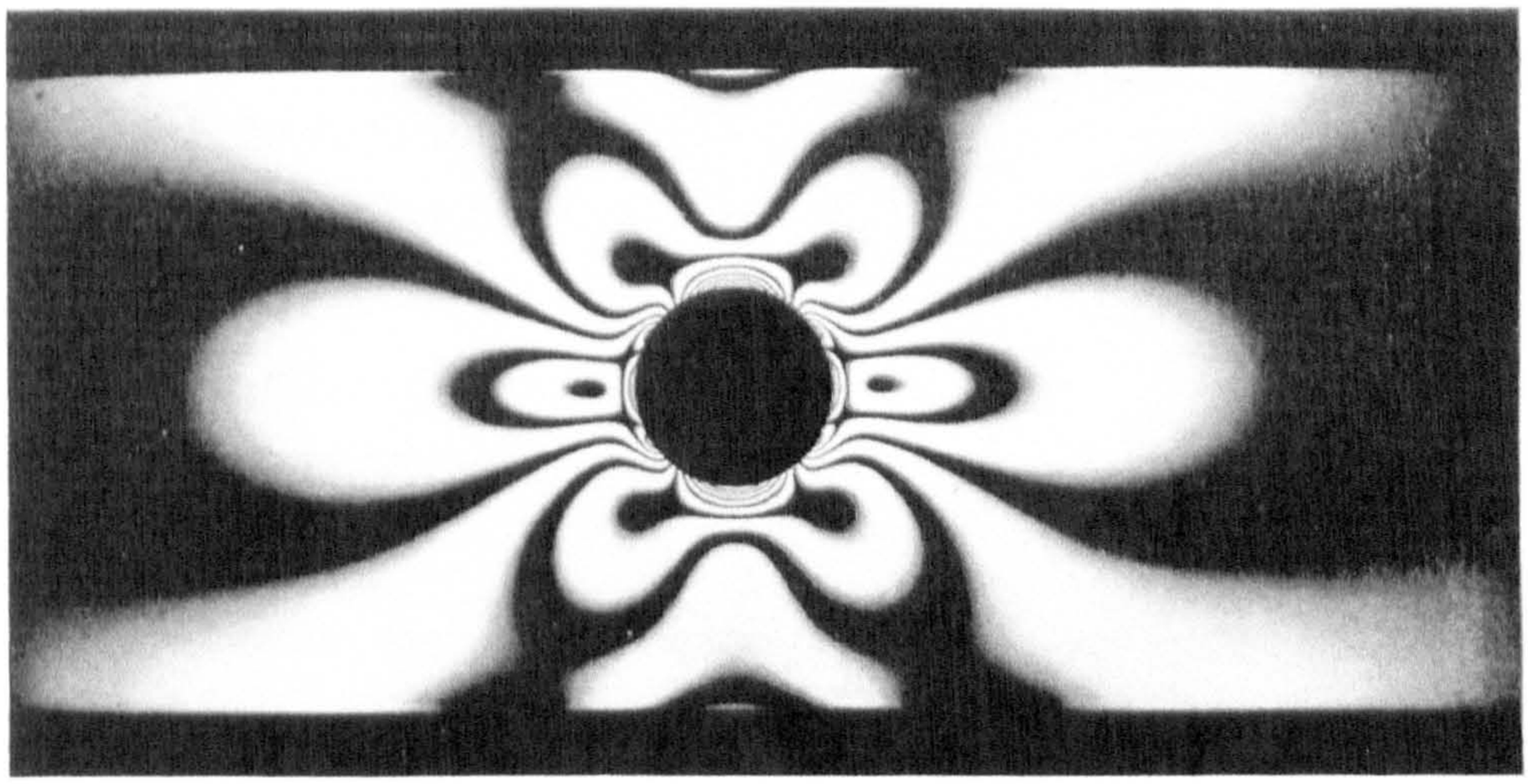

Figure 5-1. Photograph (Frocht 1941) of the photoelastic interference patterns formed on a model containing a single circular hole under tension

5.2.3 Initial Exploration

Based on standard specifications (Hendry 1966; Heywood 1952; Frocht 1941) and the procedures of foregoing photoelastic studies involving stress-raisers (North 1965; Frank and Faucett 1961; Wahl and Beeuwkes 1934), a provisional experimental programme was proposed for the statically-loaded models. This section provides an outline of this programme, which includes specification of the equipment, material and experimental procedure.

5.2.3.1 Material

The material used for all of the models tested was Araldite CT200/HT907. Epoxy resins are the most widely-used of all photoelastic materials, and, within this category, Araldite CT200/HT907 is considered to offer the optimal material properties. A rudimentary measure by which the properties of photoelastic materials are often assessed and compared is the *figure of merit*. This measurement is a simple ratio of the elastic modulus (E) to the unit fringe value (f). Materials such as CT200, which possess a high figure of merit, are particularly suitable for photoelastic applications as they exhibit a low material deflection under load and also have a high optical sensitivity. This material also has good machining properties, with little chipping, a relatively low tendency to creep under load and is able to be used for both static and stress-frozen analysis.

The properties of this material (Sharples 1981) at room temperature are listed below:

<u>**Material**: Epoxy resin, Araldite CT 200</u>

Tensile strength: 70-90 MN/m^2

Young's modulus: 2700-3400 MN/m^2

Poisson's ratio: 0.34

Material fringe value: 14.7-15.8 KN/m.fr

Unit fringe value: 0.38 MN/m^2

Figure of merit (E/f): 7130

For the experimentation, the material came in the form of cast sheets, 6mm in thickness.

5.2.3.2 Manufacture of Model

It is widely recommended (Measurement Group 1982; Sharples 1981) that any machining of photoelastic materials should be operated at very high speeds and low feeds, using pre-sharpened or new cutting tools. This not only decreases the risk of the material chipping, but it also limits the introduction of any edge stresses, which may distort the final photoelastic image. If low levels of edge stress are present in a material, they can often be removed through annealing or their influence reduced through taking a series of readings perpendicular to the machining surface and extrapolating these values to the model edge.

5.2.3.3 Equipment

The equipment used throughout the experimental work was a Sharples 250mm Diameter Field (circular) Polariscope. This polariscope contained a loading space of 500x600mm and can be used to analyse stress frozen models both in two and three dimensions. The quarter wave plates were calibrated to allow fraction fringe readings to be taken within an accuracy of 0.5% of a fringe.

Precise readings of the fringe values were taken using a travelling microscope, as illustrated in Figure 5-2. This device was fitted with a 10× magnifying microscope lens, providing a clear image of each fringe under investigation. As shown in Figure 5-2, this equipment was also fitted with a dial gauge in order to measure accurately the incremental spacings between each reading.

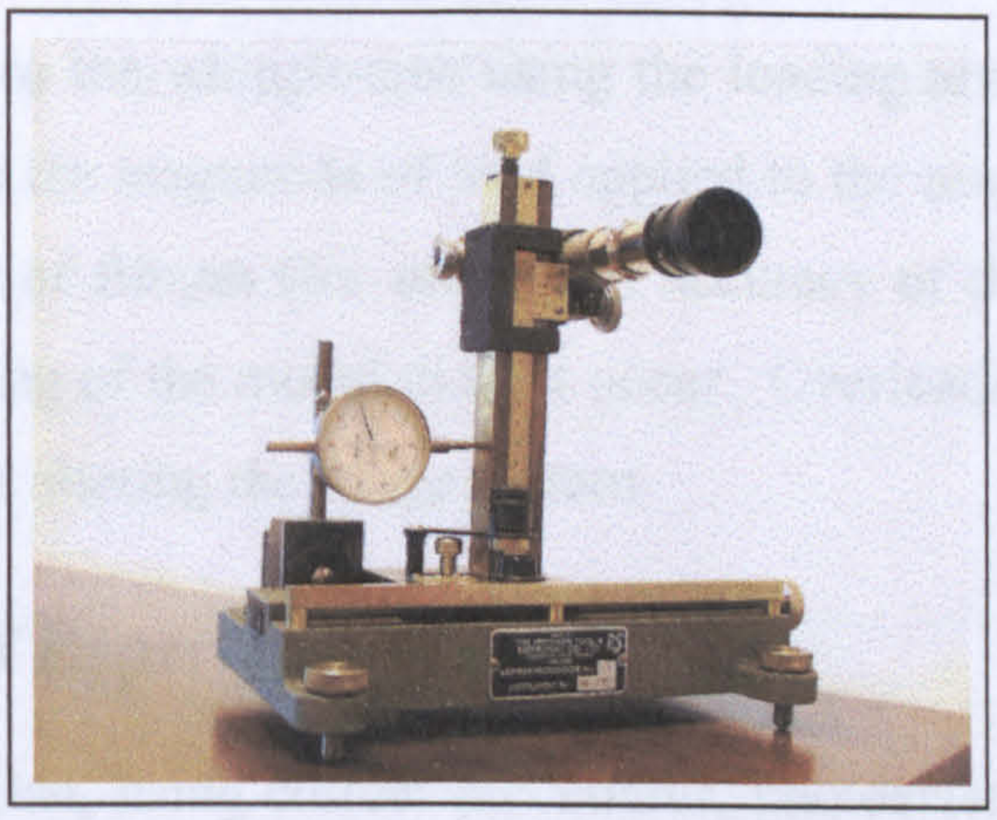

Figure 5-2. Photograph of the traveling microscope used to take accurate readings of the position and magnitude of the fringe values

5.2.3.4 Loading Arrangements

Weights were applied to each of the models though a traditional loading mechanism called a 'whipple-tree'. This device allows a point load to be distributed through the cross-section of a model using a progressive series of linkages, as illustrated in Figure 5-3. One such device was attached on either end the model to produce uniform applied tension to the specimen.

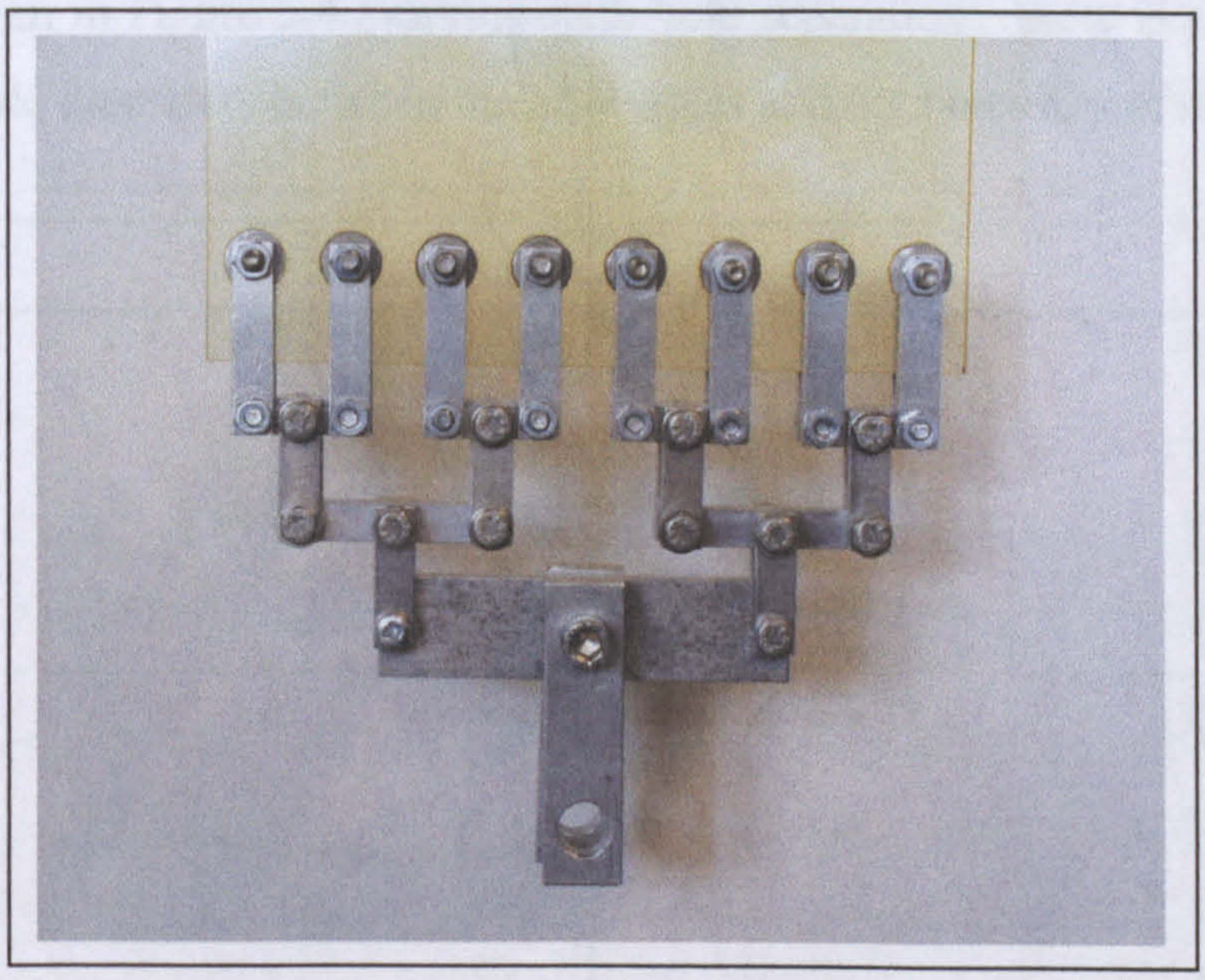

Figure 5-3. Photograph of 'whipple-tree' attached to the model for even distribution of the applied load

The whipple-tree was produced from 3mm thickness aluminium sheets, with each section bolted together using 5mm bolts. The device was attached to the model using 12mm steel ferrules, which fit into a series of holes drilled into either end of the specimen.

The load was applied to the whipple-tree using the loading arm. An optimal balance needed to be found for the magnitude of load applied to the model between generating the maximum number of fringes (for maximum accuracy of the readings) while still ensuring that overloading of the model did not occur. Overloading can cause distortion of the model, as well as altering the fringe pattern

5.2.4 Validation of Experimental Accuracy

It is widely accepted that, using correct procedures, photoelastic experimentation can yield results within a ±2% accuracy. To achieve the desired confidence in the results obtained from the photoelastic tests in this research, the accuracy was validated for the particular experimental arrangements to be used. This validation was undertaken by analysing the case of two equal holes in an infinite plate under tension, to allow a comparison to be made between an appropriate analytical treatment (Haddon 1967) and the photoelastic results generated here.

A series of models was produced from Araldite CT200/HT907, with two equal holes of various separation distances, as illustrated in Figure 5-4. For each of the four geometries given in Figure 5-4 (varying with hole separation), there is a distance of at least of five hole diameters between the hole edges and the boundary of the plate. It has

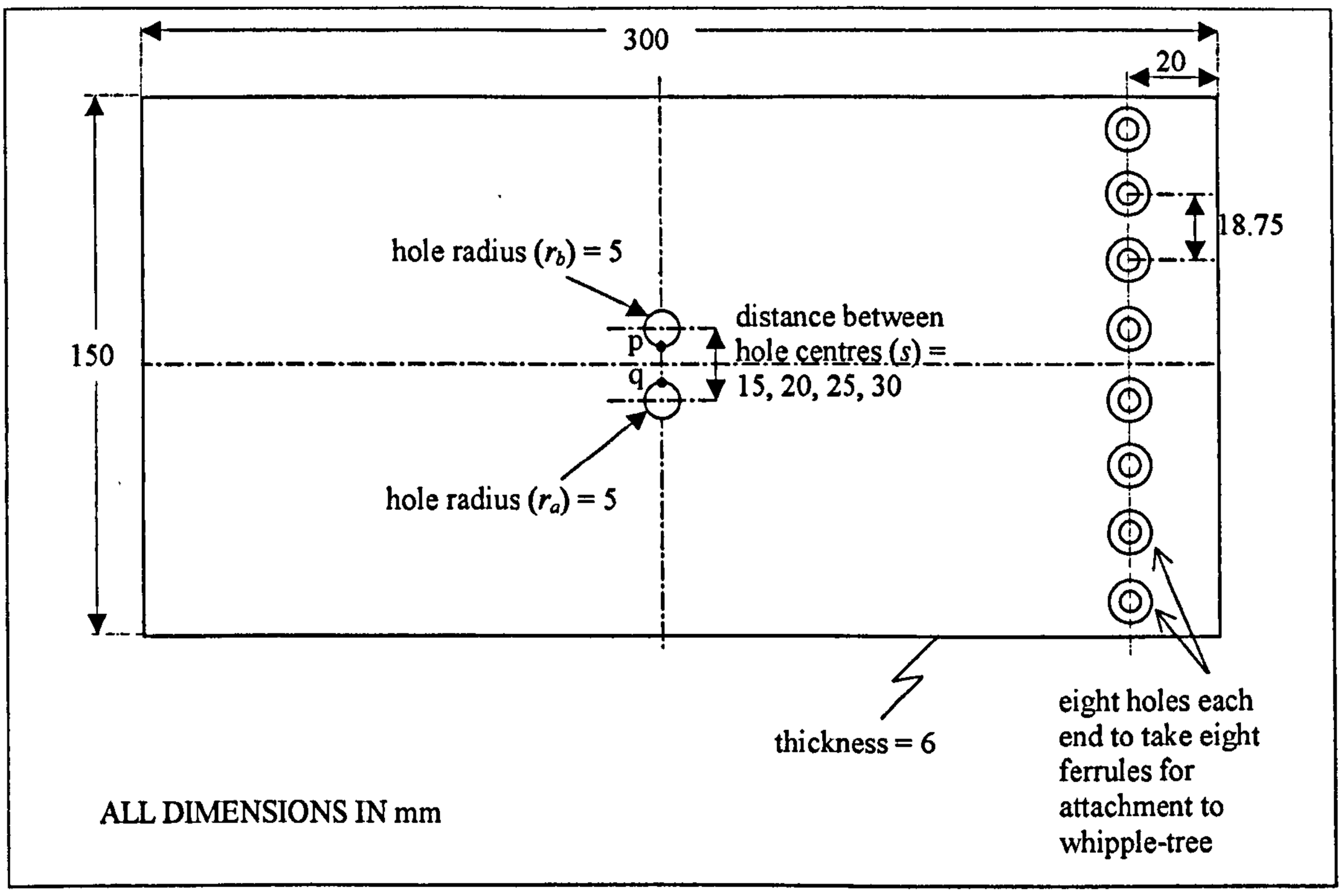

Figure 5-4. Illustration of the photoelastic model design for the analysis of two equal holes in an infinite plate under tension

been established in foregoing studies (Stranart 2000) that such separation distances are sufficient to ensure that the plate boundaries influence no stress-raising effect on the interaction problem under observation.

The models were 6mm in thickness, and contained two holes (r_a and r_b) of radius 5mm at four different separation distances (s=15, 20, 25 and 30mm). Each model was loaded statically in a perpendicular direction to the line of the holes, with a total applied weight of 6Kg. A photograph of the model within this loading arrangement is given in Figure 5-5.

All well accepted and documented procedures (Hendry 1966; Heywood 1952; Frocht 1941) were adhered to, both in the preparation of the model and in the determination of the results. For each model, readings were taken every 0.5mm through the ligament p-q

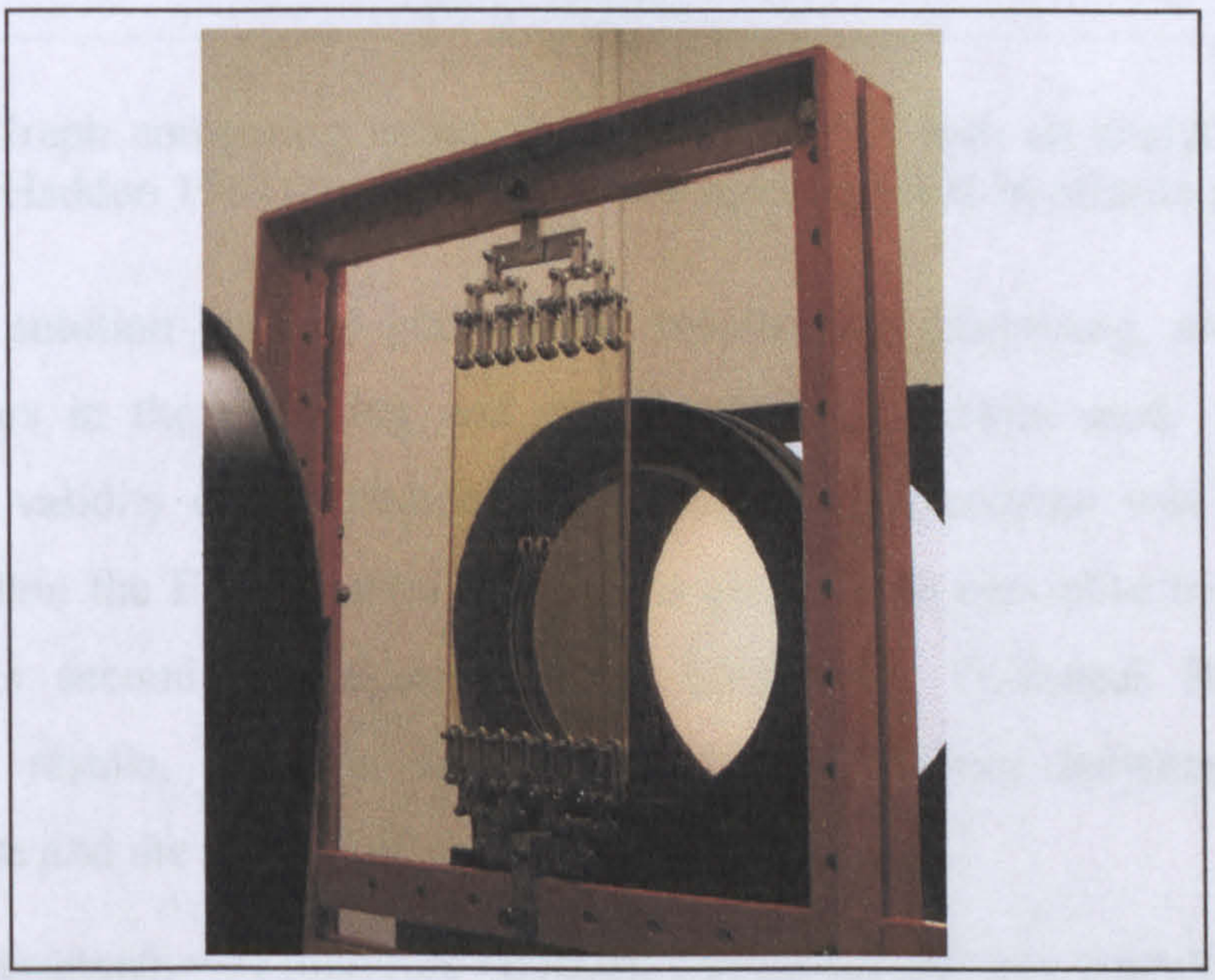

Figure 5-5. Photograph illustrating the photoelastic loading arrangement

between the hole centres (see Figure 5-4), and every 0.25mm close to each of the features, with the final readings taken 0.25mm from the hole edges. These data points were then used to form a polynomial which was extrapolated to the hole edges to determine the value of the stress levels at these critical positions (points p and q).

The resulting maximum stress concentration data for each test of the four geometries are given in Figure 5-6 alongside the results from an equivalent analytical solution for this geometry (Haddon 1967). This graph illustrates a significant discrepancy between the theoretical results and those determined photoelastically, with the experimental results falling 10-20% lower than those predicted values. These levels of deviation between

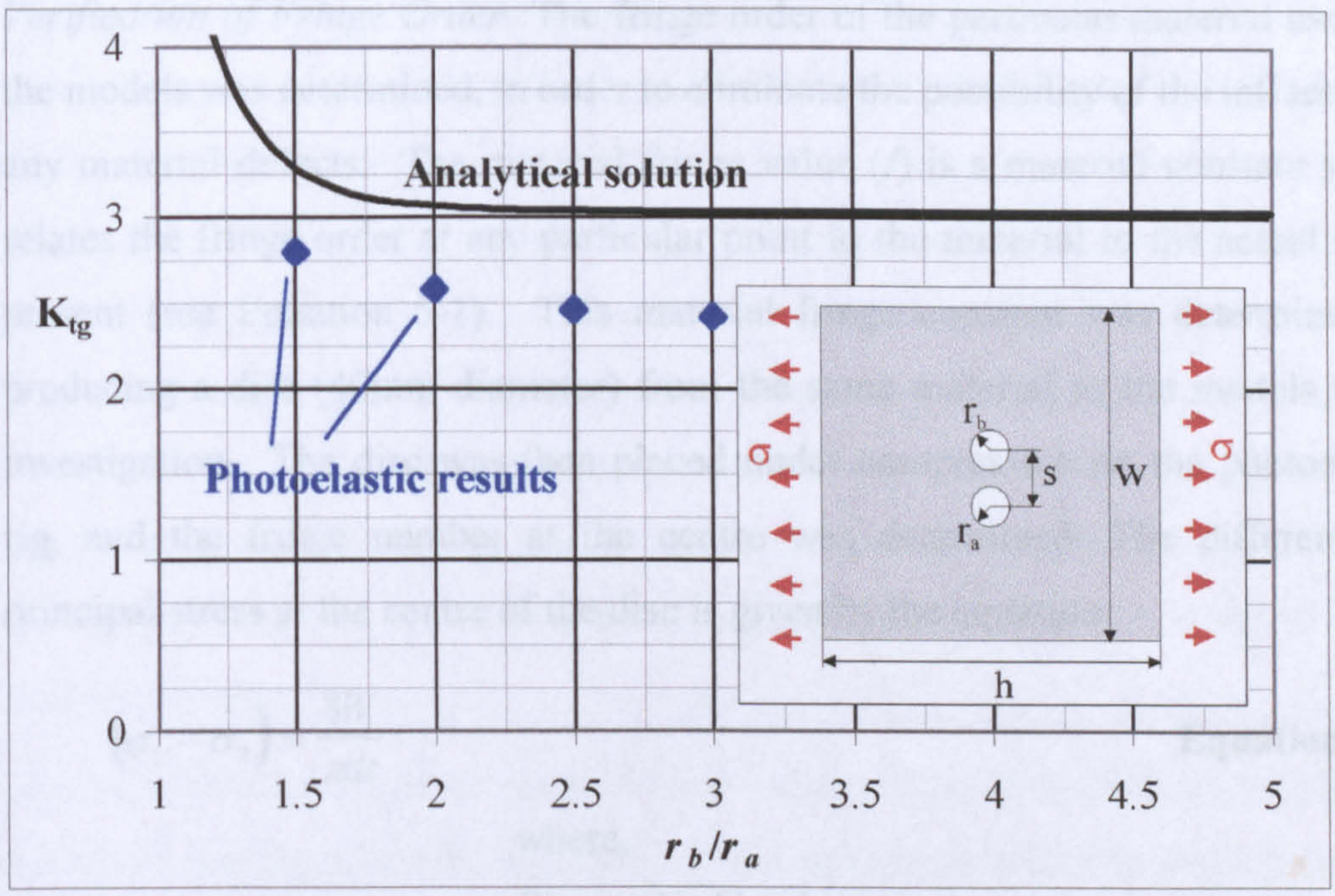

Figure 5-6. Graph comparing initial photoelastic results with an analytical solution (Haddon 1967) for the case of two equal holes in an infinite plate

the theoretical solution and the photoelastic results were surprising, and suggested significant errors in the modeling and experimental procedures used. In order to investigate the validity of the photoelastic results, the experiment was repeated by Airbus UK, within the Experimental Mechanics group, who specialise in photoelastic analysis. This second investigation (BAE SYSTEMS Technical Report 2000) confirmed the results, with an equally significant disparity between the lower photoelastic data and the theoretical solution.

A series of experiments was therefore conducted to investigate any potential sources of error within the system. A brief outline of these investigations is given below:

(i) *Analysis of Stress Frozen Model* Each of the models was stress frozen, to determine whether the use of this alternative technique would affect the levels of stress displayed around the holes. Each model was sent to Sharples Stress Engineering* for the stress freezing process, and was subsequently tested on its return. However, on analysis of each of these models, it was found that the stress levels recorded were almost identical to those found under the static loading conditions.

---

* Sharples Stress Engineers, Bamber Bridge, Preston, Lancashire, UK

(ii) *Verification of Fringe Order* The fringe order of the particular material used for the models was determined, in order to eliminate the possibility of the influence of any material defects. The material fringe value (f) is a material constant which relates the fringe order at any particular point in the material to the actual stress present (see Equation 5-1). This material fringe constant was determined by producing a disc (40mm diameter) from the same material as the models under investigation. The disc was then placed under compression on the photoelastic rig, and the fringe number at the centre was determined. The difference in principal stress at the centre of the disc is given by the equation:

$$(\sigma_1 - \sigma_2) = \frac{8W}{\pi d t} \qquad \textbf{Equation 5-1}$$

where,

W = applied load

d = disc diameter

t = material thickness

The fundamental photoelastic equation is given as:

$$(\sigma_1 - \sigma_2) = \frac{nf}{t} \qquad \textbf{Equation 5-2}$$

Therefore, the material fringe value can be defined:

$$f = \frac{8W}{\pi d n} \qquad \textbf{Equation 5-3}$$

Therefore, using the experimentally determined fringe number (n) and the given applied load and disc diameter, the material fringe value can be found to a high degree of accuracy. In this experiment, for optimum accuracy, the discs were stress frozen under compression. On investigation of a number of such discs, a material fringe value of 0.26 KN/m.fr was determined. This fell within the recommended range (Sharples 1981) of 0.24-0.28KN/m.fr for the particular material used, Araldite CT200/HT901.

(iii) *Investigation into the Adverse Effects of Overloading* It was postulated that one potential source of error could be caused by local distortion in the model, produced from overloading of the specimen. An investigation was therefore conducted to study the effect of variation of load on the stress frozen model. Four tests were carried out for applied weights on the scale pan of 3Kg, 1.5Kg, 0.75Kg and 0.375Kg for the same model geometry, where r_a=r_b=5mm and s=20mm (see

Figure 5-4). Each of the models was then stress frozen, and the analysis of each was conducted in situ, immediately after the model had cooled from the oven. The analysis of each of the stress frozen models produced surprising values for the stress concentration, providing results that were very close to the theoretical model (±4%). In terms of the four different loading conditions, there was very little discrepancy between these results, although the model under the 0.375Kg load showed the highest deviation from the theory. From this investigation into the effect of applied load, it would be recommended that the highest load (3Kg) should be used for frozen stress analysis, as it allows for the greatest ease of fringe order determination.

The outcome of the final of these investigations indicated that the accuracy in the results recorded could be significantly improved if the specimen under examination were analysed very soon after being removed from the oven. Comparisons between the stress patterns of the original models tested and the patterns of the stress frozen model on removal from the oven indicated that the original models contained bands of high compressive stress around the specimen edge and the machined surfaces. These compressive stresses were identified as *time-edge effects* caused by the absorption of moisture in the cut edges of the models over time.

5.2.5 Refinement of Experimental Procedures

The underlying problem with the original results was found to be the existence of time-edge effects. This effect gave rise to a high compressive stress around the hole edges, which distorted the tensile stress in these regions, thus displaying much lower levels of stress than was actually present. These effects develop over time when the material has been exposed to atmospheric conditions and temperatures, and occur at edges and machining surfaces, which are often the critical regions for analysis. The literature (Leven 1963) suggests that the models would need to have been exposed to atmospheric conditions for over a week to accumulate the levels of time-edge influence sufficient to affect the stress readings to the extent illustrated in Figure 5-6. However, the models used in these experiments had only been exposed to room temperature conditions for a matter of hours. Common practice (Strannigan 1964) for removal of these time-edge influences recommends storage in an oven at a stable temperature of 70°C. However, these procedures were not found to eliminate these effects fully, and storage of the models at 80°C for 24 hours reduced the time-edge influence to a much lower level.

These findings reveal some significant flaws in the current suggested procedures for measuring stress levels using photoelasticity, which assume a 2% accuracy, when actual results may deviate by up to 20%.

Through storage of the models at 80°C, and execution of the full photoelastic analysis within two hours of cooling from the oven, the resulting stress concentration values were found to be within 4% of the benchmark values predicted by Haddon (Haddon 1967). Although this level of error is relatively low, a more accurate analysis tool was required to obtain a detailed understanding of the variation in stress levels around the features. Further investigations were conducted to highlight auxiliary refinements to improve the experimental procedures and also to identify any additional factors that would exacerbate the build-up of time-edge effects. A number of these factors had a small influence on the accuracy of the system and are listed below:

(i) Applying the load onto the model using a slow-loading arm, rather than placing large weights directly onto the whipple-tree. This avoids the *shock loading* of the specimen, which can introduce additional stresses.

(ii) Allowing the model to *settle* under the load for approximately 45 minutes before taking readings, to avoid optical creep. Optical creep is the mechanism by which photoelastic materials exhibit an increase in strain over time when subjected to an applied load. After the load has been applied for a certain period of time, this deformation increases to a limiting value. It is important that any precise measurements should be taken after this limiting strain has been reached, after which point no further increases in the displayed stress levels will be observed. A series of incremental readings was taken of the fringe values of a model from the point where load was applied over a duration of sixty minutes. The results of this investigation are given in Figure 5-7, indicating that the results do not 'settle' to a constant, accurate value of stress until 45 minutes after application of the load. As can be seen from Figure 5-7, an analysis of a specimen earlier than this time could produce results with an error of up to 2.5%.

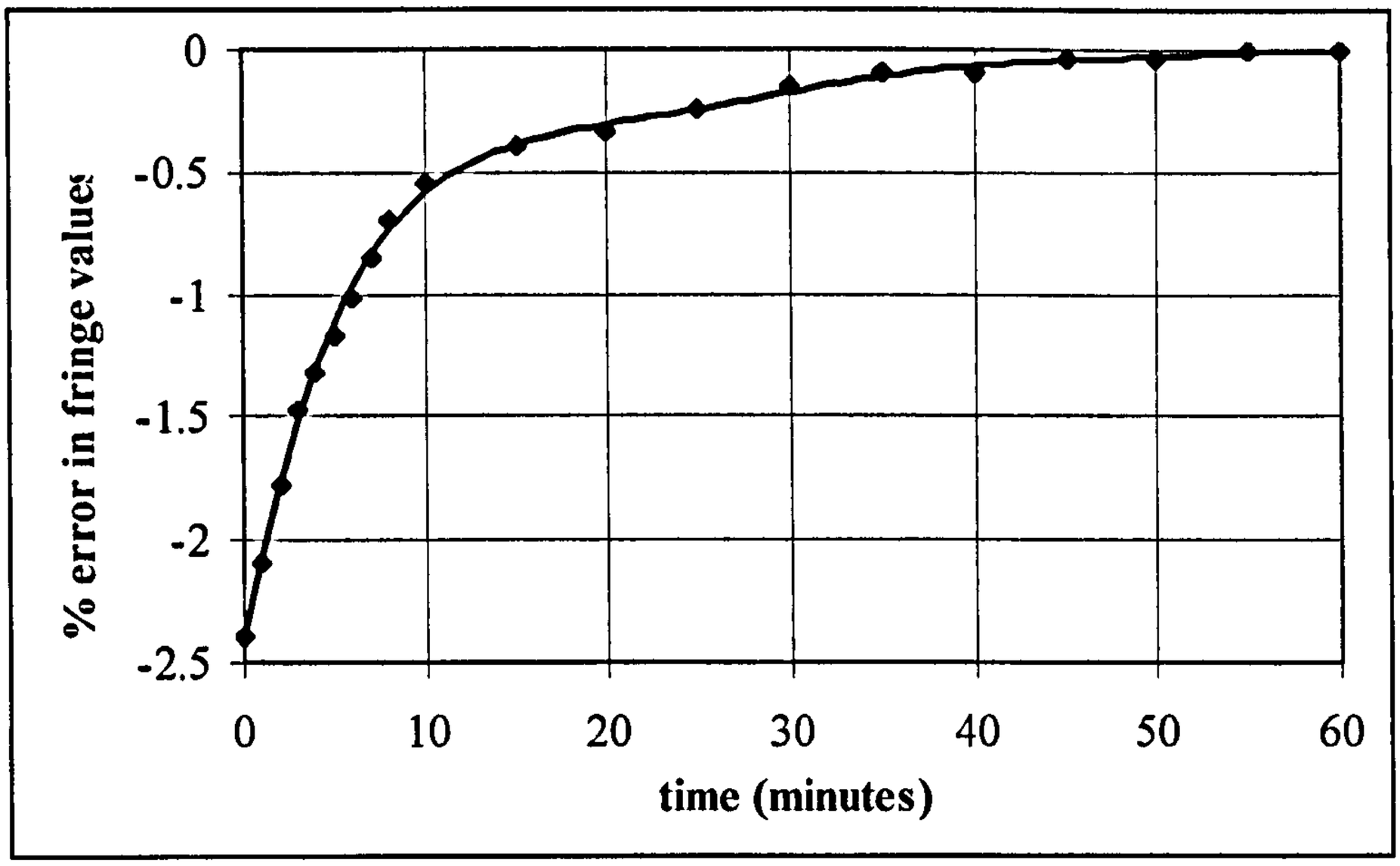

Figure 5-7. Optical Creep: A graph illustrating the variation in fringe reading over time after application of the load

(iii) It was found that the production of the specimen models on an NC machine rather than conventional hand-operated machines not only improved the accuracy of the geometry of the models but also dramatically reduced the machining stresses. The influence of machining stresses is very similar to that of time-edge effects, and the removal of these stresses improved the accuracy of the results taken, particularly around the holes. After NC machining, the precision of the geometry of the models was validated using a shadow-graph which confirmed the accuracy as ±0.02mm.

(iv) The magnification of the lens in the traveling microscope was increased to 20×, to allow more accurate readings to be taken of the fringe values at each point.

(v) An investigation was conducted to ascertain the influence of model thickness on the build-up of time-edge effects. A series of photoelastic models was constructed, of a variety of thickness, and the time-edge levels recorded for each at regular intervals over a period of five days, during which time the models were exposed to atmospheric conditions. This study revealed a relationship between the plate thickness and the susceptibility to time-edge build up, with the thicker the plate, the greater the observed influence.

(vi) Finally, the width of each of the models was reduced by a factor of two (along with proportional decreases in the geometry of the features). A narrower model allows a higher number of fringes to develop in the specimen for a given load.

These higher number of fringes increase the accuracy of the readings taken as well as improving the ease of measurement.

After all of these adjustments in experimental procedure and model manufacture had been made, a variety of models was tested. These tests included the geometry of two equal holes in tension, but also looked at cases of single features whose results could also be compared to appropriate analytical treatments. An example of the results of these tests is presented in Figure 5-8 for the case of semi-circular double-edged notches under tension, for which three different geometries were assessed using photoelasticity. This simple geometry has been treated analytically (Isida 1953), and Figure 5-8 presents a comparison of this solution alongside the photoelastic results (where r_n is the notch radius and w is the plate width). For this particular geometry, all three of the photoelastic results fell within 0.6% of those predicted by theory. After analysing a range of different geometric features, it was found that the results from all of the tests produced photoelastic measurements of stress concentration values which were within

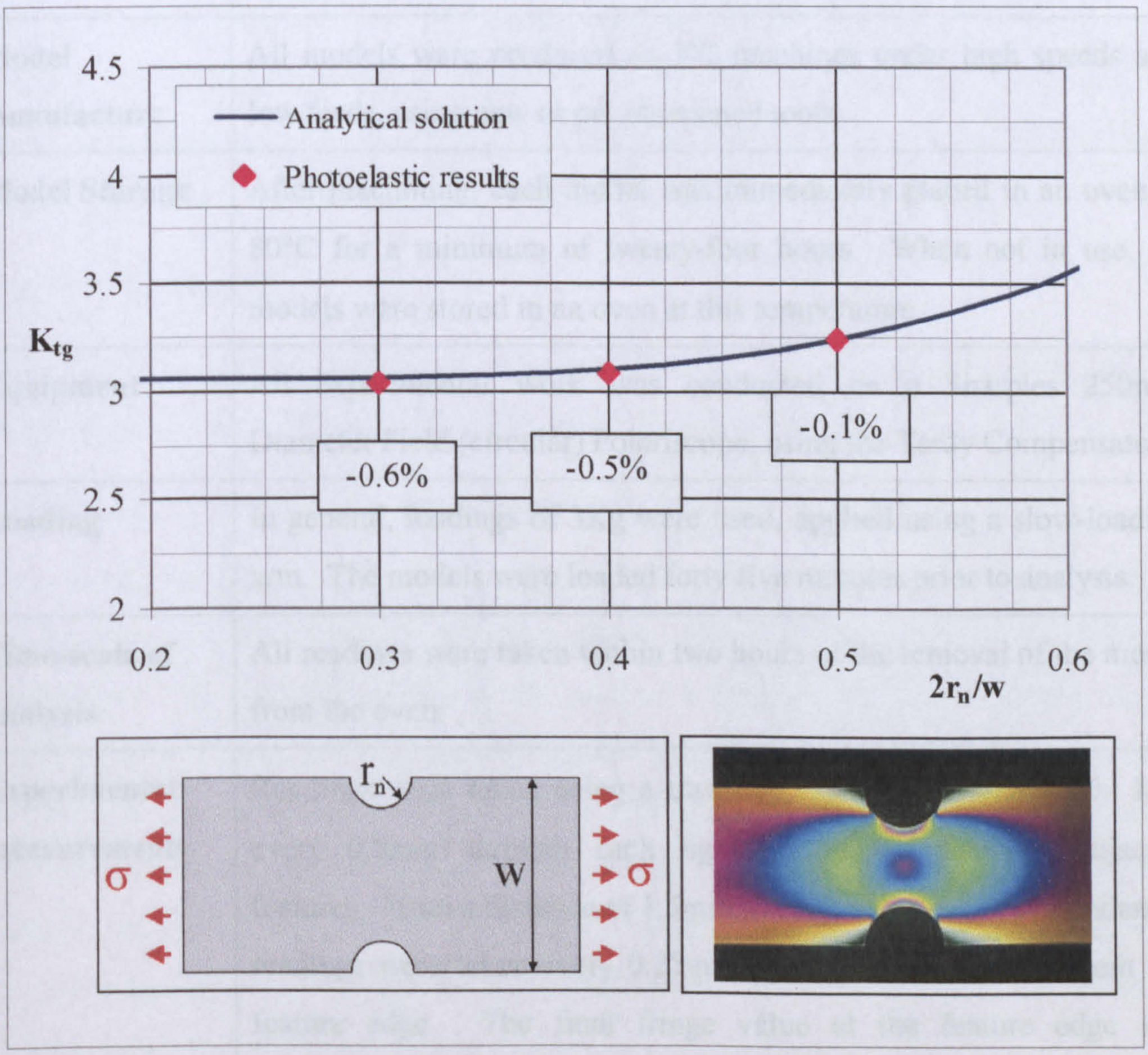

Figure 5-8. Comparison between a theoretical solution (Isida 1953) and the photoelastic results for the case of semi-circular double-edged notches

1% of those values predicted by appropriate analytical solutions.

Through the course of validating the experimental procedures used in this research, a number of interesting discoveries have been made as to the optimisation of the accuracy of the stress readings recorded. These discoveries have shown that adherence to currently accepted methods for photoelastic analysis can produce discrepancies of up to ±20% as compared to appropriate analytical treatments. In this chapter, new procedures have been proposed and validated which can reduce these errors to ±1% (as compared with analytical derivations), principally by the dramatic reduction of time-edge effects. The overall specification for these finalised procedures is summarised in the table in Figure 5-9.

Material selection	The epoxy resin Araldite CT200/HT907 was used throughout the experimentation. The material used was 3mm in thickness, and of width 150mm for models representing infinite plates, and 37.5 or 75mm in all other cases.
Model manufacture	All models were produced on NC machines under high speeds and low feeds, using new or pre-sharpened tools.
Model Storage	After machining, each model was immediately placed in an oven at 80°C for a minimum of twenty-four hours. When not in use, all models were stored in an oven at this temperature.
Equipment	All experimental work was conducted on a Sharples 250mm Diameter Field (circular) Polariscope, using the Tardy Compensator.
Loading	In general, loadings of 3Kg were used, applied using a slow-loading arm. The models were loaded forty five minutes prior to analysis.
Time-scale of analysis	All readings were taken within two hours of the removal of the model from the oven.
Experimental measurements	Readings were taken using a traveling microscope with a 20× lens every 0.5mm through each ligament section between adjacent features. From a distance of 1.5mm to each of the feature boundaries, readings were taken every 0.25mm up to a point 0.25mm from the feature edge. The final fringe value at the feature edge was determined through extrapolation of the preceding data points.

Figure 5-9. Final experimental procedures used for the photoelastic investigations

5.2.6 Model Specification

A total of five feature interaction geometries were investigated using photoelastic techniques: (i) a central hole between double-edged notches, (ii) a central hole between shoulder fillets, (iii) two holes in an infinite plate, (iv) a central hole surrounded by eight radial holes, and (v) a central hole surrounded by four radial holes. Specification drawings for each of these models are given in Appendix A. For each configuration under analysis, a number of basic photoelastic models were required, and, for each of these models, appropriate features were machined out after each subsequent analysis. For example, Figure A-2 in Appendix A illustrates the models required for the analysis containing a shoulder fillets of varying radii (r_f = 1.5, 4.5 and 9mm). An initial analysis was conducted for each of the three models containing no central hole for the purposes of validation with the theoretical derivations. On identification of the position of maximum stress at the fillet, a central hole of radius 2.5mm was then inserted at this cross-section, and a full photoelastic analysis conducted on the model. This central hole radius was then enlarged to 5, 7.5, 10 and 12.5mm, subsequent to each analysis. As with the numerical investigations, measurements were taken in each case of the position and magnitude of the point of maximum stress concentration, as well as a ligament plot of the stress concentration distribution between the features under investigation.

5.2.7 Case Studies

The case study examples provided in this section are parallel analyses to those discussed within the case studies of the previous chapter (Section 4.5).

5.2.7.1 Location of the Maximum Stress Concentration

For a number of the feature interaction configurations investigated, it was observed that the location of the point of maximum stress varied with changes in the feature dimensions. An example of this is the case of a central hole surrounded by eight satellite holes. Figure 5-10 illustrates the stress concentration recorded at the two points of maximum stress (shown in blue and red), and indicates how the point of maximum stress changes from one position to the other with variation in hole separation (s), for constant hole radii (r_c and r_s). Figure 5-11 provides photographs of the changing isochromatic pattern of the photoelastic models as the relative hole separation distance is decreased (r_s/r_c =0.5).

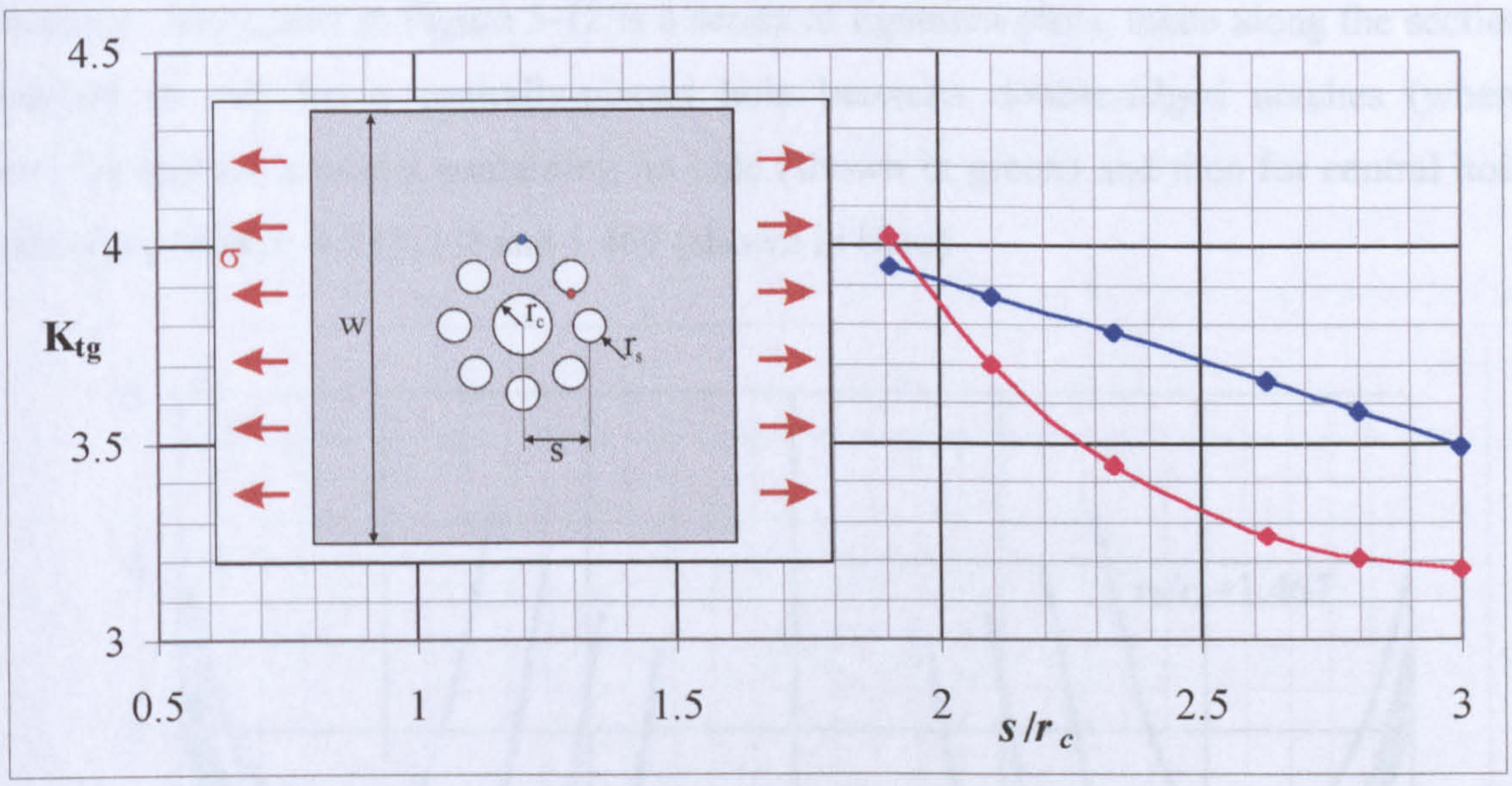

Figure 5-10. Photoelastic results for a central hole surrounded by eight satellite holes, with variation in the hole separation (where r_s/r_c =0.5)

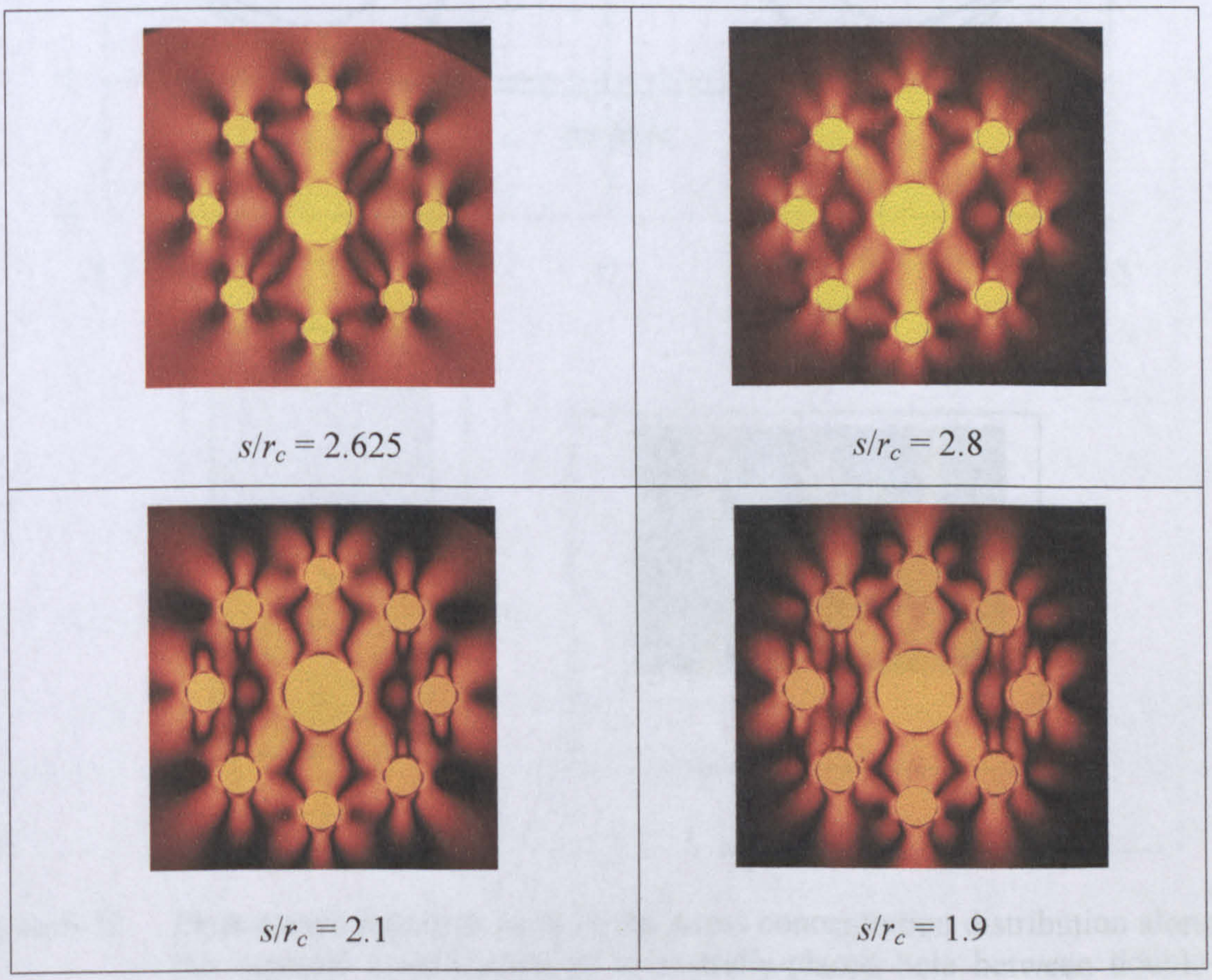

Figure 5-11. Photographs of the isochromatic stress pattern taken for a series of photoelastic models at varying values of s (where r_s/r_c =0.5)

5.2.7.2 Ligament Stress Plots

A total of sixty-six two-dimensional photoelastic models were analysed. In each case, ligament plots were taken of the distribution of stress concentration between each of the

features. Illustrated in Figure 5-12 is a series of ligament plots, taken along the section marked in red, for a centrally-placed hole between double-edged notches (where w/r_h=5) and for a model containing no hole (shown in green) and then for central hole radii r_h/r_n=0.667, 0.933, 1.2 and 1.467 (shown in blue).

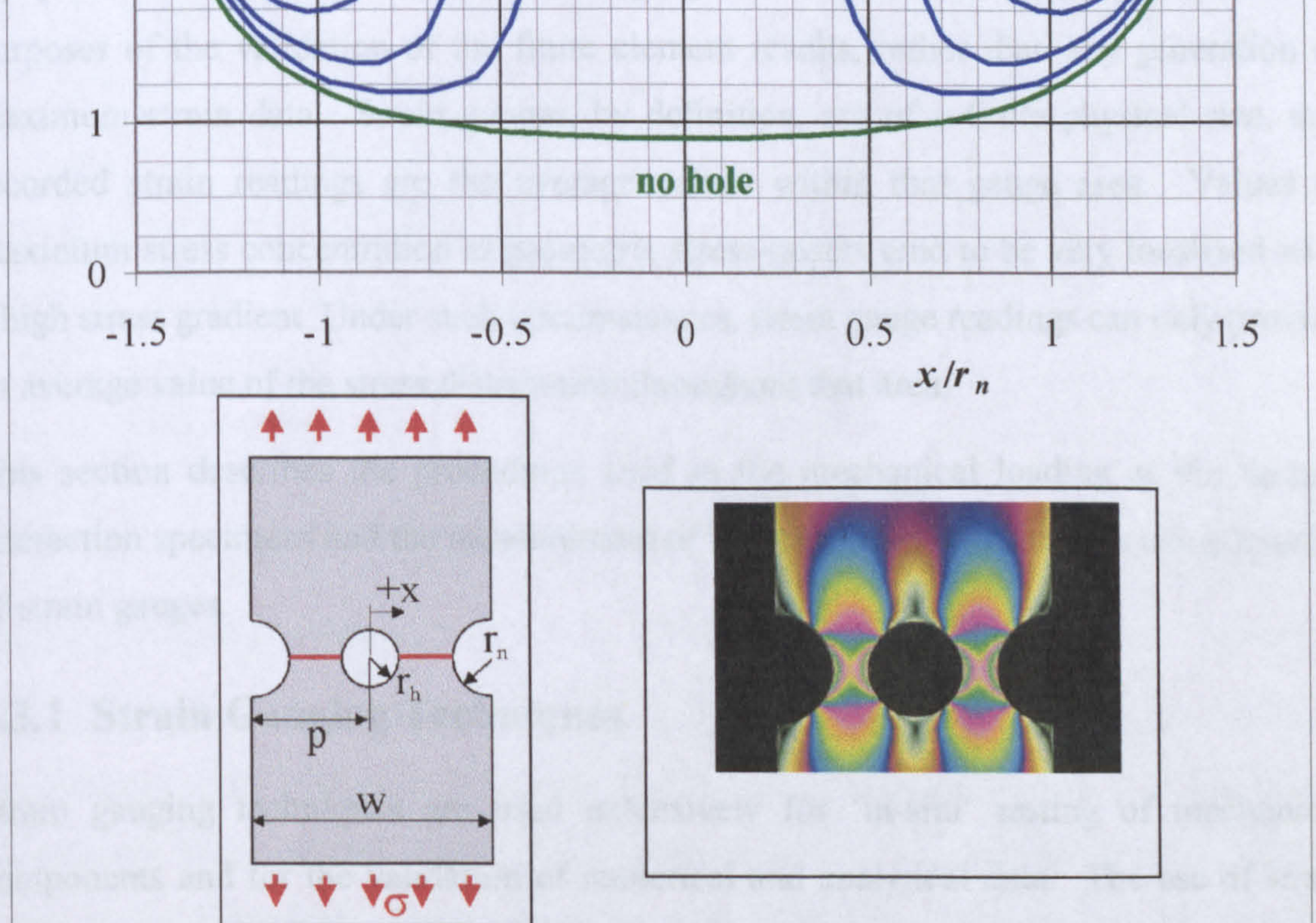

Figure 5-12. Photoelastic ligament plots of the stress concentration distribution along the nominal cross-section of a centrally-placed hole between double-edged notches

5.3 STRAIN GAUGE INVESTIGATIONS

In addition to the extensive photoelastic investigations undertaken, a number of strain gauge studies was also conducted. The primary purpose of these experimental investigations was the validation of the finite element data for those geometries that could not be analysed photoelastically; principally the three-dimensional geometries under investigation. In addition to the three-dimensional investigations, prior analysis was also conducted on a number of two-dimensional problems for the purposes of ensuring the accuracy of the experimental strain gauge procedures and techniques. Each of the geometries investigated using strain gauging techniques is shown in Figure 5-13.

It must be emphasised at this stage that, with the constraints of the experimental equipment available, the use of strain gauges in this research was purely for the purposes of the validation of the finite element results, rather than any generation of maximum strain data. Strain gauges, by definition, are of a finite physical size, and recorded strain readings are the average values within that gauge area. Values of maximum stress concentration at geometric stress-raisers tend to be very localized with a high stress gradient. Under such circumstances, strain gauge readings can only provide an average value of the stress distribution throughout that area.

This section describes the procedures used in the mechanical loading of the feature interaction specimens and the measurement of the associated strain values using a series of strain gauges.

5.3.1 Strain Gauging Techniques

Strain gauging techniques are used extensively for 'in-situ' testing of mechanical components and for the validation of numerical and analytical data. The use of strain gauges is an integral part of the full-scale fatigue test programme of all new aircraft (Tusch and Woithe 2001) and for the monitoring of operations loads for life extension analysis (Gelder et al. 2000). The underlying principle for the operation of strain gauges is the change in electrical resistance of certain materials with mechanical strain. The relationship between the change in length and the resulting change in resistance is governed by a dimensionless factor called the *strain sensitivity factor*, which typically has values in the region of two for most strain gauges.

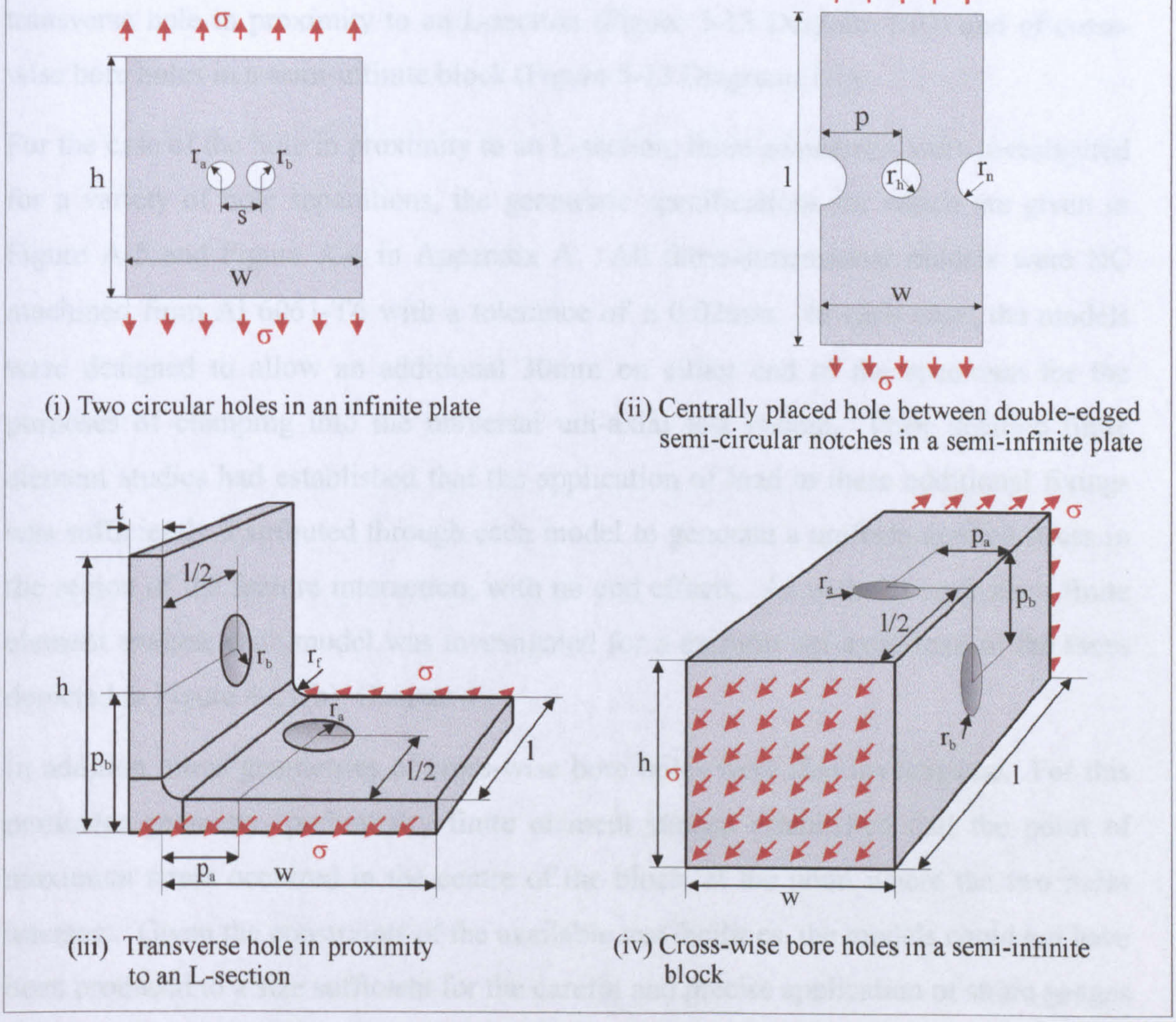

(i) Two circular holes in an infinite plate

(ii) Centrally placed hole between double-edged semi-circular notches in a semi-infinite plate

(iii) Transverse hole in proximity to an L-section

(iv) Cross-wise bore holes in a semi-infinite block

Figure 5-13. Geometries investigated using strain gauging techniques

5.3.1.1 Sample Designs

The strain gauge experimentation programme comprised the testing of two two-dimensional and two three-dimensional models, as illustrated in Figure 5-13. Although the primary focus of this work was the investigation of three-dimensional problems, initial two-dimensional models were also analysed for the purposes of validating the accuracy of the techniques adopted (Figure 5-13, Diagrams (i) and (ii)). The two-dimensional geometries investigated were two configurations of centrally-placed hole between semi-circular double-edged notches (using the models given in Figure A-1 Appendix A), and two equal holes in an infinite plate (Figure 5-4). For this analysis, the epoxy resin models that had previously been used for photoelastic analysis were employed for this strain gauge study.

The three-dimensional feature interactions investigated were the problems of a transverse hole in proximity to an L-section (Figure 5-13 Diagram (iii)) and of cross-wise bore holes in a semi-infinite block (Figure 5-13 Diagram (iv)).

For the case of the hole in proximity to an L-section, three geometries were investigated for a variety of hole separations, the geometric specifications for which are given in Figure A-5 and Figure A-6 in Appendix A. All three-dimensional models were NC machined from Al 6061-T6 with a tolerance of ± 0.02mm. In each case, the models were designed to allow an additional 30mm on either end of the specimen for the purposes of clamping into the universal uni-axial test system. Prior detailed finite element studies had established that the application of load to these additional fixings was sufficiently distributed through each model to generate a uniform applied stress in the region of the feature interaction, with no end effects. As with the equivalent finite element studies, each model was investigated for a uniform uni-axial load of the faces depicted in Figure 4-11(b), Chapter 4.

In addition, three geometries of cross-wise bore holes were also investigated. For this particular geometry, preliminary finite element studies established that the point of maximum stress occurred in the centre of the block, at the point where the two holes intersect. Given the constraints of the available test facilities, the models could not have been produced to a size sufficient for the careful and precise application of strain gauges at this position. However it was noted, during the finite element studies, that in cases where the bore hole radii were relatively large with respect to the member dimensions ($w<6r_a$ and $h<6r_b$), the overall maximum stress concentration had a significant influence on the stress concentrations recorded at the outside edge of the holes, on the surface of the block. These particular configurations of cross-wise bore geometry were therefore selected for strain gauge analysis, with the strain gauges attached to the outside surface of the block, surrounding the holes. The geometric specifications for these geometries are summarised in Figure A-7 in Appendix A.

5.3.1.2 Gauge Selection and Location

The selection of the optimal gauge type for a particular application is governed by a series of basic characteristics. For this research, particular consideration needed to be given to two of these parameters for the gauge selection process.

(i) *Gauge length* The first consideration for the selection of the appropriate gauge is the size of the region required for analysis, and the subsequent specification of the

required gauge length. For the particular application, the strain value is required at localised points in the specimen where the stress gradient is high, and it is therefore important that the gauge selected is as small as possible. In this connection, the feasibility of the accurate positioning and application of the gauge must also be considered.

(ii) *Gauge Pattern* Another important characteristic is the required gauge pattern. The two basic gauge patterns available are single gauges and rosettes. Given that the stress direction is known, and the stress gradients present are relatively high, single uni-axial gauges were considered more appropriate for this application.

With consideration to the above parameters, two gauge types were selected for use in this research: EA-06-031MH-120 and EA-06-050SB-120, from the Micro-measurements Group. The forms of these two gauges are illustrated in Figure 5-14.

EA-06-031MH-120

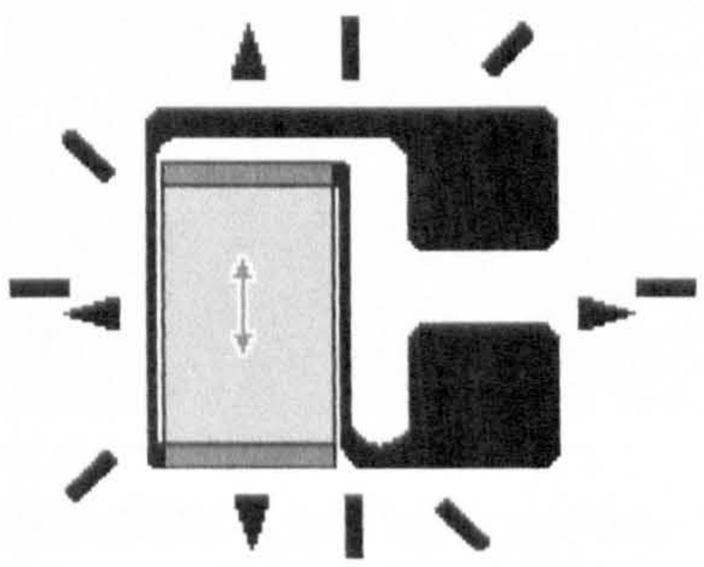

EA-06-050SB-120

Figure 5-14. Illustration of the strain gauge types used in this research (Micro-Measurements group)

These gauges both have a polymide backing and of length 0.031 and 0.05 inches respectively. EA-06-031MH-120 contains ten separate gauges, with each alternate grid running in a perpendicular direction to the line of the gauges. The application of this gauge allows the use of two or more grids in close proximity, and is often used for the measurement of stress gradients. EA-06-050SB-120 contains one gauge, of slightly larger length. This gauge was used in locations where the stress gradient was less steep. These two gauges were utilized in all of the models under investigation.

For each of the geometries investigated (see Appendix A), preliminary finite element analysis was conducted to locate the critical points of high stress concentration. The location of the strain gauges was selected to validate the finite element data in these

regions. Figure 5-15 illustrates the locations and grid directions of the two gauge designs as applied to a typical model of a hole in proximity to an L-section (Figure A-5 in Appendix A). In addition to the gauges illustrated in this figure (placed in regions of high stress), a gauge was also placed at a remote location for determination of the value of the free (applied) stress in each case. This value would not only provide an ongoing validation for the experimental calibration, but could also be used for a straight-forward calculation of the stress concentration value for each of the other gauges at positions of high stress.

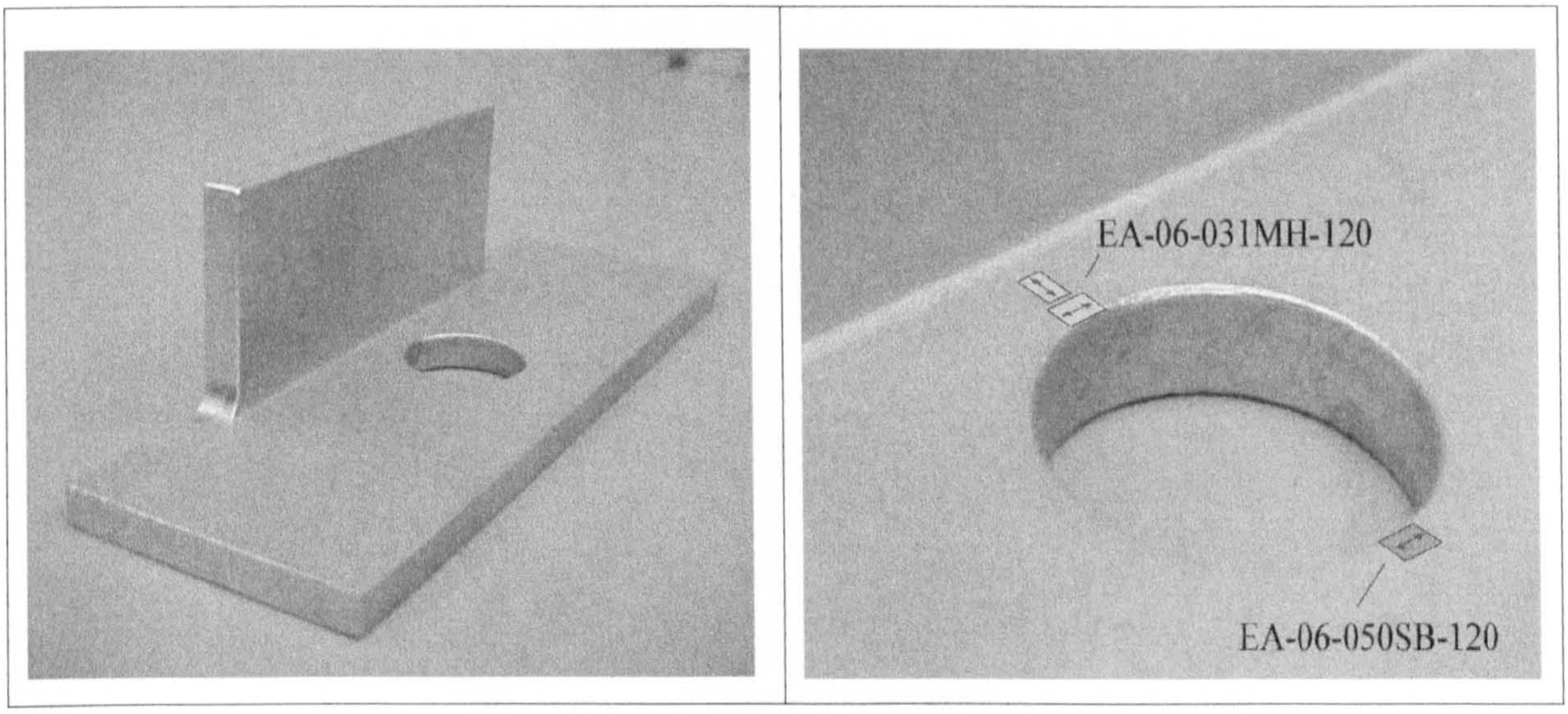

Figure 5-15. Illustration of the typical position and orientation of strain gauges for the example of a transverse hole in proximity to an L-section radius

5.3.1.3 Surface Preparation and Gauge Bonding

The aim of surface preparation is to provide a chemically clean surface with a pH value of around seven, with precise and clear gauge alignment marks. Such surface conditions ensure an accurately positioned gauge with a good bond to the material surface.

The specimens were firstly degreased with a solvent to remove any oils, greases or contaminants. The surfaces were then abraded using silicon carbide paper to remove any loosely bonded material such as rust or paint. Alignment marks were then burnished onto the material surface at the precise point at which the gauge was required. The material surface was then neutralized. The gauge, along with the appropriate solder tabs, was then carefully adhered to the specimen using a catalyst and adhesive. Details of the precise procedures are given in the Micro-Measurements instruction bulletin (Measurements Group 1996). The careful adherence to the correct surface preparation procedures was essential for successful and accurate strain gauge analysis.

5.3.2 Testing Equipment and Procedure

A series of quasi-static uniaxial tests was conducted on each model, using a Measurements Group System 500 electro-hydraulic servo-controlled testing rig, as shown in Figure 5-16.

Figure 5-16. Testing rig, showing cross-wise bore hole specimen in the hydraulic grips

The load capacity of this equipment was 15 KN, which was governed using an electronic control system. The equipment was set up with ten input channels, each of which was configurable for different strain gauge arrangements. Each channel allowed a simultaneous data acquisition rate of 10 Hz. The results were interfaced through a *pcmcia* card to a lap-top computer, which displayed the data in real time.

In each case, specimens were carefully positioned in the hydraulic grips, ensuring that the model was fully aligned. For geometries where the specimens were symmetrical (cases (i), (ii) and (iv) in Figure 5-13), two gauges were placed in identical positions on either side of the model, to detect any unwanted bending effects.

A series of loads was applied to each model in increments of 0.5 KN up to a value of 6 KN, with the corresponding strain readings recorded through an external monitoring system. The loads applied to the models were based on calculation of the elastic limit of each model. This process was repeated three times, with each cycle returning to zero to ensure that no zero-shift effects had occurred.

5.3.3 Sample Results and Validation

For each model, recorded values of the strain readings at the feature edge together with the recorded free (applied) strain provided an experimental average of the stress concentration through the gauge area. Models were viewed under a shadow-graph in order to determine accurately the positioning of each gauge. Finite element models were then constructed of each specimen such that element nodes were positioned corresponding to each corner of the gauge, with a further two nodes equally positioned along each side and in a grid fashion throughout the area. On solution of the finite element model, average values were then taken of these sixteen nodal points to produce an overall average stress concentration value for the gauge area.

Comparisons between the finite element solutions for these particular 'gauge areas' and the data generated from the strain gauge studies showed very close correlations. For example, Figure 5-17 illustrates the location of the strain gauges positioned on the cross-wise bore model. As shown in this figure, two gauges were placed either side of

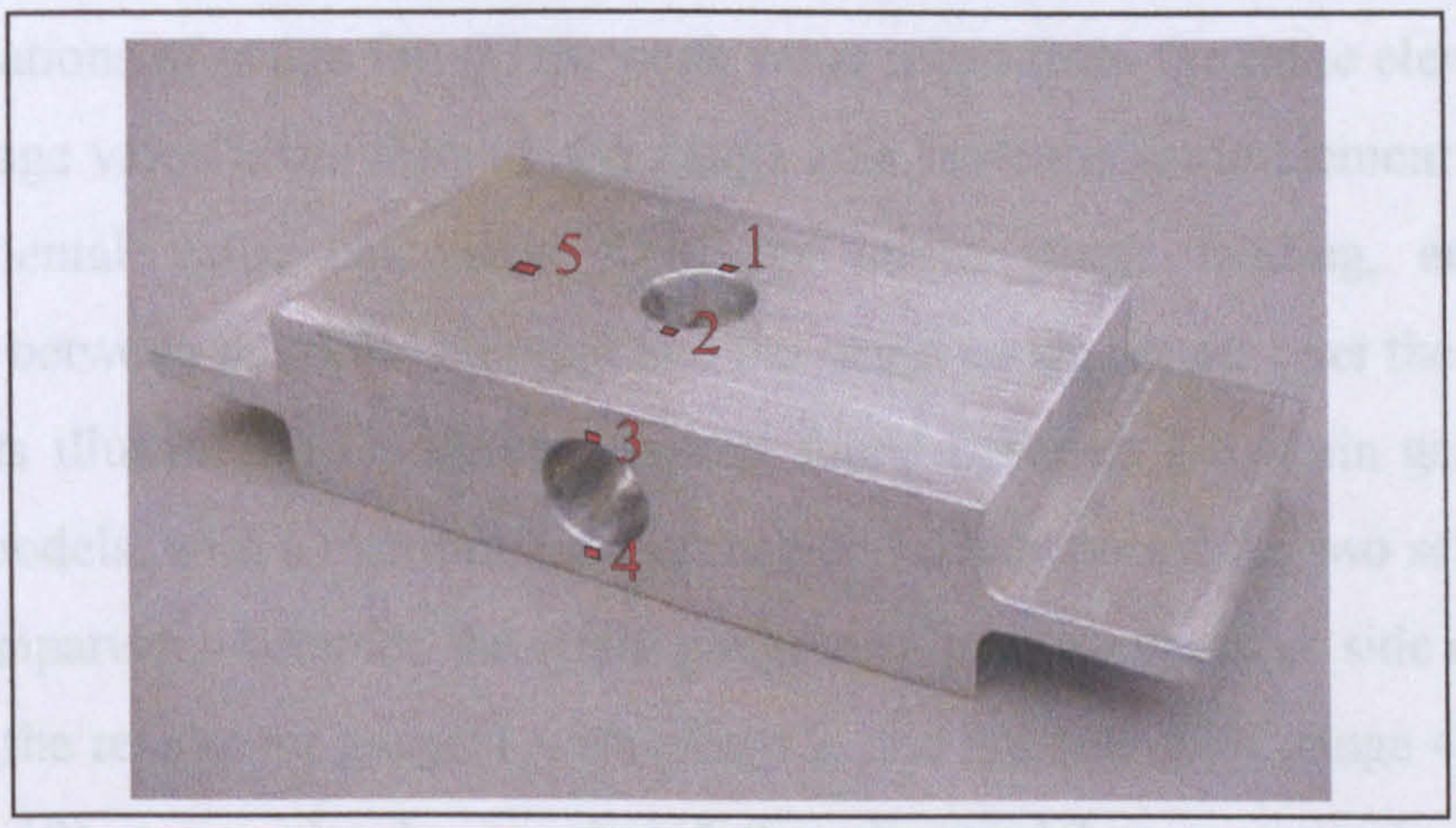

Figure 5-17. Illustration of the positioning of strain gauges on the intersecting bore-hole model

each hole (gauges 1 and 2, and gauges 3 and 4) which allowed for the detection of any bending effects due to misalignment of the model. Gauge 5 was positioned to record the applied strain to the model.

Through taking a ratio of the strain gauge readings at the hole and those values recorded at Gauge 5, stress concentration values could be obtained at each position. For example, Figure 5-18 illustrates the relationship between the free strain and the strain recorded at Gauge 3, for a series of applied loads. Through fitting a trend-line to these results, it can be seen that the free strain is equal to 0.363 times the strain at Gauge 3. This corresponds to a stress concentration factor of 2.75.

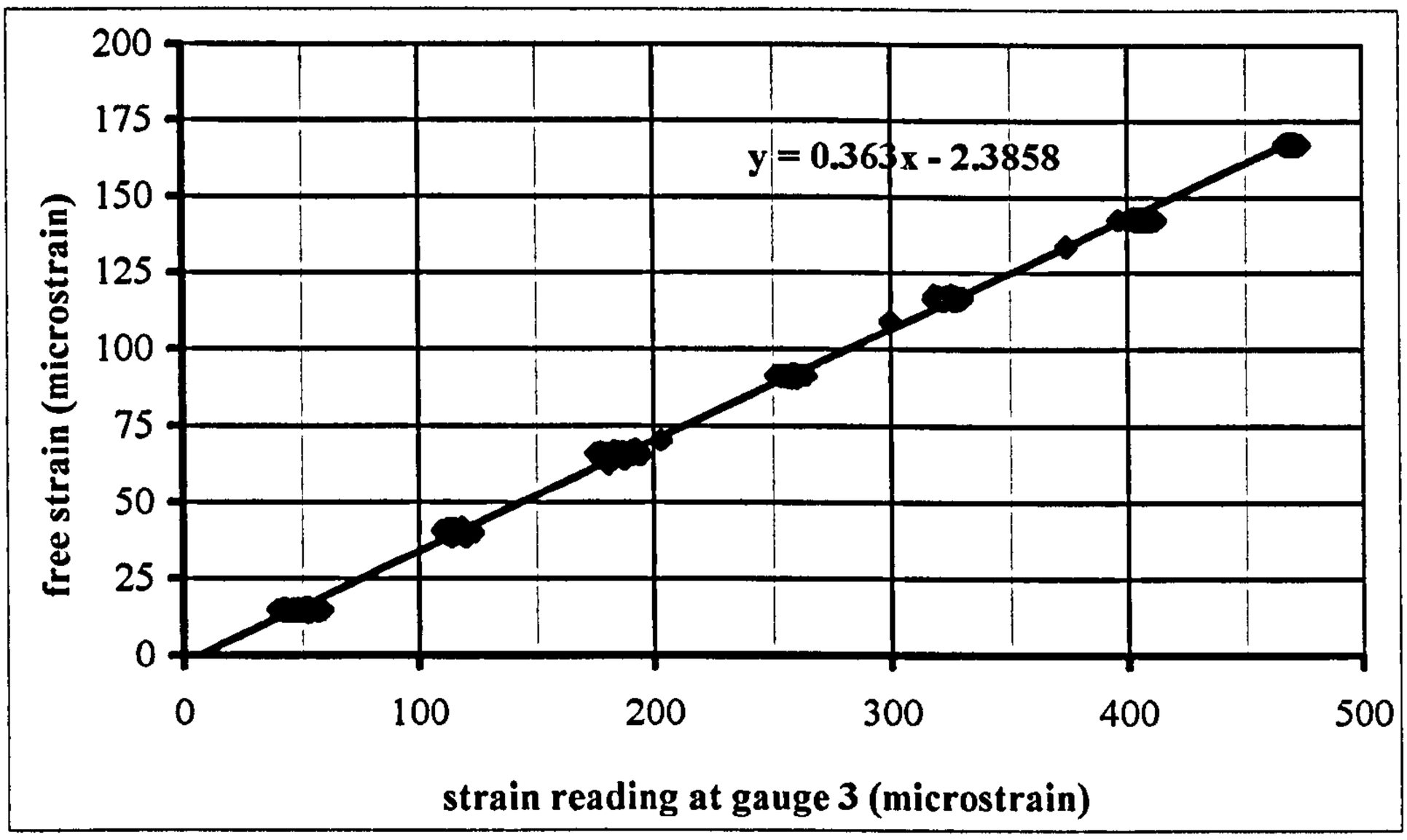

Figure 5-18. Calculation of the stress concentration factor, from incremental readings of the free strain and the strain at Gauge 3 for a range of applied loads

The data in Figure 5-19 illustrate the resulting stress concentration values at each of the four key locations of gauge for: (i) the peak value taken from the finite element model, (ii) the average value taken through the gauge area from the finite element model, (iii) the experimental value calculated from the strain gauge reading, and (iv) the discrepancy between the finite element and the strain gauge results over the gauge area. These results illustrate the close correlations found between the strain gauge and the numerical models, with a maximum difference of 7.5% between the two sets of results. Through comparisons between the strain gauge results taken at either side of each hole (comparing the results for gauge 1 with gauge 2, and gauge 3 with gauge 4 in the table in Figure 5-19) it can also be concluded that the model was correctly aligned and experienced no unwanted bending effects. Such levels of correlation between the finite element and strain gauge results were repeated throughout each of the models under investigation.

It can therefore be concluded that the strain gauge tests provided a validation of the numerical results, given the constraints of this experimental technique when applied to problems involving high stress gradients (see introduction to Section 5.3).

The strain gauge and photoelastic data were then drawn together with the finite element findings to generate the results for the overall investigation of feature interactions, as presented in the following chapter.

Gauge position	(i) Finite element results for the maximum K_t	(ii) Average finite element result over gauge area	(iii) Strain gauge result	(iv) % difference between finite element and strain gauge results o
1	3.49	1.87	1.76	6.3%
2	3.49	1.87	1.74	7.5%
3	4.27	2.64	2.75	4.0%
4	4.27	2.64	2.79	5.7%

Figure 5-19 Comparison between stress concentration values for strain gauge and finite element results for the selected gauges illustrated in Figure 5-17

CHAPTER 6

RESULTS

The aim of this chapter is to present the experimental, numerical and analytical data generated during this research, to be subsequently used as the basis of a rigorous predictive tool. The particular geometric parameters of each feature interaction problem considered were carefully selected in order to provide a comprehensive understanding of the correlations between these variables and their associated stress concentrations.

For each configuration considered, details are presented of the geometric parameters and loading conditions analysed. Validations are then provided of the data accuracy through comparisons between sample numerical, analytical and experimental data. Finally, specific results are given for each problem, providing data for the position, direction and magnitude of the maximum stress concentration, as well as plots of the stress concentration distribution between adjacent features.

6.1 INTRODUCTION

This chapter presents the results generated during the finite element, photoelastic, strain gauge and analytical studies of the two- and three-dimensional problems of feature interaction under consideration in this research. Results are presented of the position, magnitude and direction of the maximum stress concentration, as well as ligament plots of the stress concentration distributions between the features where appropriate.

During the investigations of all feature interaction problems, records were taken of the direction of the maximum principal stress concentration, in addition to its position and magnitude. In the majority of feature combinations analysed, this principal stress concentration occurred, for each geometry, in the y-direction of the model; i.e in the

direction of the applied stress. Unless specified otherwise, therefore, it should be assumed that the maximum stress concentration values presented in this chapter are in the direction of the applied stress.

This chapter is divided into sections corresponding to each feature combination type, dealing initially with the two-dimensional problems, and then looking at the three-dimensional configurations. The sections describe, firstly, the configuration of the particular interaction problem and the geometric parameters involved in its analysis. The sections then move on to describe the data validation process for the stress concentration results in each case, discussing the research tools used for the investigations. Finally, the sections present the overall results generated for the interaction geometry.

Due to the volume of results recorded during these investigations, it was not possible to include all of the sets of data in this chapter, particularly for the ligament plots between adjacent interacting features. A selection of representative results have therefore been provided in the initial geometry discussed, that of a hole placed between semi-circular double-edged notches, which exemplify the observed data trends and overall results. For brevity, in each of the subsequent interaction problems discussed, more concise presentations of a smaller selection of results are provided. Again, the results presented in these section are designed to illustrate the particular data trends in each case.

6.2 HOLE PLACED BETWEEN SEMI-CIRCULAR DOUBLE-EDGED NOTCHES

6.2.1 Geometries Considered

An illustration of the feature combination problem of a hole placed between semi-circular double-edged notches is given in Figure 6-1.

Shown in this figure are the geometric variables considered for this problem: the notch radius (r_n), the hole radius (r_h), the plate width (w), the positioning of the hole relative to the width (p) and the plate length (l), along with the free stress (σ) applied at the far boundary in the y-direction. Preliminary finite element studies established the length (l) at which the far boundaries of the geometry had no influence on the stress concentration levels observed around the features.

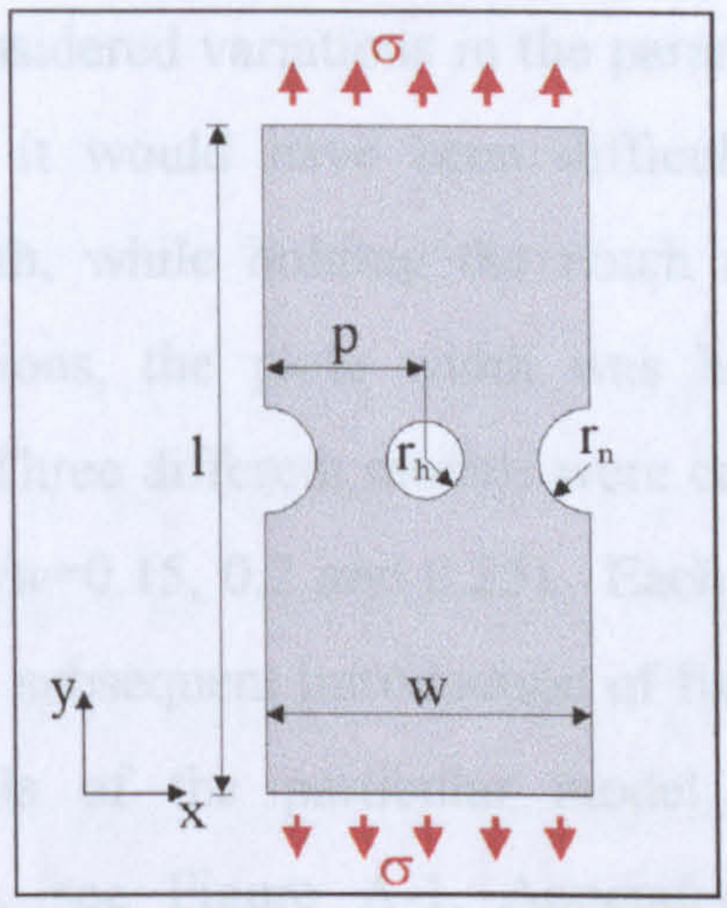

Figure 6-1. Geometric parameters involved in the problem of a hole placed between semi-circular double-edged notches

The problem of a hole and notch in proximity has four basic geometric parameters, each of which requires independent variation: the hole radius (r_h), the notch radius (r_n), the plate width (w) and the positioning of the hole relative to the width (p). For the purposes of simplification, throughout these investigations the notch radius (r_n) was held constant, and all other parameters were normalised by this value. The investigations therefore studied the effect of variation in each of the remaining geometric parameters (r_h, w and p) relative to the constant notch radius.

The research tools employed for the investigation of this problem comprised finite element analysis and photoelastic studies. Supplementary strain gauge analysis was also conducted through the re-employment of the photoelastic models, to provide additional data validation for these results.

The finite element studies considered the effect of variations in each of the geometric parameters r_h, w and p. Thirty two ratios of r_h:r_n were considered, ranging from r_h/r_n=8/75 to r_h/r_n=75/8. For each ratio of r_h:r_n, twelve plate widths (w) were also investigated, ranging from w/r_n=4 to w/r_n =24. In addition, nine geometries of hole positioning (p) were analysed, initially with the hole in a central position (p=w/2), and then for eight offset positions p=w/2–r_n(0.5, 1, 1.5, 2, 2.5, 2.75, 3 and 3.25). A total of over nine hundred finite element models were generated for this analysis, with records taken in each case of the position, magnitude and direction of the maximum stress concentration, and ligament stress concentration plots along the nominal cross-section.

The photoelastic models considered variations in the parameters r_h, and r_n. Due to the model loading constraints, it would have been difficult to allow for incremental variations in the plate width, while holding the notch radius constant. Therefore, throughout these investigations, the plate width was held constant and variations allowed in both r_h, and r_n. Three different models were constructed, each containing a notch of different radius (r_n/w=0.15, 0.2 and 0.25). Each of the models was analysed containing no hole, with the subsequent introduction of five central holes of increasing radius. For further details of the particular model geometries used for these experimental investigations, see Figure A-1, Appendix A. A total of eighteen photoelastic models were analysed, with details recorded of the maximum stress concentration as well as full ligament stress concentration plots.

6.2.2 Data Validation

The initial stage of the data validation process was an overall comparison between the data gathered for the two features individually and the analytical solution for these problems. Figure 6-2 illustrates a typical series of results of this process for the case of double-edged semi-circular notches, through comparisons between the photoelastic data, the finite element data and a well-established analytical treatment for this problem

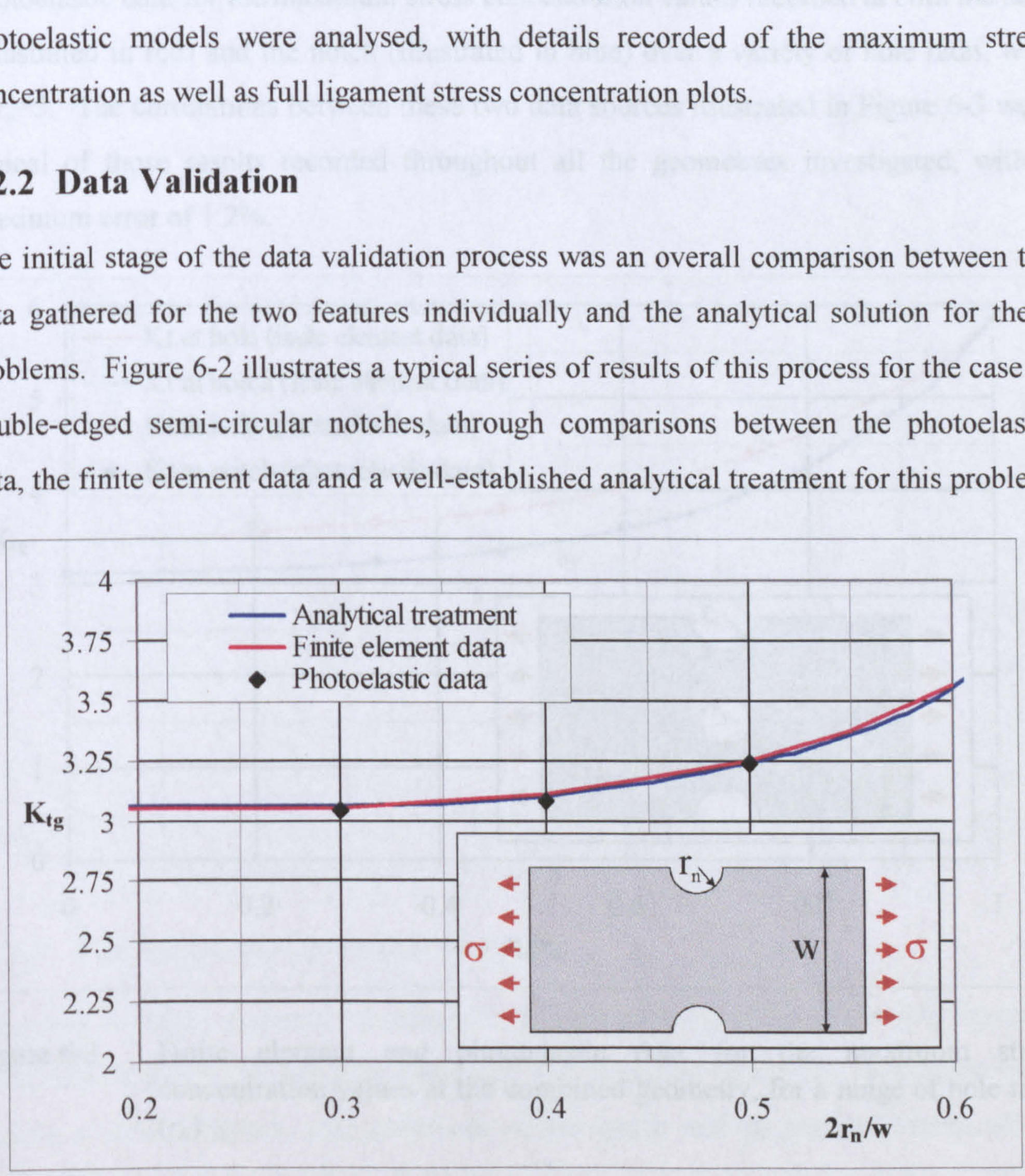

Figure 6-2. Comparisons between the photoelastic and finite element data for the double-edged notch with an appropriate analytical treatment (Ling 1967)

(Ling 1967). These results showed very close correlations between the data generated during this research and the analytical solution, with a maximum 0.8% discrepancy for the finite element data and a maximum 0.6% discrepancy for the photoelastic data.

On completion of validations for the single features, similar comparisons were carried out for the data gathered for the combined geometry. With the unavailability of appropriate analytical treatments for such problems, these validation procedures were conducted through comparisons between the strain gauge, photoelastic and finite element data. Figure 6-3 provides a comparison between finite element and photoelastic data for the maximum stress concentration values recorded at both the hole (illustrated in red) and the notch (illustrated in blue) over a variety of hole radii, with w/r_n=5. The correlations between these two data sources illustrated in Figure 6-3 were typical of those results recorded throughout all the geometries investigated, with a maximum error of 1.2%.

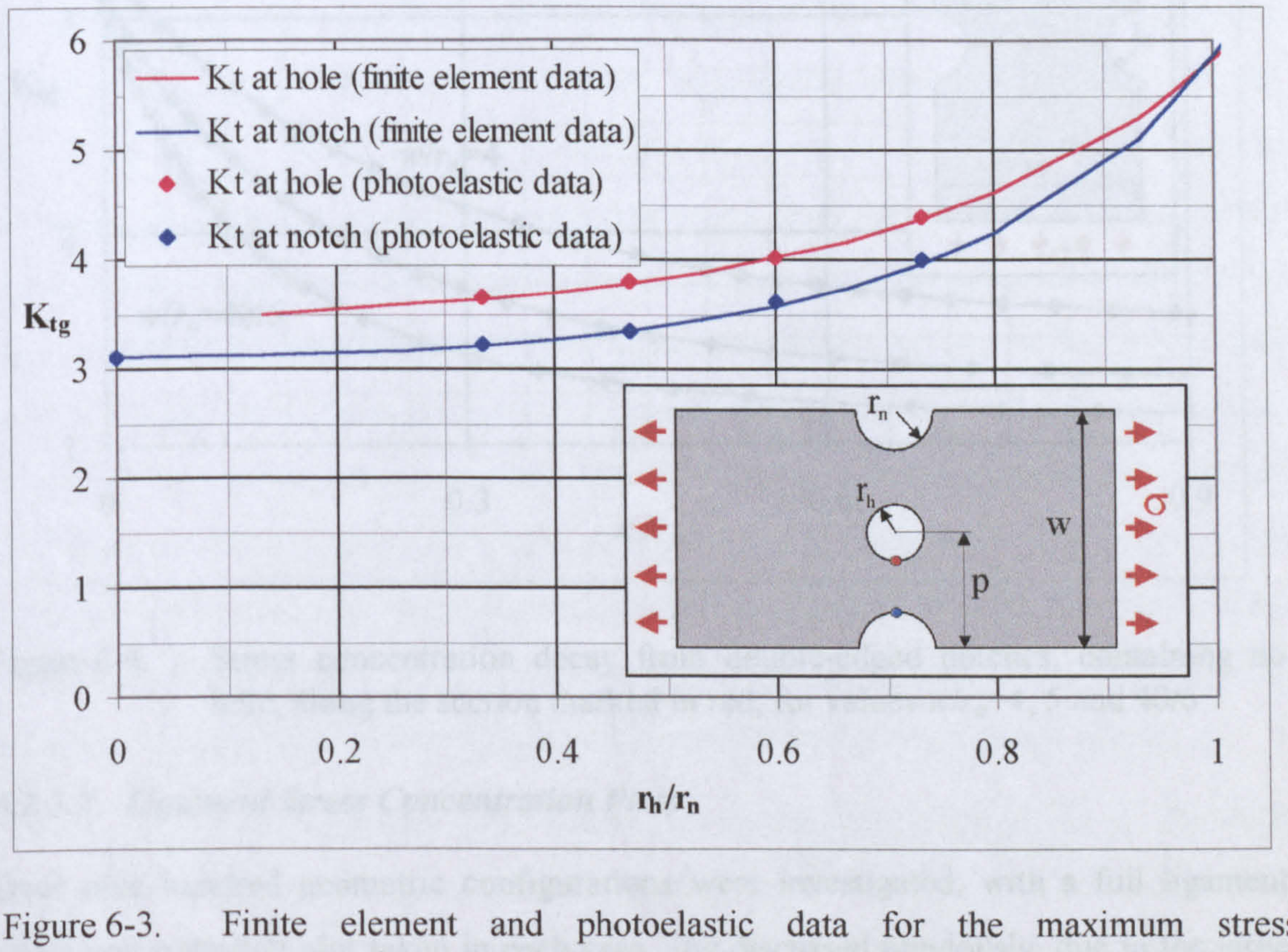

Figure 6-3. Finite element and photoelastic data for the maximum stress concentration values at the combined geometry, for a range of hole radii (r_h)

The results from the strain gauge study were also compared to the finite element results, taken over regions corresponding to the gauge areas. These comparisons showed maximum deviations of 4.7% between these two sets of results.

6.2.3 Results

For convenience, the presentation of results for this problem geometry is divided into three sections: (*i*) single feature data, (*ii*) ligament stress plots taken between the features, and (*iii*) overall results of the maximum stress concentration.

6.2.3.1 Single Feature Data

Given in Figure 6-4 are a selection of stress concentration decays from double-edged notches, measured along the section marked in red, from the notch tip. This figure illustrates the decays for three ratios of $w:r_n$, where w/r_n=4, 5 and 40/6.

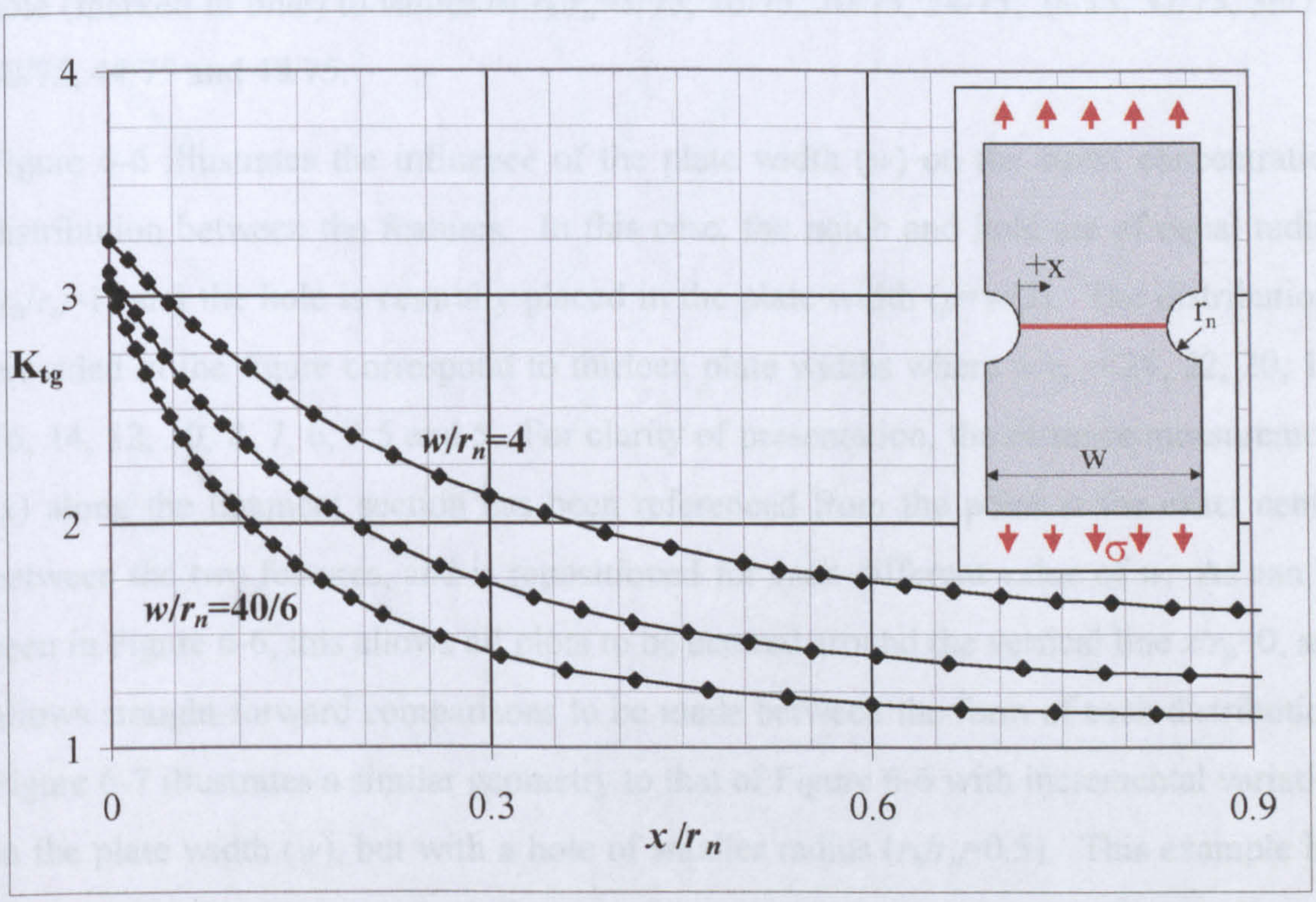

Figure 6-4. Stress concentration decay from double-edged notches, containing no hole, along the section marked in red, for values w/r_n=4, 5 and 40/6

6.2.3.2 Ligament Stress Concentration Plots

Over nine hundred geometric configurations were investigated, with a full ligament stress concentration plot taken in each case. As discussed previously, due to the large volume of data collected, only selections of the results will be presented here, which illustrate the overall trends of the findings.

The following figures illustrate the effect of variation in each of the three basic geometric parameters associated with this problem (r_h, w and p) on the ligament stress

concentration distribution between the features. In general terms, Figure 6-5 illustrates the effect of variation in the hole radius (r_h), Figure 6-6 and Figure 6-7 the effect of variation in the plate width (w) and Figure 6-8 variation in hole positioning (p).

Figure 6-5 illustrates the variation in the ligament stress concentration distribution between the notch and hole, for a series of differing radius of central hole (r_h), with both w and p constant (w/r_n=4 and p=w/2). Ligament plots are taken from the prescribed point x (see diagram in Figure 6-5) which measures the distance along the ligament section from the notch tip. This figure illustrates the changing form of the stress concentration distribution along the cross-section, from a geometry containing no hole (marked in blue) to values of r_h:r_n=8/75, 16/75, 20/75, 24/75, 28/75, 32/75, 36/75, 40/75, 44/75 and 48/75.

Figure 6-6 illustrates the influence of the plate width (w) on the stress concentration distribution between the features. In this case, the notch and hole are of equal radius (r_h/r_n=1) and the hole is centrally placed in the plate width (p=w/2). The distributions provided in the figure correspond to thirteen plate widths where w/r_n = 24, 22, 20, 18, 16, 14, 12, 10, 8, 7, 6, 5.5 and 5. For clarity of presentation, the distance measurement (x) along the ligament section has been referenced from the point at the exact centre between the two features, and is repositioned for each different value of w. As can be seen in Figure 6-6, this allows all plots to be centred around the vertical line x/r_n=0, and allows straight-forward comparisons to be made between the form of each distribution. Figure 6-7 illustrates a similar geometry to that of Figure 6-6 with incremental variation in the plate width (w), but with a hole of smaller radius (r_h/r_n=0.5). This example has been provided to illustrate the influence of the relative feature sizes on the overall stress concentration distribution. Again, this plot is based on the distance measured along the ligament section (x) taken from the central point between the two feature edges.

Finally, Figure 6-8 provides data illustrating incremental changes in p, the hole positioning relative to the plate width, with r_h/r_n=1 and w/r_n =12. As this model does not display vertical symmetry, the ligament plot has been taken along the entire cross-section of the geometry (marked in red in the diagram in Figure 6-8). The particular case where the hole is centrally placed (p=w/2) is marked in blue, and each subsequent hole positioning of p=w/2–r_n(0.5, 1, 1.5, 2, 2.5, 2.75, 3 and 3.25)in black. The distance measurement along the cross-section, x, is placed in each case at the centre of the hole.

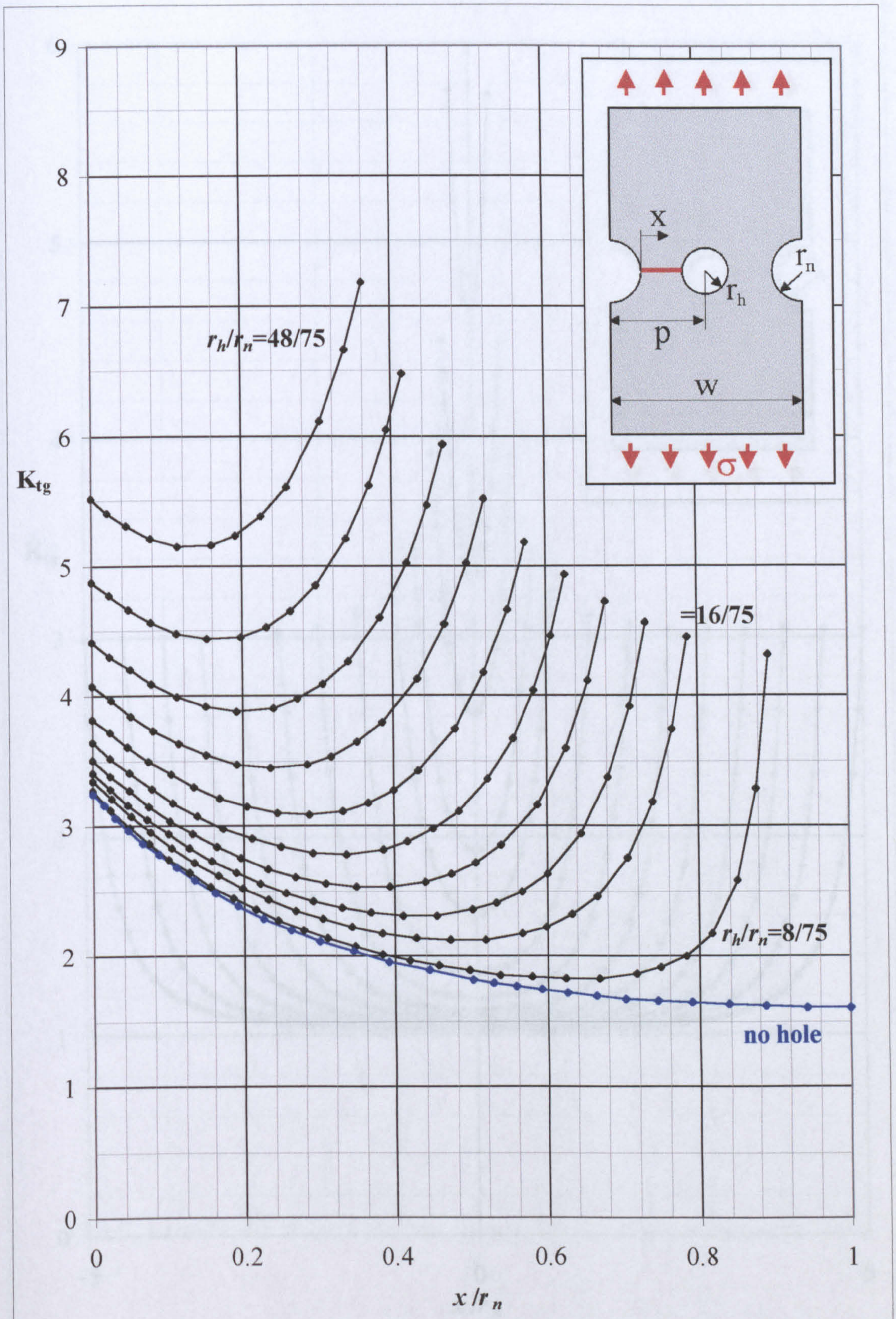

Figure 6-5. Ligament stress concentration plot for variable hole radius (r_h), along section marked in red, with $w=4r_n$ and $p=w/2$. Plots are provided for a model containing no hole (shown in blue) and for ten geometries of hole radii: $r_h:r_n$=8/75, 16/75, 20/75, 24/75, 28/75, 32/75, 36/75, 40/75, 44/75 and 48/75

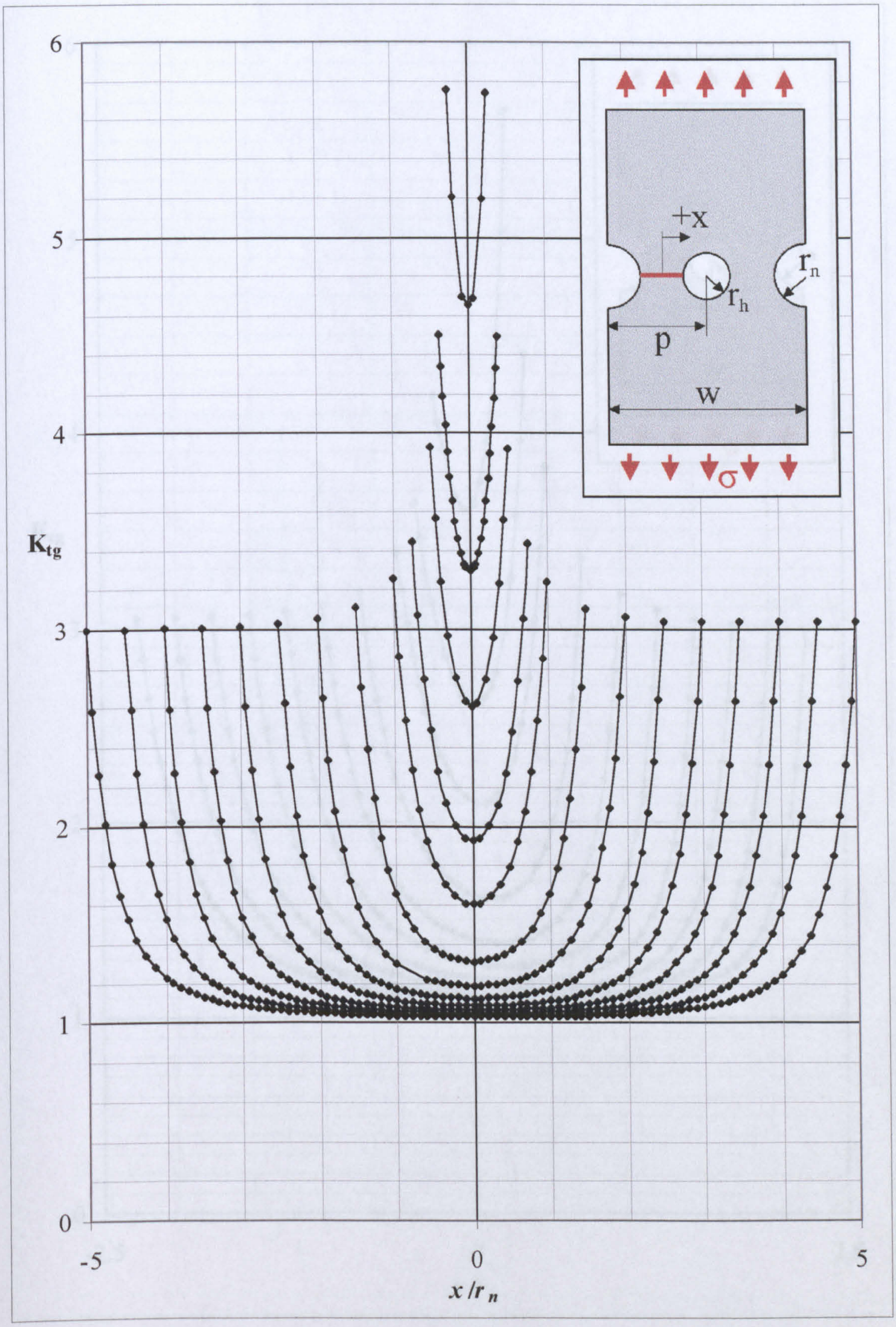

Figure 6-6. Ligament stress concentration plots for variable plate width (w), along section marked in red, for r_n=r_h and p=w/2. Plots are provided for thirteen geometries of plate width, where w/r_n = 24, 22, 20, 18, 16, 14, 12, 10, 8, 7, 6, 5.5 and 5

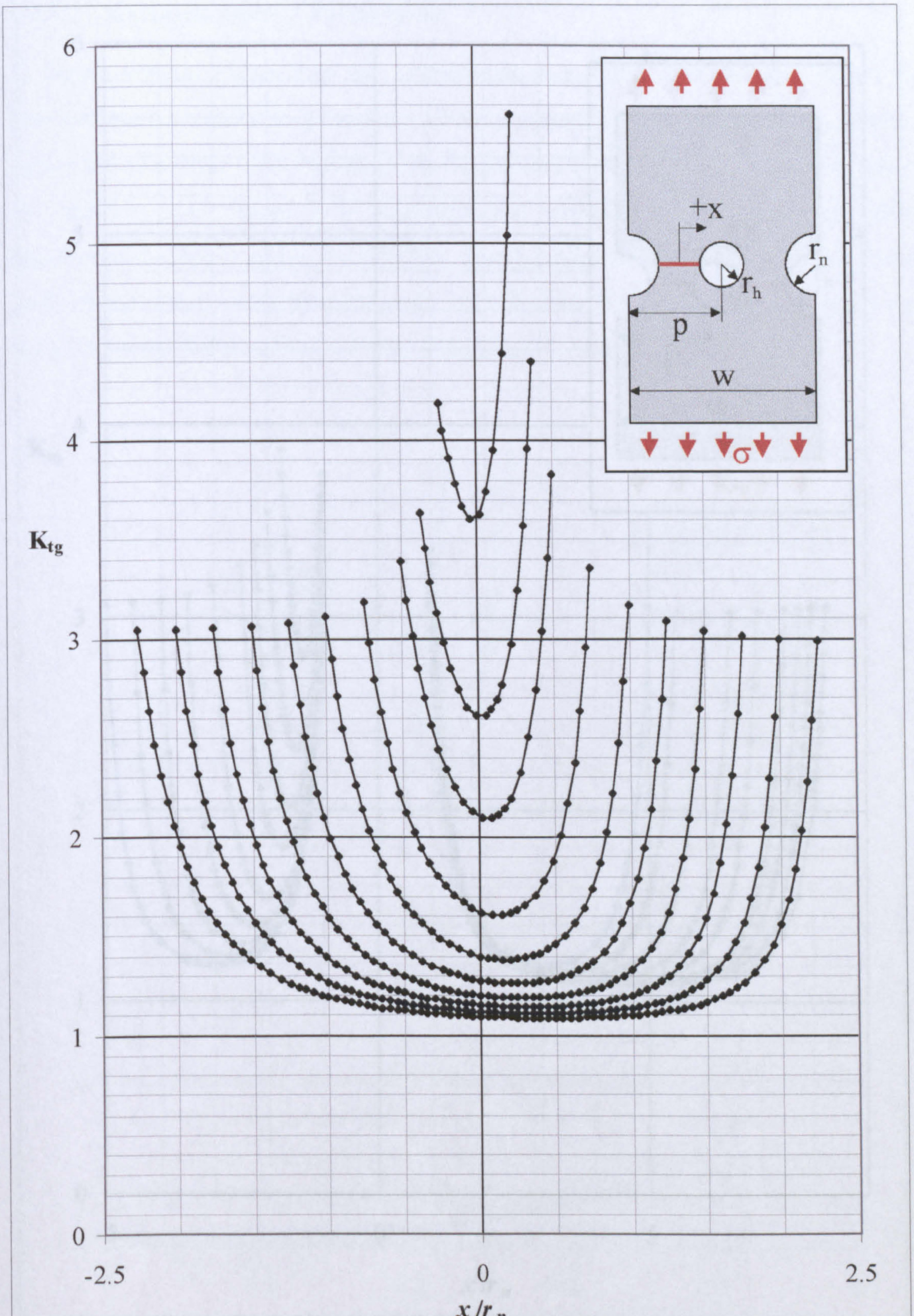

Figure 6-7. Ligament stress concentration plots for variable plate width (w), along section marked in red, for $r_h=r_n/2$ and $p=w/2$. Plots are provided for ten geometries of plate width, where w/r_n = 12, 11, 10, 9, 8, 7, 6, 5, 4.5 and 4

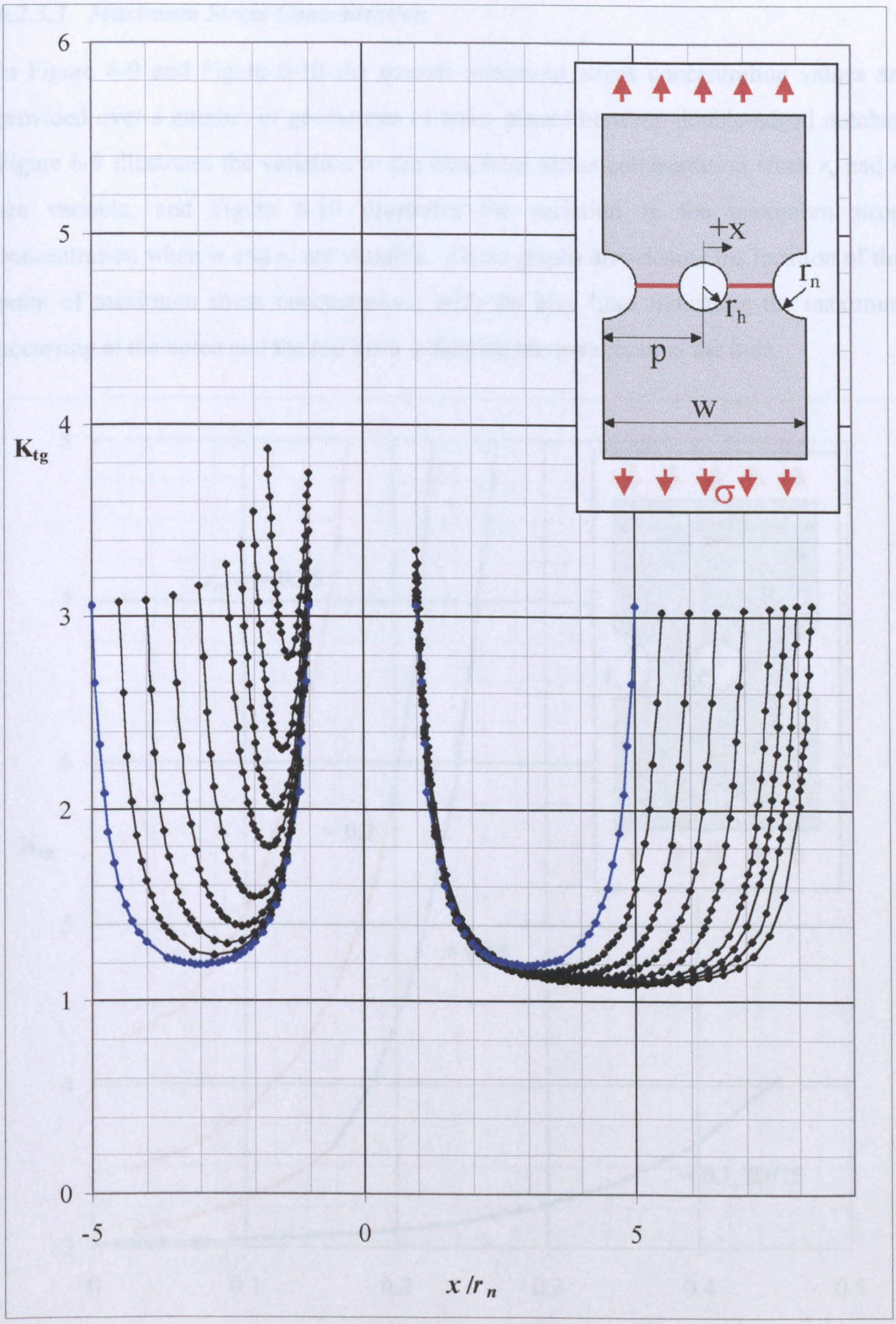

Figure 6-8. Ligament stress concentration plots for hole positioning (p), along sections marked in red, for r_n=r_h and w=12r_n. Plots are provided for the particular case of a central hole, p=w/2 (shown in blue) and eight geometries of off-set holes where p=w/2 –r_n(0.5, 1, 1.5, 2, 2.5, 2.75, 3 and 3.25)

6.2.3.3 Maximum Stress Concentration

In Figure 6-9 and Figure 6-10 the overall maximum stress concentration values are provided over a number of geometries of holes placed between double-edged notches. Figure 6-9 illustrates the variation in the maximum stress concentration when r_n and r_h are variable, and Figure 6-10 illustrates the variation in the maximum stress concentration when w and r_n are variable. These graphs also denote the location of this point of maximum stress concentration, with the blue lines indicating the maximum occurring at the notch and the red lines indicating the maximum at the hole.

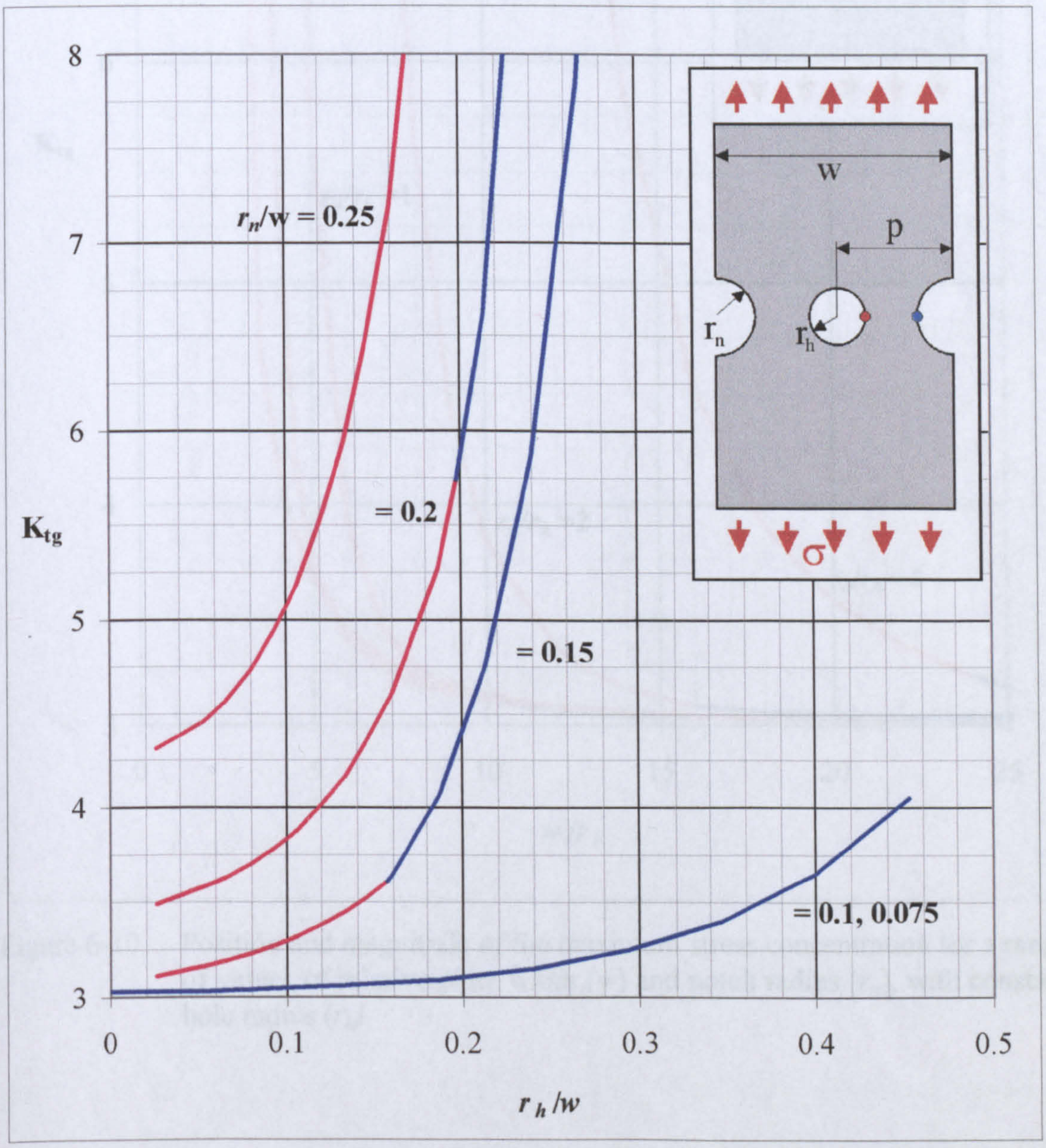

Figure 6-9. Position and magnitude of the maximum stress concentration for a range of values of relative hole radius (r_h) and notch radius (r_n) with constant plate width (w)

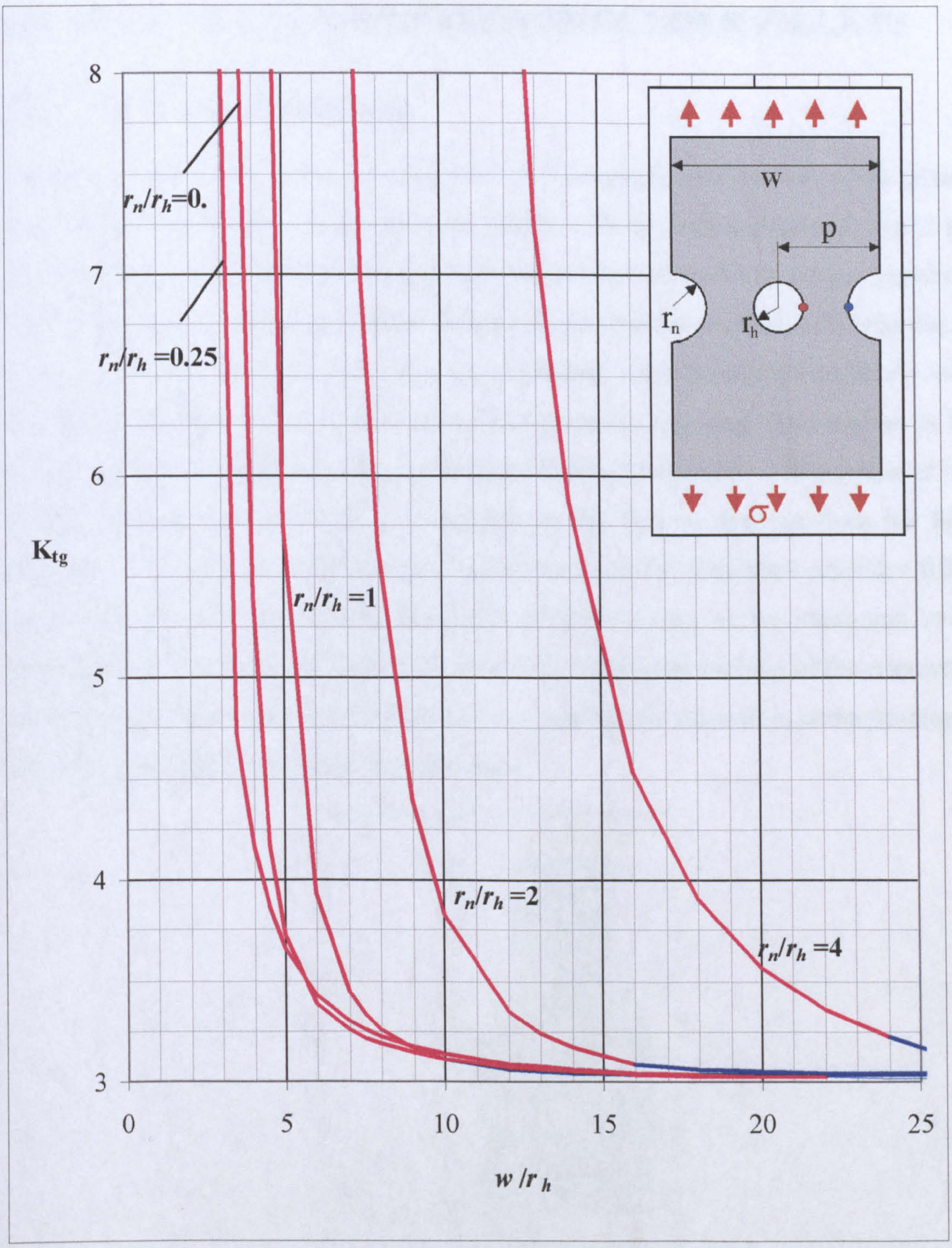

Figure 6-10. Position and magnitude of the maximum stress concentration for a range of values of relative plate width (w) and notch radius (r_n), with constant hole radius (r_h)

6.3 HOLE PLACED BETWEEN SHOULDER FILLETS

6.3.1 Geometries Considered

Shown in Figure 6-11 is an illustration of the geometric problem of a hole placed between shoulder fillets. As discussed in Chapter 3, the geometric problems considered in this research were identified as particular 'worst case' scenarios by fatigue experts at BAE SYSTEMS. Preliminary finite element studies for the problem of a hole placed between shoulder fillets revealed that the maximum stress concentration levels were consistently highest when the hole centre was placed at the same cross-section as the maximum stress concentration for the shoulder fillets individually. The position of this critical cross-section, labelled p_y, is defined as the vertical distance from the fillet shoulder. A series of initial studies was carried out for individual shoulder fillets (containing no hole) to identify this exact positioning (p_y) of the maximum stress concentration for a range of fillet radii. For each subsequent analysis of the interacting geometry, the hole centre was positioned at the appropriate value of p_y corresponding to the particular fillet radius under consideration.

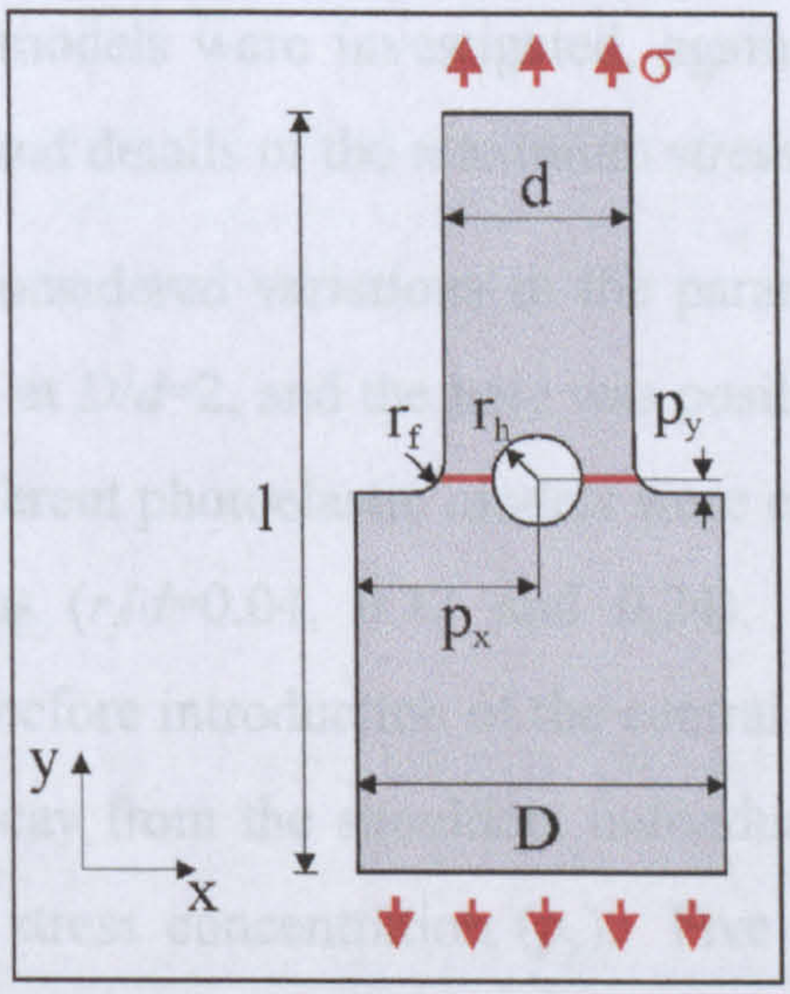

Figure 6-11. Geometric parameters involved in the problem of a hole placed between shoulder fillets

Shown in Figure 6-11 are the geometric variables considered for this problem: the shoulder radius (r_f), the hole radius (r_h), the outer plate width (D), the filleted plate width (d), the positioning of the hole relative to the outer width (p_x), the vertical positioning of the hole relative to the fillet edge (p_y) and the plate length (l), along with the free stress (σ) applied at the far boundary in the y-direction. Again, preliminary

finite element studies identified the plate length (l) for which the far boundaries had no stress-raising influence on the geometric features.

Five independent geometric parameters were considered for this problem: the shoulder radius (r_f), the hole radius (r_h), the outer plate width (D), the filleted plate width (d) and the positioning of the hole relative to the outer width (p_x). Note that p_y is not considered as a geometric variable, since it is wholly dependant on r_f. Throughout the investigations, the filleted plate width (d) was held constant, and all other parameters normalised by this value. The investigation of this problem comprised a series of photoelastic and finite element studies.

The finite element studies considered the effect of variations in each of the geometric parameters r_h, r_f, p_x and D. Fifteen ratios of r_h:d were investigated, r_h/d=2/75, 4/75, 6/75, 8/75, 10/75, 12/75, 14/75, 16/75, 18/75, 20/75, 22/75, 24/75, 26/75, 28/75 and 30/75. Fourteen ratios of r_f:d were considered, ranging from r_f/d=0.05 to r_f/d=0.42. In addition, five horizontal hole positions were considered, initially with the hole centrally-placed, p_x=D/2, and then for four offset positions p_x=D/2-(0.1d, 0.2d, 0.3d and 0.4d). Finally, the two most common ratios of D:d were investigated D/d=2 and 1.5. A total of over six hundred models were investigated, again with records taken of the appropriate ligament plots and details of the maximum stress concentration.

The photoelastic models considered variations in the parameters r_h, and r_f, while the ratio D:d was held constant at D/d=2, and the hole was positioned centrally between the fillets (p_x=D/2). Three different photoelastic models were constructed, each containing a different shoulder radius (r_f/d=0.04, 0.12 and 0.24). Preliminary analysis was conducted on each model, before introduction of the central hole, in order to investigate the stress concentration decay from the shoulders individually, as well as identify the position of the maximum stress concentration (p_y). Five central holes of increasing radii were then introduced to the model (r_h/d=0.067, 0,133, 0.2, 0.267 and 0.333). A total of eighteen experimental models were considered. For more details of the photoelastic model geometries, see Figure A-2, Appendix A.

6.3.2 Data Validation

A thorough validation process was conducted using comparisons between the finite element and photoelastic data. The results showed very close correlations between

these two sets of data, with a maximum discrepancy of 0.9%. An example of these correlations is given in Figure 6-12 illustrating the finite element data (shown in black) and the photoelastic data (shown in blue) for the ligament stress connection plot through the cross-section marked in red. This particular example is taken from the case of a centrally-placed hole (p_x=D/2), where r_h/d=0.133 and r_f/d=0.04.

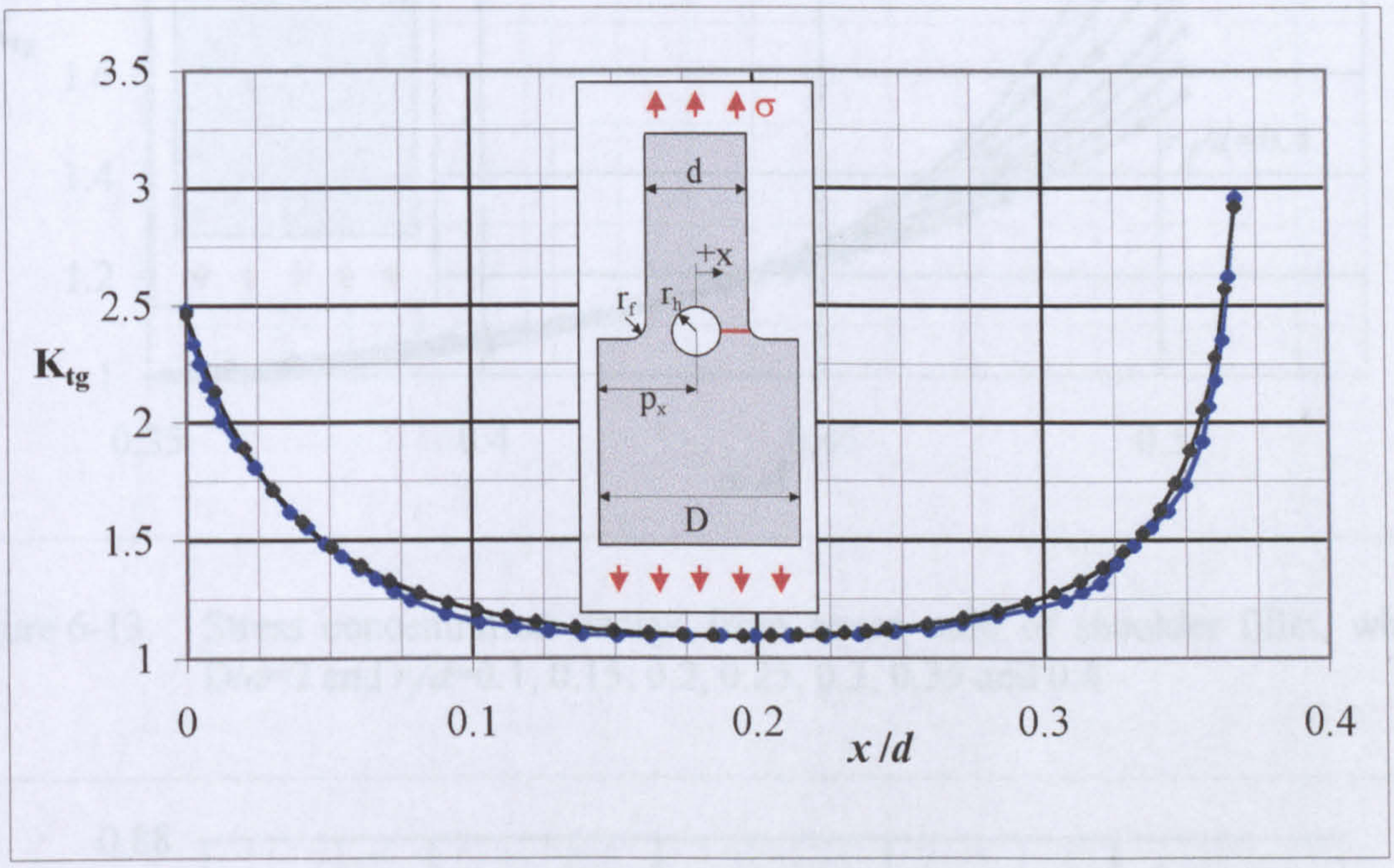

Figure 6-12. Comparison between finite element data (shown in black) and photoelastic results (shown in blue) for a ligament stress concentration plot along the section marked in red, where r_h/d=0.133, and r_f/d=0.04

6.3.3 Results

6.3.3.1 Single Feature Data

The initial stage of this work was to investigate the stress concentrations associated with each shoulder fillet individually, looking at the magnitude and decay of the stress concentration from this feature, and also at the positioning of the maximum stress (p_y). Figure 6-13 illustrates a selection of the stress decays from the shoulder fillets generated from this study, for seven radii of shoulder fillet, where r_f/d=0.1, 0.15, 0.2, 0.25, 0.3, 0.35 and 0.4, and D/d=2. Figure 6-14 illustrates the relative vertical position (p_y/r_f) of each of the points of maximum stress, for a variety of shoulder radii, and two ratios of D:d (D/d=2 and 1.5).

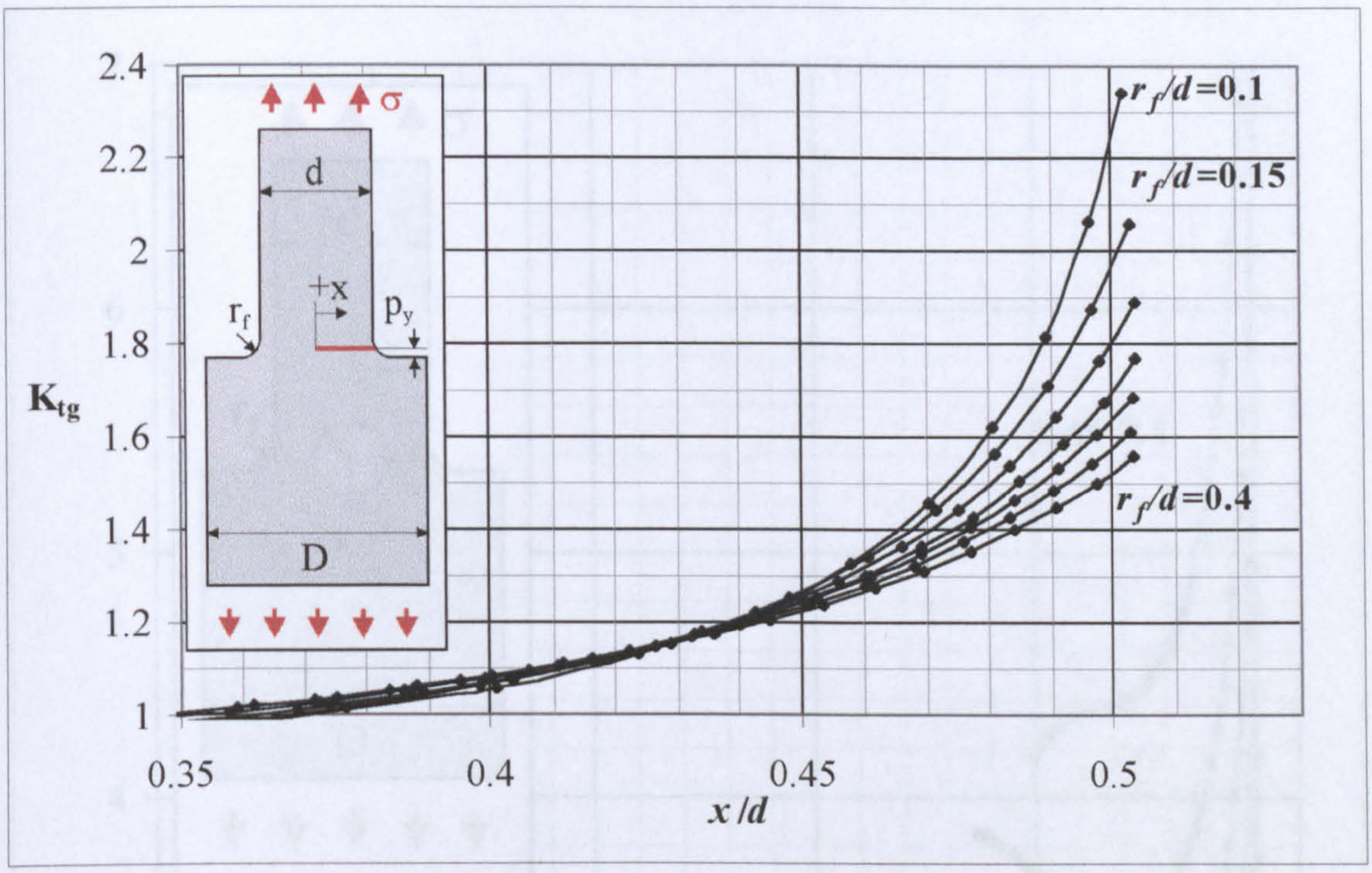

Figure 6-13. Stress concentration decays from seven radii of shoulder fillet, where D/d=2 and r_f/d=0.1, 0.15, 0.2, 0.25, 0.3, 0.35 and 0.4

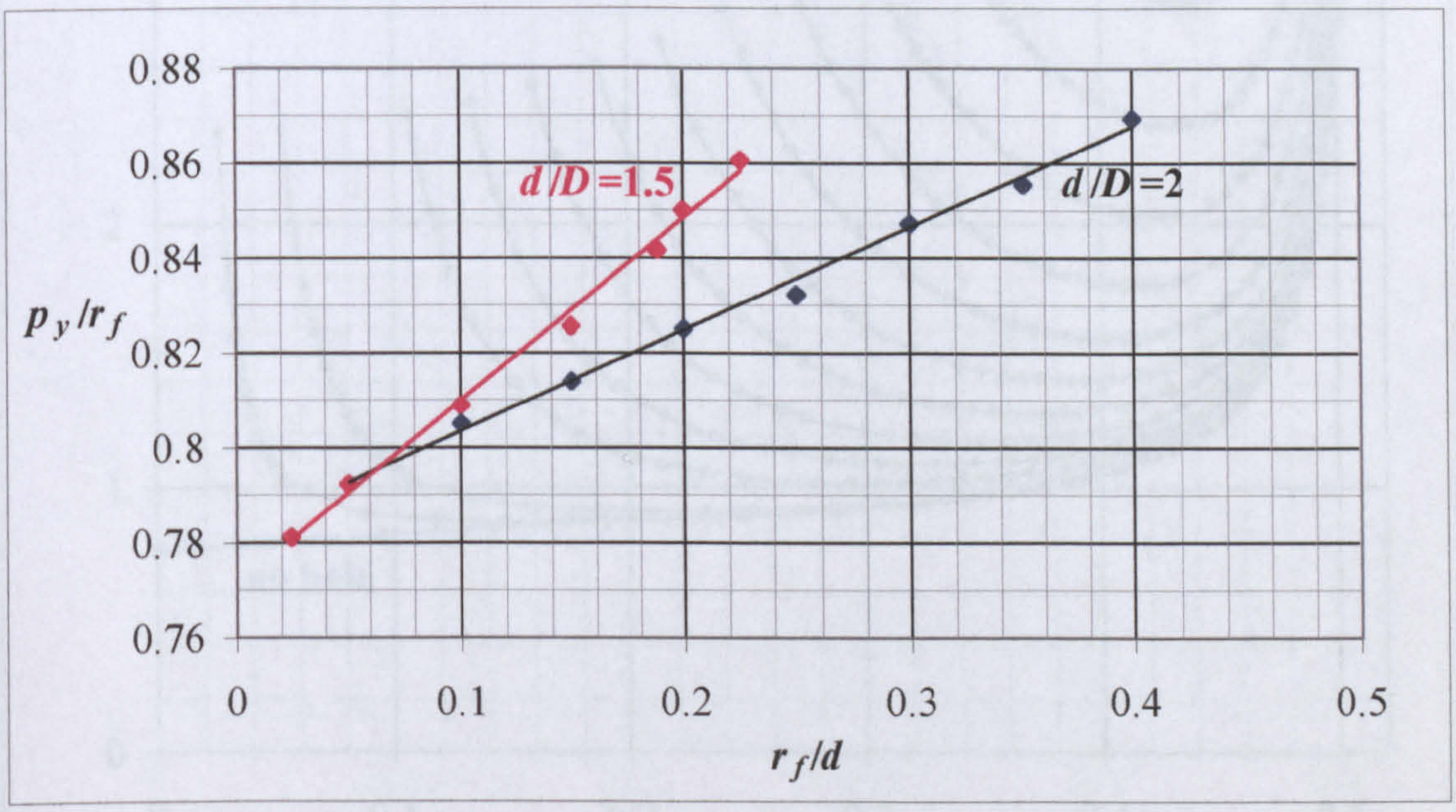

Figure 6-14. The relationship between the shoulder radius and the relative positioning of the corresponding maximum stress (p_y/r_f) for D/d=1.5 and 2

6.3.3.2 Ligament Stress Concentration Plots

Figure 6-15 and Figure 6-16 illustrate the variation in the ligament stress concentration distribution between the hole and shoulder fillet, for a series of differing radius of

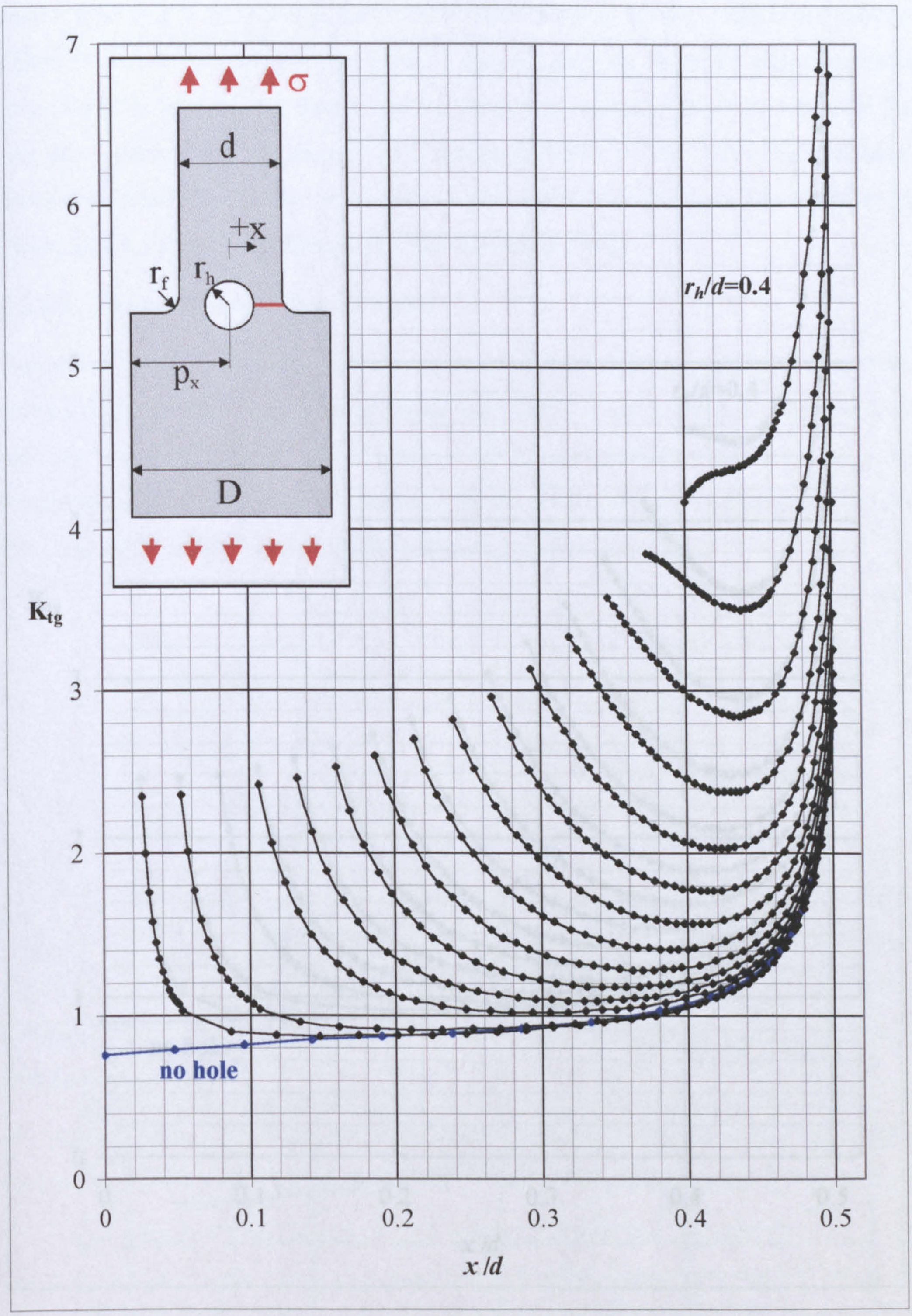

Figure 6-15. Ligament stress concentration plot for variable hole radius (r_h), along section marked in red, with r_f=0.06d and p_x=D/2. Plots are provided for a section containing no hole (shown in blue) along with fifteen geometries of hole radius (shown in black), where r_h/d=2/75, 4/75, 6/75, 8/75, 10/75, 12/75, 14/75, 16/75, 18/75, 20/75, 22/75, 24/75, 26/75, 28/75 and 30/75

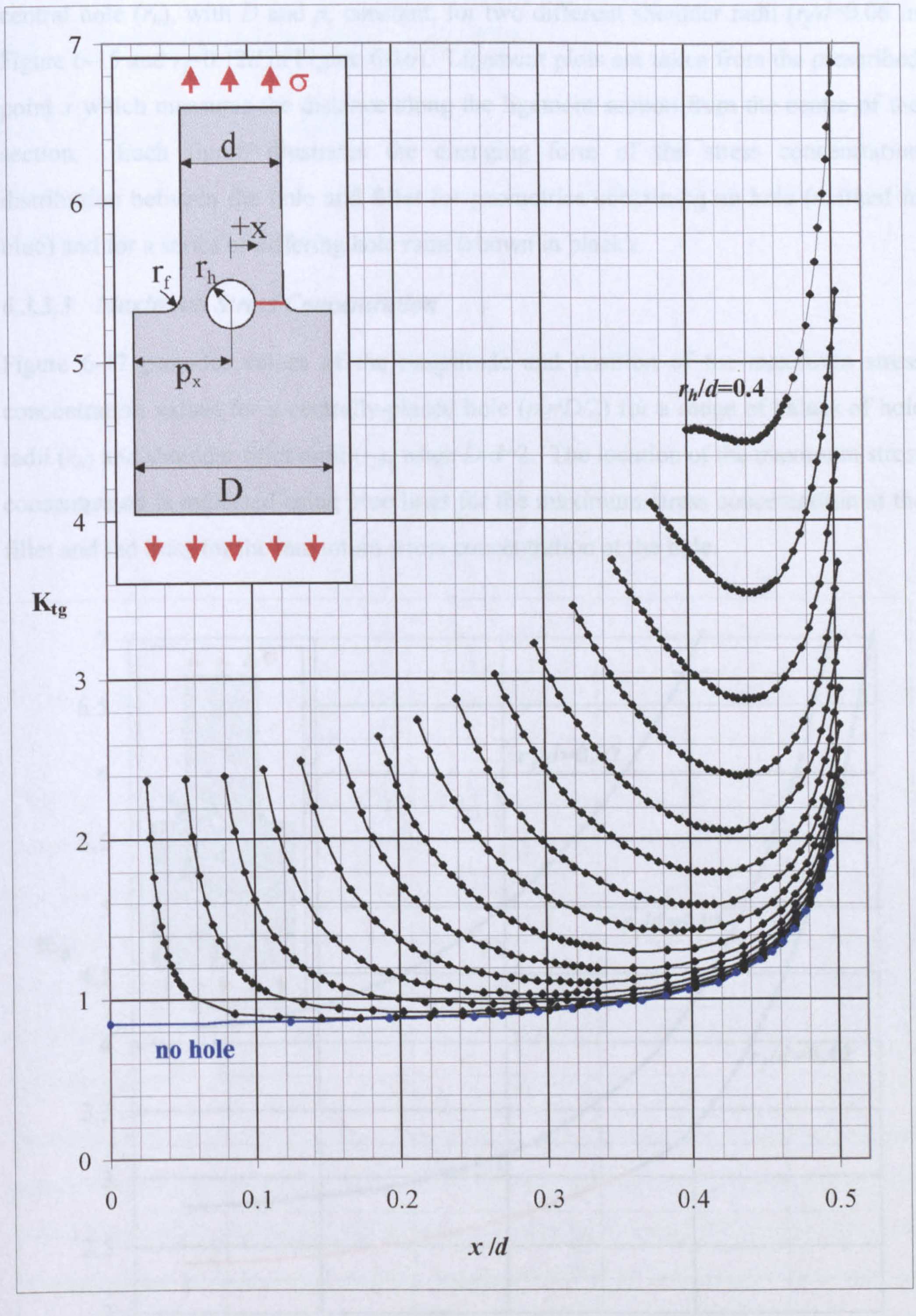

Figure 6-16. Ligament stress concentration plot for variable hole radius (r_h), along section marked in red, with r_f=0.12d and p_x=D/2. Plots are provided for a section containing no hole (shown in blue) along with fifteen geometries of hole radius (shown in black), where r_h/d=2/75, 4/75, 6/75, 8/75, 10/75, 12/75, 14/75, 16/75, 18/75, 20/75, 22/75, 24/75, 26/75, 28/75 and 30/75

central hole (r_h), with D and p_x constant, for two different shoulder radii (r_f/d=0.06 in Figure 6-15 and r_f=0.12d in Figure 6-16). Ligament plots are taken from the prescribed point x which measures the distance along the ligament section from the centre of the section. Each figure illustrates the changing form of the stress concentration distribution between the hole and fillet for geometries containing no hole (marked in blue) and for a series of differing hole radii (shown in black).

6.3.3.3 Maximum Stress Concentration

Figure 6-17 provides values of the magnitude and position of the maximum stress concentration values for a centrally-placed hole (p_x=D/2) for a range of values of hole radii (r_h) and shoulder fillet radii (r_f), when D/d=2. The location of the maximum stress concentration is indicated using blue lines for the maximum stress concentration at the fillet and red lines for the maximum stress concentration at the hole.

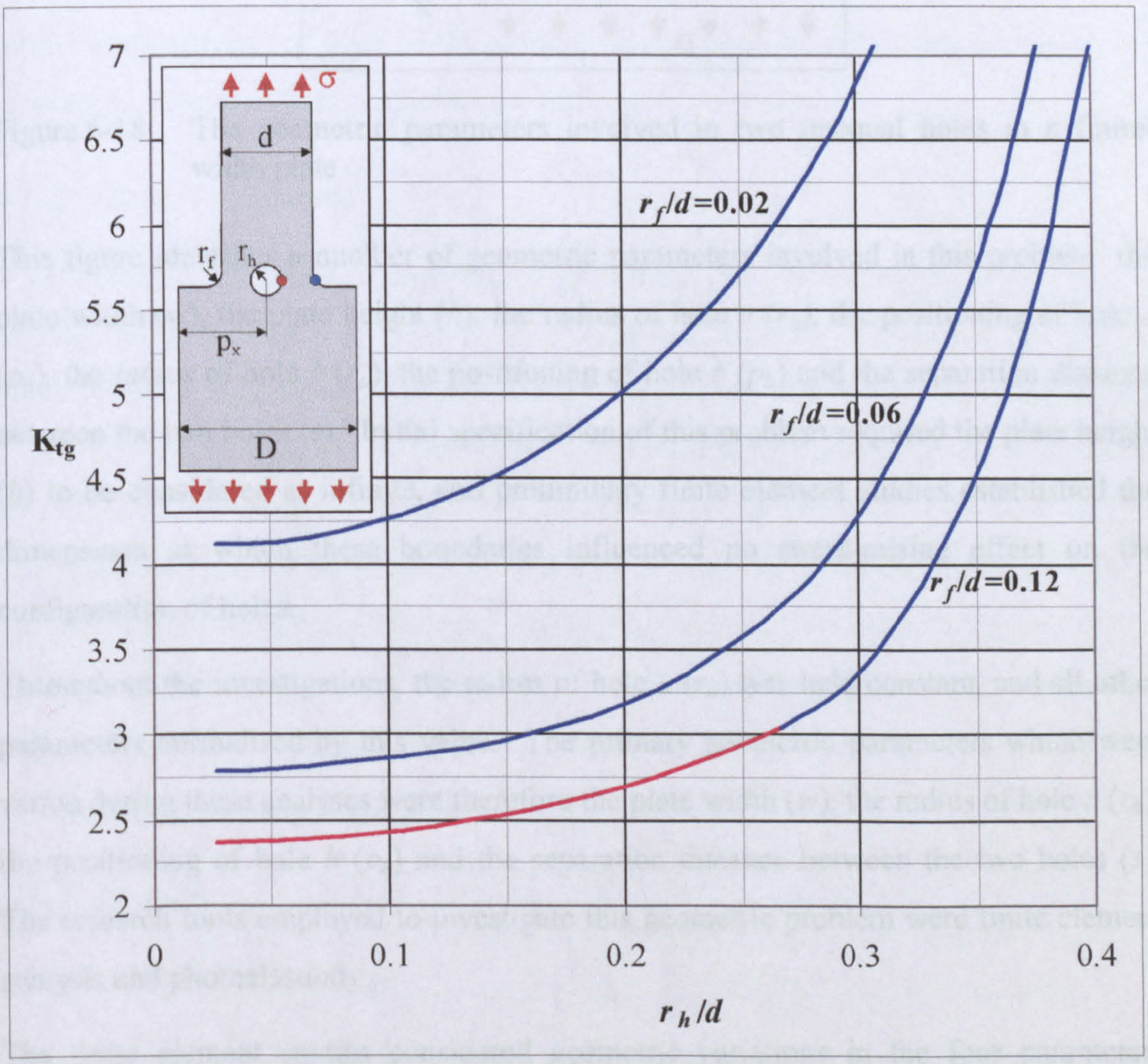

Figure 6-17. Position and magnitude of the maximum stress concentration for values of shoulder fillet radius (r_f) and hole radius (r_h), for D/d=2 and p_x=D/2

6.4 TWO HOLES IN PROXIMITY

6.4.1 Geometries Considered

Illustrated in Figure 6-18 is the feature interaction problem of two unequal holes positioned in a finite-width plate under tension.

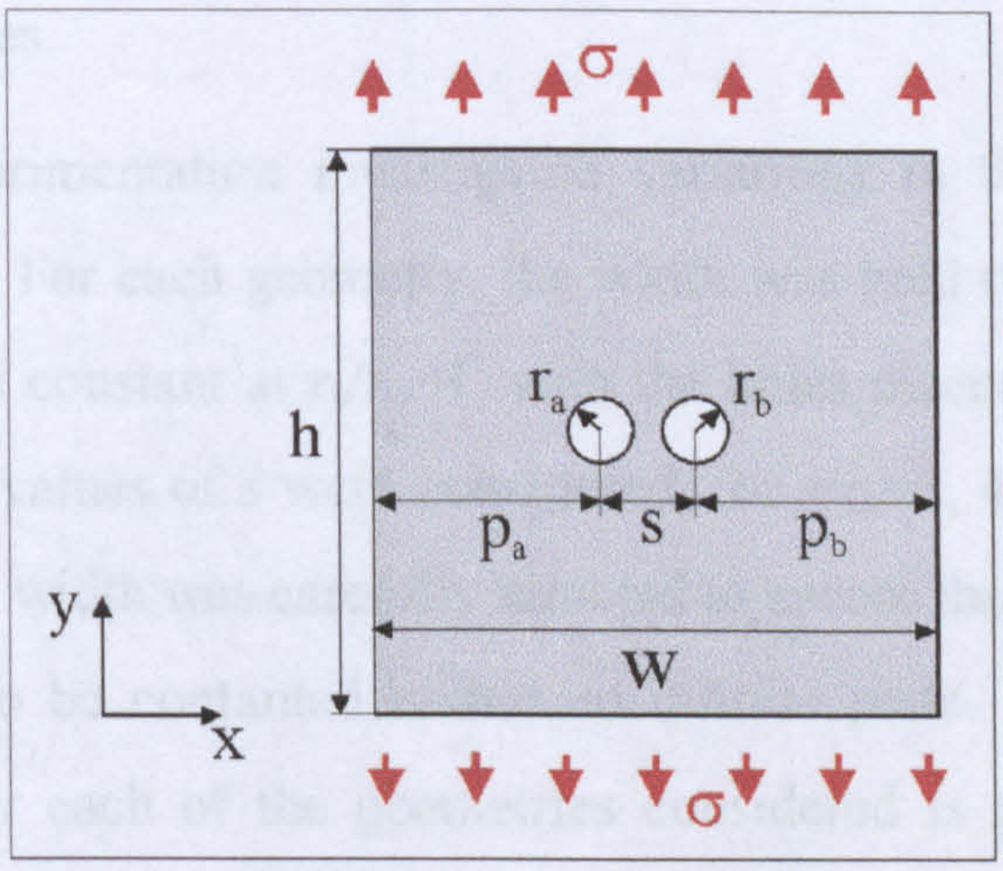

Figure 6-18. The geometric parameters involved in two unequal holes in a finite-width plate

This figure identifies a number of geometric parameters involved in this problem: the plate width (w), the plate height (h), the radius of hole a (r_a), the positioning of hole a (p_a), the radius of hole b (r_b), the positioning of hole b (p_b) and the separation distance between the two holes (s). Initial specification of this problem required the plate height (h) to be considered as infinite, and preliminary finite element studies established the dimensions at which these boundaries influenced no stress-raising effect on the configuration of holes.

Throughout the investigations, the radius of hole a (r_a) was held constant, and all other parameters normalised by this value. The primary geometric parameters which were varied during these analyses were therefore the plate width (w), the radius of hole b (r_b), the positioning of hole b (p_b) and the separation distance between the two holes (s). The research tools employed to investigate this geometric problem were finite element analysis and photoelasticity.

The finite element studies considered geometric variations in the four parameters described above (w, r_b, p_b and s). Six values of the plate width were investigated, for w/r_a=10, 12, 14, 16, 18 and 20. Seven values of the positioning of hole b were

considered, for p_b/r_a=2, 3, 4, 5, 6, 7 and 8. In addition, five values of the hole separation s were investigated, for s/r_a =2, 3, 4, 5 and 6. For each of these geometric configurations, a series of ratios of r_b:r_a was considered, ranging from r_b/r_a=0.4 to r_b/r_a=4 where appropriate, in increments of r_b/r_a=0.2. A total of over eight hundred finite element models were generated, and data collected for the position and magnitude of the maximum stress concentration, along with ligament stress concentration plots between the two features.

The photoelastic experimentation investigated variations in the separation distance between the holes (s). For each geometry, the width was held constant at w/r_a=30 and the ratio r_b:r_a was held constant at r_b/r_a=1, with the holes placed symmetrically within the plate width. Four values of s were considered, for s/r_a=3, 4, 5 and 6. For each of these models, the plate width was carefully selected to ensure that the geometry of holes could be considered to be contained within an infinite plate. An illustration of the model construction for each of the geometries considered is provided in Figure 5-4 Chapter 5. A total of four photoelastic models were investigated.

6.4.2 Data Validation

As discussed in Chapter 5, this particular geometry of feature interaction was utilised to validate the photoelastic procedures adopted in this research, through the comparison between these experimental results and an appropriate analytical treatment for two holes in an infinite plate (Haddon. 1967). After a series of experimental refinements, the disparity between the photoelastic results and those results generated by the analytical solution for this geometry was found to be within 0.8%. In addition, for those model configurations studied numerically, for which the plate width could be considered as infinite (i.e. p_a>11r_a and p_b>11r_b), the finite element results were also found to be within 1.3% of the analytical treatment. Further details of this validation process are provided in Chapter 5.

6.4.3 Results

6.4.3.1 Single Feature Data

Given in Figure 6-19 is a selection of the stress concentration decays from a single central hole in a finite-width plate under tension, measured along the section marked in red. Illustrated in this figure are the decays for a variety of plate thicknesses where

w/r_a=0.1, 0.15, 0.2, 0.25 and 0.3. For clarity, the case for which w/r_a=0.3 is illustrated in blue.

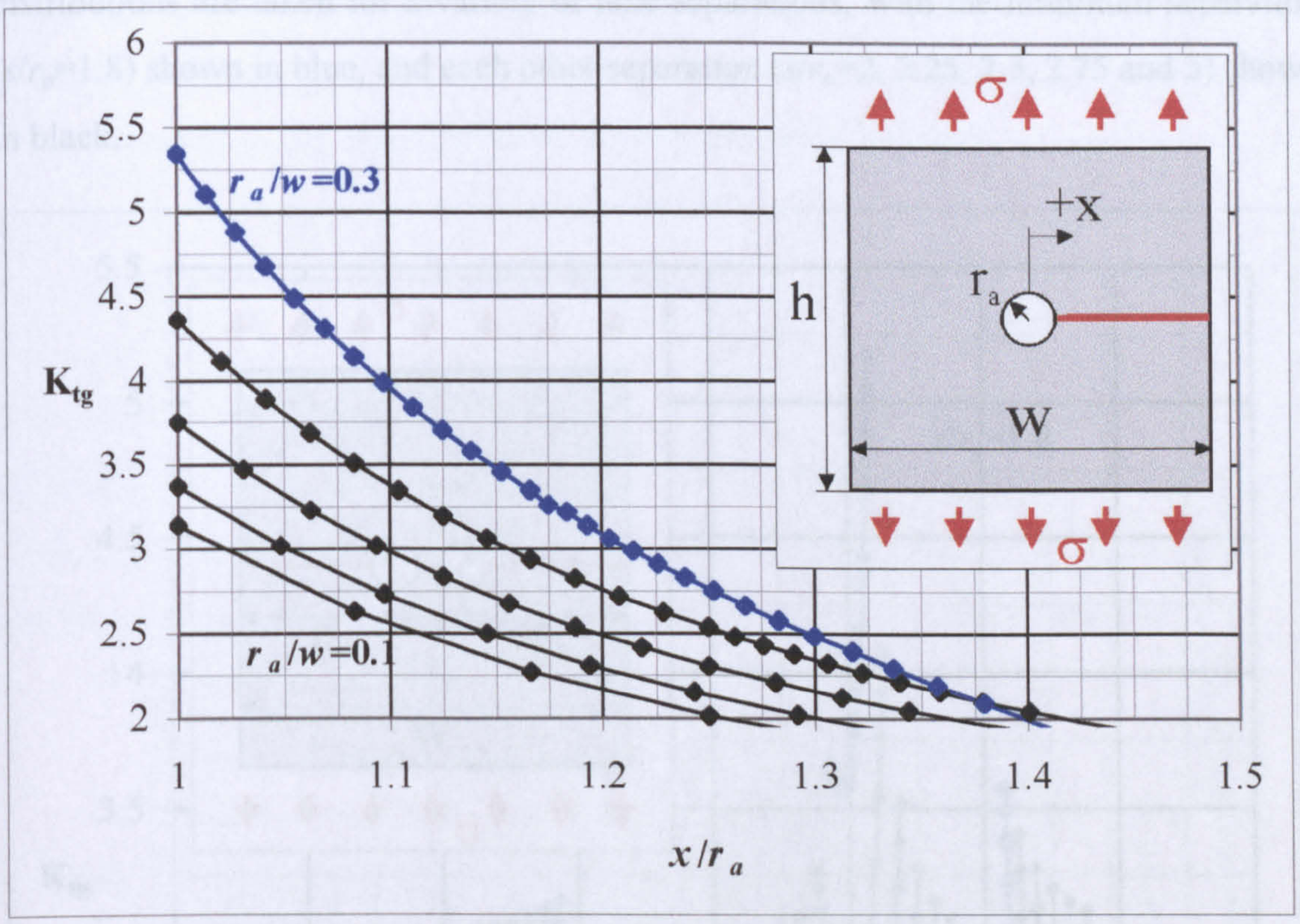

Figure 6-19. Stress concentration decay from a central hole in a finite-width plate, along the section marked in red, for r_a/w=0.1, 0.15, 0.2, 0.25 and 0.3

6.4.3.2 Ligament Stress Concentration Plots

Through the investigation of this geometric problem, it was established that the overall maximum stress concentration can occur at any one of four discrete points, at the edges of each of the holes along a line perpendicular to the applied stress. Ligament stress concentration plots were therefore taken through the entire nominal cross-section of the problem, in order to gain an understanding of the stress concentration decay surrounding each of these four points.

Due to the complexity of the stress concentration pattern taken through the entire nominal cross-section of the models, developing a clear display of these ligament data on a single graph proved difficult. Therefore, the following figures illustrate only small samples of the stress concentration distributions surrounding two interacting holes.

Figure 6-20 illustrates the variation in the ligament stress concentration distribution for two centrally-placed (p_a=p_b) holes contained within an infinite plate, with variable hole

separation (s). Ligament plots are taken along the section marked in red from the position (marked x) at the central point between the two holes. Stress concentration distributions are taken for a variety of hole separations, with the minimum separation (s/r_a=1.8) shown in blue, and each other separation (s/r_a=2, 2.25, 2.5, 2.75 and 3) shown in black.

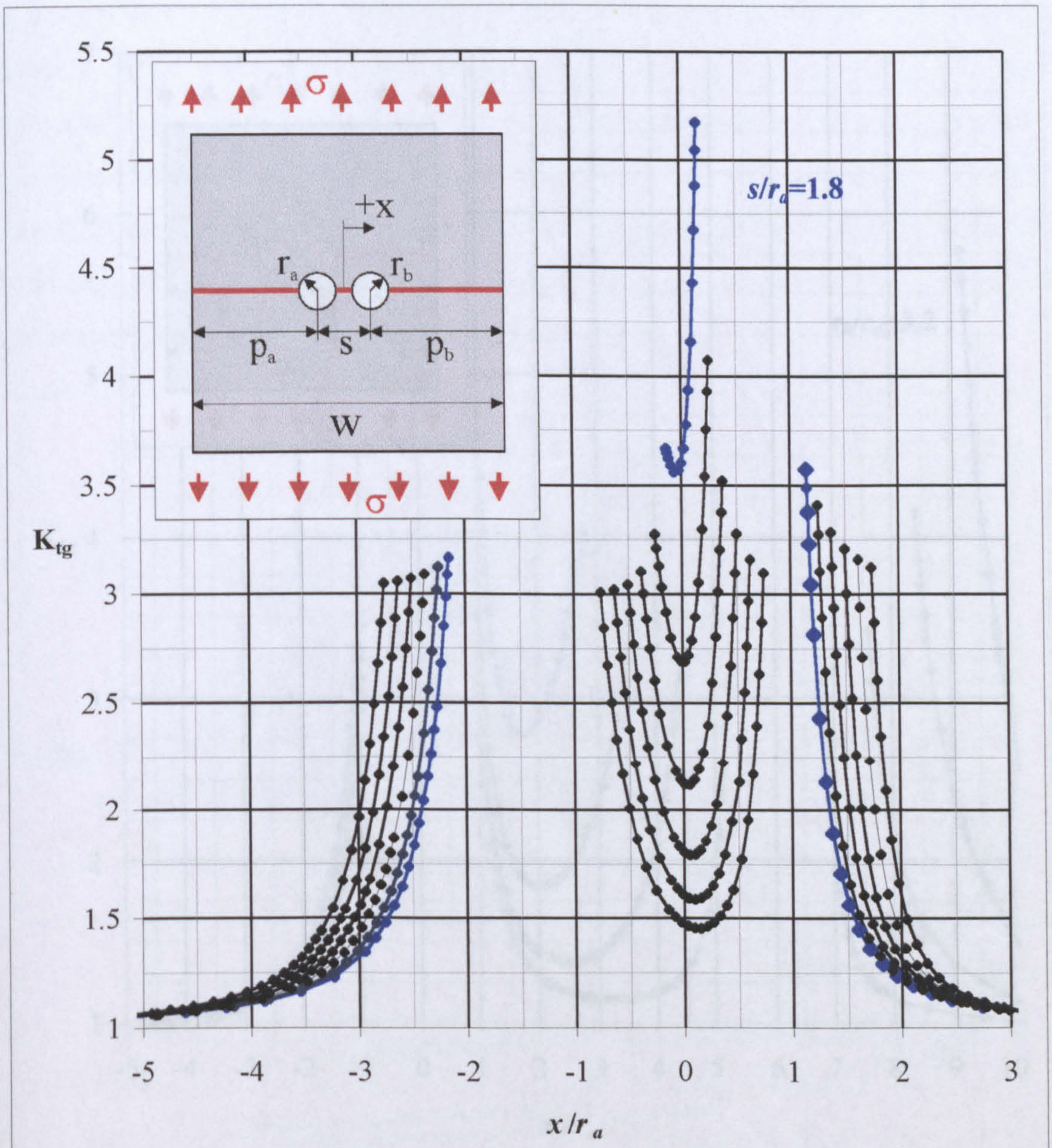

Figure 6-20. Ligament stress concentration plots for two centrally-placed (p_a=p_b) holes in an infinite plate, with constant hole radii (r_b/r_a=0.5). Plots are provided for a variety of hole separations where s/r_a=1.8, 2, 2.25, 2.5, 2.75 and 3, with the separation s=1.8 shown in blue

Figure 6-21 illustrates the variation in the ligament stress concentration for two centrally-placed (p_a=p_b) holes contained within a finite-width plate, for variation in the

radius of hole *b*. For this geometry, the plate width, hole positionings and hole separations are constant, where s/r_a=6, p_a/r_a= p_a/r_a=5 and w/r_a=16. Four different values of hole *b* radius are provided, where r_b/r_a=0.8, 1.6, 2.4 and 3.2, with the particular case of r_b/r_a=3.2 shown in blue. For clarity, the ligament plots, taken along the line marked in red, and referenced from the centre of hole *a*.

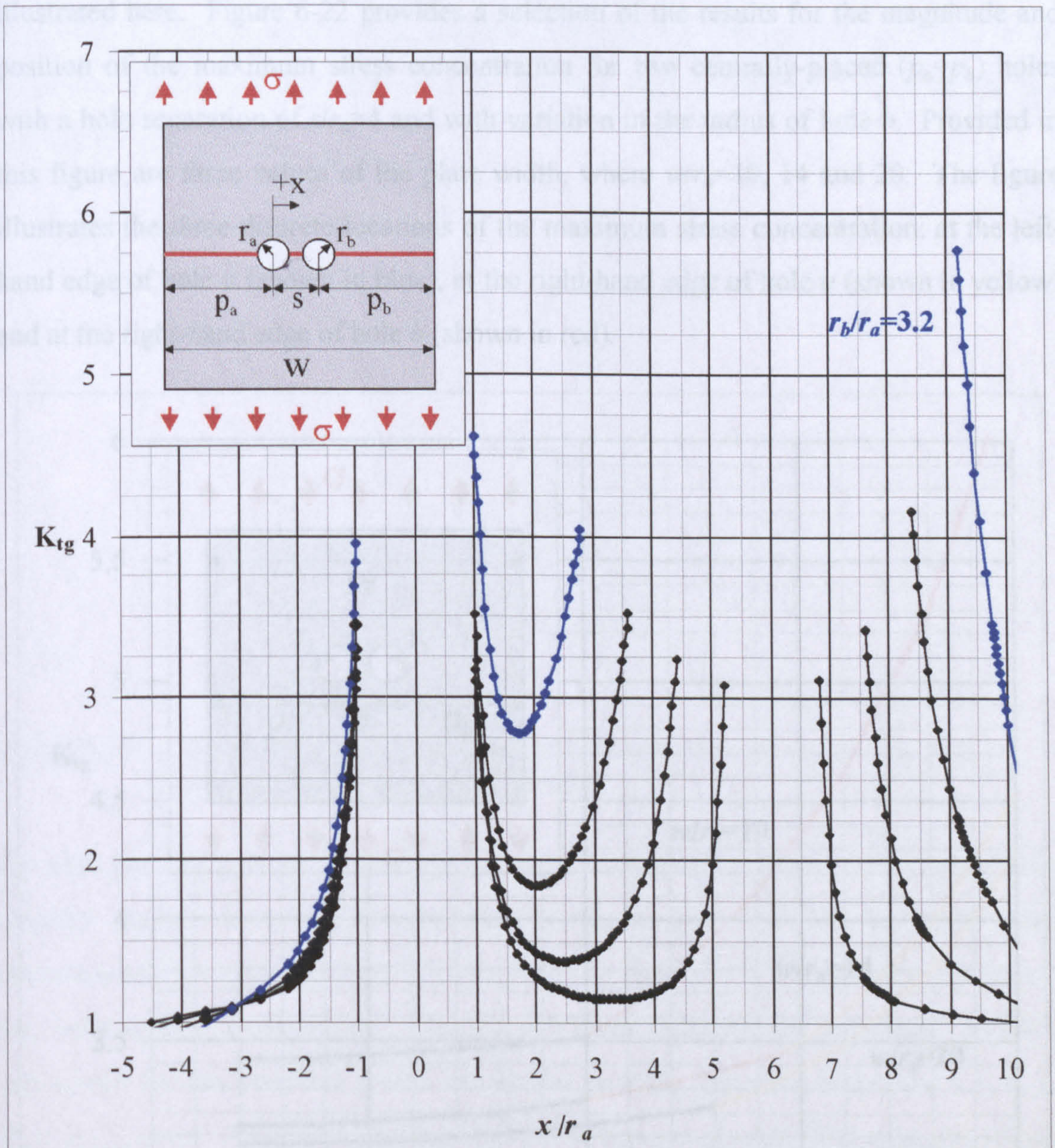

Figure 6-21. Ligament stress concentration plots for two centrally-placed (p_a=p_b) holes in a finite-width plate, with constant hole separation and plate width (s/r_a=6 and w/r_a=16). Plots are provided for a variety of radii of hole *b*, where r_b/r_a=0.8, 1.6, 2.4 and 3.2, with r_b/r_a=3.2 shown in blue

6.4.3.3 Maximum Stress Concentration

Due to the large volume of data collected for this feature combination, over a series of geometric parameters, the results generated for the overall maximum stress concentration required a large number of graphs for their clear presentation. For this reason, only a very small sample of the maximum stress concentration data can be illustrated here. Figure 6-22 provides a selection of the results for the magnitude and position of the maximum stress concentration for two centrally-placed (p_a=p_b) holes with a hole separation of s/r_a=4 and with variation in the radius of hole b. Provided in this figure are three values of the plate width, where w/r_a=10, 14 and 20. The figure illustrates the three discrete locations of the maximum stress concentration: at the left-hand edge of hole a (shown in blue), at the right-hand edge of hole a (shown in yellow) and at the right-hand edge of hole b (shown in red).

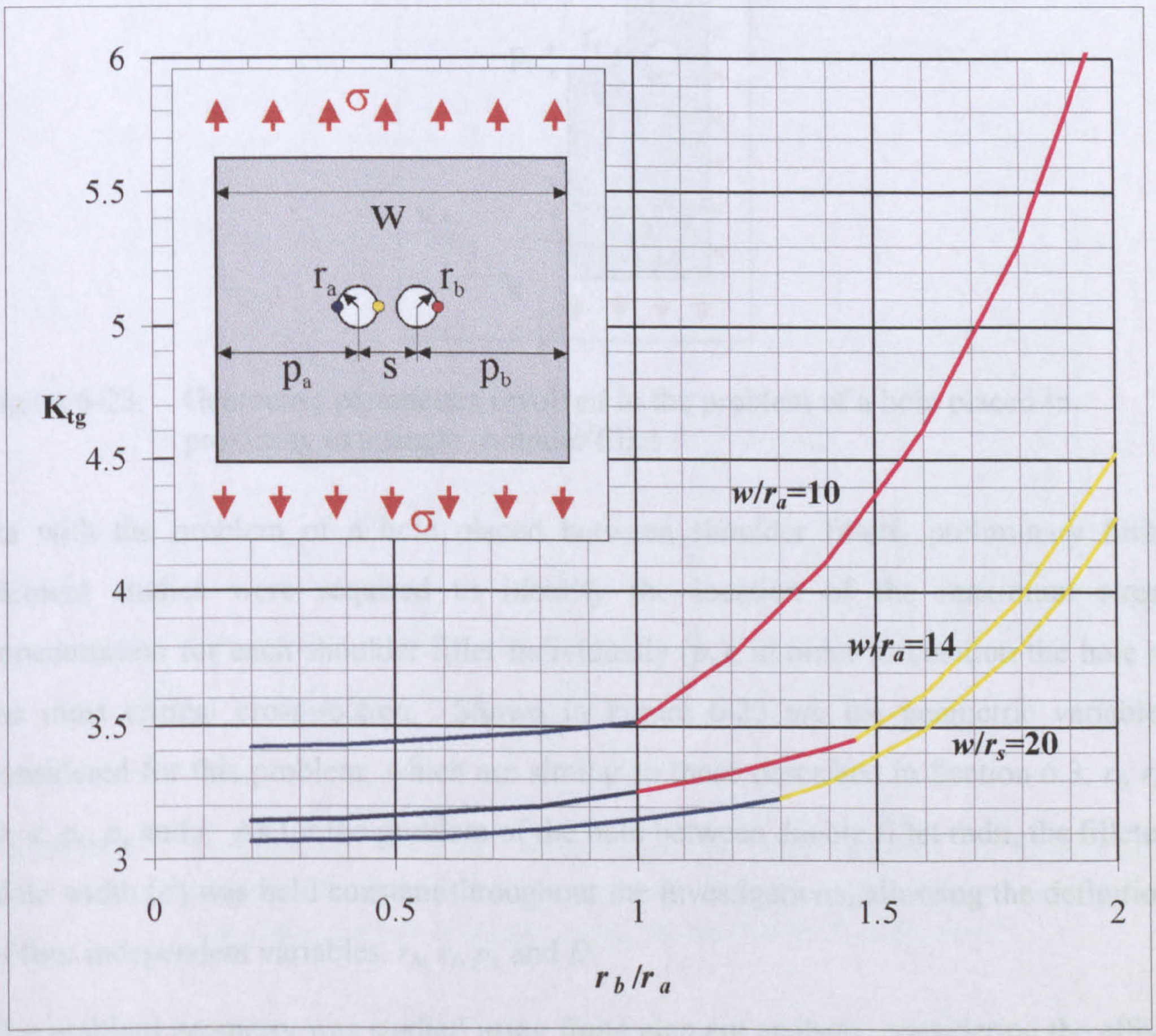

Figure 6-22. Position and magnitude of the maximum stress concentration for a constant hole separation (s/r_a=4) over a range of radii of hole b, and for a variety of values of plate width (w/r_a=10, 14 and 20)

6.5 HOLE IN PROXIMITY TO A SINGLE SHOULDER FILLET

6.5.1 Geometries Considered

The problem of a hole in proximity to a shoulder fillet is illustrated in Figure 6-23. This geometry has been identified as a particular case found in integrally machined sections, under y-direction applied load, with the vertical face constrained in the x-direction (Trevelyan et al. 2001).

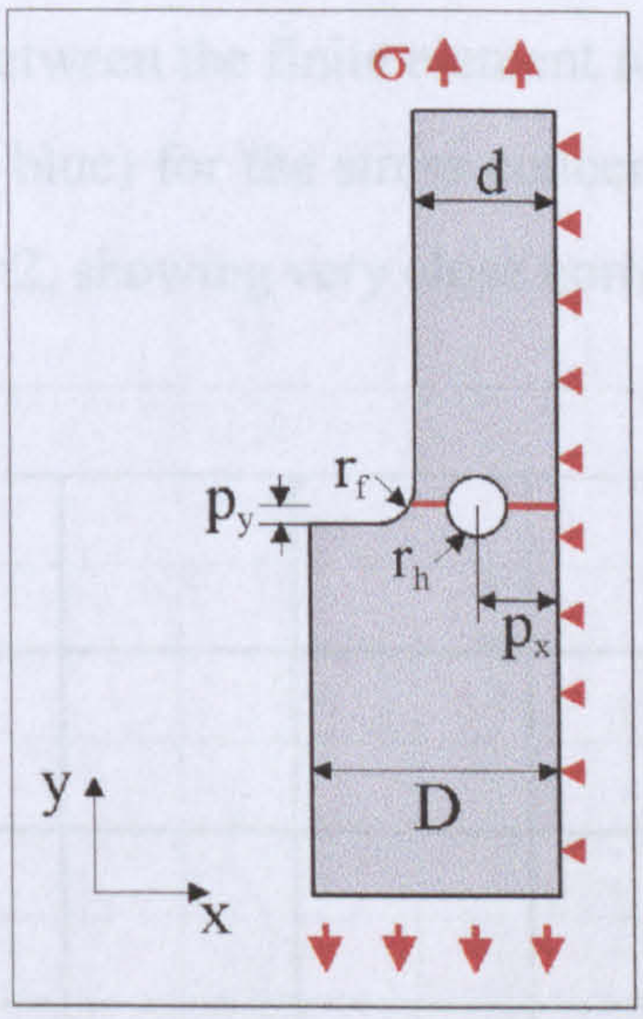

Figure 6-23. Geometric parameters involved in the problem of a hole placed in proximity to a single shoulder fillet

As with the problem of a hole placed between shoulder fillets, preliminary finite element studies were required to identify the location of the maximum stress concentration for each shoulder fillet individually (p_y), in order to position the hole at the most critical cross-section. Shown in Figure 6-23 are the geometric variables considered for this problem, which are similar to those described in Section 6.3; r_f, r_h, D, d, p_x, p_y and l. As for the problem of the hole between double fillet radii, the filleted plate width (d) was held constant throughout the investigations, allowing the definition of four independent variables: r_h, r_f, p_x and D.

The problem geometry was studied using finite element analysis, considering the effect of variations in each of the parameters r_h, r_f, p_x and D. Eight ratios of r_h:d were investigated, r_h/d=0.05, 0.1, 0.15, 0.2, 0.25, 0.3, 0.35 and 0.4. Fourteen ratios of r_f:d were considered, r_f/d=0.05, 0.06, 0.1, 0.12, 0.15, 0.18, 0.2, 0.24, 0.25, 0.3, 0.35, 0.36,

0.4 and 0.42. In addition, six horizontal hole positions were considered, p_x/d=0.4, 0.48, 0.56, 0.64, 0.72 and 0.8. Finally, the two most common ratios of D:d were analysed D/d=2 and 1.5. Over five hundred models were investigated, again with records taken of the appropriate ligament plots and details of the maximum stress concentration.

6.5.2 Data Validation

Due to the x-direction constraints on the vertical face of this model (see Figure 6-23), the simple geometry of the single shoulder fillet with no hole present can be analysed in the same fashion as the problem of double shoulder fillets containing no hole. Given in Figure 6-24 is a comparison between the finite element results (shown in black) and the photoelastic results (shown in blue) for the stress concentration decay from a shoulder fillet where r_f/d=0.06 and D/d=2, showing very close correlations (<0.9% error).

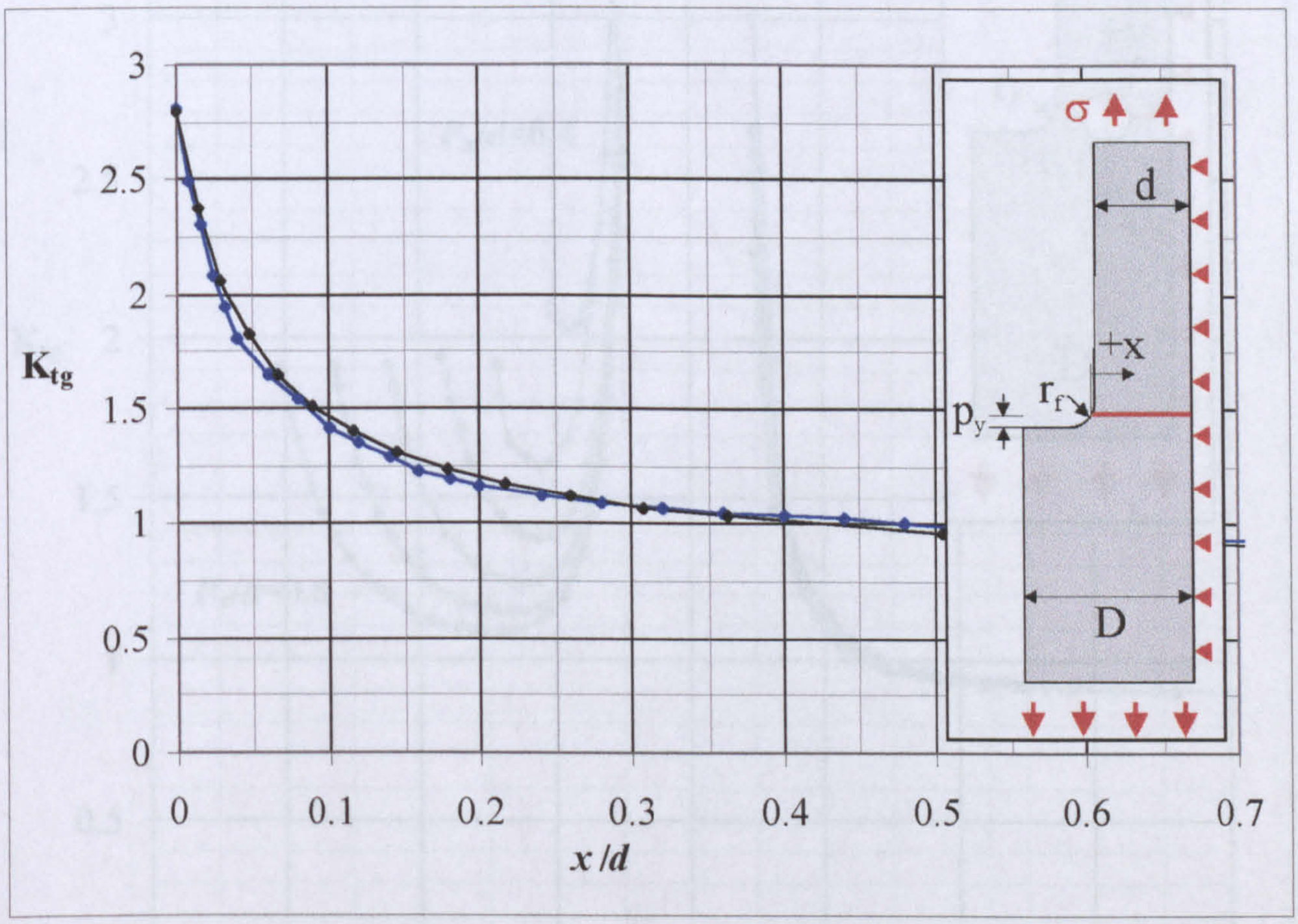

Figure 6-24. Comparison between finite element data (shown in black) and photoelastic results (shown in blue) for a ligament stress concentration plot along section marked in red, where r_f/d=0.06 and D/d=2

6.5.3 Results

6.5.3.1 Ligament Stress Concentration Plots

Given in Figure 6-25 is a selection of ligament stress concentration plots (along the line shown in red) for variations in the hole positioning (p_x) where r_h/d=0.1, r_f/d=0.4 and for values of p_x/d=0.4, 0.48, 0.56, 0.64, 0.72 and 0.8 (when x is measured in each case from the hole centre).

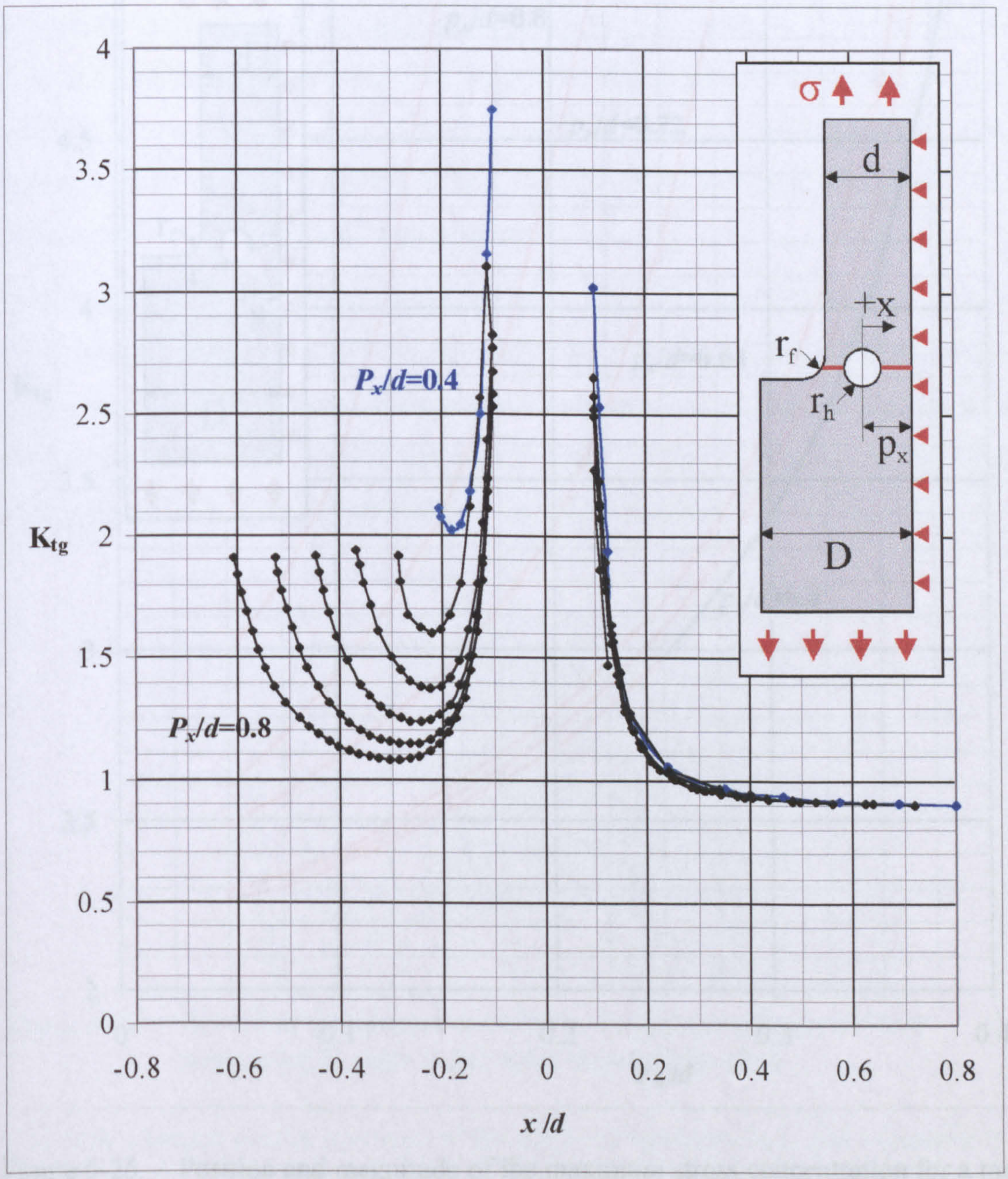

Figure 6-25. Ligament stress concentration plots for variable horizontal hole position (p_x), along sections marked in red, for r_h=0.1d and r_f=0.4d. Plots are provided for the hole positions, p_x/d=0.4, 0.48, 0.567, 0.64, 0.72 and 0.8, with the position p_x/d =0.4 marked in blue for clarity

6.5.3.2 Maximum Stress Concentration

Figure 6-26 illustrates the variation in the magnitude and position of the maximum stress concentration for variations in the hole radius (r_h) and the hole positioning (p_x) for values of D/d=2 and r_f/d=0.2. Six geometries of hole position are illustrated in this figure p_x/d=0.4, 0.48, 0.567, 0.64, 0.72 and 0.8.

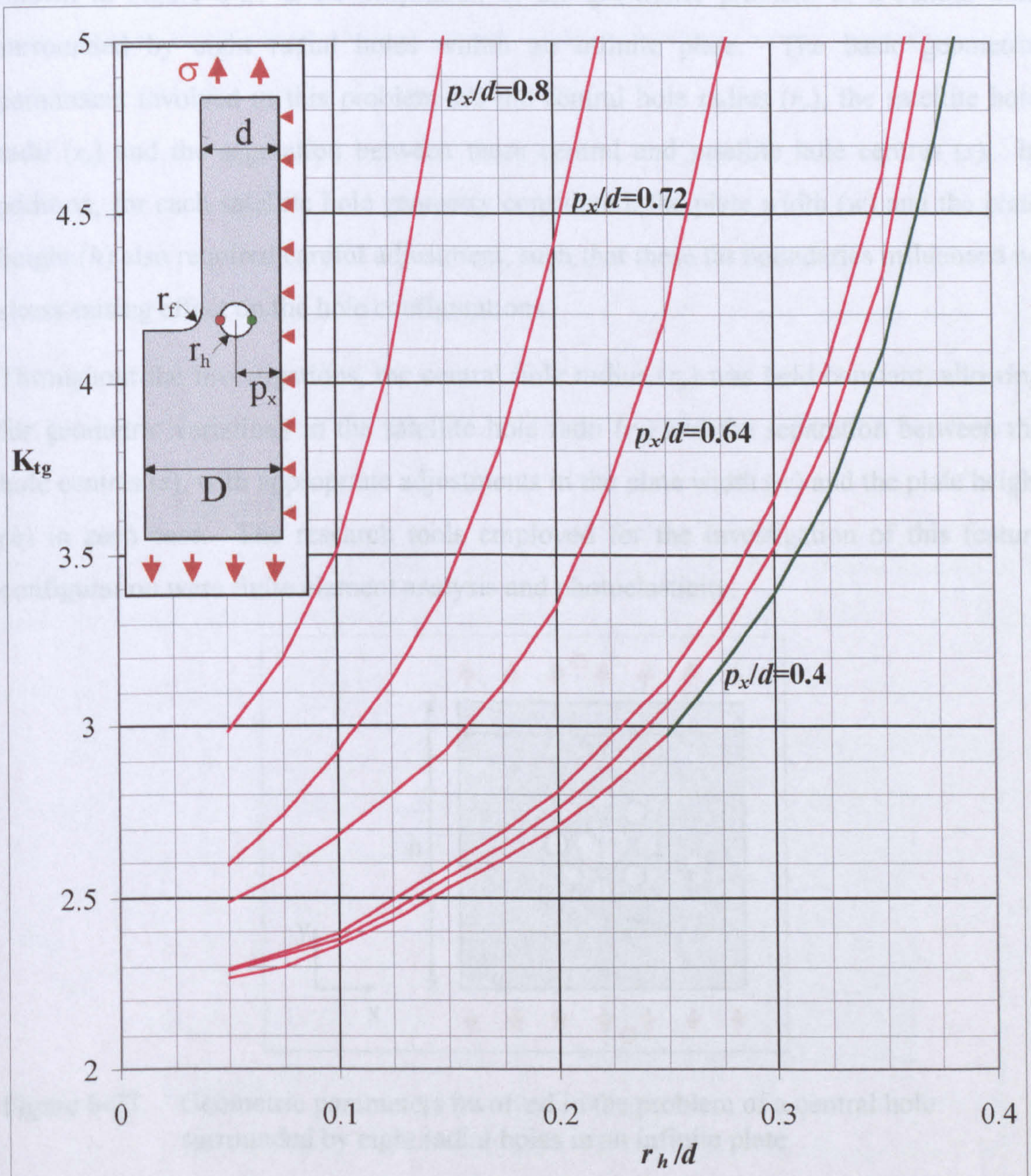

Figure 6-26. Position and magnitude of the maximum stress concentration for a range of values of hole positioning (p_x) and hole radius (r_h), for D/d=2, r_f/d=0.2 and p_x/d=0.4, 0.48, 0.567, 0.64, 0.72 and 0.8

6.6 CENTRAL HOLE SURROUNDED BY EIGHT SATELLITE HOLES

6.6.1 Geometry Considered

Shown in Figure 6-27 is an illustration of the geometric problem of a central hole surrounded by eight radial holes within an infinite plate. The basic geometric parameters involved in this problem are the central hole radius (r_c), the satellite hole radii (r_s) and the separation between these central and satellite hole centres (s). In addition, for each satellite hole geometry considered, the plate width (w) and the plate height (h) also required careful adjustment, such that these far boundaries influenced no stress-raising effect on the hole configurations.

Throughout the investigations, the central hole radius (r_c) was held constant, allowing for geometric variations in the satellite hole radii (r_s) and the separation between the hole centres (s), with appropriate adjustments in the plate width (w) and the plate height (h) in each case. The research tools employed for the investigation of this feature configuration were finite element analysis and photoelasticity.

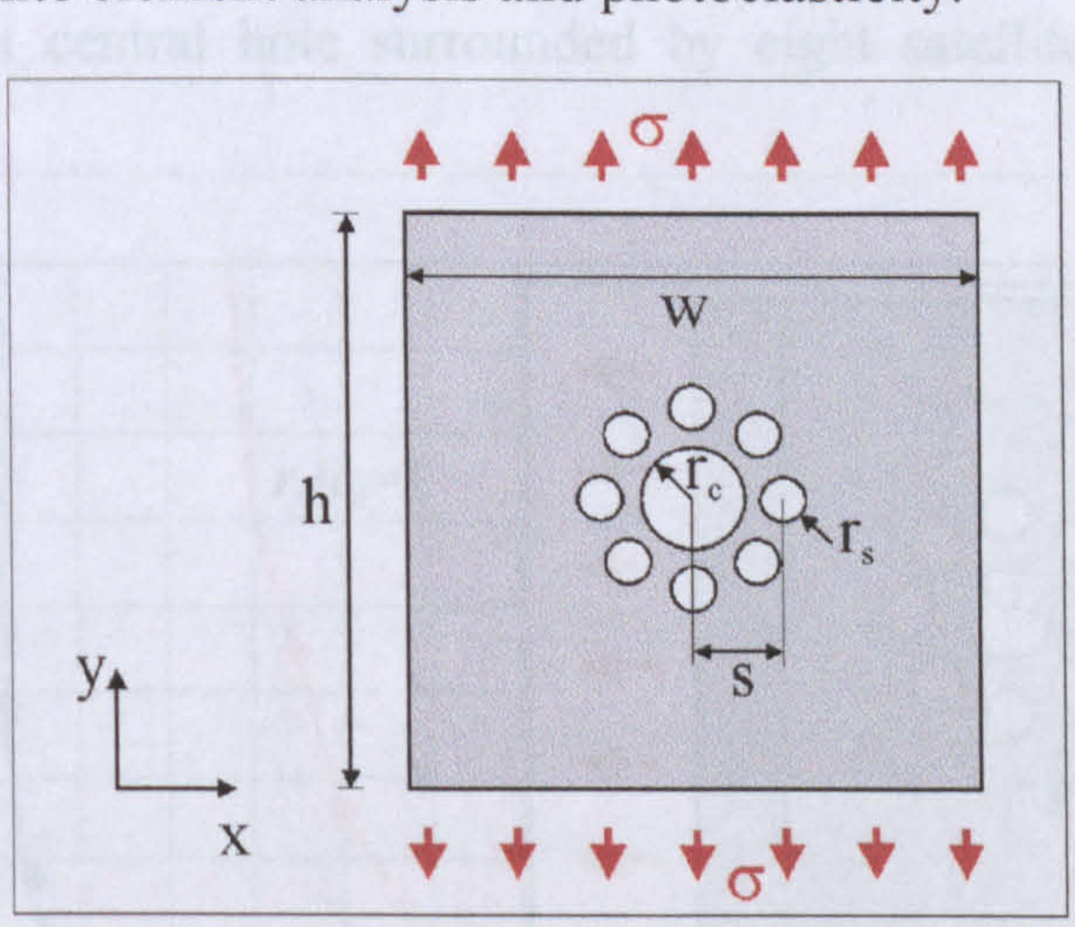

Figure 6-27. Geometric parameters involved in the problem of a central hole surrounded by eight radial holes in an infinite plate

The finite element studies investigated the effect of variations in r_s and s (relative to r_c) on the position, magnitude and direction of the maximum stress concentration. In addition, stress concentration distribution plots were also taken around the circumference of the holes displaying the high stress concentration values. Five separate ratios of r_s:r_c were considered, r_s/r_c=0.25, 0.5, 1, 2 and 4. For each of these

hole dimensions, a total of twenty five hole separation distances (s) were considered, ranging from $s=20r_c$ to $s=1.2(r_c+r_s)$. A total of one hundred and twenty five feature configurations were investigated. For each of these geometries, the plate width and height were incrementally varied to identify the point at which these dimensions no longer had a significant stress-raising influence on the geometry under consideration. This particular investigation was conducted for the enhancement of the final methodology, providing the fatigue analyst with an awareness of the constraints of the member dimensions, when defining an infinite plate.

The photoelastic studies considered variations in the parameters r_c and r_s. Throughout the investigations both the ratio $r_s:r_c$ and the separation between the central and satellite hole (s), were held constant. Two photoelastic models were constructed, for the investigation of two ratios of $r_s:r_c$, where r_s/r_c =0.5 and 1. Seven separate central and satellite hole radii were introduced to each model (for more details see Figure A-3, Appendix A). A total of fourteen models were considered for the photoelastic analysis.

6.6.2 Data Validation

Shown in Figure 6-28 is a comparison between a selection of the photoelastic and finite element results for a central hole surrounded by eight satellite holes. This figure

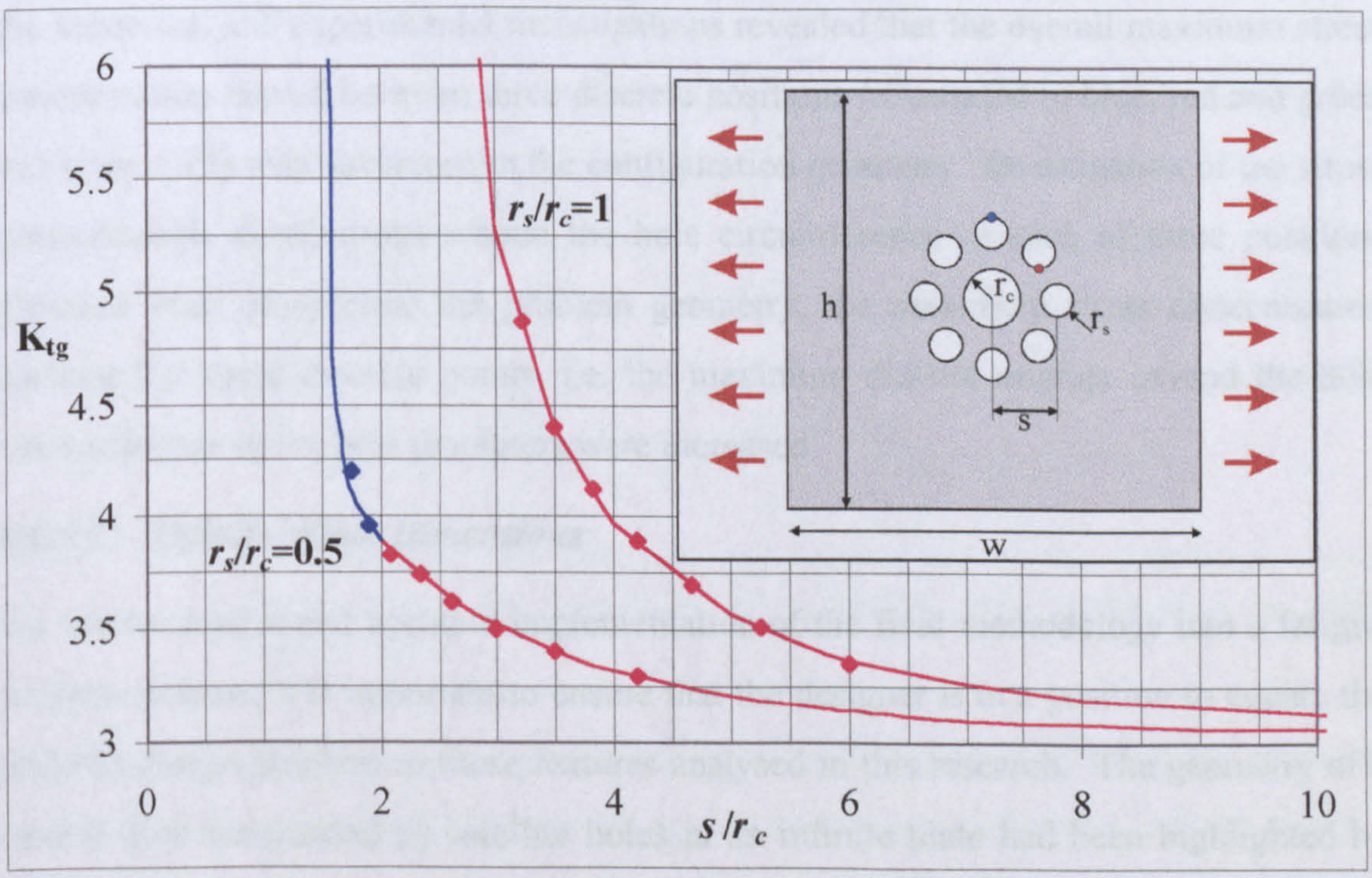

Figure 6-28. Comparison between photoelastic data (marked with a diamond symbol) and finite element data (marked with a line) for values of r_s/r_c=0.5 and 1

illustrates the photoelastic data (denoted by a diamond symbol) and the finite element data (shown by a continuous line) for two values of r_s:r_c (r_s/r_c=0.5 and 1) and over a range of values of s/r_c. Two discrete positions of the maximum stress concentration are illustrated in the figure, shown in blue and red. These results showed very close correlations between the two data sources, with a maximum discrepancy of 0.7%.

6.6.3 Results

Due to the configuration of this feature interaction geometry, the investigation of ligament stress concentration plots between adjacent holes was found to provide no meaningful information. Investigations of these geometries therefore involved the recording of stress concentration data (in both magnitude and direction) at a variety of points around the hole configurations, which were found to have regions of high stress. In addition, details of the stress concentration distribution around the circumference of the holes in regions of high stress was also taken.

6.6.3.1 Maximum Stress Concentration

Figure 6-29 illustrates the overall position and magnitude of the maximum stress concentration for a central hole surrounded by eight radial holes. The figure illustrates the maximum stress concentration values with variations in s and r_s. The results from the numerical and experimental investigations revealed that the overall maximum stress concentration moved between three discrete positions (illustrated in blue, red and green in Figure 6-29) with variations in the configuration geometry. Investigation of the stress concentration distributions around the hole circumference in each of these positions revealed that, irrespective the problem geometry, the maximum stress concentration remained at these discrete points, i.e. the maximum did not migrate around the hole circumference as the hole diameters were increased.

6.6.3.2 'Infinite' Plate Dimensions

For the successful and accurate implementation of the final methodology into a fatigue analysis process, it is important to ensure that the designer is in a position to equate the real-life design problem to those features analysed in this research. The geometry of a central hole surrounded by satellite holes in an infinite plate had been highlighted by BAE SYSTEMS as a particular geometric problem, occurring in such designs as

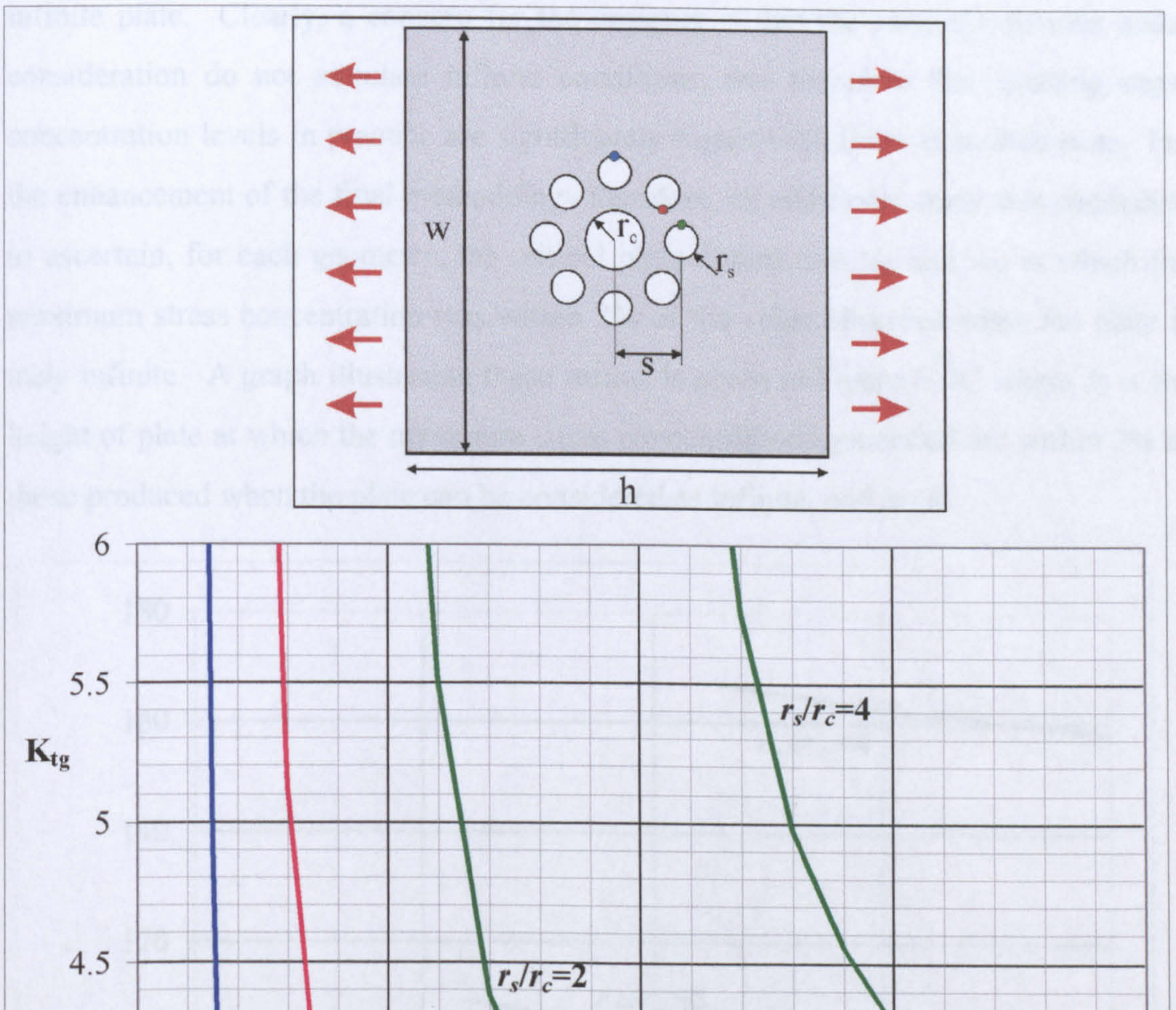

Figure 6-29. Illustration of the position and magnitude of the maximum stress concentration for geometries of a central hole surrounded by eight satellite holes

hydraulic pipe fastenings, access holes and equipment fastenings. During this research, the investigations of satellite hole problems therefore were designed to ensure, for each geometry, that the far boundaries of the plate exerted no stress-raising effect on the configurations of holes, such that the model could be assumed to be contained within an

infinite plate. Clearly, a concern for the designer is that the plate dimensions under consideration do not simulate infinite conditions, and therefore the resulting stress concentration levels in practice are significantly higher than those described here. For the enhancement of the final methodology therefore, an additional study was conducted to ascertain, for each geometry, the critical plate dimensions (h_i and w_i) at which the maximum stress concentration was within 2% of the value observed when the plate is truly infinite. A graph illustrating these results is given in Figure 6-30, where h_i is the height of plate at which the maximum stress concentrations generated are within 2% of those produced when the plate can be considered as infinite, and h_i=w_i.

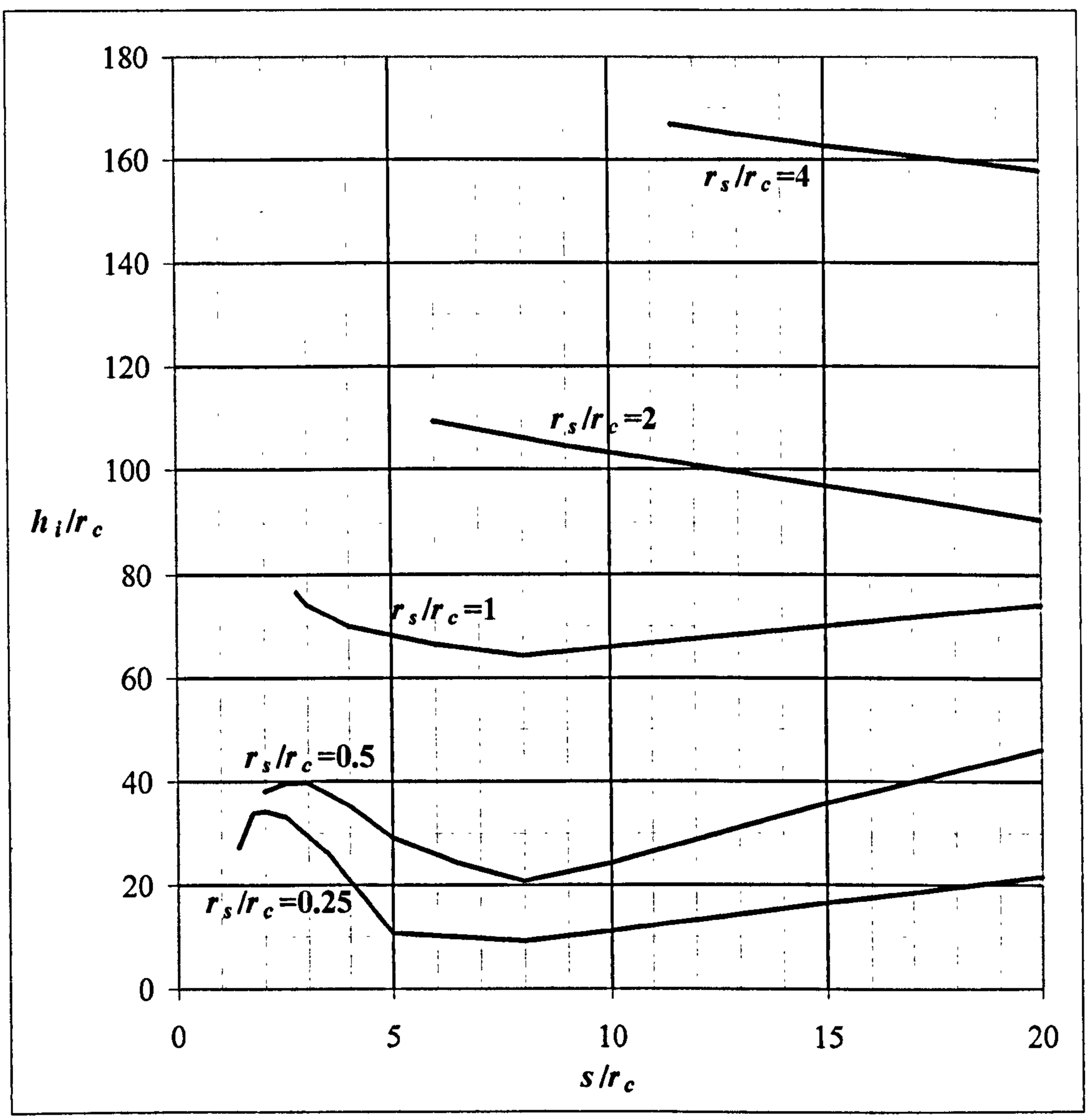

Figure 6-30. Plate height (h_i) at which the maximum stress concentration found at satellite hole geometries fall within 2% of those recorded values when the plate can be considered as infinite, where h_i=w_i

6.7 CENTRAL HOLE SURROUNDED BY FOUR SATELLITE HOLES

6.7.1 Geometry Considered

Illustrated in Figure 6-31 are the geometric parameters involved in the investigation of a central hole surrounded by four radial holes in an infinite plate. As with the problem involving eight radial holes, the basic geometric parameters for this problem are r_c, r_s and s, along with the variables w and h which require careful adjustment to ensure the simulation of 'infinite' conditions. Again, for the purposes of the investigations, the central hole radius (r_c) was held constant, allowing for relative variations in the parameters r_s, s, w and h.

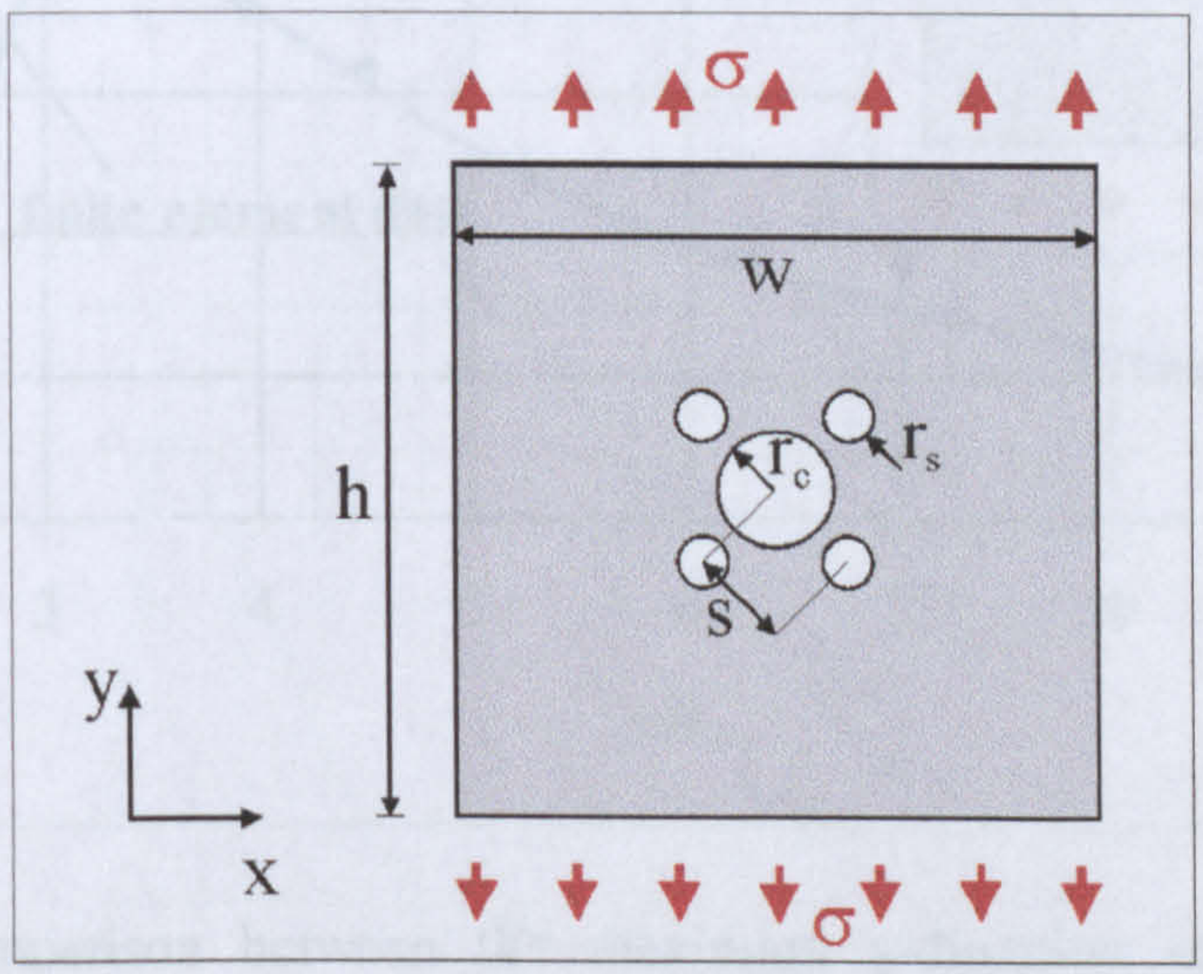

Figure 6-31. Illustration of the geometric problem of a central hole surrounded by four radial holes in an infinite plate

The investigations of this problem comprised photoelastic and finite element studies. For each of these techniques used, the geometries considered were equivalent to those investigated for the eight hole satellite problem (see Section 6.6.1). Therefore, the finite element investigations considered were for r_s/r_c=0.25, 0.5, 1, 2 and 4 and for values of s ranging from s=20r_c to s=1.2(r_c+r_s). The finite element studies also investigated the position of the maximum stress, stress concentration plots along the hole circumferences and the values of h and w for which the plate could be considered as infinite. Details of the photoelastic models considered are given in Figure A-4 Appendix A, which are again equivalent to those photoelastic geometries considered for the eight satellite hole problem.

6.7.2 Data Validation

Figure 6-32 illustrates a comparison between a sample of the photoelastic and finite element data for the case where r_s/r_c=1. This diagram illustrates not only close similarities (<0.8% error) between the magnitudes of the two sets of data, but also shows that both techniques identify the same maximum stress concentration position.

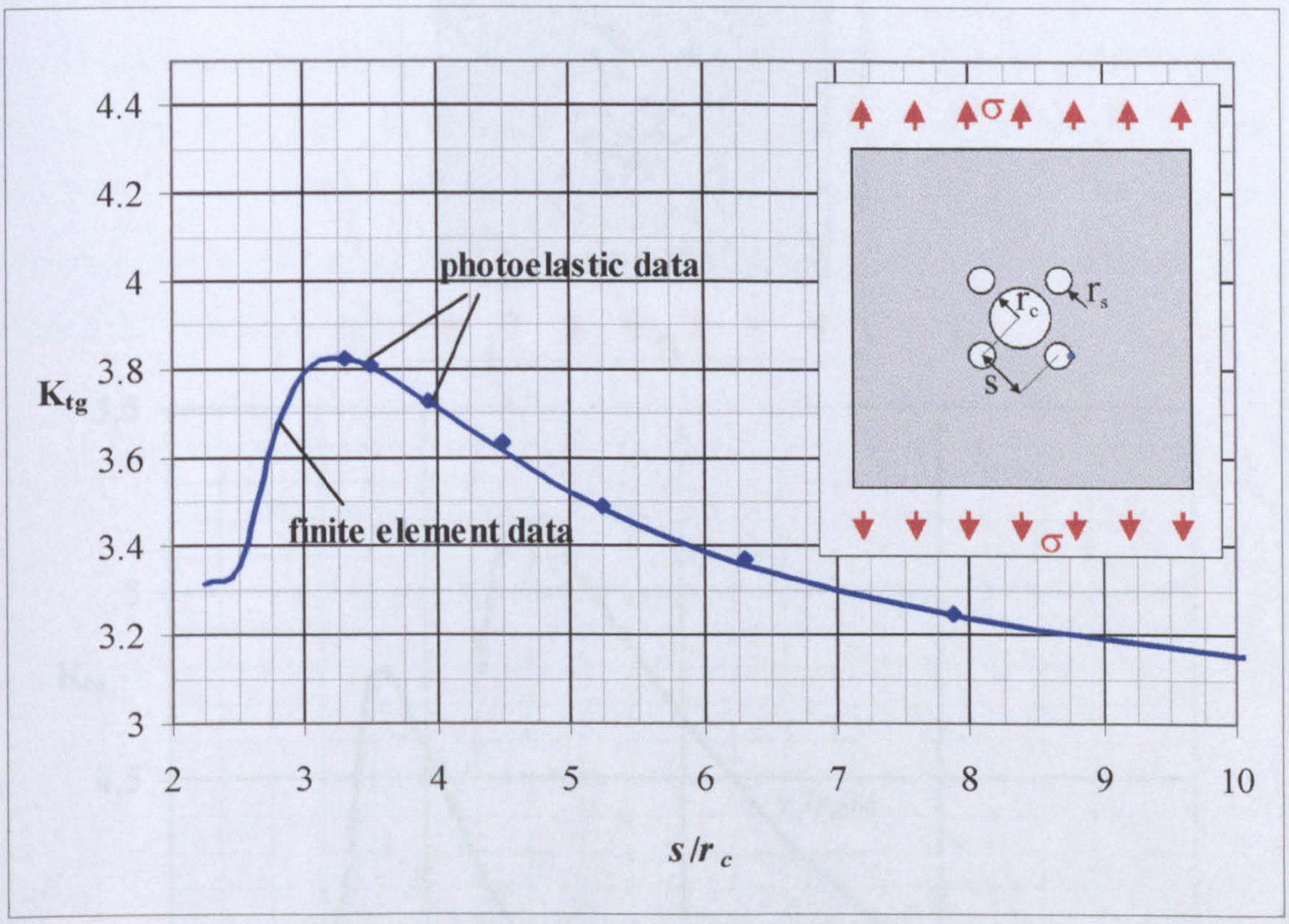

Figure 6-32. Comparison between the maximum y-direction stress concentration photoelastic and finite element results for r_s/r_c=1, for values of s/r_c

6.7.3 Results

The investigation of this problem geometry generated results in four main aspects: (i) the overall maximum stress concentration, (ii) the variation in the location of the points of high stress, (iii) the changes in the stress direction, and (iv) the definition of the plate width (w_i) and height (h_i) to ensure infinite conditions for the model. An overview of the results from each of these areas is given below.

6.7.3.1 Maximum Stress Concentration

Figure 6-33 illustrates both the position and magnitude of the maximum stress concentration for the geometry of a central hole surrounded by four radial holes, for

values of r_s/r_c=0.25, 0.5, 1, 2 and 4, and for a variety of hole separation distances (s/r_c). The values shown in this graph are for the y-direction maximum stress concentration.

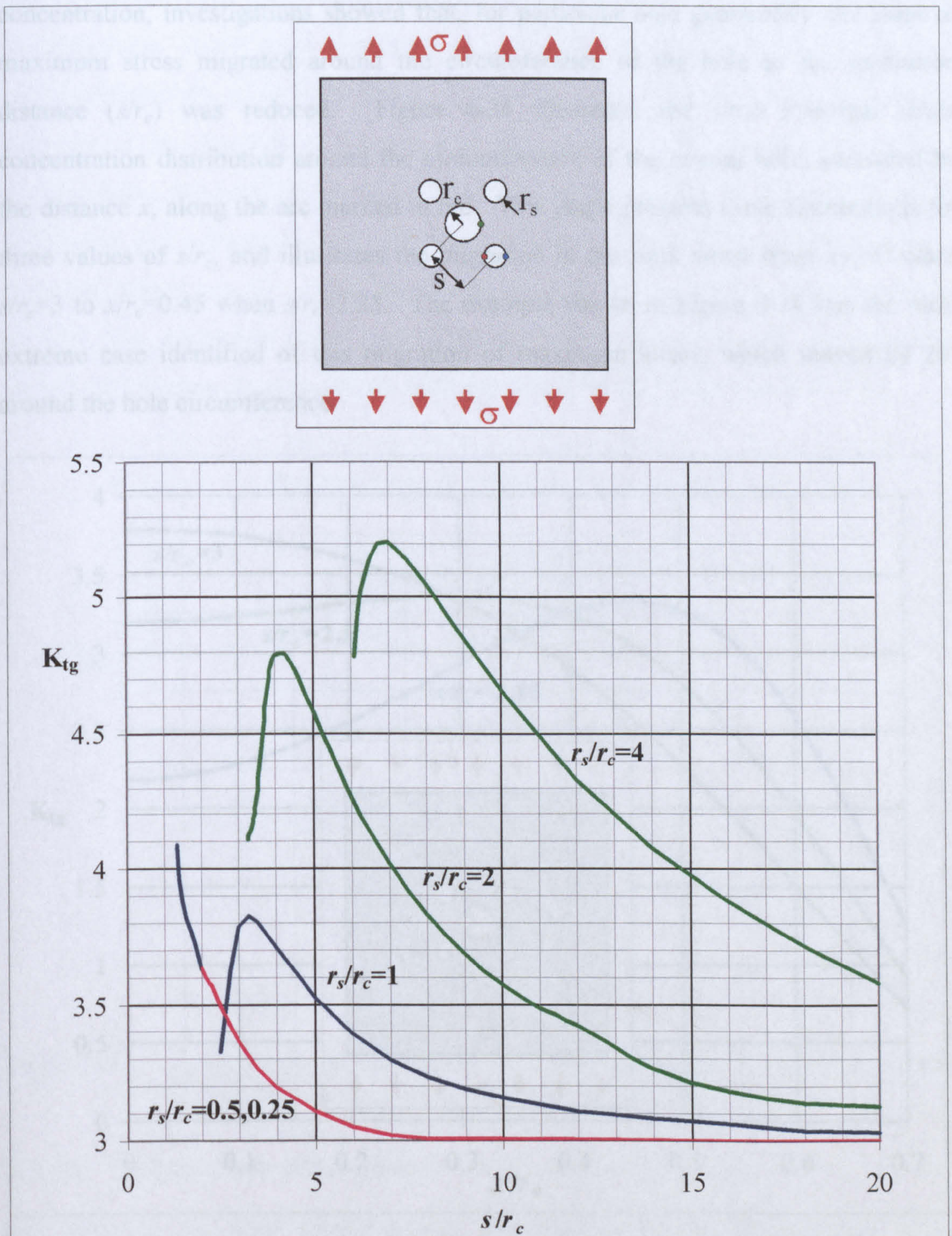

Figure 6-33. The position and magnitude of the maximum y-direction stress concentration for a central hole surrounded by four radial holes in an infinite plate

6.7.3.2 Location of the Maximum Stress

Although Figure 6-33 illustrates the general position of the maximum stress concentration, investigations showed that, for particular hole geometries, the point of maximum stress migrated around the circumference of the hole as the separation distance (s/r_c) was reduced. Figure 6-34 illustrates the First Principal stress concentration distribution around the circumference of the central hole, measured by the distance x, along the arc marked in red. This graph presents these distributions for three values of s/r_c, and illustrates the migration in the peak stress from x/r_c=0 when s/r_c=3 to x/r_c=0.45 when s/r_c=2.25. The example shown in Figure 6-34 was the most extreme case identified of this migration of maximum stress, which moved by 26° around the hole circumference.

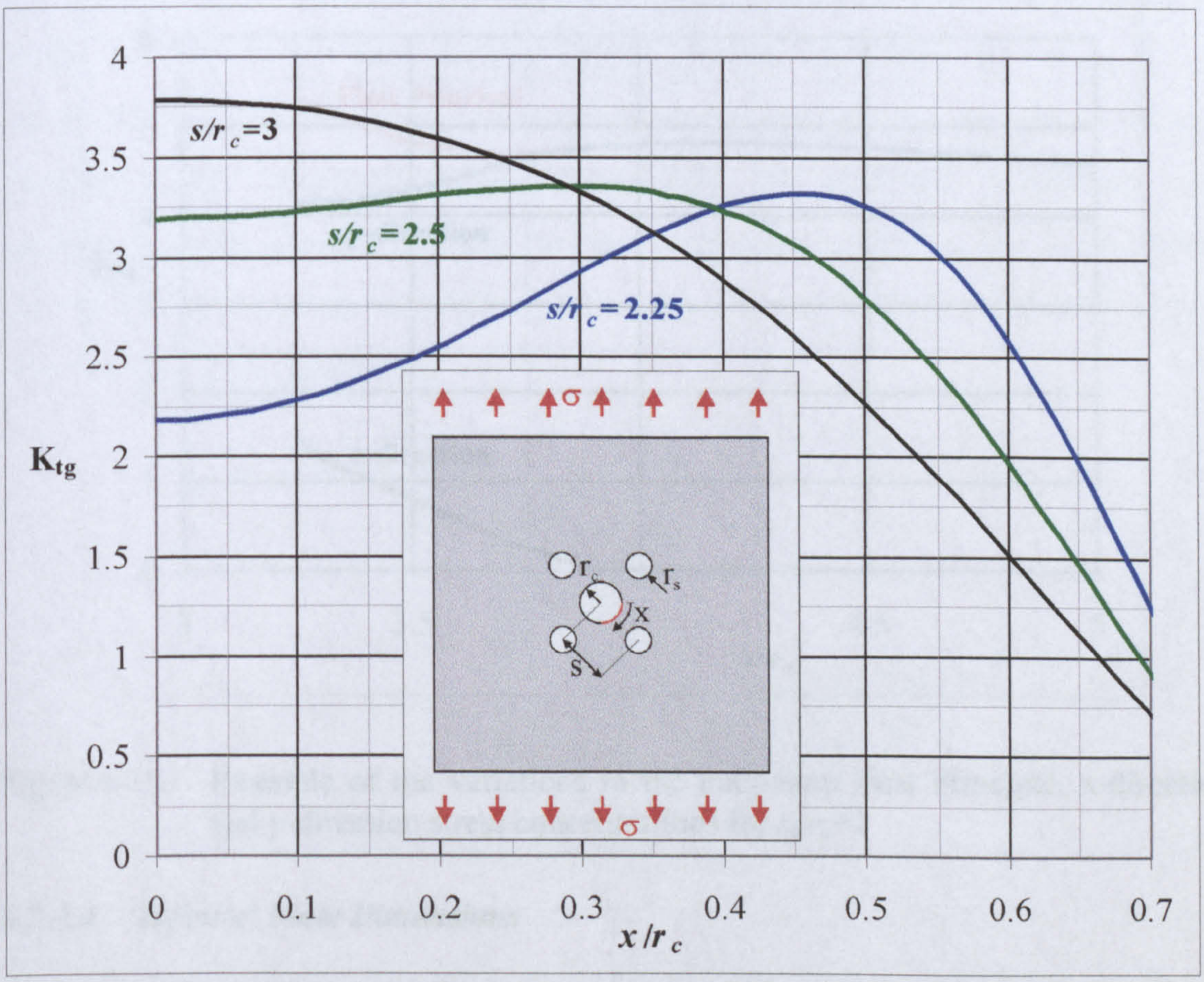

Figure 6-34. First Principal stress concentration distribution, along the hole circumference marked in red, for r_s/r_c=1, and s/r_c=2.25, 2.5 and 3

6.7.3.3 Variation in the Direction of the Maximum Stress

As discussed in the introduction to this chapter, for most geometries investigated, the direction of the maximum stress concentration was coincident with the y-direction of

the problem. In a number of geometries for the central hole surrounded by four radial holes, the point of maximum stress concentration migrated away from a boundary which was perpendicular to the direction of the applied stress, around the hole circumference. Under these conditions, it is unlikely that the direction of the stresses will continue to be in the y-direction. Therefore, it was important to investigate the variation in the direction of the stress as the separation distance between the hole configurations was reduced. Figure 6-35 illustrates the variation in the First Principal, x-direction and y-direction stress concentrations for changing hole separation (s/r_c) in geometry where r_s/r_c=2. This graphs shows that, for separation distances below s/r_c=3.9, the x-direction stress concentration becomes non-zero, and the y-direction stress concentration starts to deviate from the First Principal stress concentration.

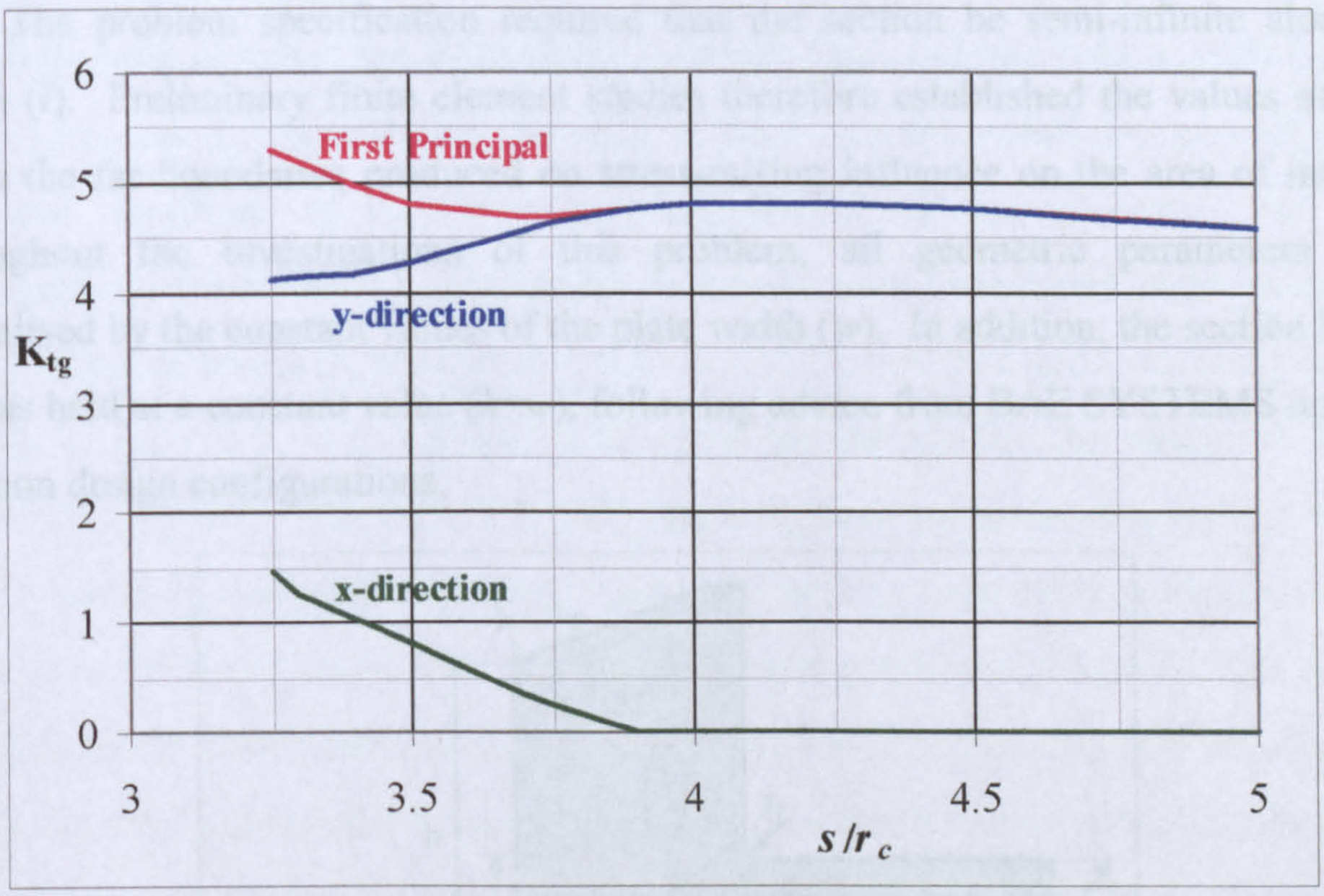

Figure 6-35. Example of the variations in the maximum First Principal, x-direction and y-direction stress concentrations for r_s/r_c=2

6.7.3.4 'Infinite' Plate Dimensions

For each of the hole configurations investigated, records were taken of the corresponding values of w and h for which the far boundaries had no significant influence on the interacting problem. In all cases, these 'infinite' plate dimensions (h_i and w_i) were found to be almost identical to those values illustrated in Figure 6-30.

6.8 TRANSVERSE HOLES IN PROXIMITY TO AN L-SECTION

6.8.1 Geometry Dimensions

Given in Figure 6-36 are the geometric parameters involved in the problem of two holes in opposite faces of a radiused L-section. This figure illustrates the nine geometric variables associated with the problem under investigation: the height of the vertical face (h), the section thickness (t), the width of the horizontal face (w), the section length (l), the radius of hole a (r_a), the positioning of hole a relative to the width (p_a), the radius of hole b (r_b), the positioning of hole b relative to the height (p_b) and the radius of the fillet (r_f). The problem specification required that the section be semi-infinite along its length (l). Preliminary finite element studies therefore established the values of l for which the far boundaries produced no stress-raising influence on the area of interest. Throughout the investigations of this problem, all geometric parameters were normalised by the constant values of the plate width (w). In addition, the section height (h) was held at a constant value (h=w), following advice from BAE SYSTEMS on most common design configurations.

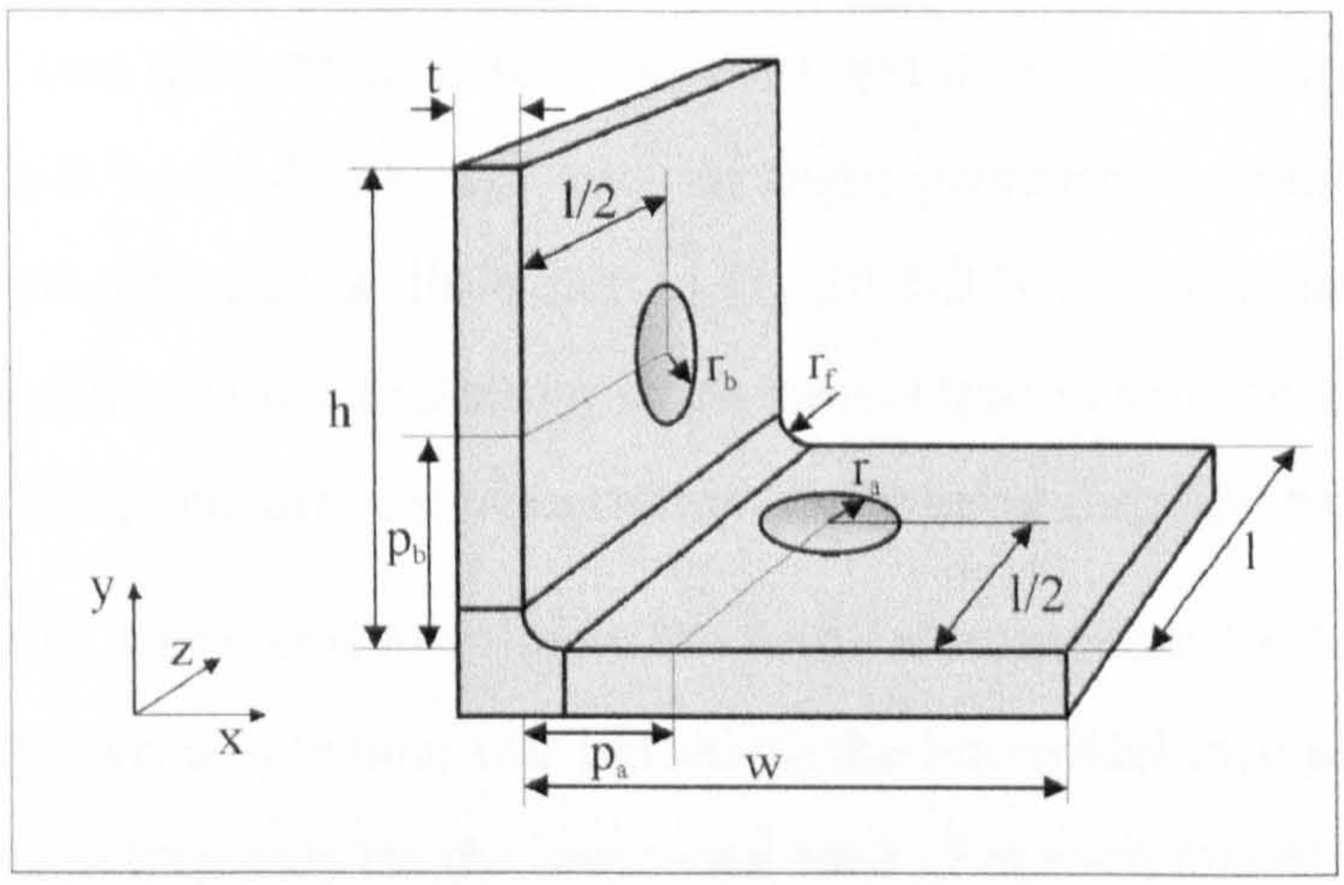

Figure 6-36. The geometric parameters involved in the three-dimensional problem of two holes in opposite faces of a radiused L-section

This problem was analysed under two separate states of loading, as specified by fatigue experts at BAE SYSTEMS. The loading conditions were for uni-axial tension along the length of the section, acting (i) on the whole cross-section of the L-section and (ii) acting on the horizontal face, as illustrated in Figure 6-37.

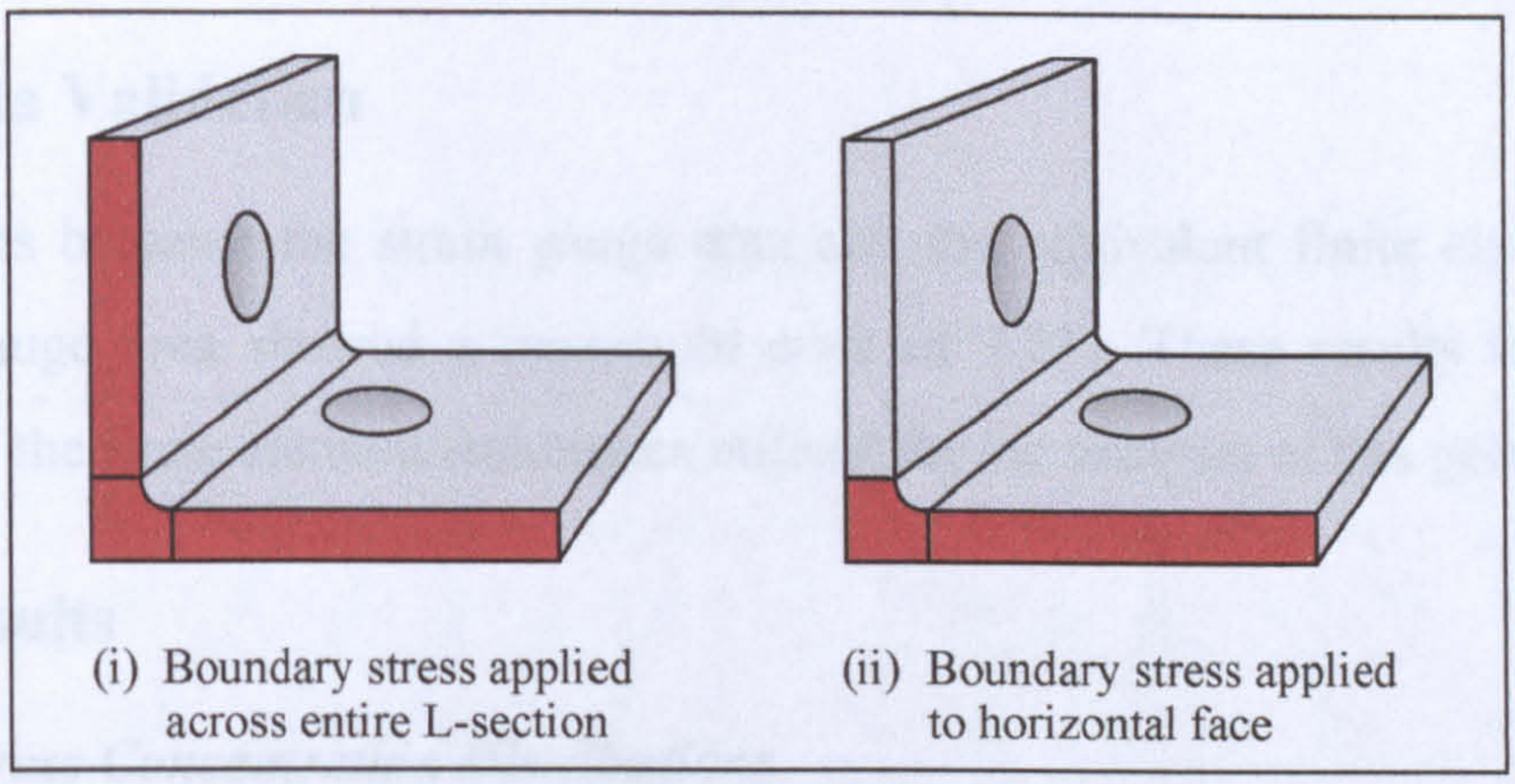

Figure 6-37. The two loading conditions considered during the analysis of this problem, with the stress applied normal to the faces marked

This interaction problem was analysed using finite element and strain gauge studies.

The finite element studies comprised three major components, for investigations of (i) one single hole in either the horizontal or vertical face, (ii) one hole in each face for which r_a=r_b and p_a=p_b, and (iii) one hole in each face for which any geometric and positional variations of the holes are independent of one another. For these investigations, the following geometrical variations were considered: eight geometries for the radius of hole a (r_a/w=0.05, 0.1, 0.15, 0.2, 0.25, 0.3, 0.35 and 0.4), four positions of hole a (p_a/w=0.2, 0.3, 0.4 and 0.5), eight geometries for the radius of hole b (r_b/w=0.05, 0.1, 0.15, 0.2, 0.25, 0.3, 0.35 and 0.4), four positions of hole b (p_b/w=0.2, 0.3, 0.4 and 0.5), two plate thicknesses (t/w=0.05 and 0.1) and three geometries of filet radius (r_f/w=0.05, 0.1 and 0.15). For each of these geometric variations, two loading conditions were considered (as illustrated in Figure 6-37). In each case, details of the position and magnitude of the maximum stress concentration were recorded, along with plots of the cross-sectional stress concentration distribution through the model width.

Strain gauge studies were used to validate the finite element data for particular cases of the problem where one single hole was placed on the horizontal face of the model, with loading conditions acting only on the horizontal face. For each model, one strain gauge was placed either side of the hole, in a line perpendicular to the applied stress. An additional gauge was placed in a region remote to the hole, for measurement of the applied strain. Further details of the dimensions of the test specimens are given in Figure A-5 and Figure A-6 in Appendix A.

6.8.2 Data Validation

Comparisons between the strain gauge data and the equivalent finite element model over the gauge area showed a maximum error of 7.2%. These results validated the accuracy of the finite element techniques utilised for the analysis of this geometry.

6.8.3 Results

6.8.3.1 Stress Concentration Distributions

To reflect the original investigations, three sets of sample stress concentration distribution data are provided here, corresponding to the analyses of (i) a single hole in the horizontal face, (ii) equally positioned and dimensioned holes in the horizontal and vertical faces, and (iii) holes in the horizontal and vertical faces of independent positioning and radius. In all cases, the stress distribution plots are measured from the fillet root, using the measurements x and y, as illustrated in Figure 6-38.

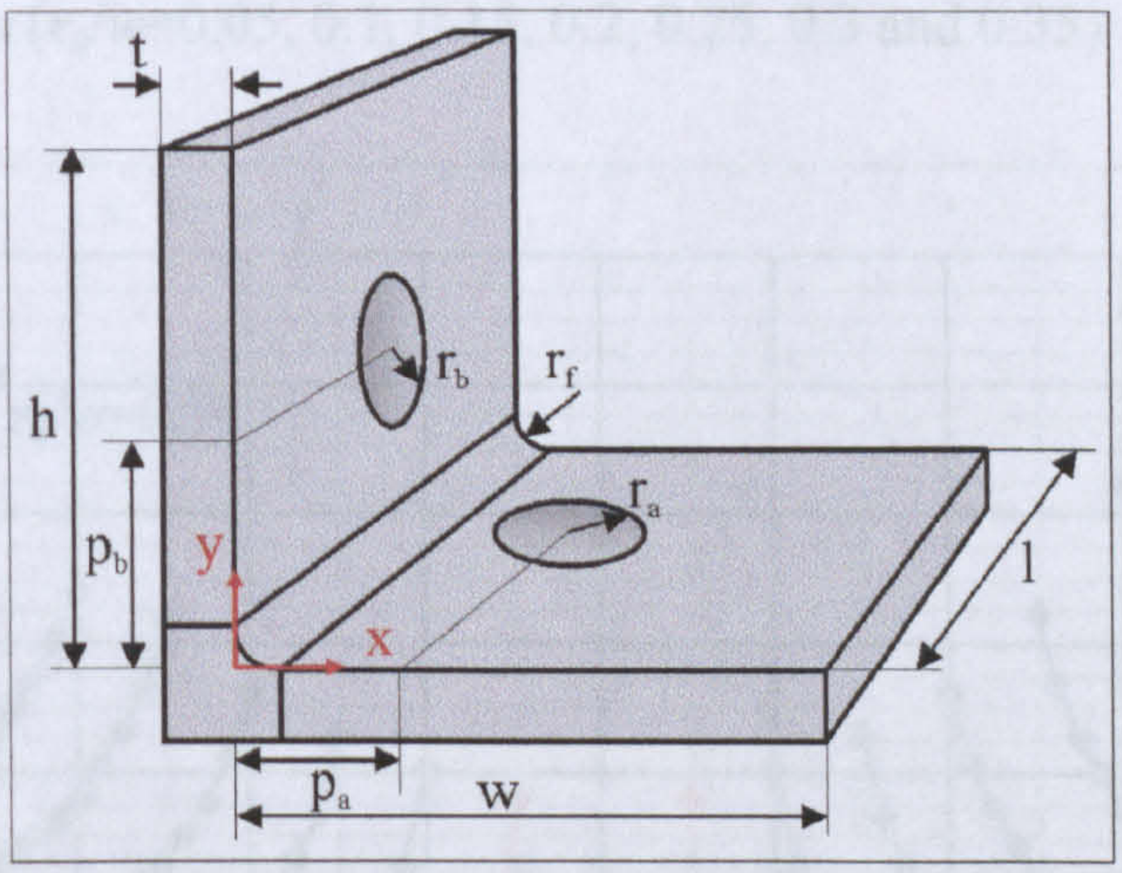

Figure 6-38. Illustration of the variables x and y, measuring the distance along the horizontal and vertical cross-sections from the root of the fillet

The data presented in Figure 6-39 was generated from a single hole in the horizontal face of the model, with the load applied to the entire cross-section. This figure illustrates the variation in the stress concentration distribution along the horizontal face for a variety of hole radii (r_a/w=0.05, 0.1, 0.15, 0.2, 0.25, 0.3 and 0.35), and where p_a/w=0.5, r_f/w=0.1 and t/w=0.05. For clarity, r_a/w=0.05 is shown in red and r_a/w=0.35 is shown in blue. Figure 6-40 illustrates a comparable set of results to that of Figure 6-39, but in this case an additional hole is placed in the vertical section, such that r_a=r_b and p_a=p_b. The figure considers the variation in stress concentration distribution along the

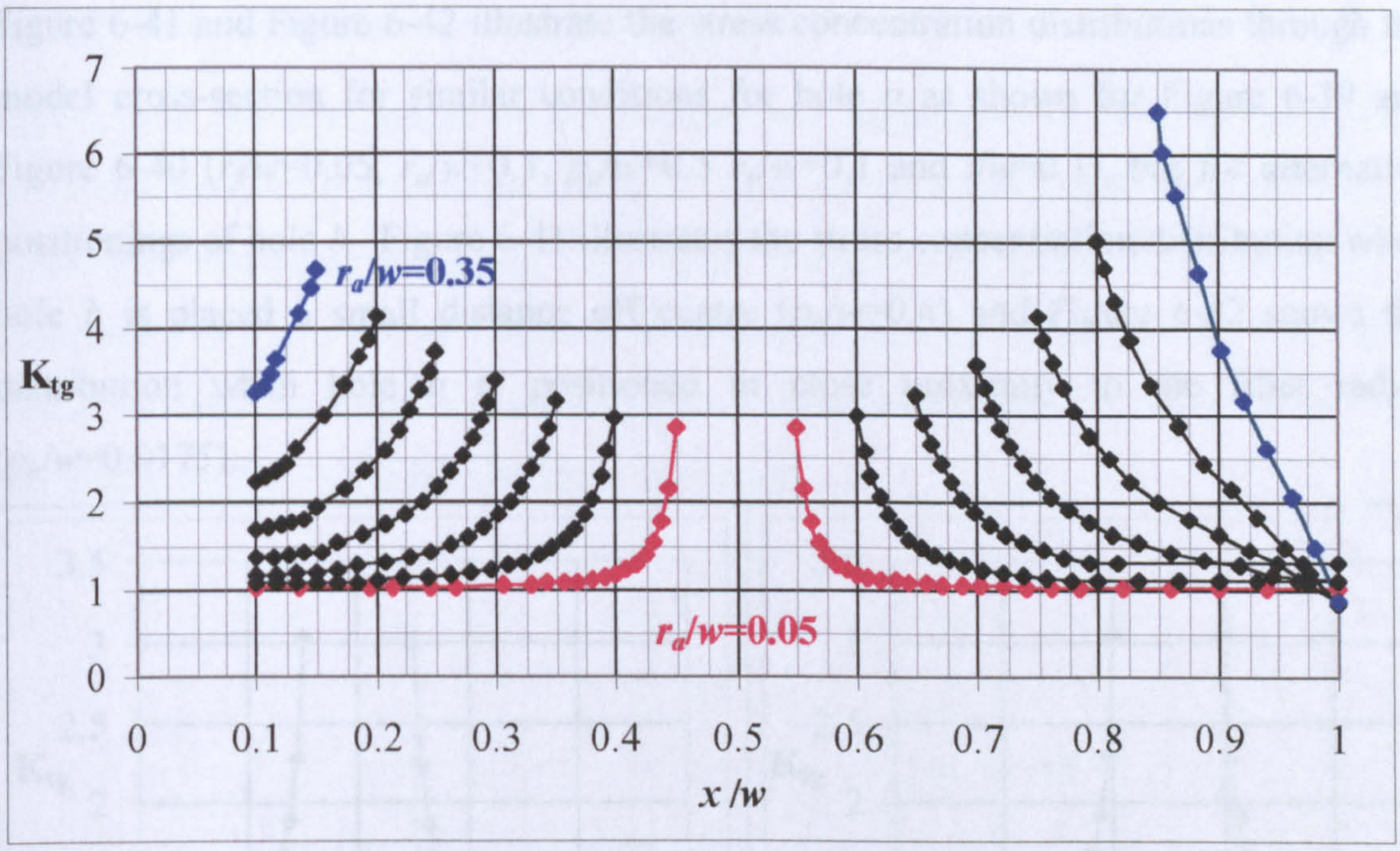

Figure 6-39. Stress concentration distributions for a single hole in the horizontal face of the section, where p_a/w=0.5, r_f/w=0.1, t/w=0.05 and for seven radii for hole a (r_a/w=0.05, 0.1, 0.15, 0.2, 0.25, 0.3 and 0.35)

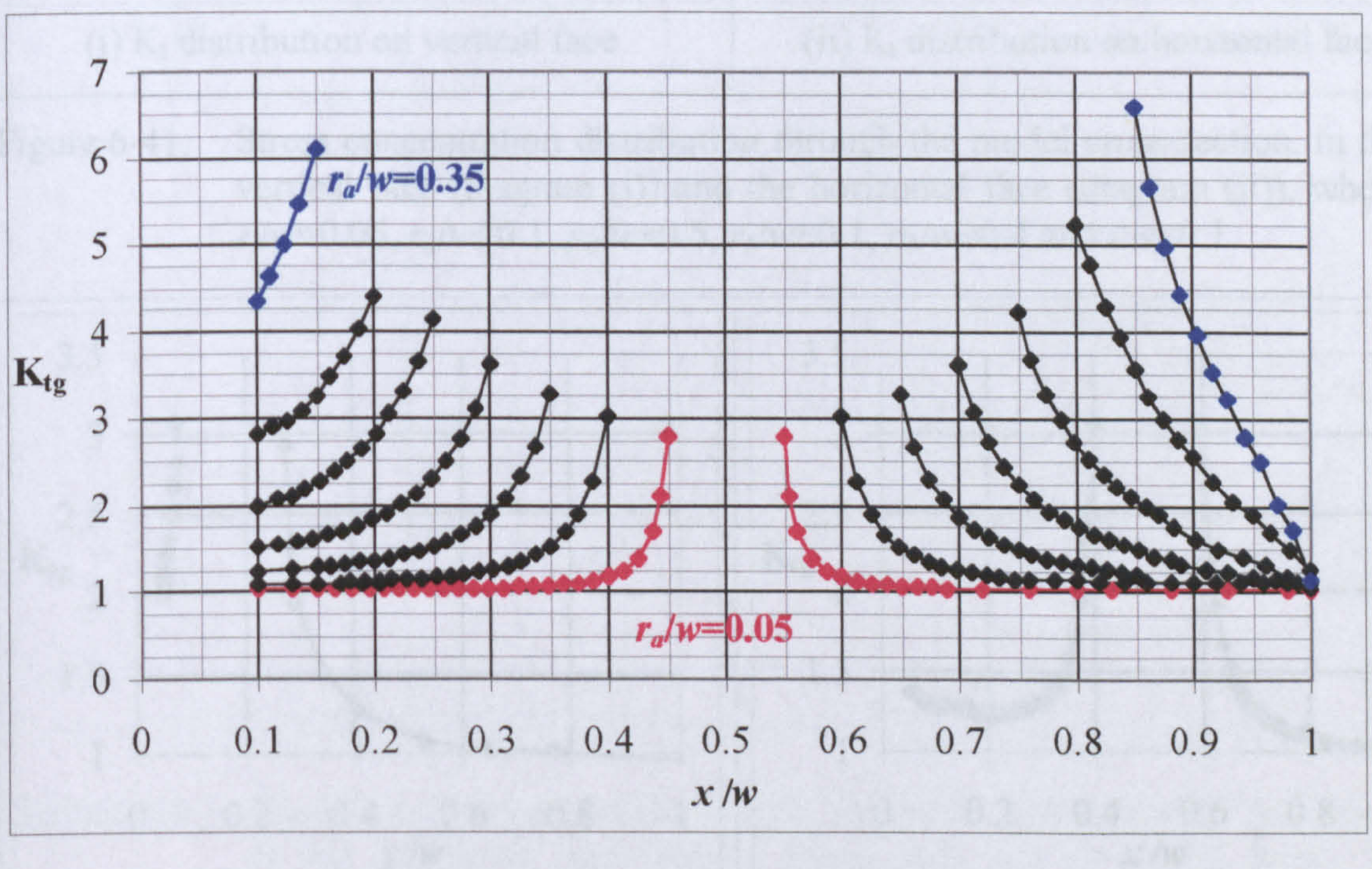

Figure 6-40. Stress concentration distributions for a two symmetrical holes in either face of the section, where p_a/w=p_b/w=0.5, r_f/w=0.1, t/w=0.05 and for hole a and hole b (r_a/w= r_b/w=0.05, 0.1, 0.15, 0.2, 0.25, 0.3 and 0.35)

horizontal face (which displays identical results to the vertical face) for hole radii (r_a/w=r_b/w=0.05, 0.1, 0.15, 0.2, 0.25, 0.3 and 0.35). The boundary stress concentration is applied to the entire cross-section, with p_a/w=p_b/w=0.5, r_f/w=0.1 and t/w=0.05.

Figure 6-41 and Figure 6-42 illustrate the stress concentration distributions through the model cross-section for similar conditions for hole *a* as shown for Figure 6-39 and Figure 6-40 (r_f/w=0.05, r_a/w=0.1, p_a/w=0.5 r_b/w=0.1 and t/w=0.1), but for alternative positionings of hole *b*. Figure 6-41 illustrates the stress concentration distribution when hole *b* is placed a small distance off centre (p_b/w=0.4) and Figure 6-42 shows the distribution when hole *b* is positioned in close proximity to the fillet radius (p_b/w=0.0175).

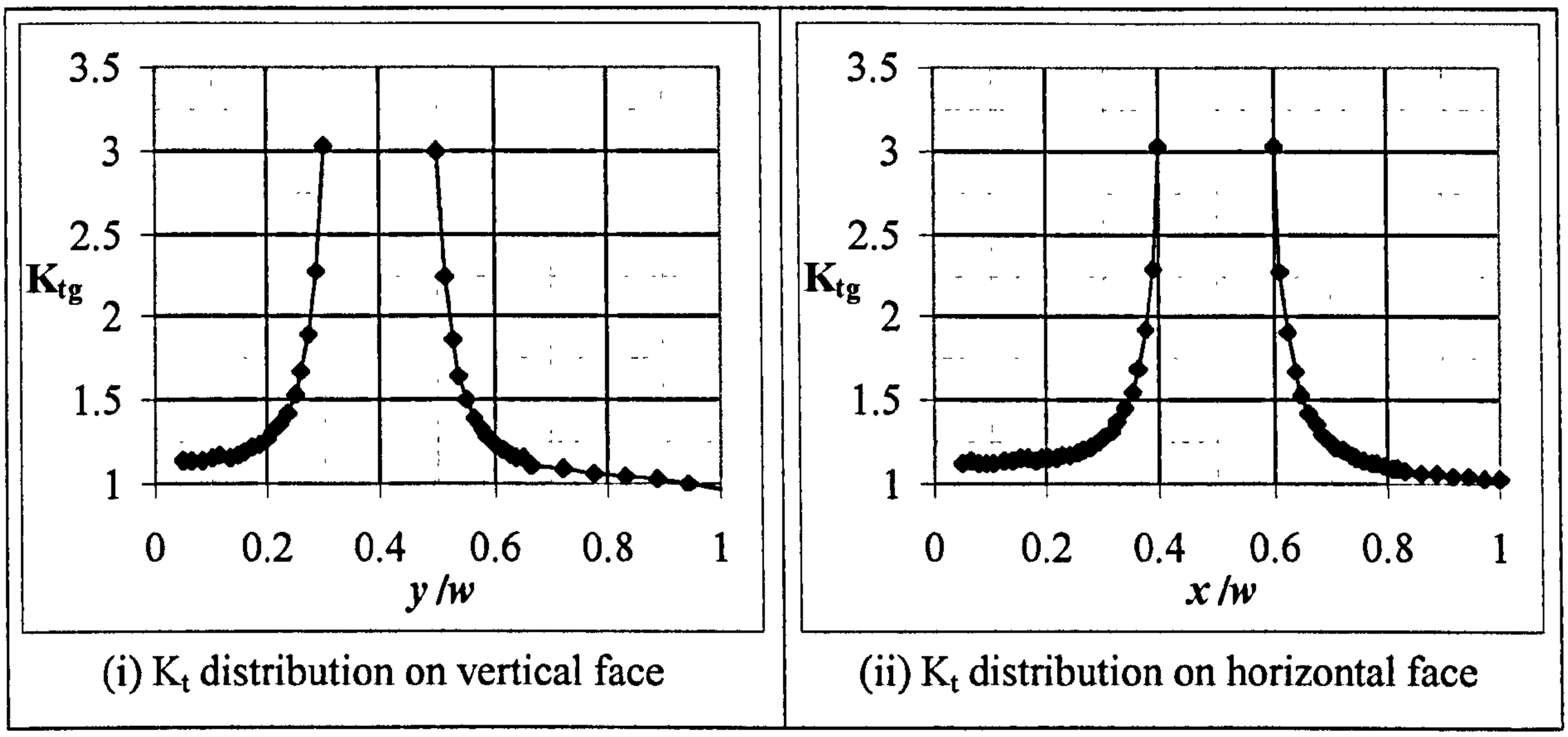

(i) K_t distribution on vertical face

(ii) K_t distribution on horizontal face

Figure 6-41. Stress concentration distribution through the model cross-section, in the vertical face (diagram (i)) and the horizontal face (diagram (ii)), where r_f/w=0.05, r_a/w=0.1, p_a/w=0.5, r_b/w=0.1, p_b/w=0.4 and t/w=0.1

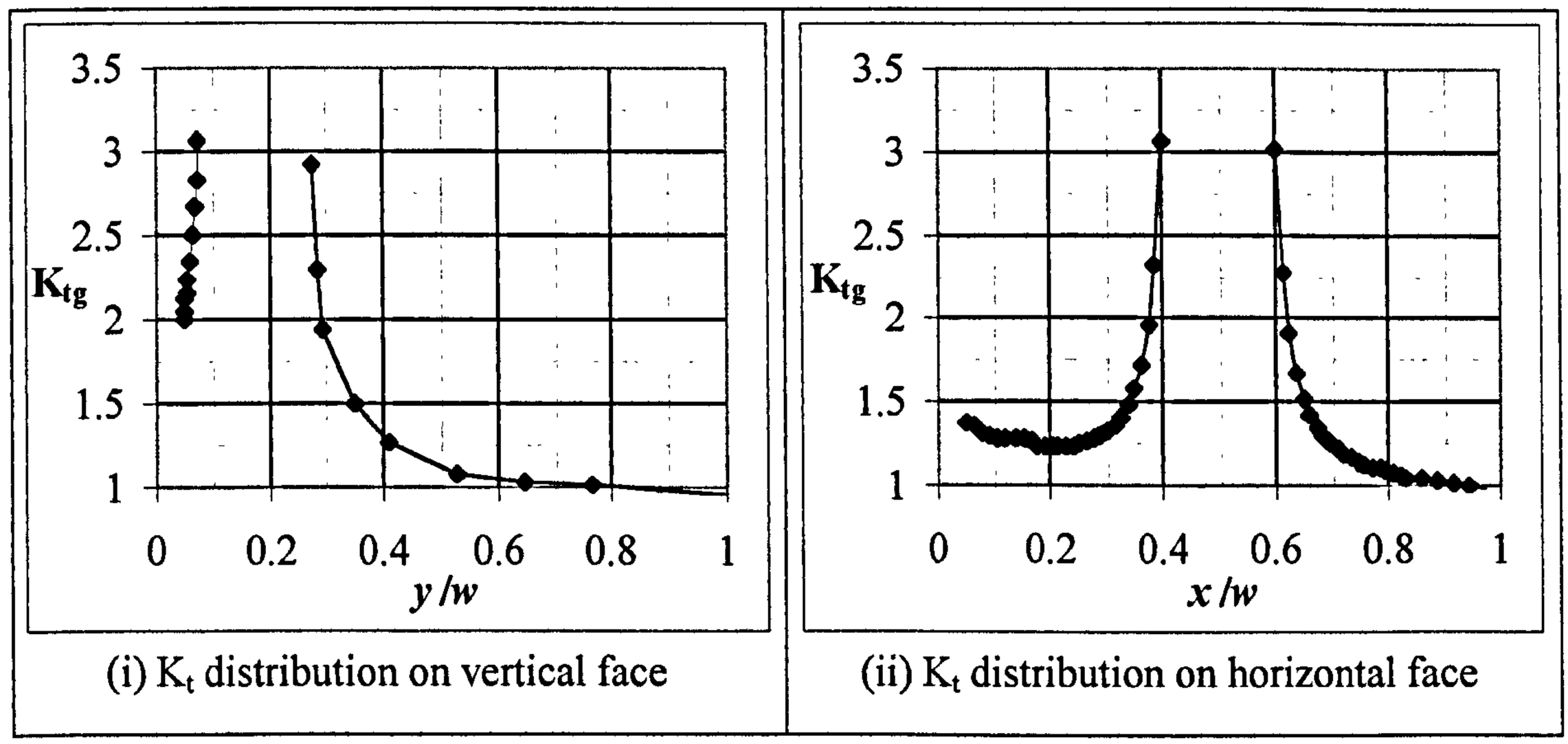

(i) K_t distribution on vertical face

(ii) K_t distribution on horizontal face

Figure 6-42. Stress concentration distribution in the vertical and horizontal faces, where r_f/w=0.05, r_a/w=0.1, p_a/w=0.5, r_b/w=0.1, p_b/w=0.0175 and t/w=0.1

6.8.3.2 Maximum Stress Concentration

Figure 6-43 provides values of the position and magnitude of the maximum stress concentration for the case where one hole is placed on both the horizontal and vertical faces, such that r_b=r_a and p_b=p_a. This figure illustrates the impact of variation in the hole radius (r_a) and a series of hole positionings (p_a/w=0.2, 0.3, 0.4 and 0.5) on the overall maximum stress concentration. For this example, r_f/w=0.05 and t/w=0.1, and the load is applied to the full model cross-section.

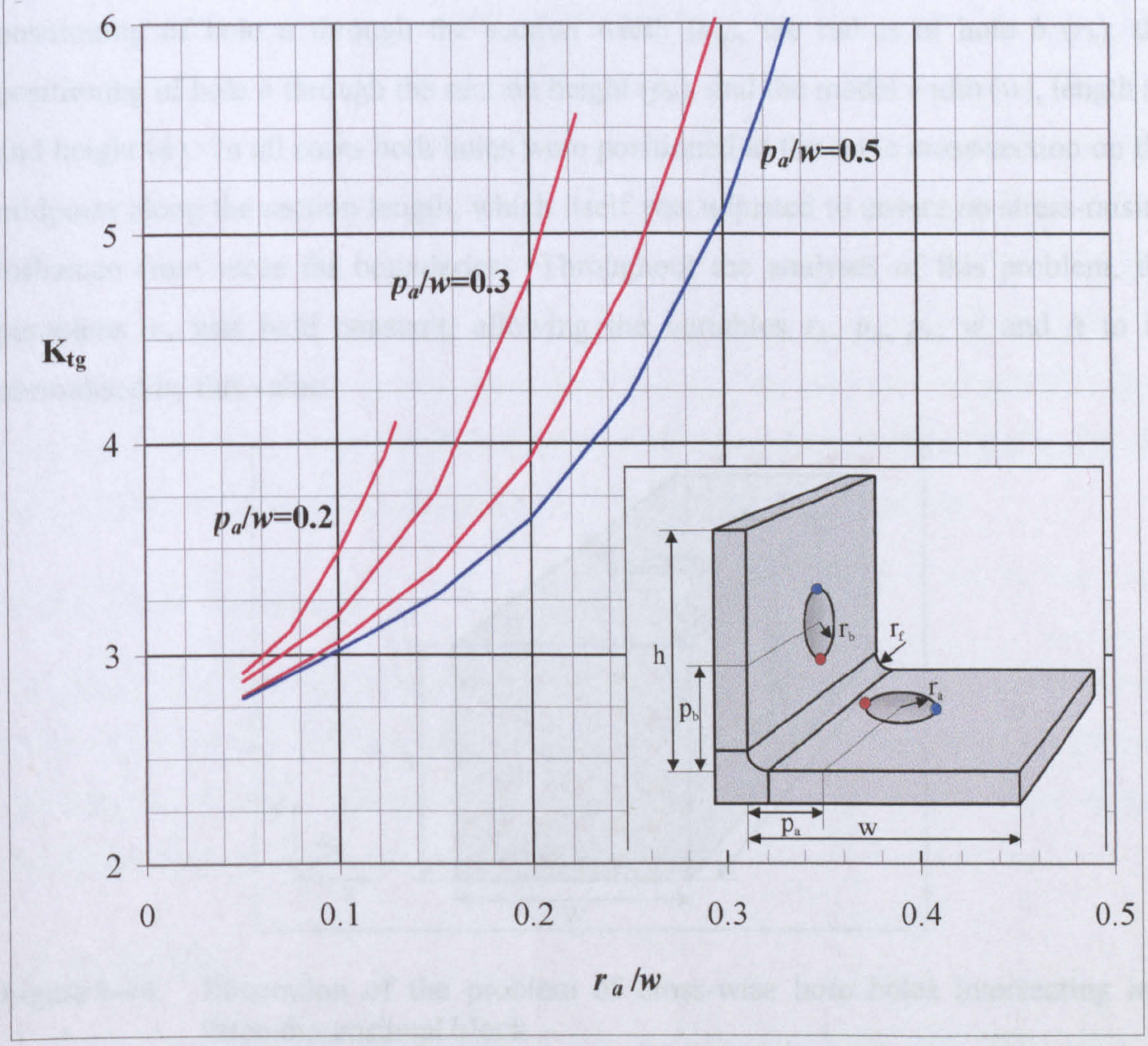

Figure 6-43. Maximum stress concentrations for two holes, symmetrically positioned on the horizontal and vertical faces such that r_b=r_a and p_b=p_a, for variation in the hole radii and positioning, for the values p_a/w=0.2, 0.3, 0.4 and 0.5, where r_f/w=0.05 and t/w=0.1

6.9 CROSS-WISE BORE HOLES

6.9.1 Geometry Considered

Figure 6-44 provides an illustration of the geometric parameters and the loading condition of intersecting cross-wise bore holes. Such three-dimensional problems occur in a variety of design configurations, such as grease holes, where two perpendicular intersecting holes both extend through to the opposite face of the section. The geometric parameters involved in this problem are, the radius of hole a (r_a), the positioning of hole a through the section width (p_a), the radius of hole b (r_b), the positioning of hole b through the section height (p_b), and the model width (w), length (l) and height (h). In all cases both holes were positioned at the same cross-section on the midpoint along the section length, which itself was adjusted to ensure no stress-raising influence from these far boundaries. Throughout the analyses of this problem, the parameter r_a was held constant, allowing the variables r_b, p_a, p_b, w and h to be normalised by this value.

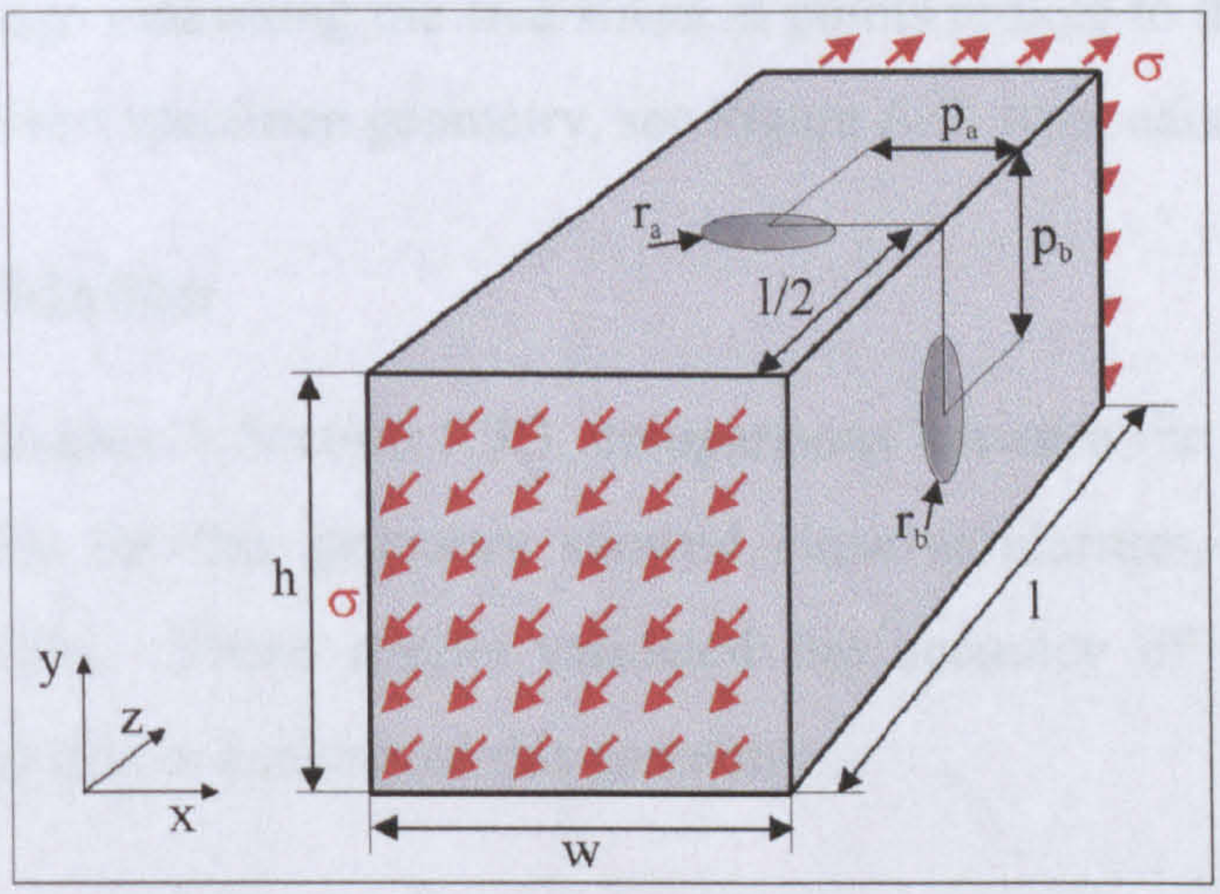

Figure 6-44. Illustration of the problem of cross-wise bore holes intersecting in a three-dimensional block

Finite element analyses and strain gauge techniques were used to analyse this problem.

The finite element studies investigated the influence of r_b, p_a, p_b, w and h on the position and magnitude of the maximum stress concentration. In addition, for each geometry, stress concentration distribution plots were taken along the shaft of each hole from their point of intersection to the specimen surface. Six geometries of r_b were considered, r_b/r_a=1, 0.5, 0.25, 0.125, 0.1 and 0.05. Between ten and twenty values of w

were investigated, ranging from w=2.5r_a to 20r_a (the number varying according to the particular geometry under consideration). Between ten and twenty values of h were investigated, ranging from values of h=2.5r_b to 20r_a. Four values of p_a were analysed, p_a=w/2, w/3, w/4 and w/5. Similarly, four values of p_b were analysed p_b=h/2, h/3, h/4 and h/5.

As discussed in Chapter 5 Section 5.3.1.1, preliminary finite element studies had established that the maximum stress concentration for any configuration of intersecting bore holes, occurred at the centre of the block, at the point of intersection. Due to the experimental constraints, it was not possible to create a physical test specimen which could accommodate any arrangement of strain gauge in the block centre. However, finite element studies had also established that the magnitude of the stress concentration observed at the block centre, produced a significant stress-raising effect on the specimen surface, in the area surrounding the holes. A series of strain gauges were therefore positioned at the edges of each hole, for the purposes of validation of the finite element data. Two gauges were placed at the edge of each of the holes, along with one larger gauge measuring the free strain at points remote to the interaction. For more details of the test specimen geometry, see Figure A-7, Appendix A.

6.9.2 Data Validation

As described in Chapter 5 Section 5.3.3, comparisons between the finite element and strain gauge results for this geometry showed close similarities, with a maximum discrepancy of 7.5%. These results validated the accuracy of the finite element techniques adopted for the analysis of this geometry.

6.9.3 Results

Illustrated in this section are samples of the stress concentration plots taken along the hole shafts, and a selection of the maximum stress concentration data. In all cases, it was found that the maximum stress concentration occurred at the intersection of the holes, at the two edges along a perpendicular line to that of the applied stress. Due to the very large volume of data gathered for this geometry, only a small selection of the data can be presented here.

6.9.3.1 Stress Distribution Plots

For each geometry of r_b, p_a, p_b, w and h analysed, a ligament plot was taken along the shaft of each hole, along the sections marked y_a and x_b in Figure 6-45. For clarity, this figure illustrates only the two intersecting holes. As shown in Figure 6-45, each of these stress concentration plots is taken from the point of maximum stress (where y_a=x_b=0) to the point where the hole meets the specimen surface.

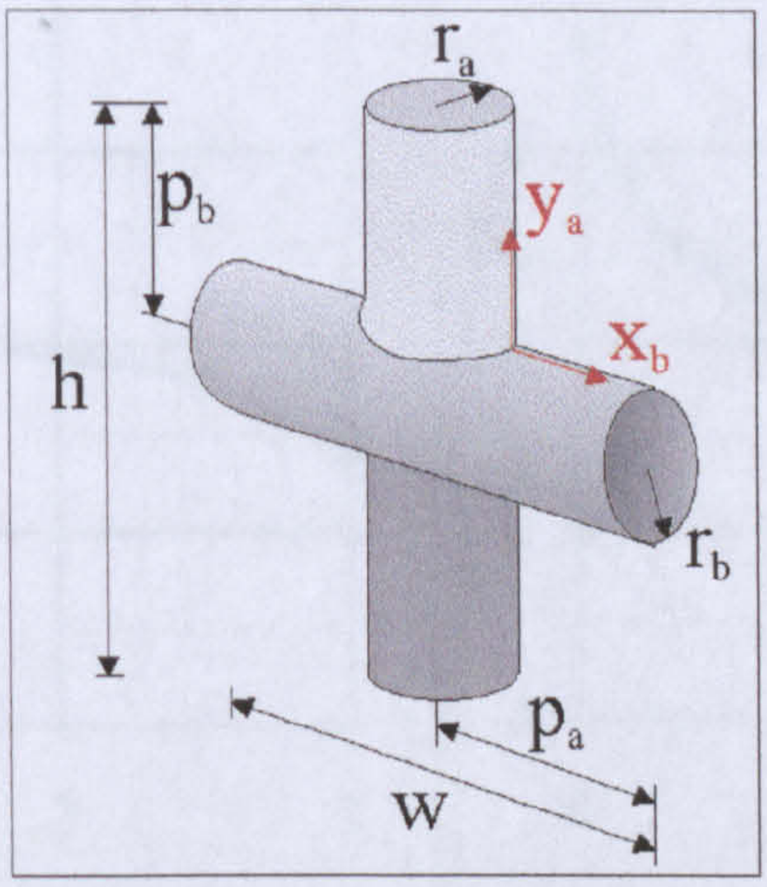

Figure 6-45. Illustration of the sections of the hole shafts taken for stress concentration distribution plots

Shown in Figure 6-46 is an example of the data gathered of the stress concentration distribution plots, where r_b/r_a=1, w/r_a=12, p_a=w/2, h/r_a=3 and p_b=h/2. Shown in

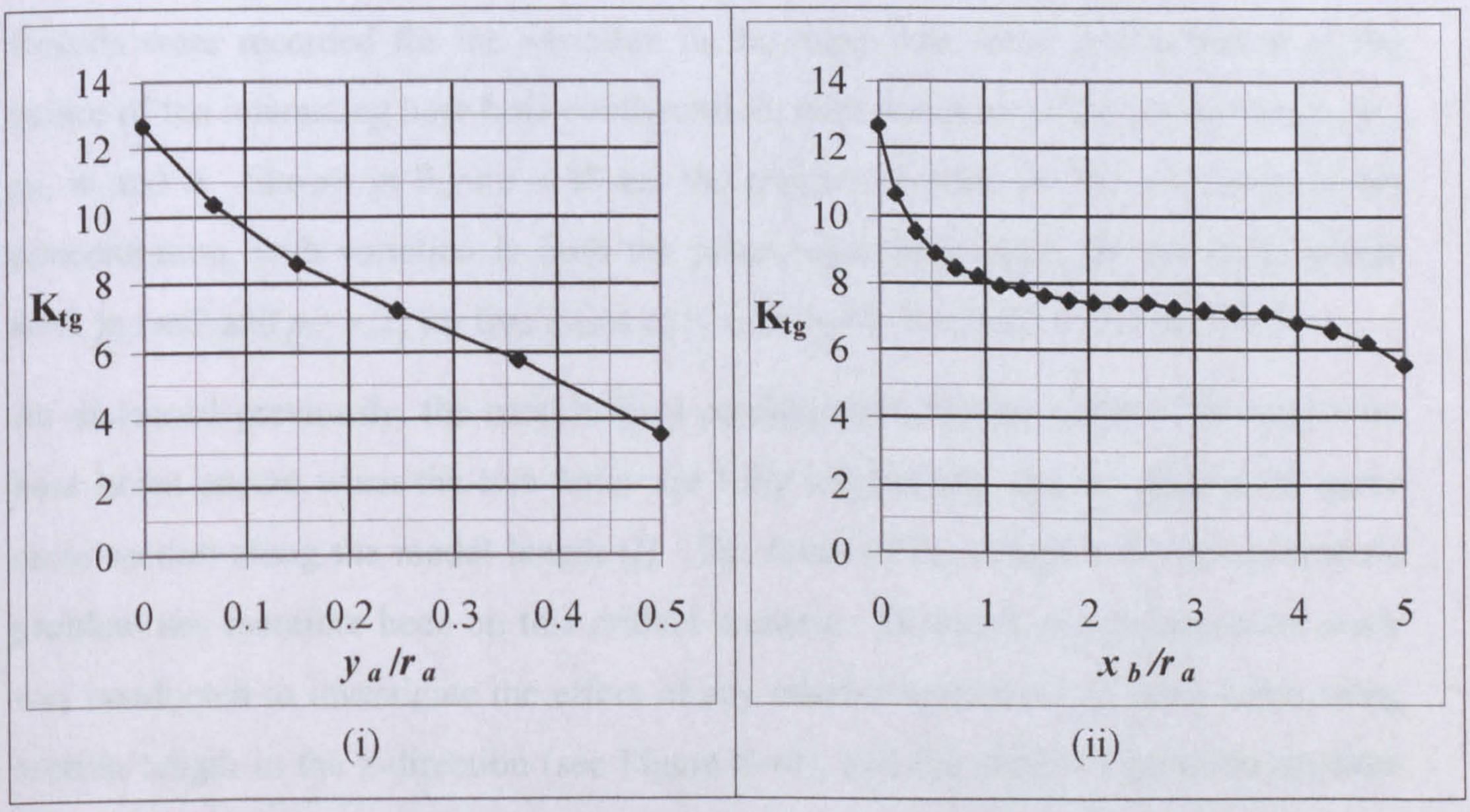

Figure 6-46. Stress concentration distributions for hole *a* (see Diagram (i)) and hole *b* (see Diagram (ii)) for r_b/r_a=1, w/r_a=12, p_a=w/2, h/r_a=3 and p_b=h/2

Diagram (i) is the distribution taken down the vertical shaft of hole *a* along the distance y_a, and in Diagram (ii) is the distribution taken across the horizontal shaft of hole *b* along the distance x_b. Similarly, Figure 6-47 illustrates the stress concentration distribution along the hole lengths for alternative section width and height, where r_b/r_a=1, w/r_a=h/r_a=8, p_a=w/2, and p_b=h/2.

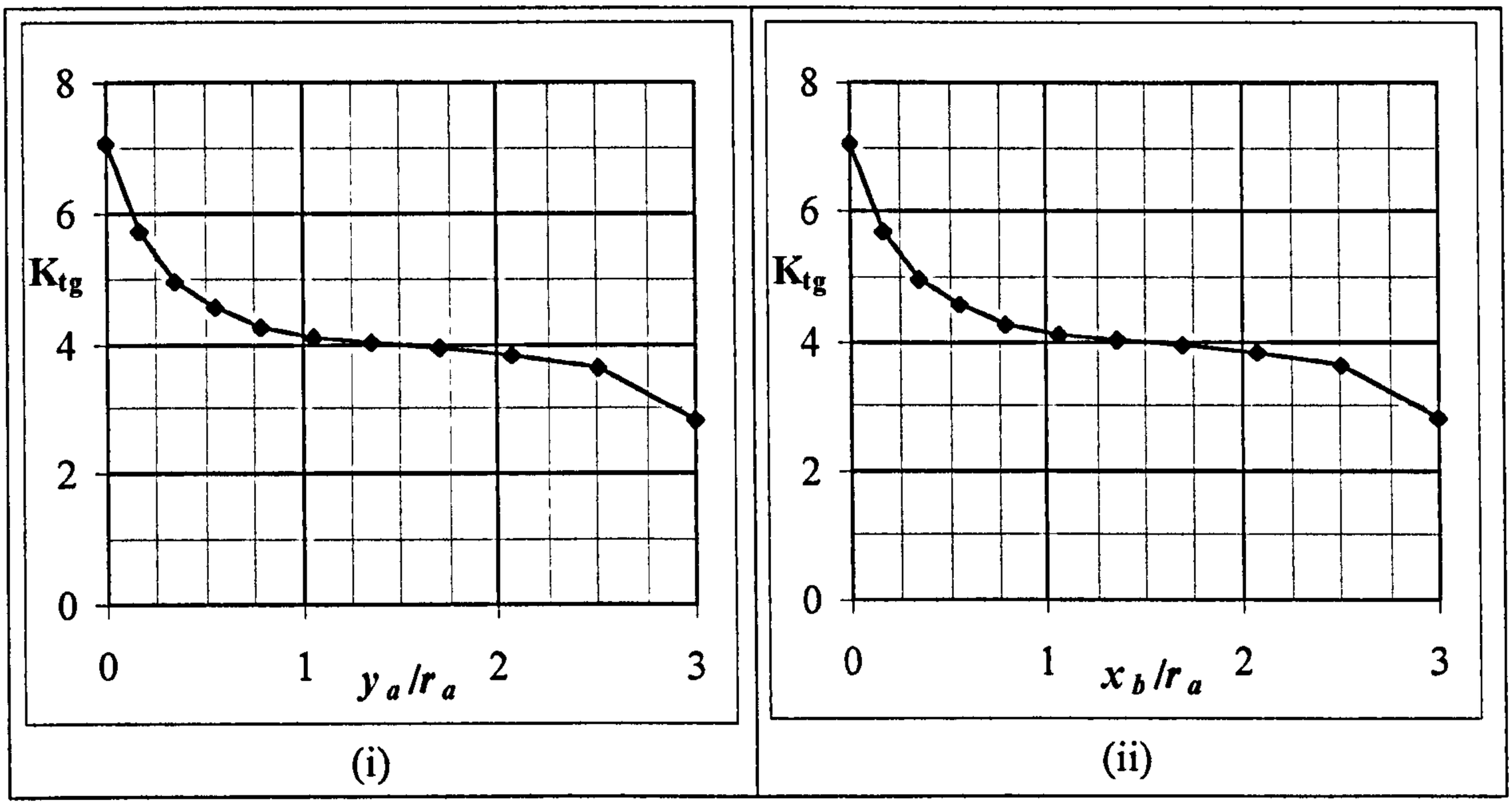

Figure 6-47. Stress concentration distributions for hole *a* (Diagram (i)) and hole *b* (Diagram (ii)) for r_b/r_a=1, w/r_a=h/r_a=8, p_a=w/2, and p_b=h/2

6.9.3.2 Maximum Stress Concentration

Results were recorded for the variation in the maximum stress concentration at the centre of the interacting bore hole configuration, with variation in the parameters r_b, p_a, p_b, w and h. Shown in Figure 6-48 are the results recorded for the maximum stress concentration, with variation in both the plate height and width, for the cases where w=h, p_a=w/2 and p_b=w/2, for five ratios of r_b:r_a (r_b/r_a=1, 0.5, 0.25, 0.125 and 0.05).

As discussed previously, the most critical configuration for the problem of cross-wise bore holes occurs when the two holes are fully intersecting and are placed the same cross-section along the model length (l). The focus of the research for this geometric problem has therefore been on this critical scenario. However, a supplementary study was conducted to investigate the effect of any relative movement of these holes along section length in the z-direction (see Figure 6-44), and the critical separation distance between the holes after which no stress-raising influence occurs. Figure 6-49 illustrates

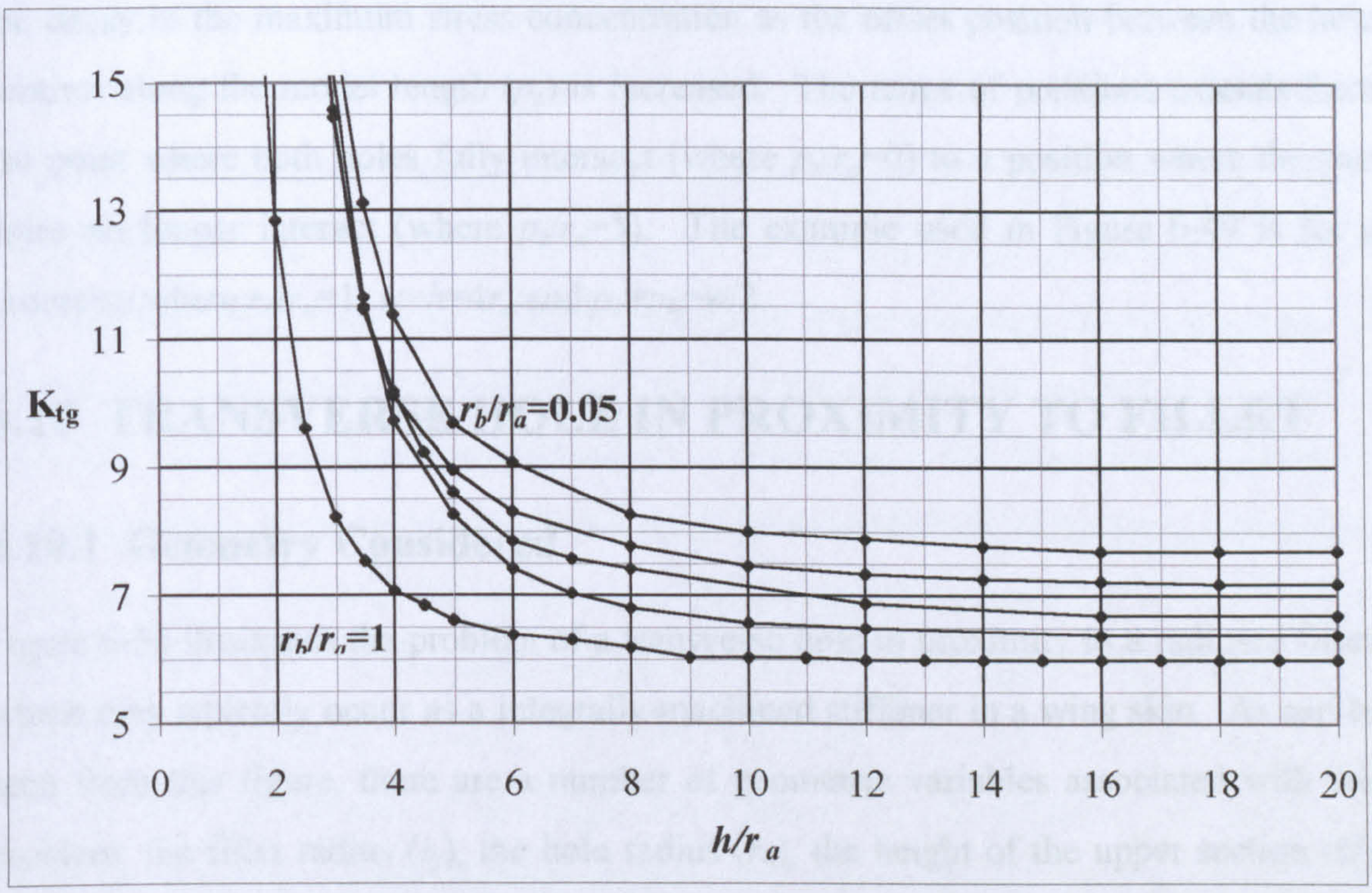

Figure 6-48. Maximum stress concentration for variations in the plate dimensions h and w (where h=w), for of values of r_b/r_a=1, 0.5, 0.25, 0.125 and 0.05

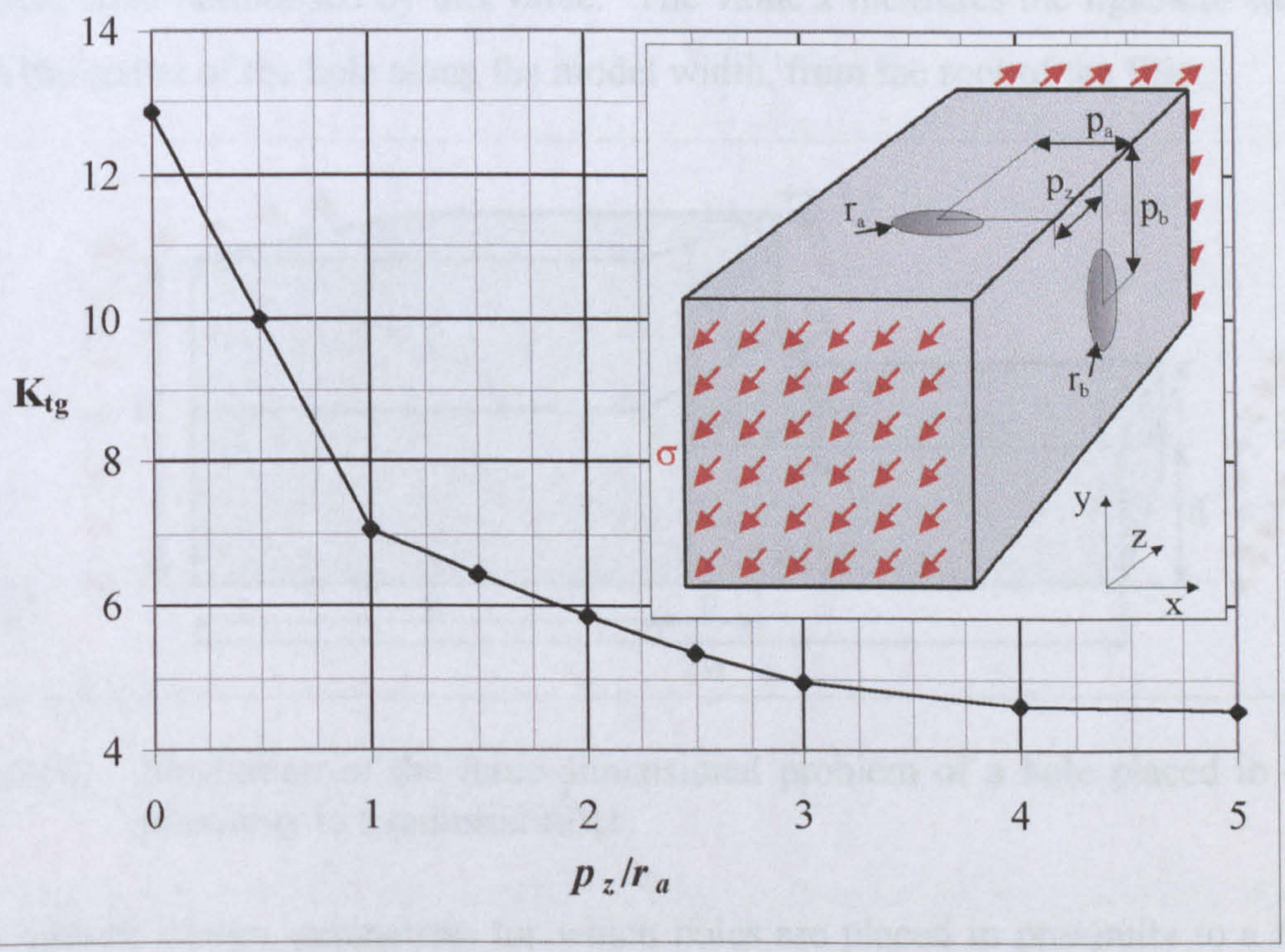

Figure 6-49. The variation in maximum stress concentration with the relative offset position of the two holes (p_z), for r_b/r_a=1, w=h=4r_a and p_a=p_b=w/2

the decay in the maximum stress concentration as the offset position between the hole centres, along the model length (p_z) is increased. The range of positions extends from the point where both holes fully intersect (where p_z/r_a=0) to a position where the two holes no longer interact (where p_z/r_a=5). The example used in Figure 6-49 is for a geometry where r_b/r_a=1, w=h=4r_a and p_a=p_b=w/2.

6.10 TRANSVERSE HOLE IN PROXIMITY TO FILLET

6.10.1 Geometry Considered

Figure 6-50 illustrates the problem of a transverse hole in proximity to a radiused fillet, which may typically occur as a integrally-machined stiffener in a wing skin. As can be seen from this figure, there are a number of geometric variables associated with this problem: the fillet radius (r_f), the hole radius (r_h), the height of the upper section (D), the height of the filleted section (d), the model length (l), the model width (w) and the positioning of the hole relative to the fillet (p). For the purposes of simplification, the filleted height (d) was held constant throughout the investigations, and all other parameters were normalised by this value. The value x measures the ligament section through the centre of the hole along the model width, from the root of the fillet.

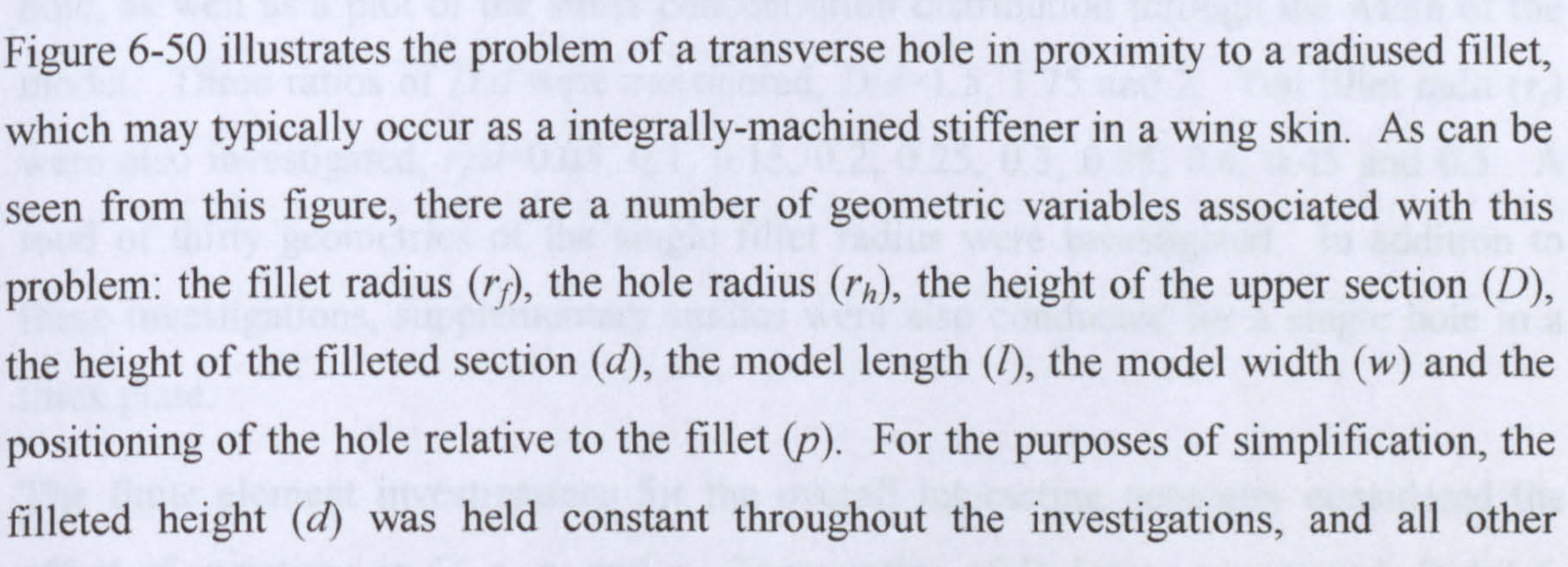

Figure 6-50. Illustration of the three-dimensional problem of a hole placed in close proximity to a radiused fillet

Within aircraft design, geometries for which holes are placed in proximity to a three-dimensional fillet occur commonly throughout the structure. However, during the evaluation of manufacturing defects, situations often arise where the hole is misplaced and positioned in a closer proximity to the fillet radius than specified in the design, or,

in some cases, placed through the radius itself. For this investigation, it was therefore important to analyse a wide range of hole positions (p) throughout the model width.

This three-dimensional problem was investigated using finite element analysis. These investigations required preliminary analyses of the individual problems of a three-dimensional fillet containing no hole. This study began with establishing the values of w and l for which these far boundaries had no influence on the stress concentration at the fillet. This investigation considered the influence of r_f and D on the magnitude and position of the maximum stress concentration produced for this geometry, containing no hole, as well as a plot of the stress concentration distribution through the width of the model. Three ratios of D:d were considered, D/d=1.5, 1.75 and 2. Ten fillet radii (r_f) were also investigated, r_f/d=0.05, 0.1, 0.15, 0.2, 0.25, 0.3, 0.35, 0.4, 0.45 and 0.5. A total of thirty geometries of the single fillet radius were investigated. In addition to these investigations, supplementary studies were also conducted for a single hole in a thick plate.

The finite element investigations for the overall interacting geometry considered the effect of variations in D, r_f, r_h and p. Three ratios of D:d were considered, D/d=1.5, 1.75 and 2. Ten fillet radii (r_f) were also investigated, r_f/d=0.05, 0.1, 0.15, 0.2, 0.25, 0.3, 0.35, 0.4, 0.45 and 0.5. Four hole radii were considered r_h/d=0.1, 0.2, 0.3 and 0.4. Finally, for each geometry, a series of between twenty and forty hole positions (p) were considered, in the range p/d=-1.5 to 1.5. A total of over eight hundred models were considered. In each case, records were taken of the location and magnitude of the maximum stress concentration, as well as ligament plots through the model width. In addition, for each model considered, the values of w and l were carefully adjusted to ensure no additional stress-raising influence from the model boundaries.

6.10.2 Results

6.10.2.1 Single Feature Data

The primary stage of the investigation of this three-dimensional geometry was the analysis of the individual problems of the radiused fillet and of the hole in a thick plate.

The investigation of the radiused fillet involved the generation of stress concentration distribution plots, through the width of the model, illustrating the influence of r_f and D on the position and magnitude of the maximum stress concentration, and the stress

decay from this point. Figure 6-51 illustrates a typical set of results for this study, providing the data for the stress concentration distribution through the model width for values D/d=2 and r_f/d=0.1. These results also show the position (x/d=0.08) and the magnitude (K_{tg}=2.01) of the maximum stress concentration. Similar investigations were conducted for the range of values of D and r_f. Figure 6-52 and Figure 6-53 illustrate a selection of the results generated during the investigations for D/d=2, providing data for the magnitude of the maximum stress concentration, and the relative position of this maximum along the fillet radius. These investigations also established that the length and width boundaries of the section produced no stress-raising effect on the fillet radius if $w > 20r_f$, and $l > 20r_f$.

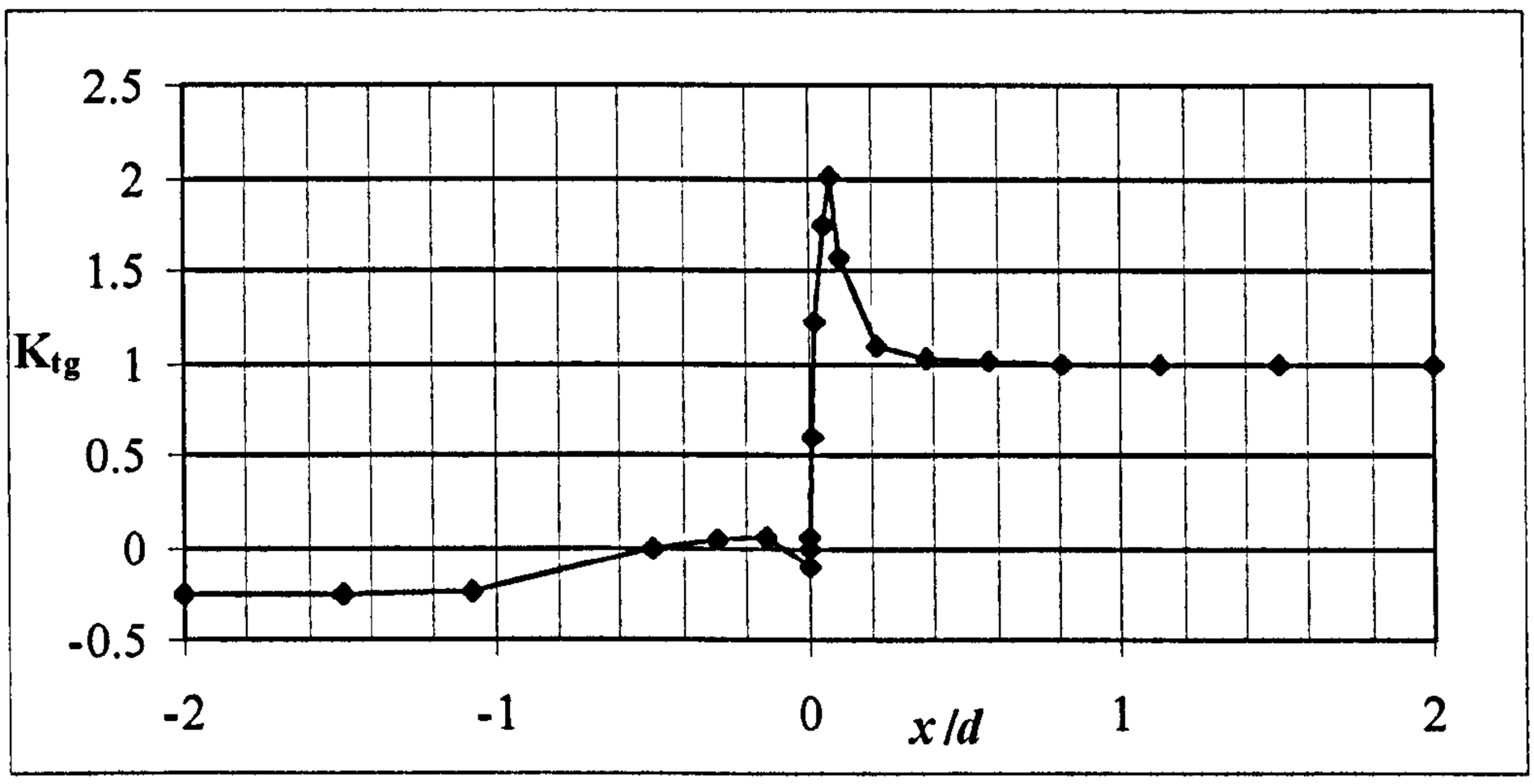

Figure 6-51. Stress concentration distribution through model width, for D/d=2 and r_f/d=0.1

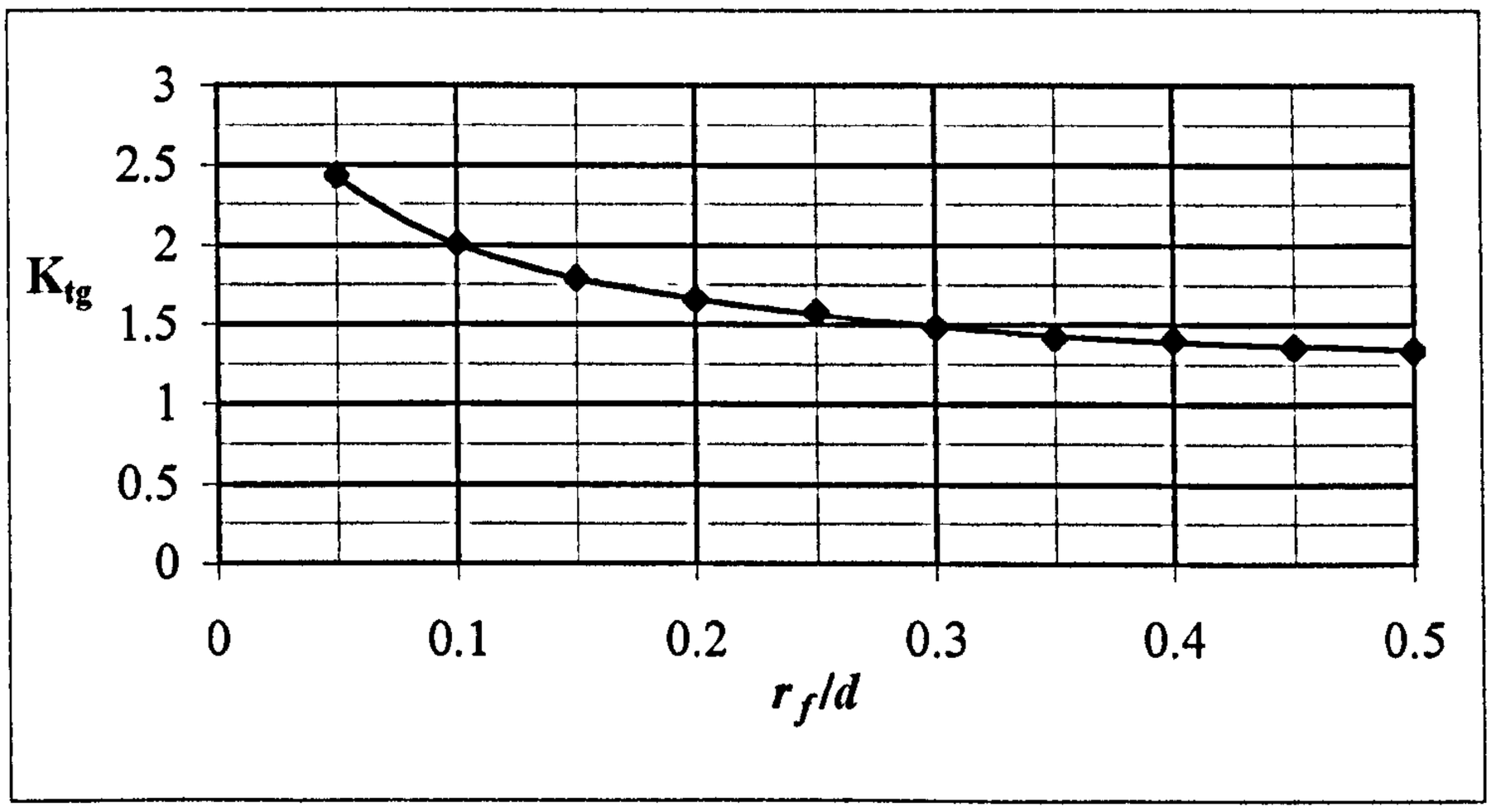

Figure 6-52 Maximum stress concentration variation for a series of fillet radii, for D/d=2

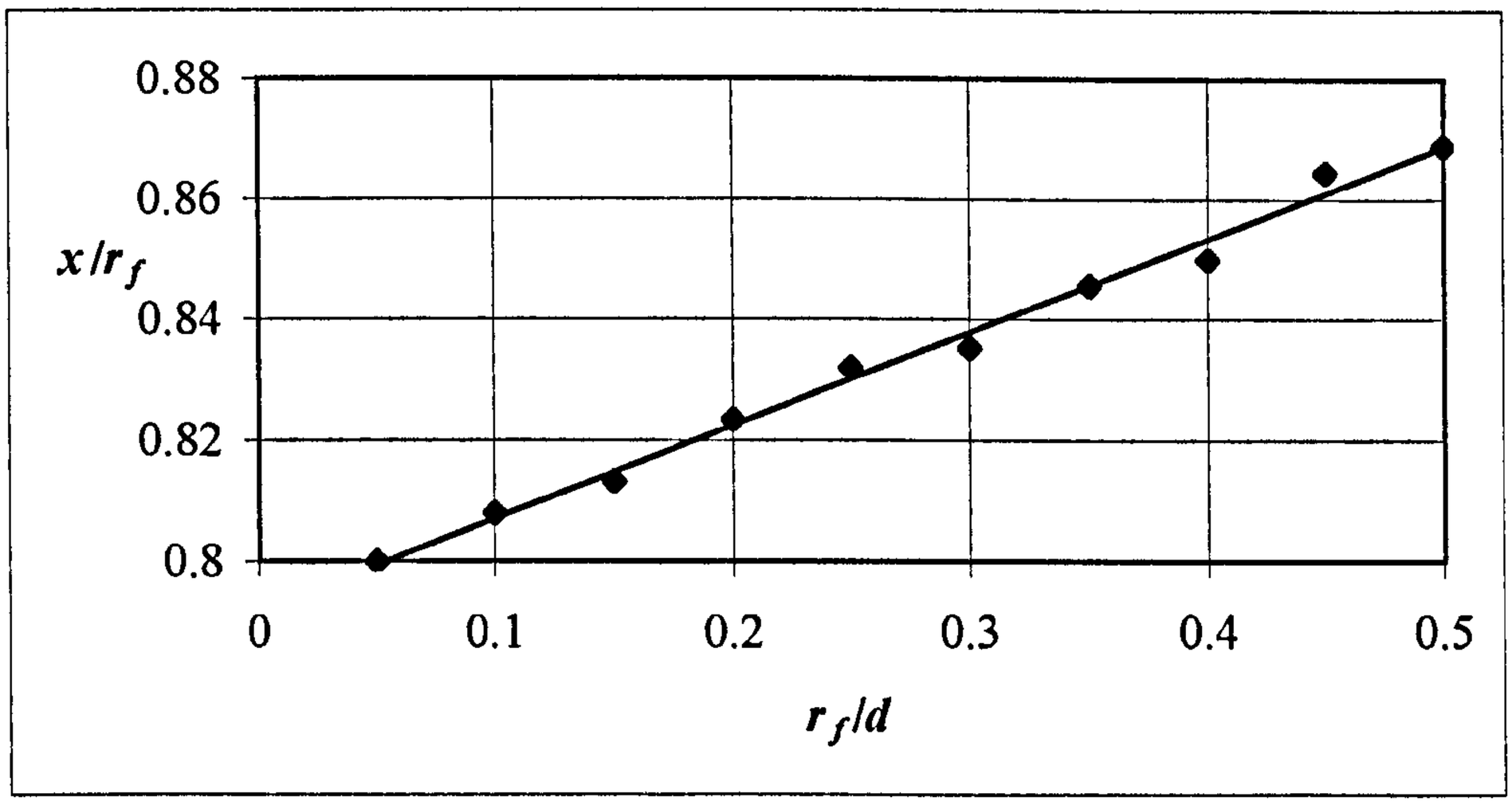

Figure 6-53. The position of the maximum stress concentration, relative to the fillet radius (r_f), for a series of fillet radii, where D/d=2

Investigations into the stress concentration associated with a hole in an infinite thick plate under these conditions revealed that the K_{tg}=3.2 in all cases.

6.10.2.2 Results for the Interacting Geometry

A series of investigations was then conducted for the introduction of the hole, analysing over eight hundred configurations of r_f, r_h, D and p. For each given geometry of r_f, r_h and D, solutions were developed for a series of incremental values of hole position (p) in the range p/d=-1.5 to +1.5. Figure 6-54, Figure 6-55 and Figure 6-56 illustrate the magnitude of the maximum stress concentration for forty hole positions where D/d=0.5 and r_h/d=0.2, for three different fillet radii (r_f/d=0.1, 0.2 and 0.4 respectively).

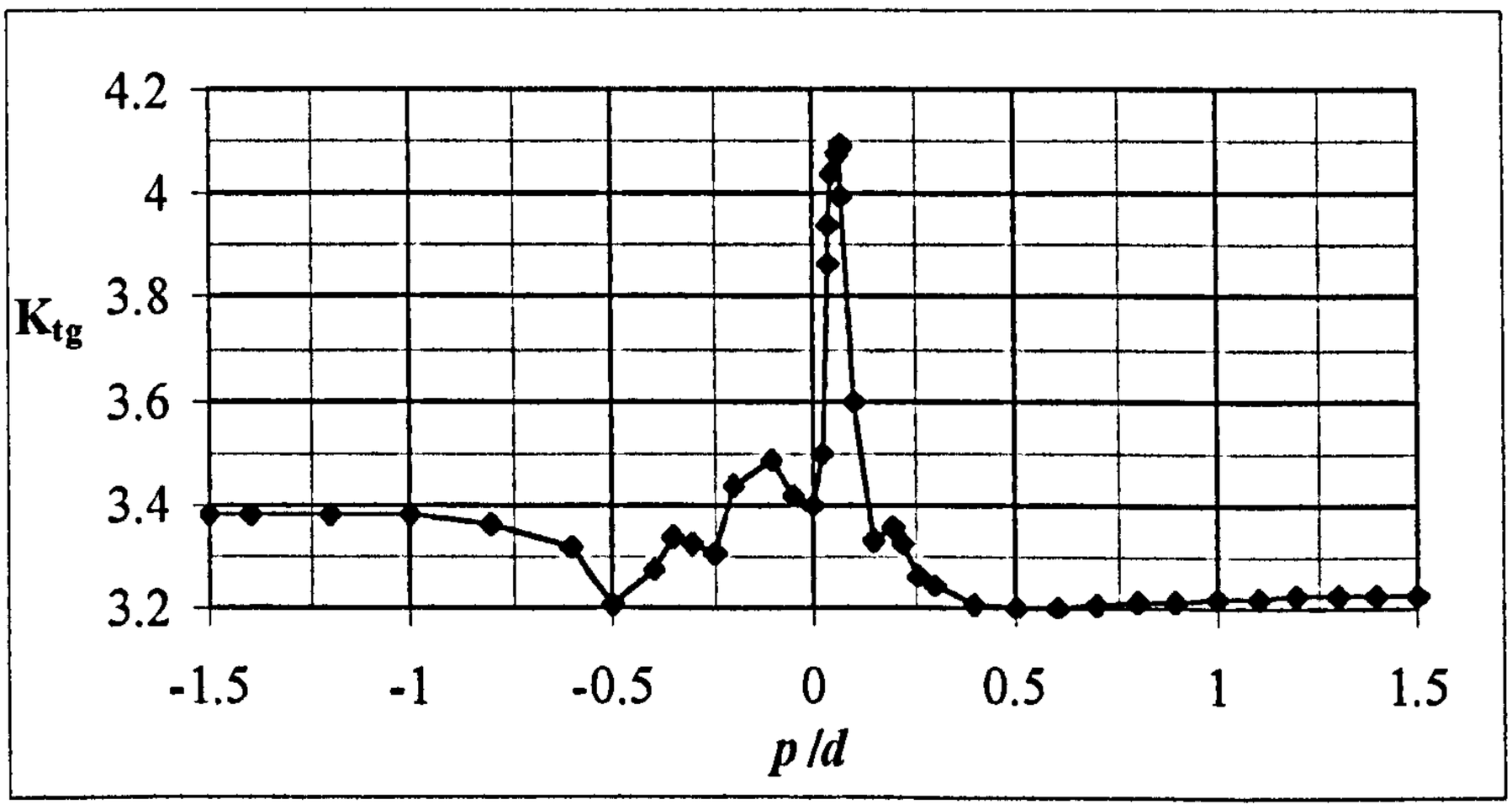

Figure 6-54. Maximum stress concentration for each of a series of hole positioning (p) in the range p/d=-1.5 to +1.5, where D/d=0.5, r_h/d=0.2 and r_f/d=0.1

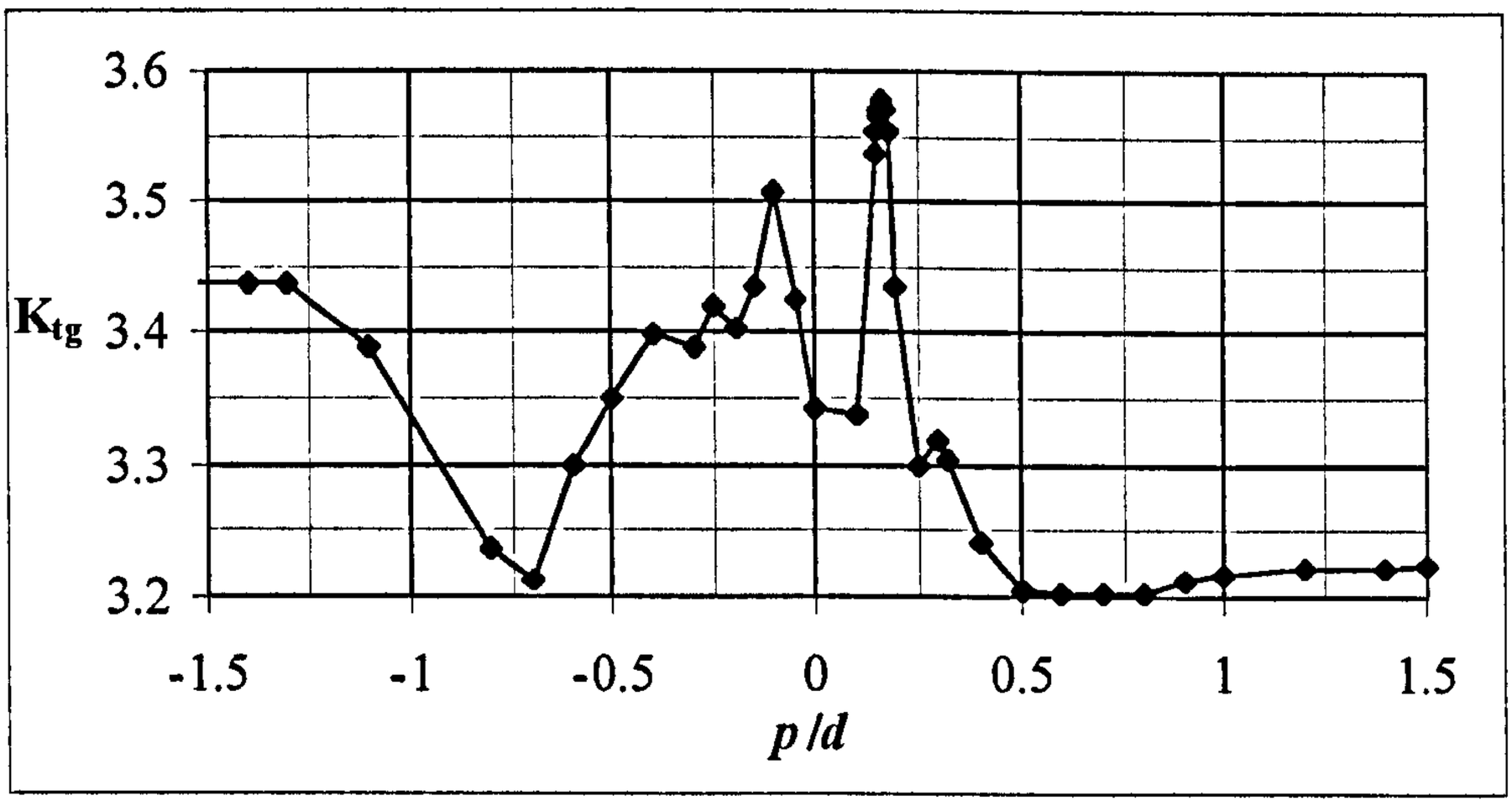

Figure 6-55. Maximum stress concentration for each of a series of hole positioning (p) in the range p/d=-1.5 to +1.5, where D/d=0.5, r_h/d=0.2 and r_f/d=0.2

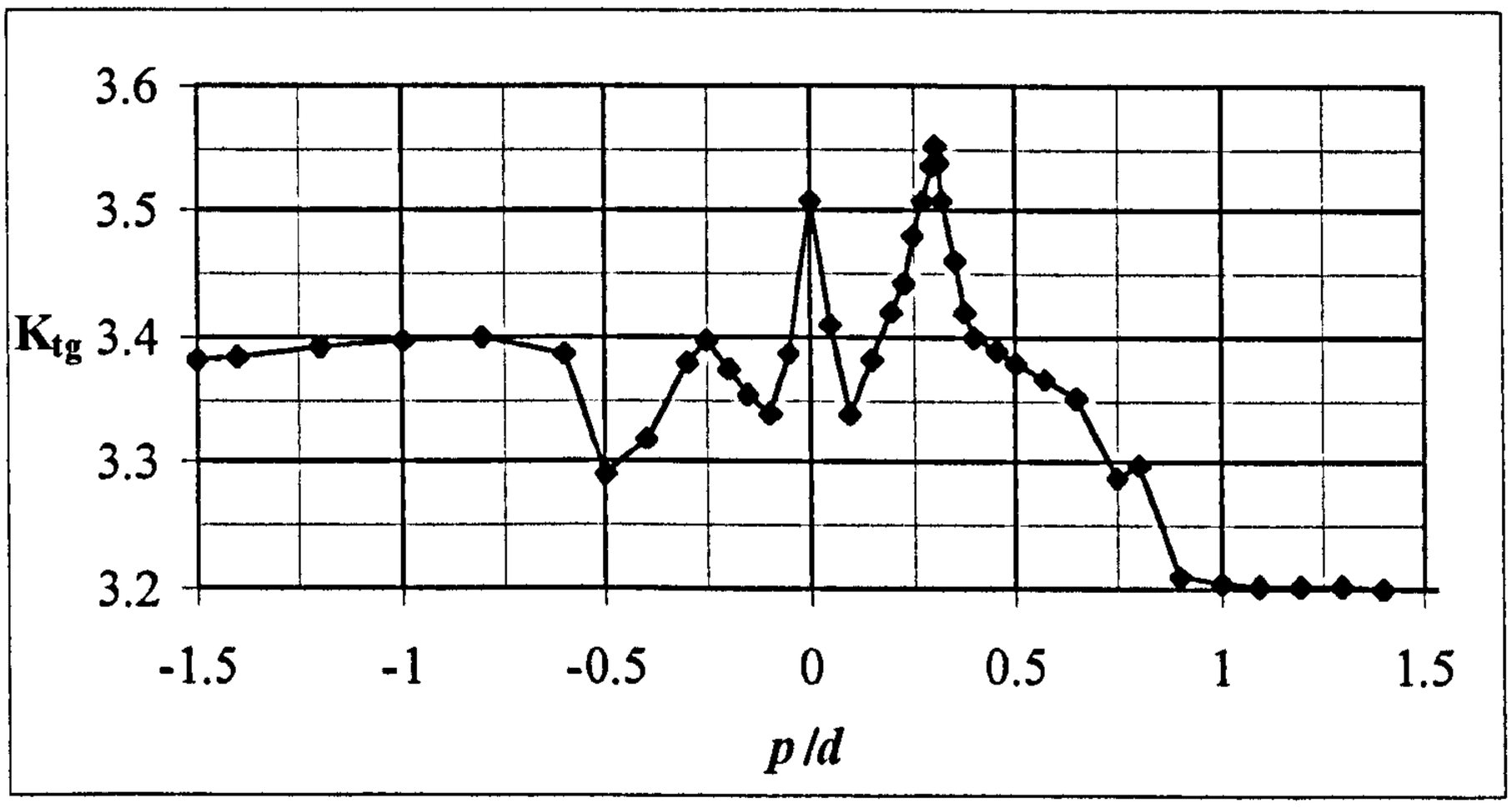

Figure 6-56. Maximum stress concentration for each of a series of hole positioning (p) in the range p/d=-1.5 to +1.5, where D/d=0.5, r_h/d=0.2 and r_f/d=0.4

From each of these figures, it can be seen that there is a particular hole position (p) for which a peak maximum stress concentration is generated. These results have been gathered together to provide values, for given r_f, r_h and D, for the overall maximum stress concentration formed for cases where the hole is placed in its most critical position. A selection of these results is given in Figure 6-57 for values of r_f/d=0.05, 0.1, 0.2 and 0.4, r_h/d=0.1, 0.2, 0.3 and 0.4, and D/d=0.5.

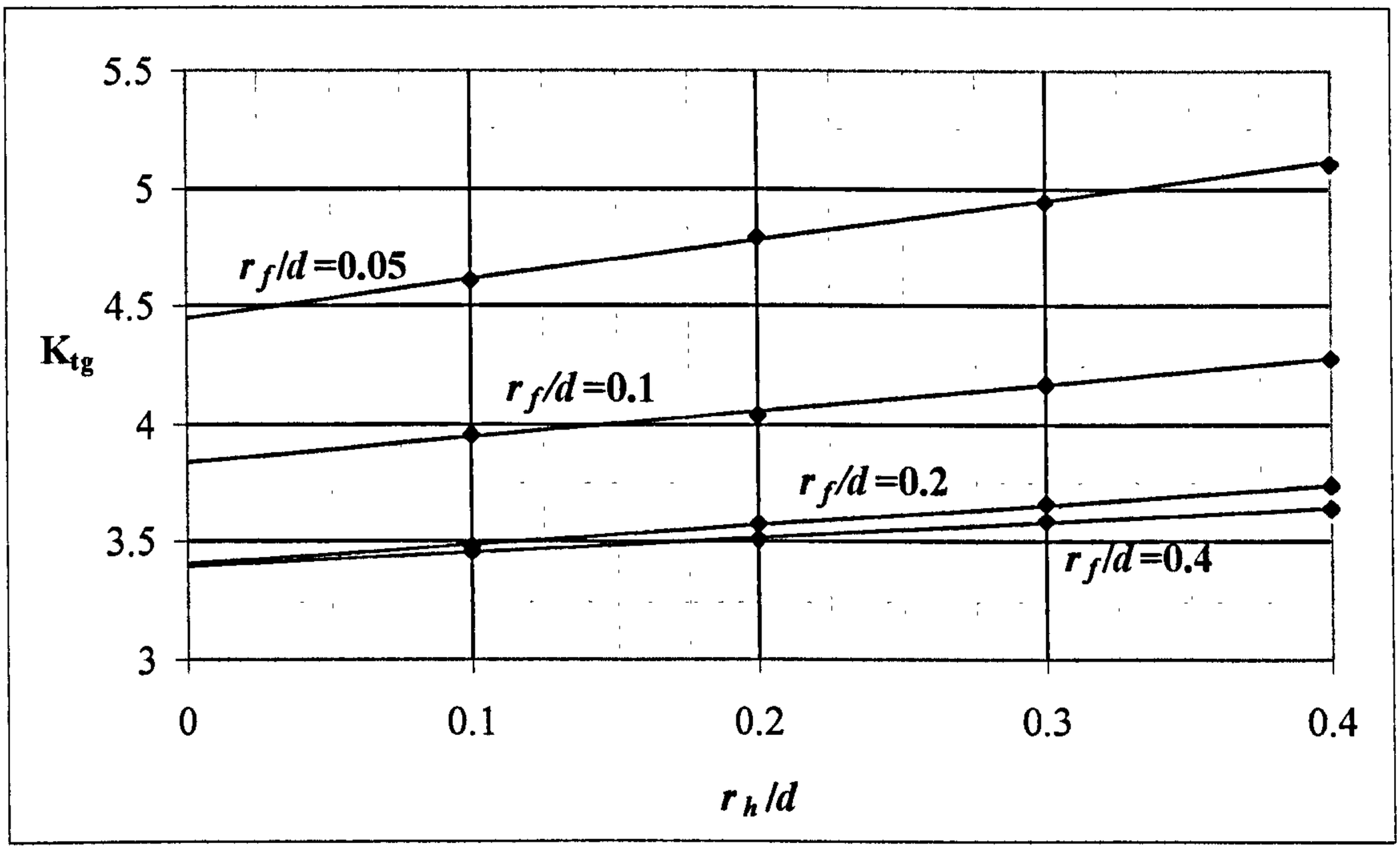

Figure 6-57. Maximum recorded stress concentration for configurations where the hole is positioned at the most critical location, for a series of values of r_f and r_h, and for D/d=0.5

CHAPTER 7

DATA ANALYSIS AND METHODOLOGICAL DEVELOPMENT

This chapter describes the development of methodologies for the evaluation of stress-raisers in proximity. The chapter begins with a detailed analysis of the experimental, numerical and analytical results generated during this research, drawing out particular correlations and highlighting unexpected patterns in the data. Through this process of data analysis, common trends are identified between particular feature interaction problems, allowing these geometries to be classified into two broad problem types: (i) those stress-raisers which lie on a common cross-section, and (ii) those stress-raisers of alternative alignment. Evaluation methodologies are then developed and presented for each of these problem categories, with particular focus on the application of the techniques within the industrial context. The analysis techniques generated for category (i) were found to be generic in nature, enabling the potential for any new feature interaction problems to be integrated into the basic form of this predictive tool. Finally, the process of methodological validation and implementation is presented.

7.1 INTRODUCTION

Having reviewed the results of the experimental and numerical investigations, this chapter is concerned with the analysis of the data obtained, and with the development of methodologies for the prediction of the maximum stress concentration associated with the interaction of features.

Section 7.2 deals with the process of data analysis, drawing together common trends and similarities between each of the feature combination types. Due to the high degree

of accuracy observed between the numerical, analytical and experimental results presented in Chapter 6, it was possible to conduct the data analysis process with confidence in the precision of the stress concentration patterns generated.

Based on the insights gained from this thorough analysis process, Section 7.3 is concerned with the development of predictive methodologies for the analysis of the feature interaction problems considered in this research.

Finally, Section 7.4 provides an overview of the validation of the methodologies developed here, and discusses their implementation as standard practice within the fatigue analysis process at BAE SYSTEMS.

7.2 DATA INTERPRETATION

In Chapter 6, comprehensive results were provided for each of the feature combination categories considered in this research. For each of these geometries, the data collected were presented in terms of the following four key aspects:

(i) single feature data,

(ii) stress concentration distributions,

(iii) magnitude of the maximum stress concentrations, and

(iv) location of the maximum stress concentration.

The identification of these four aspects for each geometry proved to be crucial in understanding the explanatory variables of the problem, such as relative feature size and feature separation distance. For this reason, the following sections have been structured according to these four aspects. In addition, a section has also been included where the definition of infinite boundary conditions for problems of feature interactions is discussed. This section is concluded with a summary of the key findings from the data analysis process.

7.2.1 Single Features

For each problem of feature interaction considered in this research, the initial task in the process of model analysis was an investigation into the stress concentrations associated with each of the features *individually*. It was envisaged that an understanding of the

form and influencing factors of the stress concentration for the individual features would provide an insight into the effect of placing such features in proximity.

A number of interesting characteristics were identified during these preliminary analyses of individual features. One initial observation was that each individual feature generated its own distinctive stress-field, and no detailed similarities could be drawn between the stress concentration decays produced by each geometry. Moreover, it was observed that even the manner in which the form of the stress concentration decay changed with geometric variations was not consistent throughout the individual features investigated. For example, comparisons between Figure 6-4 Chapter 6 (showing the decay from a double-edged notch), and Figure 6-19 Chapter 6 (showing the decay from a single hole) indicate that, although in both cases the maximum stress concentration increases with increased relative feature size, the variation in the gradient of the decay differs in pattern between the features. Figure 6-4 Chapter 6 illustrates that, as the relative size of the notch is increased, the gradient of the stress concentration decay from the feature edge is reduced. In contrast, it can be seen from Figure 6-19 Chapter 6 that, as the relative size of the hole increases, the gradient of the stress concentration decay from the hole edge increases. This comparison illustrates the distinctive influence of each individual feature, and highlights the potential complexities in drawing overarching trends and correlations for problems where such geometries are placed in proximity.

7.2.2 Stress Concentration Distribution

Analysis of the form of the stress concentration distribution generated between geometric features in proximity provides a detailed picture of the manner in which the stress-fields surrounding the features adapt both to the introduction of a secondary feature, and also to geometric variations in the problem configuration. These stress concentration data enable one to compare the distributions observed between interacting features, with the decays generated from each stress-raiser individually. During the investigations into each feature geometry, it was determined that only stress concentration distributions taken between individual points of maximum stress concentration along a line normal to the applied stress produced results which could be utilised in a meaningful way. This factor therefore constrained the geometries for which stress concentration distributions were taken, to the following problems: (i) two

holes in a finite-width plate, (ii) a hole placed between double-edged notches, (iii) a hole placed between shoulder fillets, (iv) a hole placed in proximity to a single fillet, and (v) the three-dimensional problem of intersecting bore holes.

In general, the data have confirmed many initial assumptions relating to feature interactions. For example, the data clearly illustrate the existence of a 'critical separation distance' between the features, beyond which the stress-raisers generate no influence on the maximum stress concentration. It is interesting to note that, under such circumstances where the feature separation is greater than this critical distance, any reductions in the model cross-section due to increases in the feature size are accounted for by increases in the minimum (or base-line) stress concentration between the features, rather than through any variations in the maximum stress concentration (Figure 6-7 Chapter 6). This trend can be observed through the analysis of any of the stress concentration distribution plots provided in Chapter 6. The analysis of the stress concentration distribution data generated for problems of interacting features has highlighted additional unexpected trends, which were of particular interest.

One common pattern that was observed throughout the analysis of the distributions associated with feature interaction problems was the close correlations between the stress concentration decay from any feature individually, and the stress concentration distribution formed when a secondary feature is placed in proximity. An illustration of this association is given in Figure 6-5 Chapter 6, for the problem of a hole placed between double-edged notches. The figure provides the stress concentration distributions between the notch and hole, for a series of hole radii (r_h). This figure illustrates particularly close correlations between the decay for an individual notch (shown in blue), and the feature interaction problem for which the relative hole radius is very small (r_h/r_n=8/75), in the vicinity of the notch. This figure also illustrates another interesting trend in the data, relating to the stress concentration decay from the notch edge as the hole radius is varied (looking at the left-hand portion of the graphs given in Figure 6-5). The figure indicates that, for the constant notch radius, the gradient of the stress concentration decay from this point is independent of the hole radius, and, in fact, is always equal to the gradient of the decay from the individual notch. This trend is confirmed through analysis of the data generated for each of the alternative geometries investigated. For example, Figure 6-15 Chapter 6, illustrates the stress concentration distributions generated for the problem of a hole placed between shoulder fillets, for a

variety of hole radii. Again, this figure illustrates that the gradient of the decay from a feature of constant radius (in this case the shoulder fillet) is independent of the presence or relative size of any additional features.

The most surprising trend identified through the analysis of the stress concentration distribution data, was observed through the investigation of a centrally-placed hole between double-edged notches, for the case where the hole and notch were of constant and equal radius. Figure 6-6 Chapter 6 provides the results associated with this particular geometry, and illustrates the stress concentration distributions between the features for a variety of plate widths. The results illustrate very clearly that, for any given plate width, the maximum stress concentration and the stress concentration decays from each of these features are almost identical (i.e. the stress concentration distribution patterns are symmetrical about the point $x/r_n=0$). This result was particularly striking for the fact that the equivalent decays from the individual hole and individual notch are quite different from one another, both in form and magnitude. An explanation for this phenomenon was sought using a visualisation technique often adopted during the consideration of problems involving stress-raisers; namely the analogous problem of the flow of a fluid. Shown in Figure 7-1 is an illustration of such hypothetical 'stress flows' through the problem of a centrally-placed hole between double-edged notches, where the hole radius is equal to the notch radius.

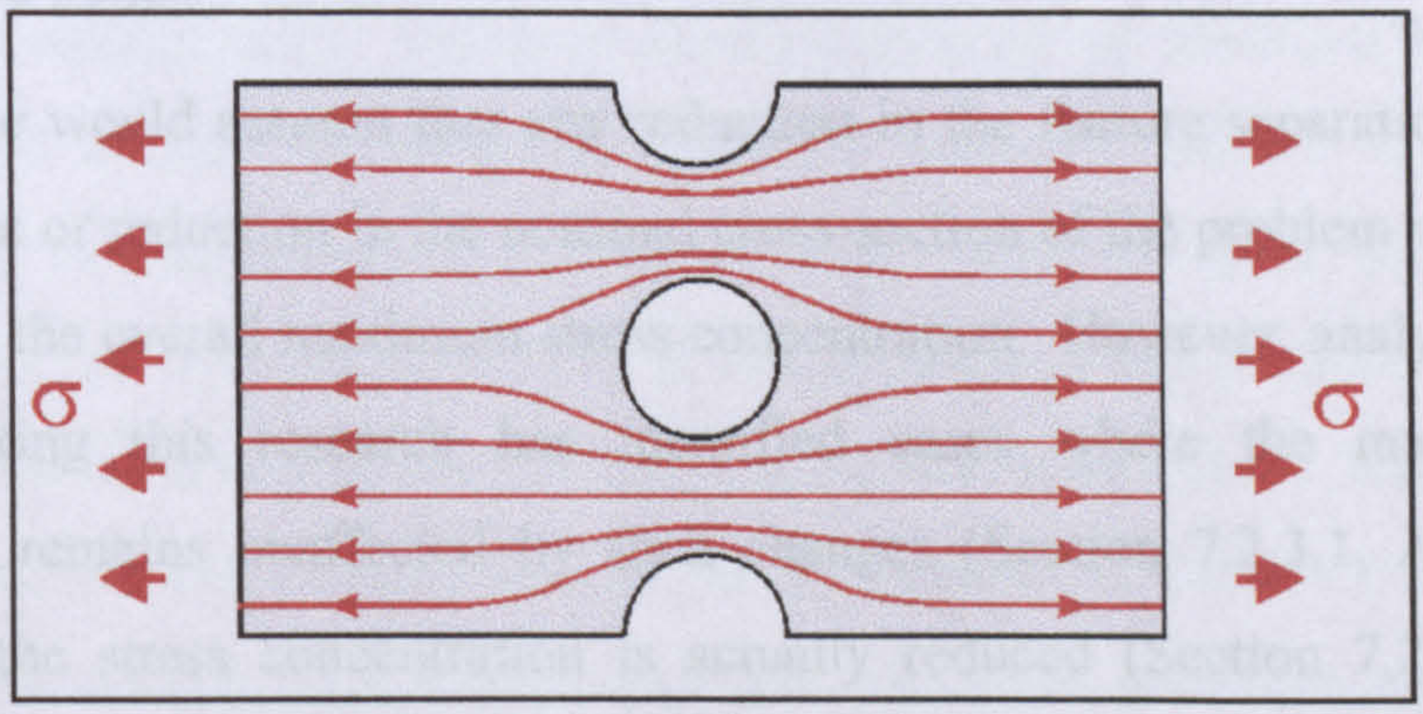

Figure 7-1. Illustration of the form of the 'stress flows' passing through a model of a centrally-placed hole between double-edged notches, for which the radius of the notches and the radius of the hole are equal

As can be seen from Figure 7-1, this particular problem configuration is symmetrical about a central horizontal line, running through the hole centre. Due to its symmetrical nature, it can be assumed that any stress patterns above this line are unaffected by any stress-raising influence in the lower portion, and vice-versa. Each portion can therefore

be considered in isolation, and, as such, are each identical to a simple problem of double-edged notches under tension. A comparison between the data presented in Figure 6-6 Chapter 6, and the appropriate geometries of double-edged notches revealed that these results were indeed identical. This result provides an insight into potential techniques which could be used to simplify problems involving stress-raisers on a common cross-section.

7.2.3 Maximum Stress Concentration

Analysis of the maximum stress concentration data provides interesting insights into the effects of geometric variations in feature interaction problems. For a number of the geometries considered in this research, clear relationships can be established between particular geometric variations, and the maximum stress concentration produced. For example, Figure 6-57 Chapter 6 illustrates the maximum stress concentrations generated from the problem of a transverse hole in proximity to a fillet section, when the hole is positioned in its most critical location. This figure displays clear linear relationships between geometric variations in the hole radius, and the resulting stress concentration value, for a variety of radii of fillet. A number of the feature combinations considered in this research displayed similar straight-forward relationships. However, further analysis of the research data revealed some significant and unexpected trends.

In general, one would assume that any reduction in the feature separation, increase in the feature size or reduction in the nominal cross-section of the problem would result in an increase in the overall maximum stress concentration. However, analysis of the data generated during this research has identified cases where the maximum stress concentration remains unaffected by such changes (Section 7.2.3.1, *No Effect*) and cases where the stress concentration is actually reduced (Section 7.2.3.2, *Negative Effect*). In addition, these data revealed that the actual increases observed in the maximum stress concentration at geometries of interacting features due to any reductions in the nominal stress, are much less significant than those that would be predicted by the aerospace industry (Section 7.2.3.3, *Reduced Effect*). This section provides a more detailed discussion of each of these issues.

7.2.3.1 No Effect

The data evaluation process of the research results revealed a number of feature interaction problems for which particular geometric variations produced no effect on the maximum stress concentration. For example, Figure 6-29 Chapter 6 provides the maximum stress concentration values for a central hole surrounded by eight satellite holes. This figure illustrates that the reduction of the relative radius of the satellite holes from r_s/r_c=0.5 to r_s/r_c=0.25, has no influence on the overall maximum stress concentration. To investigate this issue further, an additional study was conducted, analysing problems for satellite holes of radii $r_s/r_c < 0.25$. This investigation revealed that any further decreases in the relative satellite hole radii beyond r_s/r_c=0.25 had only a marginal influence on the maximum stress concentration. Similar such results were also observed in a number of the problems investigated. For example, it was also established, for the case of a hole between double-edged notches (see Figure 6-9 Chapter 6) that the influence of variation in the notch radius only played a significant role on the overall maximum stress concentration for values $r_n/w > 0.1$. This can be explained by the fact that, for the equivalent geometries of individual notches, the maximum stress concentration itself remains constant for all values of $r_n/w < 0.1$.

One feature interaction problem which was of particular interest to BAE SYSTEMS was that of the transverse hole in proximity to an L-section, containing holes in both the horizontal and vertical faces. The most common form of this structural problem, found throughout the aircraft in integrally-machined sections, occurs where both the horizontal and vertical holes are centrally placed within the plate width and height respectively (i.e. $p_a=w/2$ and $p_b=h/2$). The investigation of this problem comprised the analysis of three main components: (i) the basic problem of a single hole placed in the horizontal face, (ii) holes placed in both the horizontal and vertical faces of identical radius and position (i.e. $r_a=r_b$ and $p_a=p_b$), and (iii) holes placed in either face, with independent position and radius. The analysis of the data generated from these investigations has focussed on the effect of the introduction and geometric variation of the secondary hole on the stress concentration associated with the original hole placed in the horizontal face. For example, Figure 6-39 Chapter 6 provides stress distribution plots for the basic problem involving only a single hole (case (i)), for a series of hole radii. Figure 6-40 Chapter 6 illustrates the stress distribution through the same section (the horizontal face) but for the geometry where a secondary identical hole is placed in

the vertical face (case (ii)). Comparisons between these two sets of data reveal that, although the introduction of the secondary feature produces limited effects on the stress concentration distributions in the horizontal face, the overall maximum stress concentration remains largely unchanged (looking in each case at the right-hand section of the graphs). Moreover, it was also observed that the maximum stress concentration in both cases never exceeded the equivalent value for an offset hole in a two-dimensional plate, for corresponding values for the hole radius (r_a) and using values of the hole position as p_a+0.5t and values for the plate width as w+0.5t.

Analysis of the results from investigation (iii), with holes of independent position and radius placed in either face, revealed that the maximum stress concentration at each of the holes was unaffected by any geometric changes in the additional hole. For example, the data in Figure 6-41 Chapter 6 illustrate the stress concentration distribution in both the vertical (Diagram (i)) and horizontal (Diagram (ii)) faces, for two holes of equal radius, and of comparable offset positions (r_a/w=0.1, p_a/w=0.5, r_b/w=0.1 and p_b/w=0.4). Figure 6-42 Chapter 6 illustrates a similar geometry, but with the secondary hole positioned in proximity to the fillet radius (r_a/w=0.1, p_a/w=0.5, r_b/w=0.1 and p_b/w=0.0175). Comparisons between Diagram (ii) in Figure 6-41, and Diagram (ii) in Figure 6-42 illustrate the effect of the relative movement of the secondary hole on the stress concentration distribution around the original hole. These figures show that this movement of the secondary feature towards the radius fillet has no effect on the maximum stress concentration at the original hole. Analysis of all the data generated from such geometries revealed the same conclusions – the maximum stress concentration associated with a hole in an L-section component remains unaffected by geometric variations of any secondary hole in an opposite face, and the overall values are almost identical (±2%) to comparable stress concentration factors associated with an offset hole in a two-dimensional plate, for hole position p_a+0.5t and plate width w+0.5t.

One possible explanation for this apparent absence of interaction between the two holes could be that the fillet radius is simply acting as an artificial boundary. This result would indicate that any interaction effect observed in the two-dimensional problem of two holes in proximity could be removed by bending the material between the two holes to form an L-section, thus effectively simplifying the problem analysis to that of two independent geometries of single offset holes in a finite-width plate. From the

perspective of the industrial application of this work, an interesting question would be whether there are any circumstances under which the transformation of the two-dimensional problem of two interacting holes, into a three-dimensional L-section with a hole in either face, would actually reduce the overall maximum stress concentration. Comparisons between appropriate sets of data generated during this research for two holes in a finite-width plate (in two dimensions), and a transverse hole in proximity to an L-section (in three dimensions), revealed that the maximum stress concentration levels for the three-dimensional geometry are universally larger than those for the comparable two-dimensional cases.

7.2.3.2 Negative Effect

In general, the majority of results generated during this research displayed some level of maximum stress concentration increase as a result of either a reduction in the feature separation or an increase in the feature size. However, as illustrated in Figure 6-33 Chapter 6, one noteworthy exception to this trend was the case of a central hole surrounded by four satellite holes. The investigations of this problem geometry established that, for satellite holes of equal or greater radius to the central hole, the maximum y-direction stress concentration starts to decrease below a certain threshold separation distance. Further detailed analysis of this problem revealed two causes for this unexpected trend: (i) the migration in the point of maximum stress concentration around the hole circumference, and (ii) the change in direction of the maximum stress concentration. These two factors are discussed below.

It is well known that the maximum stress concentration for a single hole in a plate under tension occurs at either edge of the hole, along a line perpendicular to the applied stress, with a high stress gradient away from these points. For the majority of interaction problems studied during this research, the position of the overall maximum stress concentration occurs at the individual point of maximum stress concentration for one of the features present, again with a high stress gradient. However, for the case of a central hole surrounded by four satellite holes, as the configuration of holes (and thereby their associated stress fields) is drawn closer together, the overall point of maximum stress migrates from its original position, along the hole circumference in the direction of the secondary point of high stress at an adjacent hole. These changes in the stress distribution are illustrated in Figure 6-34 Chapter 6, for the case where r_s/r_c=1.

As a number of such points of high stress are drawn closer together, moving along the circumference of each respective hole, one large highly-stressed region is created, surrounded by a relatively low stress decay. In order for equilibrium throughout the model to be maintained, the magnitude of the maximum stress concentration over this relatively large area must therefore be reduced.

The second factor affecting the observed decrease in the maximum stress concentration for the problem of a central hole surrounded by four satellite holes, is variations in the direction of the maximum stress concentration. For every other geometric problem considered in this research, results have shown that the maximum stress concentration occurs at a boundary parallel to the applied stress. Therefore, for these problems, it can always be assumed that the maximum stress concentration occurs wholly in this direction. However, in the particular case of the four satellite hole problem, due to the migration of the point of the maximum stress, this stress direction can no longer be considered purely in the y-direction. Figure 6-35 Chapter 6 illustrates the x-direction, y-direction and First Principal stress concentrations for the case where r_s/r_c=2. This figure shows that, for separation distances (s/r_c) greater than approximately 3.9, the x-direction stress concentration is zero and the y-direction and First Principal stress concentrations are identical. However, at separation distances smaller than this value, the x-direction stress concentration becomes non-zero, and the y-direction stress concentration deviates from the First Principal stress concentration. Although the First Principal stress concentration displays an overall increase in value below this separation, a distinct dip is also visible at this critical value due to the plateauing of the maximum stress concentration within the hole configurations.

It is interesting to note that these effects are not observed for the associated problem of a central hole surrounded by eight satellite holes. This is simply due to the fact that, for configurations of eight radial holes, each of relatively large radius, the geometries themselves intersect before any migration effects in the maximum stress concentration can occur.

7.2.3.3 Reduced Effect

One particularly interesting outcome of the analysis of the data generated during this research was the observation that the recorded maximum stress concentration was consistently lower than those which would have been estimated by fatigue experts

within the aerospace industry, using basic engineering principles. Prior to the research investigation, it had been generally assumed that any increase in the maximum stress concentration resulting from the introduction of an additional feature would be produced by the combined action of two elements:

(i) an overall increase in the nominal stress levels due to the reduction in cross-sectional area from the addition of a new feature, and

(ii) increased maximum stresses due to the interaction between the two stress-fields.

However, on analysis of the results generated during this research, an unexpected trend was observed, which did not support this assumption.

Data evaluation revealed that only a minimal increase in the maximum stress concentration value was observed with the introduction of a relatively small secondary feature to a particular problem. As an illustrative example of this trend, the case of a hole placed between shoulder fillets will be drawn upon, results for which are given in Figure 6-17 Chapter 6. As can be seen from this figure, when r_f/d=0.06 and r_h/d=0.05, the maximum stress concentration is 2.8. However, the maximum stress concentration for shoulder fillets containing no central hole (where r_f/d=0.06) is also 2.8, indicating no initial increase in the stress concentration with the addition of the hole. These results ran contrary to the initial predictions, which assumed a base-line increase in the maximum stress concentration, rising in proportion with the reduction in cross-sectional area caused by the second feature (due to element (i) above), compounded by any interaction effect between the two features (element (ii)). Although, for the cases where r_h/d<0.2 (see Figure 6-17 Chapter 6), the separation distance between two features was thought to be sufficiently large that no significant stress field interaction was produced, an increase in stress concentration was still expected due to the reduced cross-sectional area. An investigation was therefore conducted to compare the results given in Figure 6-17 Chapter 6 with the theoretical levels of maximum stress concentration present at the shoulder if account were simply taken for the reduction in cross-section due to the introduction of the hole[1]. The results of this comparison are

---

[1] This reduction in cross-section was accounted for by multiplying the stress concentration value (K_{tg}) for the individual shoulder, by the ratio of the original cross-sectional area to the new cross-sectional area which is produced on introduction of the hole.

given in Figure 7-2 for the case where r_f/d=0.06. This graph indicates very clearly that the research results taken from the geometry of interacting hole and shoulder (illustrated in blue) are actually significantly *lower* than those values for the shoulder alone adjusted for the reduced cross-section (illustrated in black). This surprising result is accounted for by the very fact that there are two stress-raising features affecting the cross-section rather than one. The explanation for this phenomenon is given below.

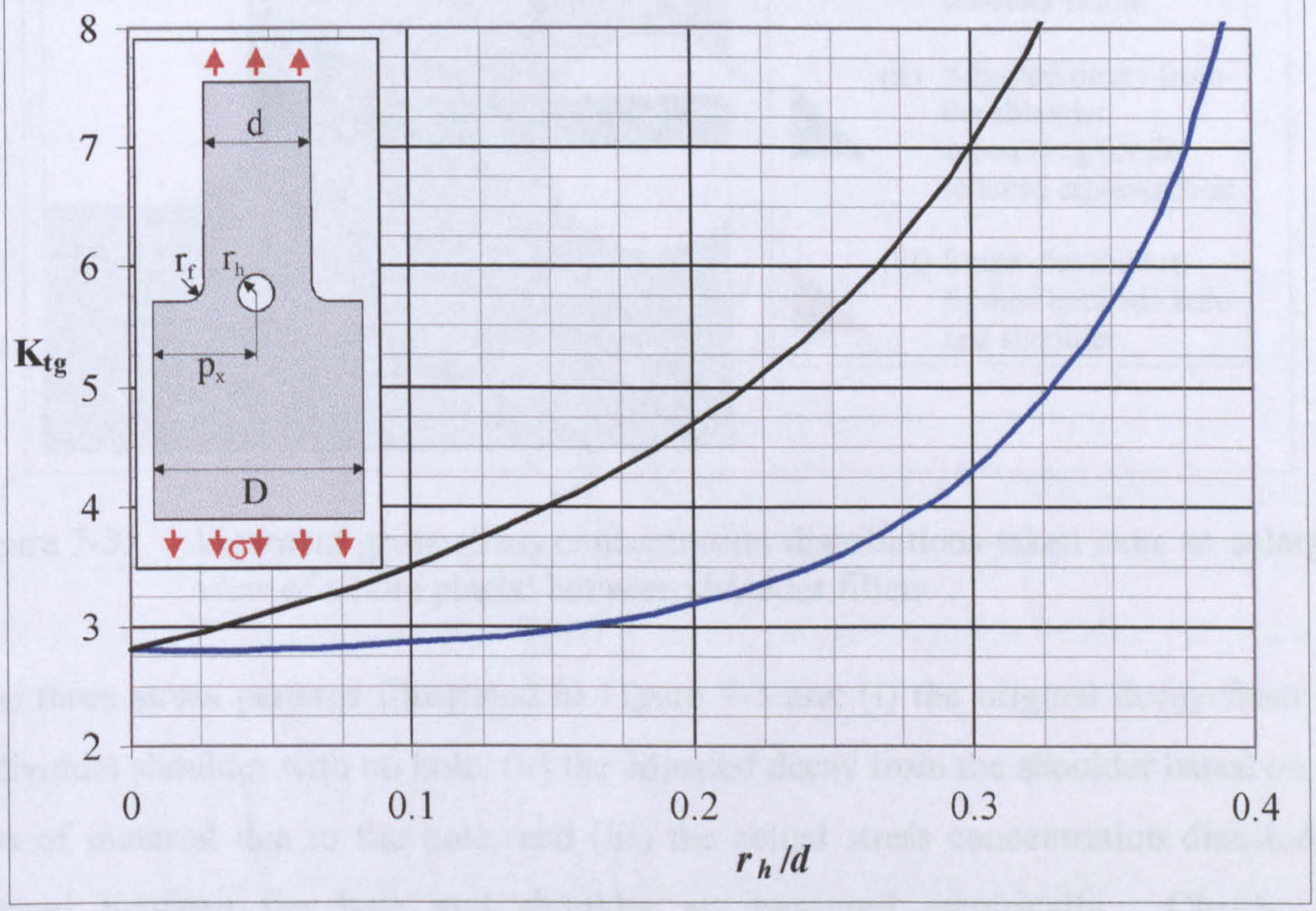

Figure 7-2. A comparison of research results for a centrally-placed hole between shoulder fillets where r_f/d=0.06 (given in blue), with corresponding values for the individual shoulder over an appropriately adjusted cross-section (given in black)

Any feature placed under tension has an associated stress pattern, running perpendicular to the applied stress, which increases to a peak at the feature edge (see Figure 6-13 Chapter 6, for stress concentration decays from shoulder fillets). The introduction of a secondary feature to that cross-section will introduce an additional stress pattern, with a corresponding peak at the feature edge. In order for stress equilibrium to be maintained in the section, the introduction of this additional region of high stress must be balanced by the lowering of the remaining stress levels through the section. The effect of this stress-redistribution is that the maximum stress levels for two particular features placed in proximity are lower than those levels found for each feature individually over an

appropriately adjusted cross-section. This result is illustrated in Figure 7-3, using the example of the hole and shoulder section placed in proximity. The figure provides an enlarged view of the section between the hole and shoulder, along with graphs depicting various stress distributions through the section.

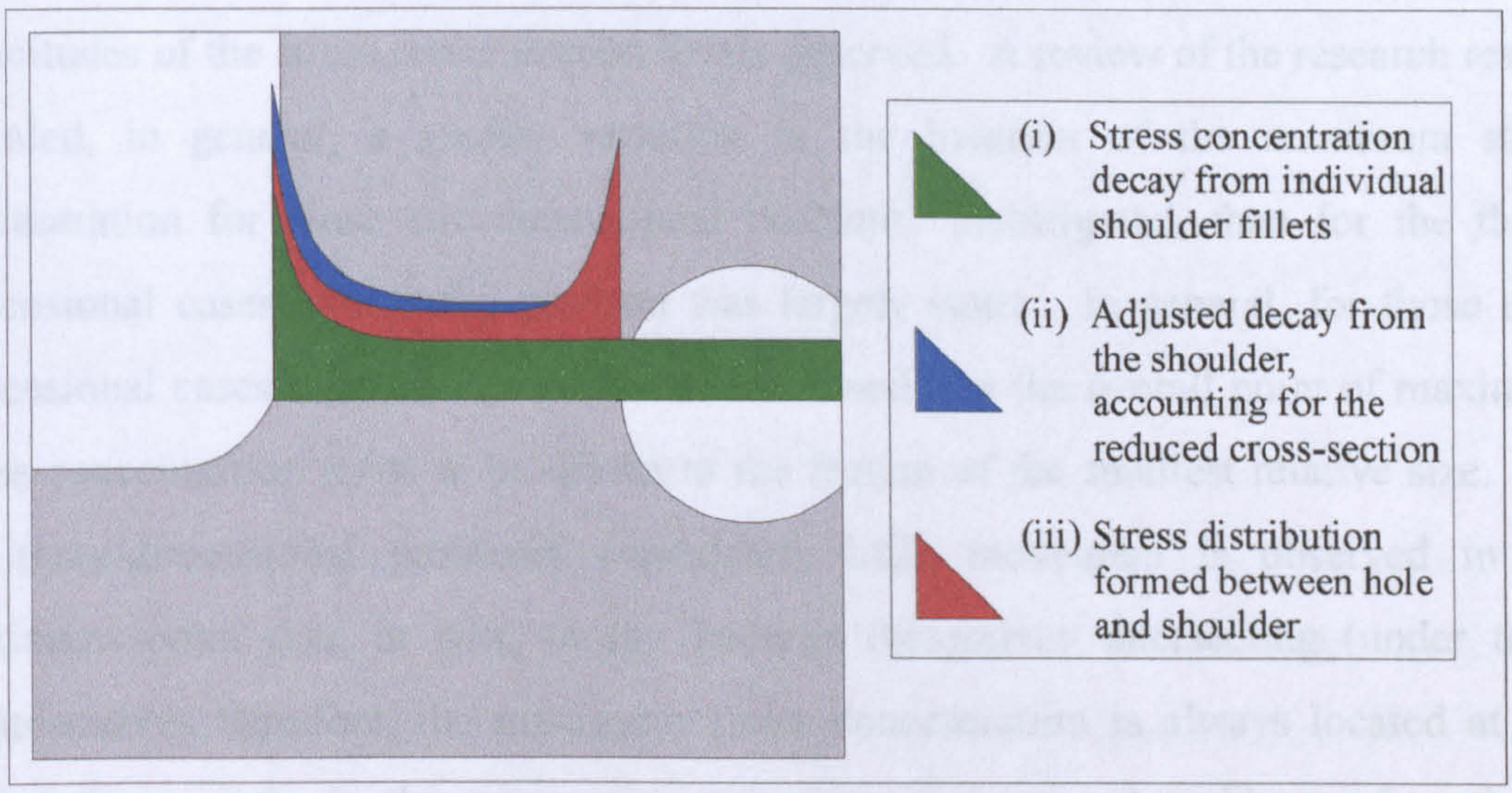

Figure 7-3. Ligament gross stress concentration distributions taken over an enlarged view of a hole placed between shoulder fillets

The three stress patterns illustrated in Figure 7-3 are: (i) the original decay from the individual shoulder with no hole, (ii) the adjusted decay from the shoulder based on the loss of material due to the hole, and (iii) the actual stress concentration distribution formed between the hole and shoulder as measured empirically. Clearly, for equilibrium to be maintained, the area under curve (ii) must be equal to that under curve (iii), as they are both acting over the same area. Figure 7-3 illustrates that, although the maximum stresses formed by the two features in proximity (pattern (iii)) are greater than the maximum stress of the individual shoulder (pattern (i)), they are still significantly lower than the stress formed at the shoulder for the reduced cross-section (pattern (ii)).

As can be seen in Figure 7-2, this apparent stress-lowering effect has a significant influence on the levels of maximum stress concentration present in a geometry involving features in proximity. However, it is not currently accounted for by fatigue analysts within the aerospace industry, and would also not have been predicted by any approximation methods currently available. The discovery of this effect is therefore of particular interest, and will form an element of the final method of analysis.

7.2.4 Position of the Maximum Stress Concentration

Investigation of the position of the maximum stress concentration for each of the problems under consideration has provided a number of insights into the impact of geometric variation, and in particular, the significance of particular feature types on the magnitudes of the stress concentration levels observed. A review of the research results revealed, in general, a greater variation in the location of the maximum stress concentration for those two-dimensional problems investigated, than for the three-dimensional cases, where the position was largely static. In general, for those two-dimensional cases considered, it can be determined that the overall point of maximum stress concentration tends to be drawn to the feature of the smallest relative size. For the three-dimensional problems considered, little movement is observed in the maximum point due, in part, to the features themselves intersecting (under these circumstances therefore, the maximum stress concentration is always located at this intersection point). In this connection, two three-dimensional problems of particular interest were those of the cross-wise bore-holes and the hole placed in proximity to a fillet radius. Each of these two cases is discussed in more detail below in Sections 7.2.4.1 and 7.2.4.2 respectively.

7.2.4.1 Cross-Wise Bore-Holes

The problem of the cross-wise bore-holes provided an interesting geometry for analysis, as, not only did the features fully intersect for each possible geometric configuration, but this point also coincided with the location of each of the maximum stress concentrations for each feature individually. As demonstrated by the study results, this configuration therefore generated very high stress concentration values. Figure 6-48 Chapter 6 illustrates that, for bore holes of equal radius (r_b/r_a=1), as the block dimensions h and w tend to infinity, the maximum stress concentration value tends to six. This result was of particular interest, as similarities can be drawn with the two-dimensional problem of a hole in a plate under tension, where, as the plate width tends to infinity, the maximum stress concentration at the hole tends to three. Due to the coincidence of the two individual points of maximum stress concentration, further data analysis was conducted, to ascertain whether any correlations existed between the maximum stress concentration results generated for this geometry, and the standard stress concentration results for individual two-dimensional offset holes in finite-width

plates under tension, using equivalent values for r_a, w, p_a, r_b, h and p_b. This investigation revealed that the overall maximum stress concentration for the problem of cross-wise bore holes was directly proportional to the product of the equivalent two-dimensional problems for each of the features individually. Further investigations of these direct relationships indicated that an accurate prediction of the maximum stress concentration for any geometry of cross-wise bore-holes could be generated by the simple multiplication of the individual stress concentration values for each hole in two dimensions (based on the appropriate plate dimensions and hole positioning) adjusted by an appropriate factor. Details of this method are provided in Section 7.3.1.6.

7.2.4.2 Transverse Hole in Proximity to Fillet

Analysis of the research data for the problem of a transverse hole in proximity to a fillet required investigations in three stages: (i) evaluation of the stress distributions through the simple problem of a fillet containing no hole (Figure 6-51 Chapter 6), (ii) analysis of the effect of the introduction of a hole to this geometry, over a series of hole positions (Figure 6-54, Figure 6-55 and Figure 6-56 Chapter 6), and (iii) evaluation of the overall maximum stress concentration for each of these geometries, where the hole is placed at the most critical position (Figure 6-57 Chapter 6). The geometric problem of a hole in proximity to a fillet section typically occurs within integrally machined structures. The issue of specific interest to BAE SYSTEMS was the geometry, typically occurring during manufacturing concessions, where the hole was misplaced, either in closer proximity to the fillet than originally designed, or positioned through the fillet radius itself. In particular, BAE SYSTEMS required a quantification of the magnitude of the 'worst case' stress concentration generated from a range of problem geometries, along with an identification of the exact position of the hole under these circumstances. As discussed in Section 7.2.3, these maximum stress concentration values are a linear function of the hole radius, for given values of the radius of the fillet. In this section, the particular hole positions which generate such maximum stress concentrations are discussed.

Given in Figure 6-51 Chapter 6 is the stress concentration distribution through the radiused fillet section, for a model containing no hole. This figure illustrates a significant peak in the stress concentration at a localised point along the fillet radius. As illustrated in Figure 6-53 Chapter 6, the location of these points of maximum stress

for the individual fillet vary with the fillet radius. The results generated from the introduction of a transverse hole, at a series of positions, to this geometry is given in Figure 6-54, Figure 6-55 and Figure 6-56 Chapter 6. These graphs indicate two localised hole positions which generate peaks in the maximum stress concentration. The larger of the two peaks, in each case, is located at the same point as the individual maximum stress concentration from the individual fillet, and is therefore the result of the full intersection of the maximum stresses associated with each of the features. The secondary peak in each case is located marginally below the point p/d=0, and is generated from the hole centre, and therefore its associated maximum stress concentration, being positioned in very close proximity to the change in cross-section.

It is also interesting to note that, for those geometries where the hole is placed beyond a relatively small distance from the radius (approximately where p=2.5r_f), the two features produce no interacting influence.

7.2.5 Infinite Plate Width

The initial specifications provided for each of the two- and three-dimensional problems considered in this research, required at least one of the structural dimensions to be considered as 'infinite'. For most of the geometries investigated, this simply required preliminary finite element studies to establish the geometric constraints for which the 'infinite' boundaries produced no interacting effect on the region of interest. During such studies of the four and eight hole satellite problems, however, it was noted that, in many cases, the plate dimensions required to simulate infinite conditions were surprisingly large. Therefore, a comprehensive analysis was conducted, to ascertain the plate width and height (w_i and h_i respectively), over each geometric configuration, for which that plate could be considered as infinite. The results of this study are given in Figure 6-30 Chapter 6. Further analysis of these data established that the infinite plate height (h_i, for which w_i=h_i) was a function of the hole separation (s), over a series of satellite hole radii (r_s/r_c). These relationships are presented in Figure 7-4.

The investigation of additional geometries for which s/r_c>20, indicated that each of the graphs given in Figure 7-4 seemed to be asymptotic to particular values of $h_i r_c/s$. This observation was consistent with the original stress-concentration results generated for the satellite hole problem (Figure 6-29 Chapter 6), where all the data were asymptotic to stress concentration of three, where s/r_c>25 (i.e. beyond this point, no interaction

effects were observed). Further analysis of the data presented in Figure 7-4 revealed that each graph was asymptotic to a different value of $h_i r_c/s$, based on the following relationship:

$$h_i=2(s/r_c) + 6(r_s/r_c)$$

In other words, beyond a critical separation distance where the configuration of holes no longer interact, the infinite boundaries can simply be positioned at a distance of $5(r_s/r_c)$ beyond the satellite hole edge, in order for these boundaries to produce no stress-raising influence.

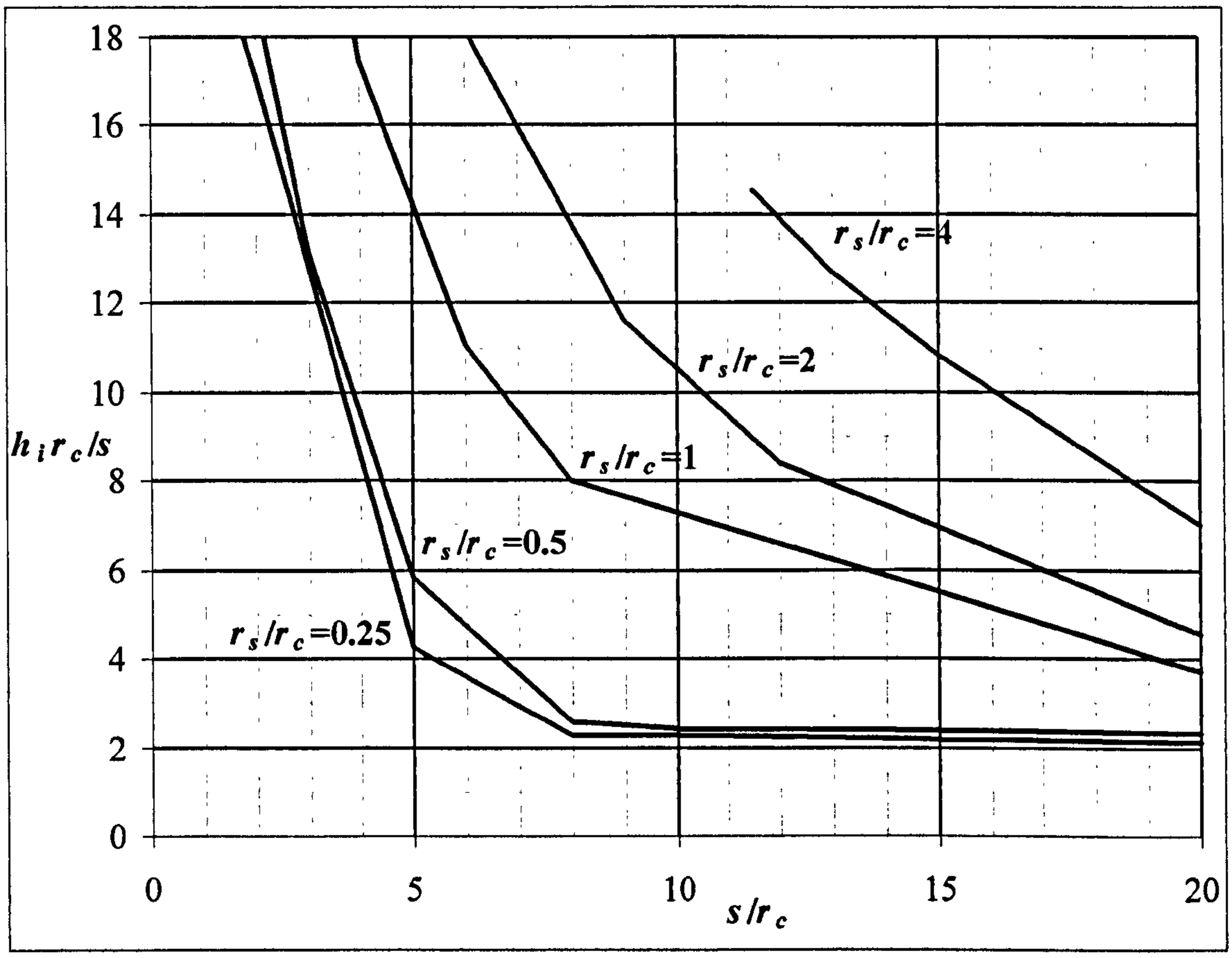

Figure 7-4. Illustration of the relationships identified between the relative 'infinite plate dimensions' (h_i, where $h_i=w_i$) and the relative hole separation distance (s) for problems involving four or eight satellite holes surrounding a central hole

7.2.6 Key Characteristics of the Overall Results

This data interpretation section has described a wide range of issues drawn out from the analysis of the analytical, numerical and experimental results generated during this research. The analysis has highlighted a number of unexpected results, such as the

apparent absence of stress-field interaction between holes placed on adjacent faces within an L-section. However, a number of general characteristics were identified, across all problem types, which would prove to be crucial to the development of stress concentration models. These are listed below:

- correlations have been identified between the maximum stress concentration associated with features individually, and the value of the maximum stress concentrations observed when such features are placed in proximity,
- correlations have been identified between geometric variations in the problem model, and the resulting changes in the maximum stress concentration,
- in general, for features placed in proximity, the overall maximum stress concentration tends to be drawn to the feature of smaller relative size, and
- in all cases investigated, the maximum stress concentration was significantly lower than would have been predicted using current estimation tools within the aerospace industry.

There was also a large number of geometric problems for which it was possible to generate stress concentration distribution plots between the features under consideration. For these features, it was possible to gain additional insights into the influence of geometric variation in the problem geometry. In particular, it was possible to generate detailed comparisons between the stress concentration decay from individual features, and the overall stress concentration distribution formed when such features are placed in proximity. One trend of particular interest, drawn out from such comparisons, was that the gradient of the stress concentration decay from a given feature is independent of any additional geometric influences (i.e. this decay remains constant, irrespective of the presence or size of any additional feature). This result is of particular interest, as it removes a potentially complex variable from the problem analysis, thus simplifying the stress-field model for the evaluation of these problems.

7.3 METHODOLOGICAL DEVELOPMENT

The data analysis presented in this chapter has identified a number of correlations between geometric variations in the configuration of feature interaction problems, and their effects on the overall stress concentration. The aim of this section is to utilise these relationships to generate robust methodologies for the prediction of the position

and magnitude of the maximum stress concentration under such circumstances. It must be noted, however, that these formulations will be estimates, based on the comprehensive empirical data generated as part of this research. Any exact solutions that do not rely on such empirical relationships could only be generated from analytical treatments. As discussed previously, treatments of this type would provide relationships of such a highly complex and specific nature as to render them unusable in any industrial context.

The data analysis presented in the previous section described two broad categories of feature interaction problem:

(i) those problems whose stress-field interaction can be represented meaningfully by stress concentration distributions between the features, and

(ii) those geometries for which the stress-field interaction can only be characterised by the location and magnitude of the maximum stress concentration.

These two broad classifications can be more conveniently described as:

(i) those problems involving features which lie on a common cross-section (normal to the applied stress), and

(ii) those geometries containing features of alternative alignment.

Detailed analysis of these feature interaction categories indicated that two differing approaches would be required for the generation of predictive methodologies in each case. Analysis of those features which lie on a common cross-section indicated that a generic evaluation tool could be developed, based on an understanding of the form and influencing factors of the stress concentration distributions between the features. In contrast, analysis of the data generated from those features of alternative alignment revealed no overarching trends or similarities, due to the inherent differences in the geometries considered. For these latter problems, it was therefore anticipated that individually-tailored analysis tools would be required for each geometry.

In this section, the methodological development is described for the two feature interaction categories, (i) features which lie on a common cross-section (Section 7.3.1), and (ii) features of alternative alignment (Section 7.3.2). Finally, in Section 7.3.3, a summary is provided of all the evaluation methodologies developed.

7.3.1 Multiple Features at a Common Cross-Section

Those features considered in this research which lie on a common cross-section normal to the applied stress are: (i) two holes in a finite-width plate, (ii) a hole placed between double-edged notches, (iii) a hole placed between shoulder fillets, (iv) a hole placed in proximity to a single fillet, and (v) the three-dimensional problem of transverse bore-holes. This section discusses, initially, those factors which proved critical to the generation of predictive methodologies, followed by presentations of the resulting evaluation tools for each of the geometric problems under consideration.

7.3.1.1 Modelling Considerations

One particular issue drawn out in the data analysis process was found to be of particular relevance in the formation of the prediction methodology. This was based on correlating the stress concentration at given points between the interacting features, with the stress concentration levels associated with each feature individually at equivalent points.

The development of methodologies for the evaluation of interacting features required the quantification of the relationships between the *individual* stress concentrations for the single features and the *interacting* stress concentrations for the combined geometry, through a process of focused data manipulation. In this connection, a number of important factors needed to be considered in detail:

(i) the basic nature of the relationship between the *individual* and *interacting* stress concentration values,

(ii) the actual stress concentration measure which generated the closest correlations between these two values (i.e. the choice of whether to use the *net* or the *gross* stress concentration factor), and

(iii) the particular individual stress concentration values which correlate most successfully with the interacting values (for example, the determination of the cross-section over which the individual stress concentration values are calculated).

In this section, each of these issues is discussed, along with an overview of additional adjustments designed to improve the accuracy of the methodologies under development.

The initial stage of the process of methodological development involved the identification of the general nature of the relationship between the stress concentrations associated with the two features individually, and that of their combination. The two obvious models under consideration were based on the *sum* and the *product* of these individual values.

It was considered that the sum might prove to be a plausible method, as summation is the basis for the prediction of the stress concentrations associated with problems of combined loadings (British Aerospace Defence Limited 1996). In these cases, the overall stress concentration is estimated by taking the sum of the stress concentrations associated with each loading condition individually. However, this model did not prove promising in predictive terms, for the problems considered in this research, with no clear correlations identified between the *individual* and *interacting* stress concentrations for a given geometry.

The second avenue for exploration was based on the product of the individual values. This manipulation technique proved to be much more fruitful, with the identification of clear correlations between individual and interacting stress concentrations throughout all of the models under consideration. The success of the product model over that of the sum was not entirely surprising for the following reasons:

(i) the idea that the sum would form the basis of a suitable model derives from the assumption that inherent commonalties exist between problems of multiple features and problems of multiple loading conditions. It is well known that multiple loading conditions can be equated to the superposition of each individual applied load, and therefore, in this application, the choice to sum the individual stress concentrations is logical. However, the combination of multiple features produces highly complex interaction effects, which cannot simply be represented by any superposition of the individual levels, and therefore the argument for a summation model is inappropriate,

(ii) intuitively, stress concentrations are measured as 'factors', and as such can be thought to contribute in some multiplicative manner to the overall effect, and

(iii) given that the base-line value for which no stress-raising effect is experienced is represented by a stress concentration factor of one (rather than zero), it might suggest that a multiplicative rather than an additive model is more appropriate

(mathematically, one is the identity element under multiplication, whereas zero is the identity element under addition).

Another important consideration in the generation of the predictive methodology was which particular stress concentration measure would produce the more accurate and consistent prediction tool; the *net* or the *gross* value. After the generation of a series of comparable models, it was established that, for all geometries investigated, manipulations of the gross stress concentration values were found to provide much stronger correlations than the equivalent analysis using the net stress concentration values. In practical terms, this facilitated the generation of a more straight-forward evaluation tool. Net stress concentration factors are typically employed for geometries of a given nominal cross-section, for which 'adjustment factors' are used to account for effects such as surface finish or life improvement techniques. In the application under consideration in this research, however, the nominal cross-section varies with the problem type, and net stress concentration would therefore have been a less convenient measure to have used, when the ultimate value required is the absolute maximum stress. One possible explanation was proposed as to why, in the cases considered in this research, the predictive methodology based on the *gross* stress concentration factor proved to be more consistently accurate than those based on the *net* value. Analysis of the data has suggested that the removal of material due to the introduction and expansion of any additional features produces a much less significant effect than may have been anticipated. As discussed in Section 7.2.3.3, this phenomenon may be explained by the fact that any increases in the nominal stress from material loss are effectively counteracted by a reduction in the maximum stress levels due to the introduction of the additional area of high stress. It could be postulated that one possible result of this effect is that the only significant factor influencing the two features in proximity is the interaction of the stress-fields, with the effects due to the loss of material being rendered negligible. If this argument held true, the use of net stress concentration factors in this context would therefore clearly not provide a sound basis for any predictive tool.

The process of data analysis, for those features which were positioned on a common cross-section, revealed that, for a feature of constant relative size, the gradient of the stress decay from that feature remained constant throughout any additional geometric variations (as discussed in Section 7.2.2). The data also showed that this gradient could

be easily determined through the analysis of that feature individually (over the gross cross-section). This characteristic of the stress distribution from any interacting feature means that the stress decay from any given feature can be can be evaluated as a simple function of the maximum stress concentration at the feature edge. Therefore, although correlations between individual stress concentrations and interacting stress concentrations have been identified throughout the entire cross-section over which the problem was considered, detailed calculations are required only at the points of high stress at the feature edges. This focus of the methodology at the feature edges also targets the accuracy of the technique under development on those critical locations where the evaluation of the stress concentration is crucial.

A series of thorough investigations were conducted to evaluate the particular stress concentration values whose product correlated most successfully with the actual interacting stress concentration values. This investigation revealed that, for each of the critical points under consideration (in all cases positioned at a feature edge), the two values required were:

(i) the individual maximum stress concentration associated with the particular feature at the point of consideration (calculated over the *gross* section of the problem), and

(ii) the decayed stress concentration resulting from the individual influence of the closest boundary (be that the plate width or the second feature) at the point of consideration (again calculated over the *gross* section).

For example, for the case of two holes in a finite-width plate, the data analysis revealed that the overall maximum stress concentration could occur at any one of four distinct points, as dependent on the configuration of the problem. These four positions are illustrated as points 1, 2, 3 and 4, in Figure 7-5. In this case, the value of the product at point 2 is the maximum stress concentration due to hole *a* multiplied by the decayed stress concentration from hole *b* at this point. The value of the product at point 1 is simply the maximum stress concentration due hole *a* individually, as stress concentration influence from the plate boundary will be equal to one.

Based on each of these considerations, methodologies have been developed for the feature interaction problems which lie on a common cross-section: (i) two holes in a finite-width plate (Section 7.3.1.2), (ii) a hole placed between double-edged notches

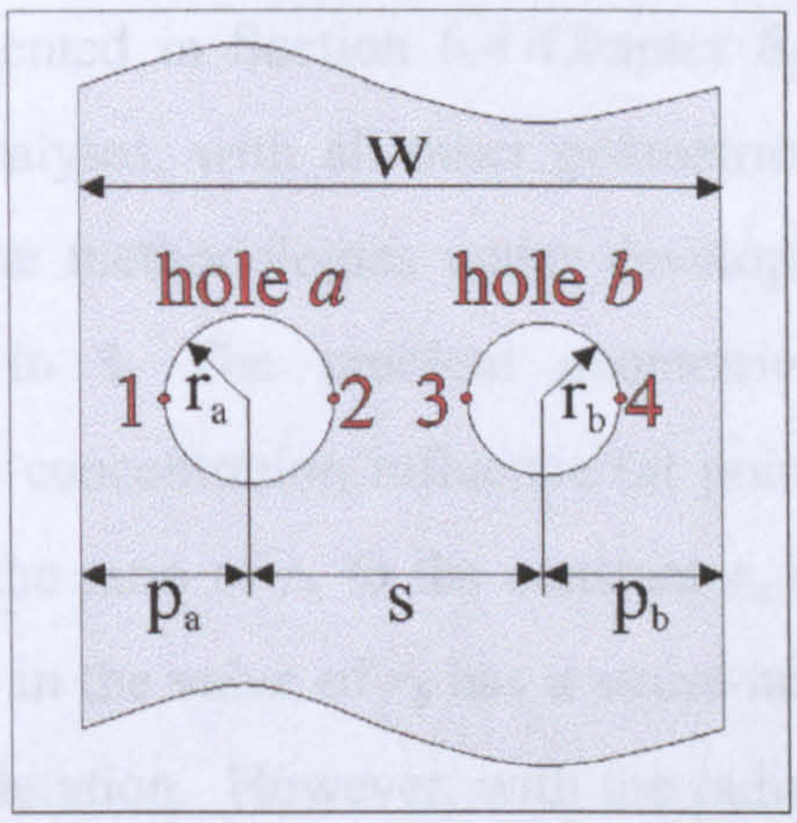

Figure 7-5. Positioning of the four potential locations of the maximum stress concentration for the problem of two holes in a finite-width plate

(Section 7.3.1.3), (iii) a hole placed between shoulder fillets (Section 7.3.1.4), (iv) a hole placed in proximity to a single fillet (Section 7.3.1.5), and (v) the three-dimensional problem of transverse bore-holes (Section 7.3.1.6). Similar techniques were used for the development of the methodologies in each case. For this reason, only in the case of the first geometry discussed (that of two unequal holes in a finite-width plate), will full details be provided of the techniques used to generate the methodology.

As will be revealed in Section 7.3.1.7, each of these methods can be drawn together into a single overarching formula that can be used to analyse any interacting features which lie on a common cross-section.

7.3.1.2 Two Holes in a Finite-Width Plate

As has been discussed in the previous section, a series of clear correlations have been observed between the stress concentration distributions recorded for problems involving interacting stress-raisers, and the product of appropriate stress concentrations for those features individually. For the case of two holes in a finite-width plate, the maximum stress concentration can occur at one of four points (marked 1, 2, 3 and 4 in Figure 7-5).

The basis of the methodological development involves the identification of the exact empirical relationship between the stress concentrations observed for the interacting holes and the product of the appropriate values for the individual holes, at each of the four points under consideration. An extensive series of comparisons was therefore generated between the actual recorded stress concentration and the product of the individual stress concentration for a wide range of geometric configurations.

In line with the data presented in Section 6.4 Chapter 6, the value of r_a was held constant throughout the analyses, with all other geometric parameters normalised by this value. In terms of the methodologies under development, this is equivalent to setting the value of r_a to 1. The problem geometries were analysed through investigations of the stress concentration influence (at points 1, 2, 3 and 4) for given values of p_a, p_b and s, as the ratio of r_b to the constant r_a was varied. The data have shown that such variations in the value of r_b has a stress-raising impact on each of the four positions under consideration. However, with the radius of r_a remaining constant, the product of the individual stress concentrations associated with points 1 and 2 were found to show little variation, and it was therefore more difficult to correlate these values with the stress concentrations for the interacting problem than it was for the equivalent stress concentrations at points 3 and 4. It was therefore determined that the problem should be viewed in two separate stages. Stage one involved scaling the original problem using r_a as the normalising unit, and taking evaluations for points 3 and 4. In stage two, the problem was then re-scaled, this time using the value of r_b as the normalising unit. By symmetry, the evaluation of point 1 was based on the same relationship form as that developed for point 4 and, in a similar way, the evaluation of point 2 was based on the same relationship form as that developed for point 3. For this reason, relationships between the *individual* stress concentrations, and the *interacting* stress concentration only needed to be developed at points 3 and 4. The development of these methodologies at these two locations will be discussed in turn.

Given in Figure 7-6 are two examples of the comparisons between the actual stress concentration for the interacting holes (shown in blue) and the product of the appropriate individual stress concentrations (shown in red) at point 3 in the geometry. These figures provide the stress concentration results for a variety of ratios of r_b/r_a, where $s=4r_a$. Comparisons between the sets of data presented in Figure 7-6 indicate similarities in the relationships between the *actual* stress concentration and the *product* of the individual stress concentrations at this point. In order to quantify this relationship, a ratio was taken of the two values (the *actual* stress concentration for the interacting features divided by the product of the two appropriate individual stress concentrations at the desired point). This value shall be referred to as R. For ease of data manipulation in this particular geometry, it was decided it would be more convenient to use a ratio based around a value of zero, rather than one (for cases where

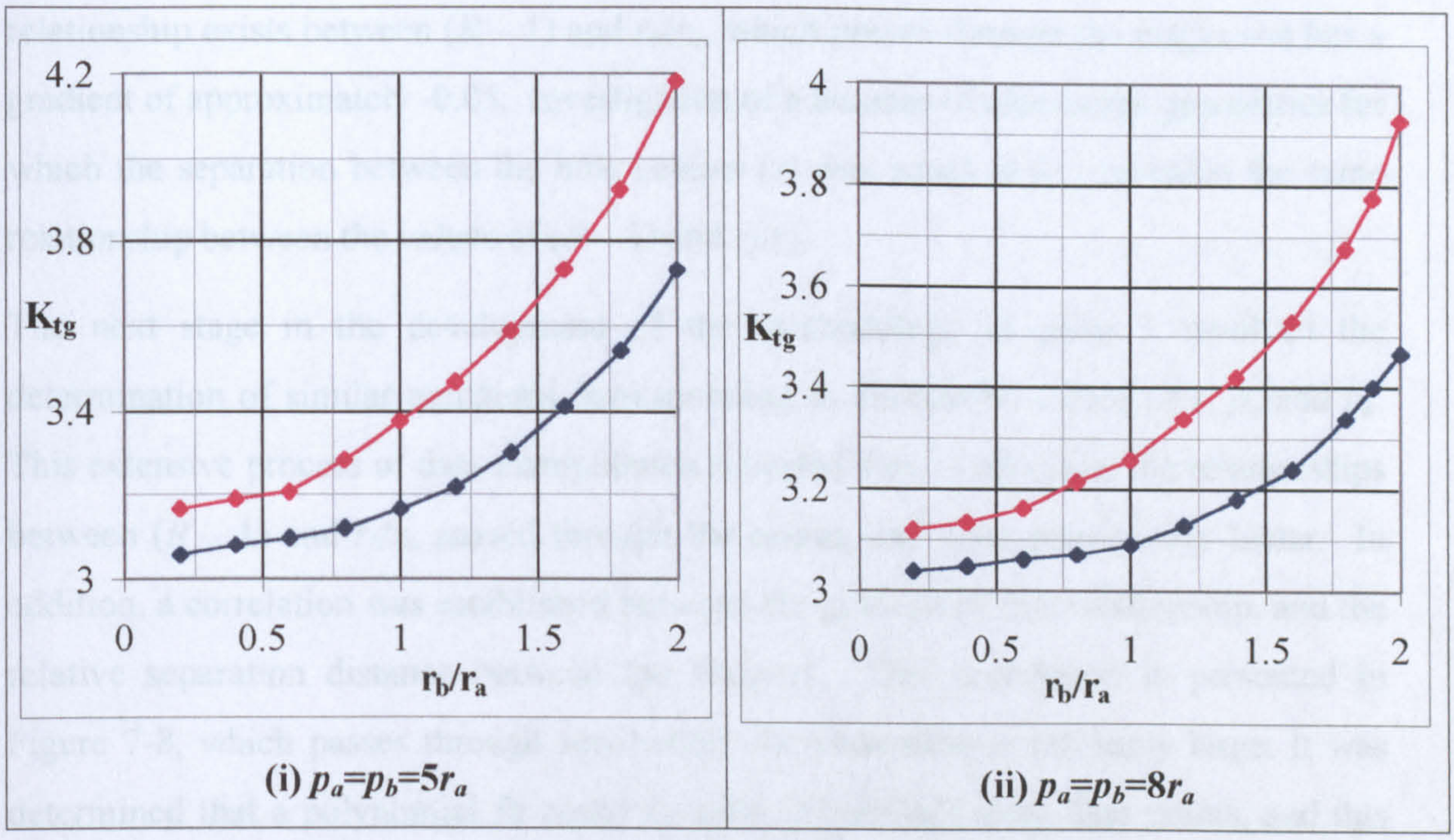

Figure 7-6. Comparisons between the actual stress concentration observed for the interacting holes (shown in blue) and the product of the appropriate individual values for each hole (shown in red) at point 3 for $s=4r_a$

the *product* was equal to the *interacting* stress concentration). For this reason, the value that was used for the data evaluation in this case was taken as this ratio minus one $(R-1)$. Figure 7-7 illustrates the variation in $(R-1)$ with values of r_b/r_a, corresponding to the data presented in Figure 7-6. These results indicate that, in both cases, a linear

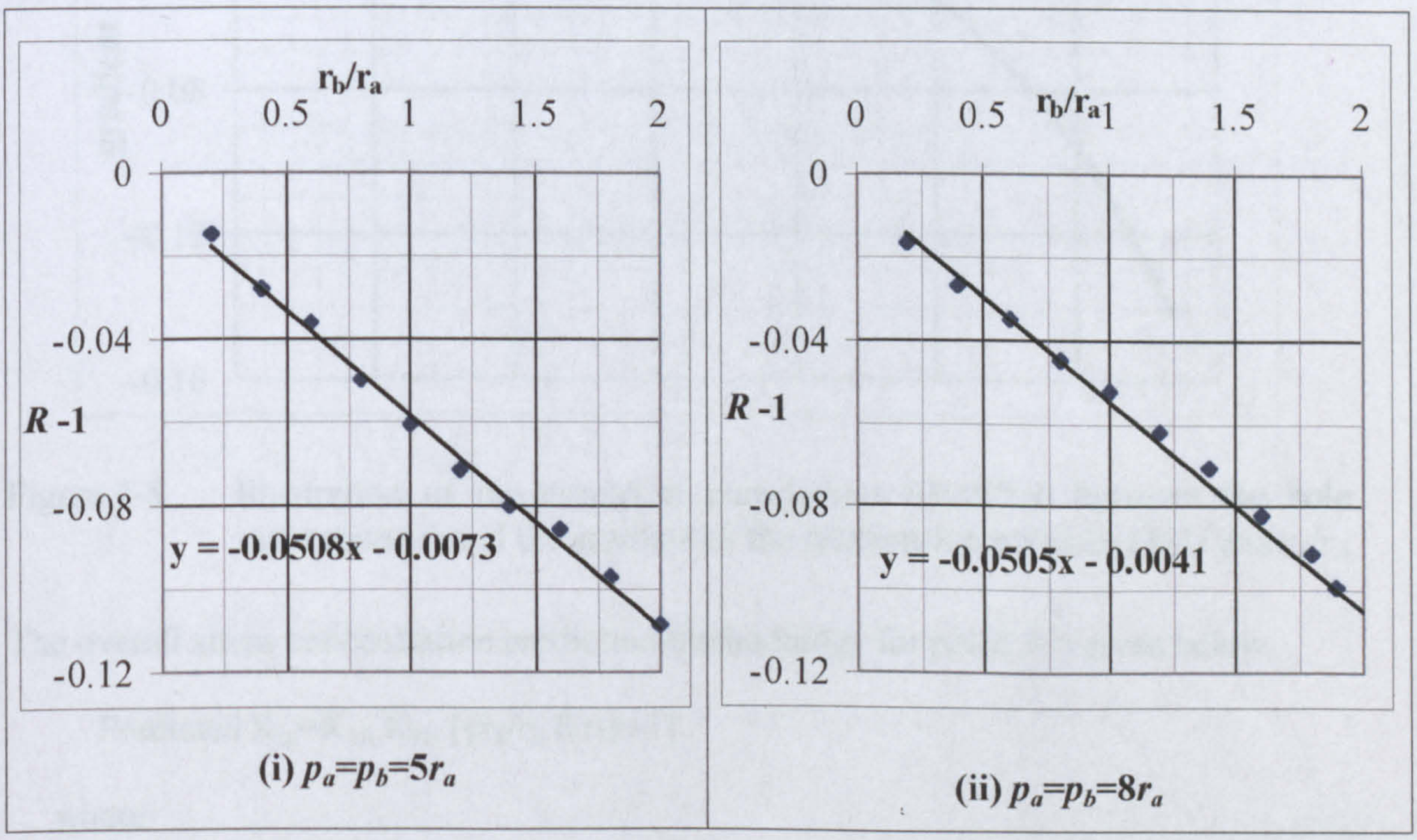

Figure 7-7. The relationship between $(R-1)$ and the relative size of hole b (r_b/r_a) at point 3 for $s=4r_a$

relationship exists between $(R-1)$ and r_b/r_a, which passes through the origin and has a gradient of approximately -0.05. Investigation of a number of alternative geometries for which the separation between the hole centres (s) was equal to $4r_a$, revealed the same relationship between the values of $(R-1)$ and r_b/r_a.

The next stage in the development of the methodology at point 3 involved the determination of similar equations corresponding to alternative values of s, p_a and p_b. This extensive process of data manipulation revealed that, in all cases, the relationships between $(R-1)$ and r_b/r_a passed through the origin, and were consistently linear. In addition, a correlation was established between the gradient of this relationship, and the relative separation distance between the features. This correlation is presented in Figure 7-8, which passes through zero where the separation is infinitely large. It was determined that a polynomial fit could be used to correlate these data points, and this relationship is the basis of the stress concentration prediction at this point.

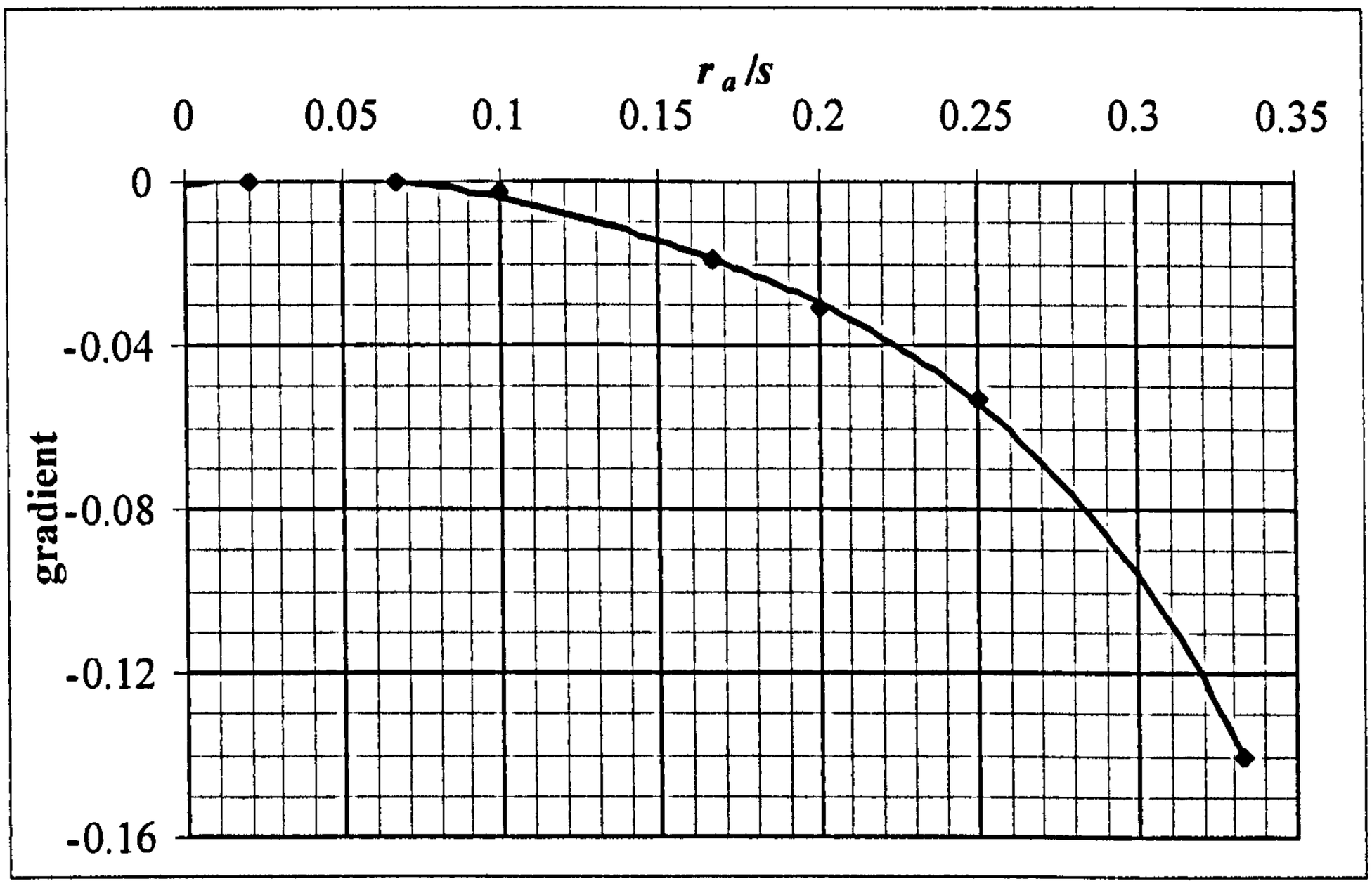

Figure 7-8. Illustration of the empirical correlations identified between the hole separation (s) and the gradient of the relationship between (R-1) and r_b/r_a

The overall stress concentration prediction methodology for point 3 is given below,

Predicted $K_{tg}=K_{3A}\,K_{3B}\,[\{r_b/r_a\,f(s)\}+1]$

where

K_{3A} is the decayed stress concentration from hole a at point 3

K_{3B} is the maximum stress concentration at point 3 due to hole *b*

$$f(s) = -2.0603\left(\frac{1}{s}\right)^4 + 2.1168\left(\frac{1}{s}\right)^3 - 1.8578\left(\frac{1}{s}\right)^2 + 0.1625\left(\frac{1}{s}\right) - 0.0026$$

The identification of the relationship between the *individual* and *interacting* stress concentrations at point 4 was conducted in a largely similar manner. However, in this case, only one individual stress concentration value was required, as the decayed stress concentration from the plate width would simply provide a stress concentration of one.

The overall stress concentration prediction methodology developed for point 4 was:

Predicted $K_t = K_{4B}[f(s)+1]$

where

K_{4B} is the maximum stress concentration at point 4 due to hole *b*

$$f(s) = 2.917\left(\frac{1}{s}\right)^3 - 1.403\left(\frac{1}{s}\right)^2 + 0.4913\left(\frac{1}{s}\right) - 0.0315$$

Using simple manipulations of the formulations derived for points 3 and 4, equivalent relationships were generated for points 1 and 2:

Point 1

Predicted $K_{tg} = K_{1A}[f(s, r_b)+1]$

where

K_{1A} is the maximum stress concentration at point 1 due to hole *a*

$$f(s, r_b) = 2.917\left(\frac{r_b}{s}\right)^3 - 1.403\left(\frac{r_b}{s}\right)^2 + 0.4913\left(\frac{r_b}{s}\right) - 0.0315$$

Point 2

Predicted $K_{tg} = K_{2A} K_{2B} [\{r_b/r_a\, f(s)\}+1]$

where

K_{2A} is the maximum stress concentration at point 2 due to hole *a*

K_{2B} is the maximum stress concentration at point 2 due to hole *b*

$$f(s, r_b) = -2.0603\left(\frac{r_b}{s.r_a}\right)^4 + 2.1168\left(\frac{r_b}{s.r_a}\right)^3 - 1.8578\left(\frac{r_b}{s.r_a}\right)^2 + 0.1625\left(\frac{r_b}{s.r_a}\right) - 0.0026$$

Validations of the prediction methodologies revealed that, for any separation distance of r_d/s and r_b/s >4, the results were within ±1% of those generated numerically, and for a separation distance of r_d/s and r_b/s >2, the results were accurate to ±2%.

7.3.1.3 Hole Placed between Double-Edged Notches

Shown in Figure 7-9 is an illustration of the geometric problem of a hole between double-edged notches.

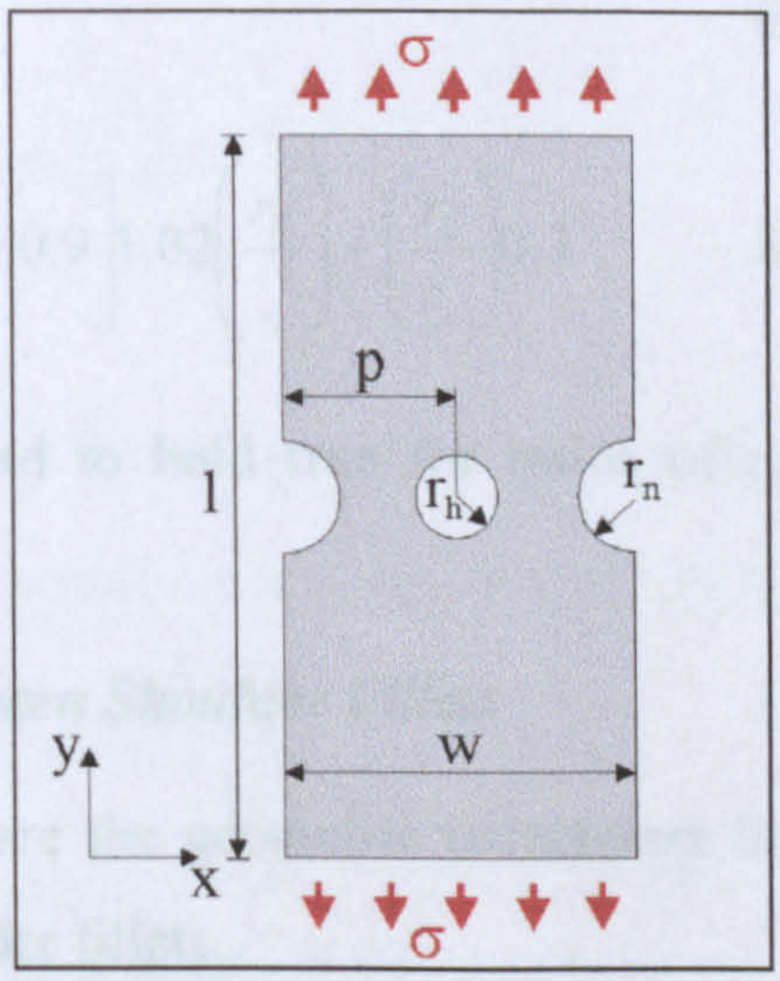

Figure 7-9. Feature interaction problem of a hole between semi-circular double-edged notches

In a similar manner to that described in Section 7.3.1.2, methodologies were developed for the problem of a centrally-placed hole between double-edged notches:

At the Notch:

Predicted $K_t = K_{nn}\, K_{nh}(f(r_h, w))$

where,

K_{nn} is the stress concentration due to the notch at the notch

K_{nh} is the stress concentration due to the hole at the notch

$$f(r_h, w) = 0.2\left(\frac{r_n}{w}\right) + 0.95 \qquad \text{for } \frac{r_h}{r_n} < -7\left(\frac{r_n}{w}\right) + 2.3$$

$$f(r_h, w) = \left[8.4\left(\frac{r_n}{w}\right) - 0.9\right]\left(\frac{r_h}{r_n}\right) + 0.3 \qquad \text{for } \frac{r_h}{r_n} > -7\left(\frac{r_n}{w}\right) + 2.3$$

At the Hole:

Predicted $K_t = K_{hh}\, K_{hn}(f(r_h, w))$

where,

K_{hh} is the stress concentration due to the hole at the hole

K_{hn} is the stress concentration due to the notch at the hole

$$f(r_h, w) = 0.9 \qquad \text{for } \frac{r_h}{r_n} < -7.4\left(\frac{r_n}{w}\right) + 2.3$$

$$f(r_h, w) = \left[7.2\left(\frac{r_n}{w}\right) - 0.9\right]1.02\left(\frac{r_h}{r_n}\right) + \left(\frac{r_h}{r_n}\right)0.3 \qquad \text{for } \frac{r_h}{r_n} > -7.4\left(\frac{r_n}{w}\right) + 2.3$$

These formulae were found to hold true for ratios of r_n:w between r_n/w=0.15 and r_n/w=0.25.

7.3.1.4 Hole Placed Between Shoulder Fillets

Illustrated in Figure 7-10 are the geometric parameters involved with a problem of a hole placed between shoulder fillets.

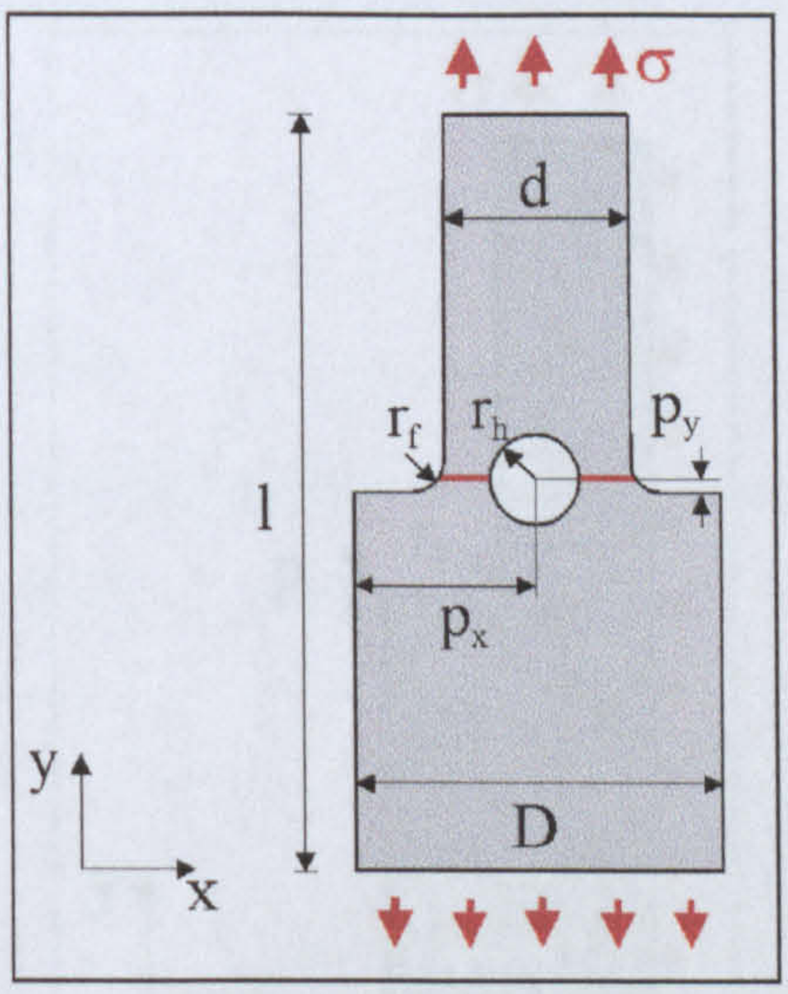

Figure 7-10. The geometric problem of a hole placed between shoulder fillets

The formulations developed for a centrally-placed hole, both at the shoulder and at the hole are :

At the Shoulder:

Predicted $K_t = K_{ss}\, K_{sh}(f(r_h, r_f))$

where,

K_{ss} is the stress concentration due to the shoulder at the shoulder

K_{sh} is the stress concentration due to the hole at the shoulder

$$f(r_h, r_f) = 0.99 \qquad \text{for } \frac{r_h}{r_f} < 5$$

$$f(r_h, r_f) = 0.21\left(\frac{r_h}{r_f}\right) \qquad \text{for } \frac{r_h}{r_f} > 5$$

At the Hole:

Predicted $K_t = K_{hh}\, K_{hs}(f(r_h, r_f))$

where,

K_{hh} is the stress concentration due to the hole at the hole

K_{hs} is the stress concentration due to the shoulder at the hole

$$f(r_h, r_f) = \left[0.43\left(\frac{r_h}{d}\right) - 0.015\right]\left(\frac{r_h}{r_f}\right) - \left(\frac{r_f}{d}\right) + 1$$

7.3.1.5 Hole in Proximity to a Single Fillet

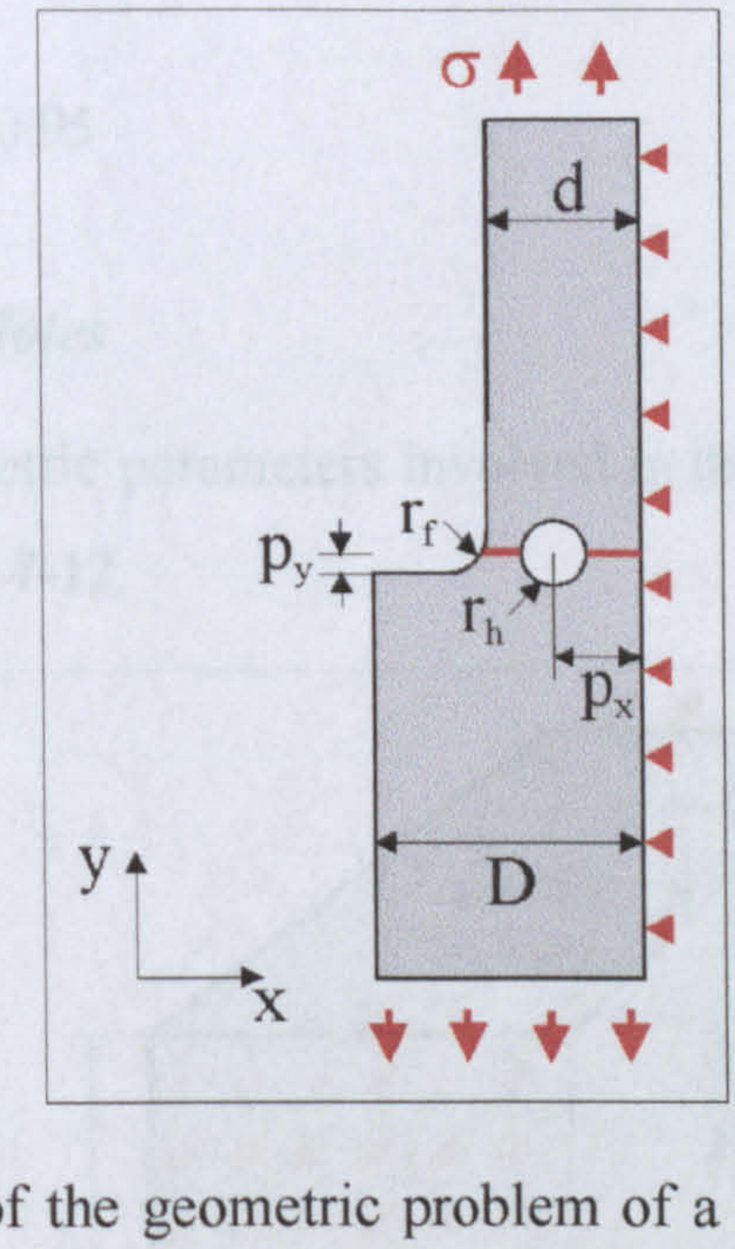

Figure 7-11. Illustration of the geometric problem of a hole in proximity to a single shoulder fillet

Again, using a similar approach to that described in Section 7.3.1.2, the following methodologies were generated for a hole (centrally-placed in the section width, *d*) in

proximity to a single shoulder fillet. Details of the geometric parameters involved in this geometry are given in Figure 7-11.

At the Shoulder:

Predicted $K_t = K_{ss}\, K_{sh}(f(r_f))$

where,

K_{ss} is the stress concentration due to the shoulder at the shoulder

K_{sh} is the stress concentration due to the hole at the shoulder

$$f(r_f) = 5.92\left(\frac{r_f}{d}\right)^2 - 5.64\left(\frac{r_f}{d}\right) + 1.54$$

At the Hole:

Predicted $K_t = K_{hh}\, K_{hs}(f(r_f)+1)$

where,

K_{hh} is the stress concentration due to the hole at the hole

K_{hs} is the stress concentration due to the shoulder at the hole

$$f(r_f) = -0.17\left(\frac{r_f}{d}\right) + 0.95$$

7.3.1.6 Transverse Bore Holes

An illustration of the geometric parameters involved in the problem of cross-wise bore holes in presented in Figure 7-12.

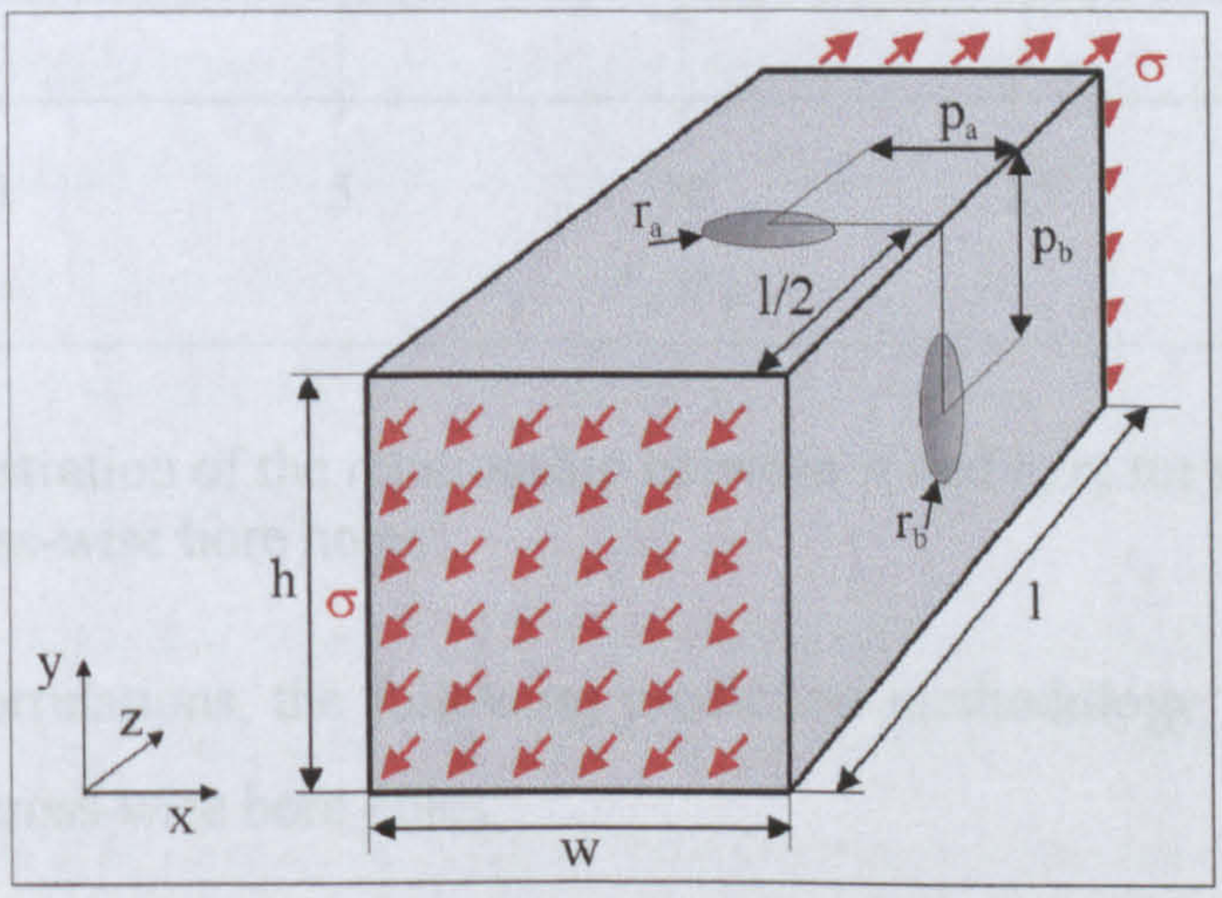

Figure 7-12. Illustration of the geometric problem of cross-wise bore holes

The approach used for the development of an evaluation methodology for cross-wise bore holes was very similar to those adopted for the analysis of the two-dimensional problems. In the evaluation of problems involving features which lie on a common cross-section, this particular geometry is only distinctive for the fact that the features fully intersect, with each individual point of maximum stress concentration coinciding at the same location to form the overall point of maximum stress concentration for the interacting geometry. In this case, therefore, the product of the two individual stress concentrations simply utilise the values of maximum stress concentration corresponding to each individual hole (as evaluated in two-dimensions). It has been established that this product is directly proportional to the actual stress concentration observed at the interacting geometry (see Section 7.2.4.1). Further investigation revealed that this relationship was independent of the plate width (w), the plate length (l) and the relative positioning of the two holes (p_a and p_b), but was only dependent on the relative radius of the two holes (r_a/r_b). This relationship, between R and values of r_a/r_b is given in Figure 7-13.

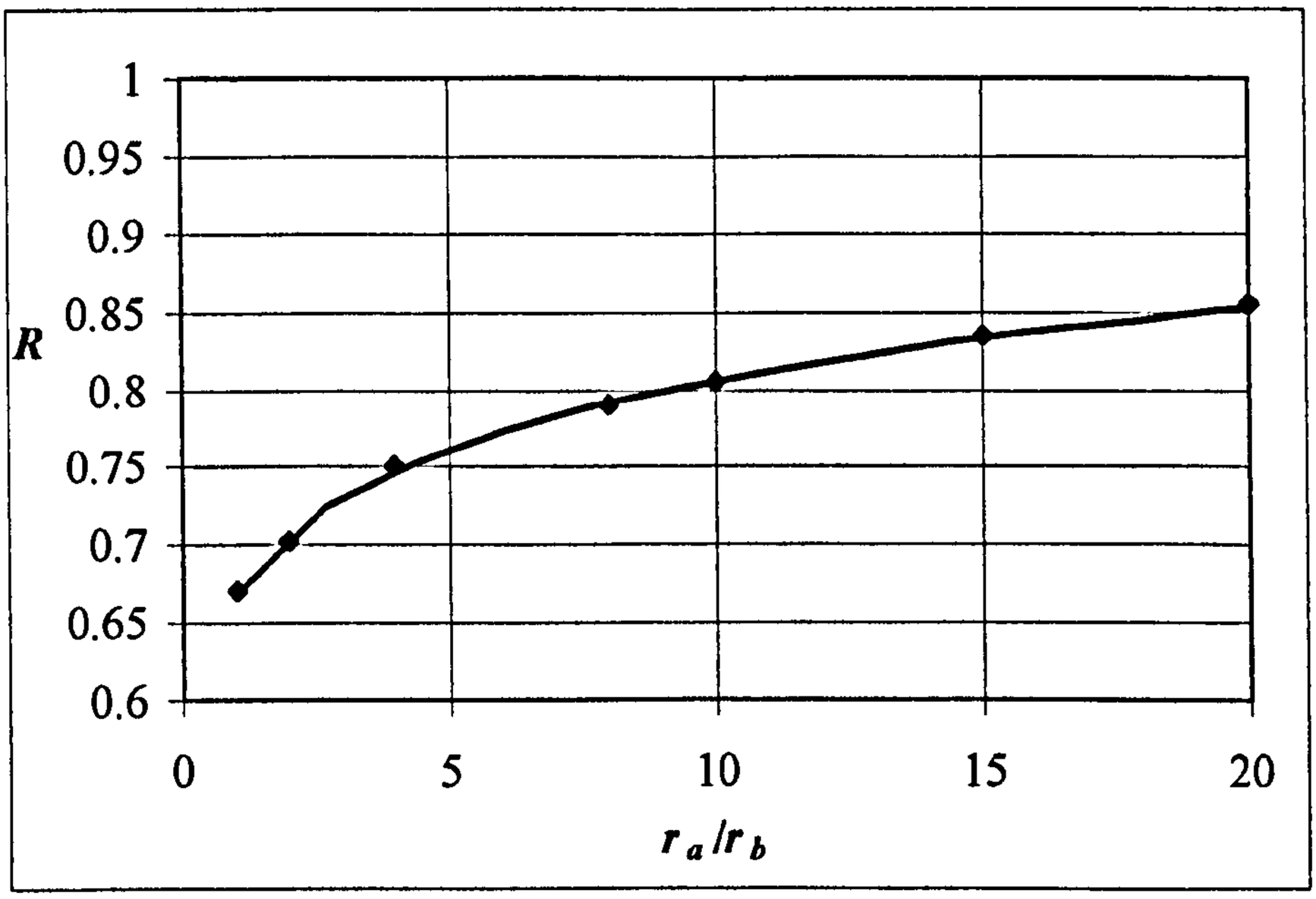

Figure 7-13. Illustration of the relationship between R and r_a/r_b for the problem of cross-wise bore holes

Based on these correlations, the following prediction methodology was developed for the evaluation of cross-wise bore holes:

$$\text{Predicted } K_t = K_a K_b(f(r_b))$$

where,

K_a is the stress concentration due to the hole *a*

K_b is the stress concentration due to the hole *b*

$$f(r_b) = 0.67\left(\frac{r_a}{r_b}\right)^{0.0812}$$

As there is no separation distance between the two features, the multiplicative function is only dependent on the relative sizes of the two features.

7.3.1.7 Form of the Methodology

It is clear from an analysis of all the methodologies presented in this section, for the evaluation of problems lying on a common cross-section, that all of the resulting formulations are of a common unifying form. In general terms, each methodology comprises two elements:

(i) the product of the two individual gross stress-concentration values at the point under consideration, and

(ii) a multiplication factor relating to the relative size of the feature associated with the point under consideration, and the distance from this point to the adjacent boundary.

More specifically, the methodologies can all be represented by the following general equation, for a point (point *1*) on the edge of a feature (feature α, of radius r_α) lying at a distance, *s*, from a free boundary or secondary feature β:

$$\textbf{Predicted } K_{tg} = K_{1\alpha}\, K_{1\beta}\, [f(s, r_\alpha)]$$

Therefore, for the prediction of stress concentrations for problems on a common cross-section, one needs simply to multiply the product of the individual stress concentrations associated with each feature involved in the problem ($K_{1\alpha}$ and $K_{1\beta}$) by a function of the separation distance between the feature under consideration and its adjacent boundary (*s*) and the relative size of the feature itself (r_α).

In order to test the accuracy of each of the methodologies generated, a number of finite element models were generated for random geometries of each of the problems considered here. These numerical results were compared to those values predicted by the evaluation methodology, and all results were found to be accurate within 2%.

7.3.2 Multiple Features of Alternative Alignment

There were a number of geometric problems considered in this research, containing features which did not lie on a common cross-section. These problems of alternative feature alignment were: (i) a central hole surrounded by eight radial holes, (ii) a central hole surrounded by four radial holes, (iii) transverse holes in proximity to an L-section, and (iv) a transverse hole in proximity to a fillet. During the experimental and numerical investigations of these geometries, it was established that the generation of data for the stress concentration distribution between adjacent features would not provide any meaningful insights into the key parameters affecting the stress-field interaction. The methodological development therefore relied on the analysis of the more basic relationships between the problem geometry and the resulting maximum stress concentration. In addition, due to the inherent differences in the geometric problems, it was also established that no overarching formulations could be derived for their evaluation, and therefore individually-tailored predictive techniques must be developed. For each of the geometric problems, the most suitable evaluation tool was developed, based on the ease of application and the accuracy of the results obtained. In this section, the development of the evaluation tools for each of the geometric problems is discussed.

7.3.2.1 Central Hole Surrounded by Four or Eight Satellite Holes

Given in Figure 7-14 is an illustration of the geometric parameters involved in the problems of a central hole surrounded by (i) eight radial holes and (ii) four radial

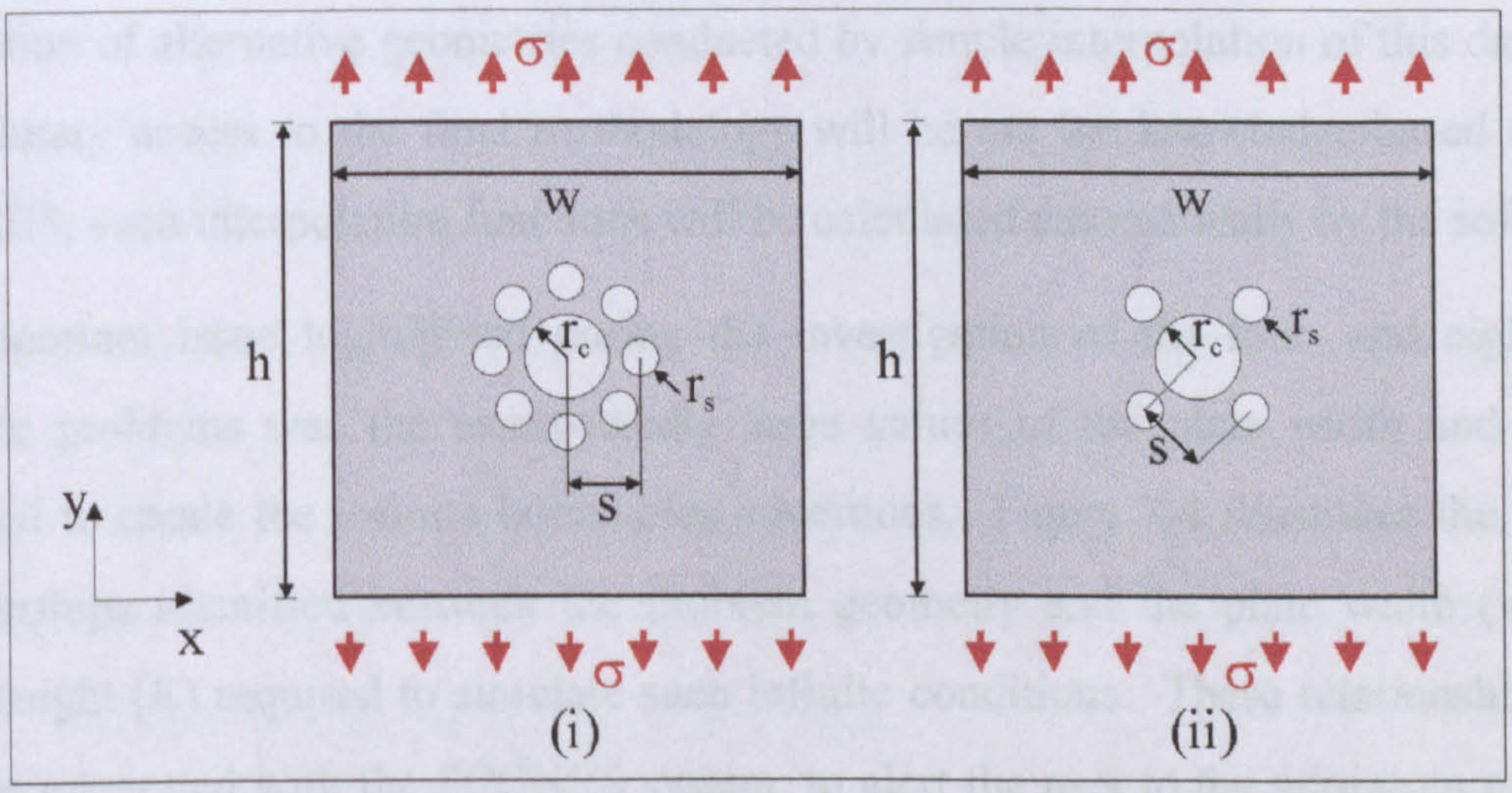

Figure 7-14. Illustration of the geometric problem of a central hole surrounded by (i) eight satellite holes and (ii) four satellite holes

holes. Analysis of the data generated from these problems revealed some general relationships existed between geometric changes in the relative satellite hole radius (r_s/r_c) and the relative separation distance (s/r_c), and the resulting maximum stress concentration. For example, it was observed that the relative sizes of the features played an important role in the location of the maximum stress concentration.

An important aspect of any methodology under development for this research is the accuracy with which it can be used to predict stress concentration values for the geometries which were not part of the original empirical data. In other words, the methodology must have the flexibility to predict accurately the stress concentration values for any geometry, within a given range. Through a process of data manipulation, a number of relationships have been developed between the geometric parameters involved in this satellite hole geometry and the maximum stress concentration. However, these relationships were based on the finite empirical values of r_s/r_c generated during the research, and the determination of any stress concentration values for alternative hole radii or separations would be based on simple data interpolation between these values. The development of methodologies for configurations of the four satellite hole geometry alternative to those exact geometries studied during this research was found to be particularly complex, due to the migration in point of maximum stress concentration around the hole circumferences, and the resulting variations in the magnitude and direction of the maximum stress concentration. It was therefore decided that using the original empirical data would provide the most straightforward and accurate basis for the determination of stress concentrations for this geometry, with the evaluation of alternative geometries conducted by simple interpolation of this data. As the primary access to the final methodology will be via the knowledge-based system SCONES, such interpolation functions will be calculated automatically by the software.

An important issue highlighted during the investigation of the four- and eight-hole satellite problems was the unexpectedly large values of the plate width and height required to create the infinite boundaries conditions. Figure 7-4 illustrates the simple relationships identified between the problem geometry and the plate width (w_i) and plate height (h_i) required to simulate such infinite conditions. These relationships will also be integrated with the SCONES system, to alert the user to the minimum required plate dimensions for each analysis.

7.3.2.2 Transverse Holes in Proximity to an L-section

An illustration of this three-dimensional problem is given in Figure 7-15. As discussed in Section 7.2.3.1, analysis of the geometric problem of transverse holes in proximity to an L-section revealed that any interaction influence between the two holes, one in each face of the L-section, had no detectable effect on the maximum stress concentration associated with either hole. The data analysis also established that, for this particular geometry, the change in section at the fillet radius acted as a free boundary, and any increases in the maximum stress concentration observed at either hole was due solely to the interaction between the hole and this boundary. The methodology developed for each hole was therefore based on the simple two-dimensional evaluation of an offset hole in a finite-width plate, where, in each case, the model width is given as (w+0.5t) and the hole position is (p_a+0.5t). The overall point of maximum stress is identified as the location of the highest of these individual stresses. As the current version of the SCONES system has access to comprehensive data for the evaluation of single features

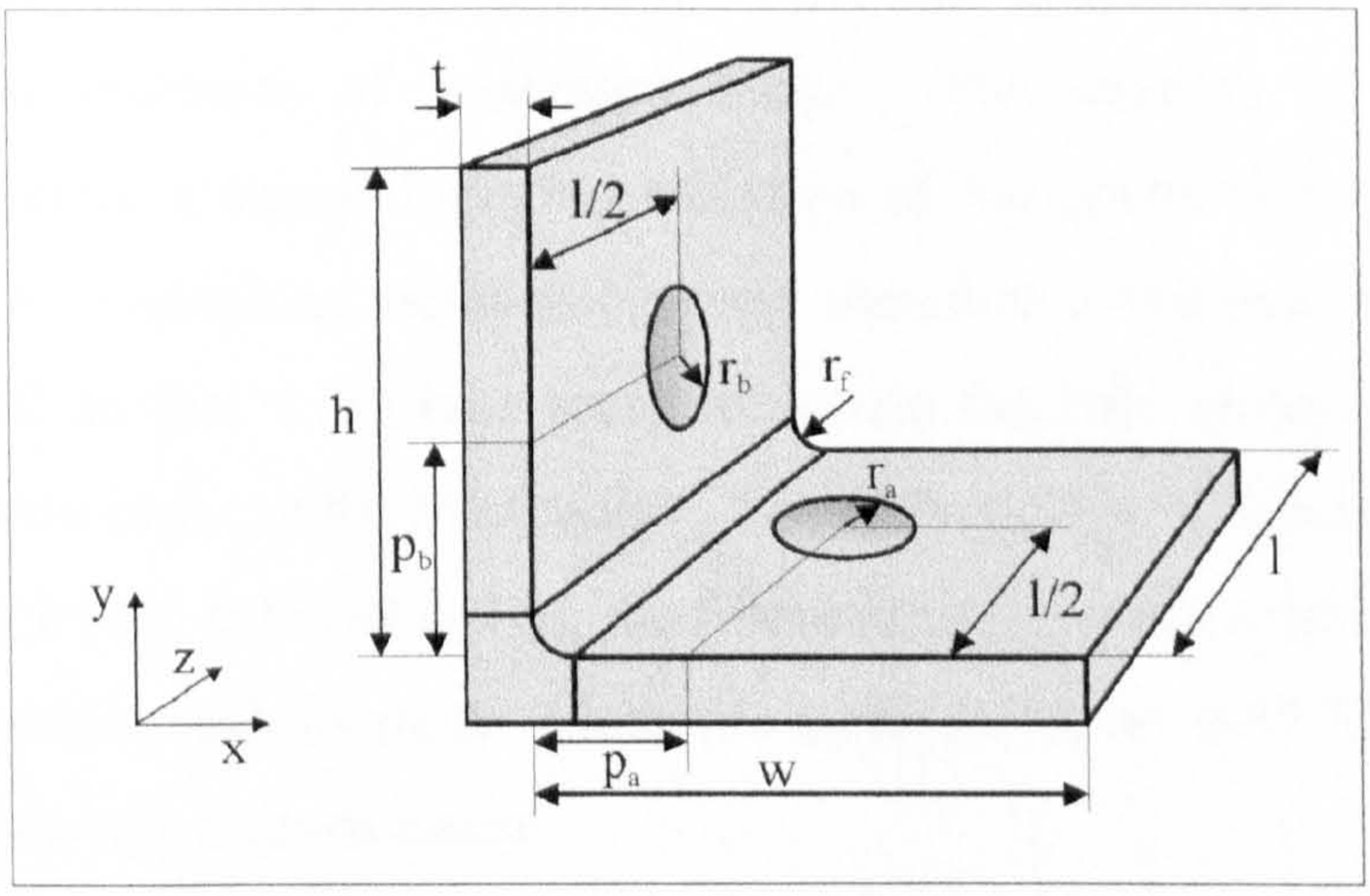

Figure 7-15. Illustration of the geometric parameters involved in the three-dimensional problem of transverse holes in proximity to an L-section

(including that of a single offset hole), the implementation of the methodology to analyse this problem of transverse holes in proximity to an L-section will be straight-forward. The use of this methodology was found consistently to overestimate the stress concentration in comparison to that found from finite element modelling by 1-1.5%.

7.3.2.3 Transverse Hole in Proximity to a Fillet

Illustrated in Figure 7-16 are the geometric parameters involved in the problem of a transverse hole in proximity to a fillet. This geometry was identified by BAE

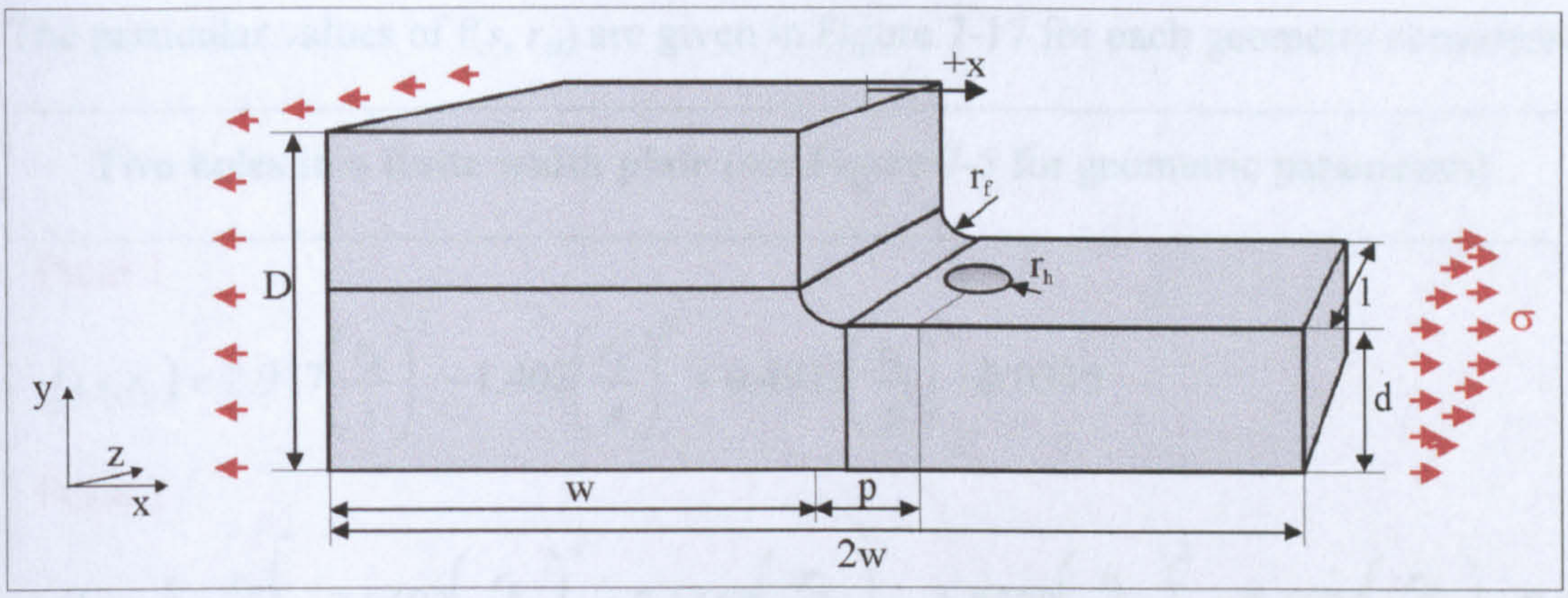

Figure 7-16. Illustration of the three-dimensional problem of a transverse hole in proximity to a radius section

SYSTEMS as a particular area of concern raised during the consideration of manufacturing concessions. As discussed in Section 7.2.4.2, when the hole is positioned such that $p>2.5r_f$, no interacting influence is observed between the two features. Typical designs within aircraft structures would rarely position such features at these distances (i.e. where $p<2.5r_f$) and therefore this methodology would principally be adopted for problems of misplaced holes. The analysis of manufacturing concessions requires a straightforward evaluation of the potential for fatigue-critical components. An evaluation methodology was therefore developed for this problem geometry, based on the 'worst-case scenario' where the hole centre is placed at the point of maximum stress, at the fillet radius. The methodology is based on relationships identified between the hole radius (r_h), the fillet radius (r_f) and the resulting maximum stress concentration (such as those values presented in Figure 6-57 Chapter 6). The resulting methodology is given below:

$$\textbf{Predicted } K_t=(0.37r_f^{-0.485})(r_h+1)+2.75$$

This evaluation methodology was found to generate stress concentration values within 3% of those predicted using finite element techniques.

7.3.3 Summary of Methodologies

7.3.3.1 Features on a common cross-section

The methodologies developed for the evaluation of multiple features at a common cross-section are of the form:

$$\textbf{Predicted } K_{tg}=K_{1\alpha}\,K_{1\beta}\,[f(s, r_\alpha)]$$

The particular values of f(s, r_α) are given in Figure 7-17 for each geometry considered.

Two holes in a finite width plate (see Figure 7-5 for geometric parameters)

Point 1

$$f(s,r_b)=2.917\left(\frac{r_b}{s}\right)^3-1.403\left(\frac{r_b}{s}\right)^2+0.4913\left(\frac{r_b}{s}\right)-0.0315$$

Point 2

$$f(s,r_b)=\frac{r_b}{r_a}\left[-2.0603\left(\frac{r_b}{s.r_a}\right)^4+2.1168\left(\frac{r_b}{s.r_a}\right)^3-1.8578\left(\frac{r_b}{s.r_a}\right)^2+0.1625\left(\frac{r_b}{s.r_a}\right)-0.0026\right]$$

Point 3

$$f(s)=\frac{r_b}{r_a}\left[-2.0603\left(\frac{1}{s}\right)^4+2.1168\left(\frac{1}{s}\right)^3-1.8578\left(\frac{1}{s}\right)^2+0.1625\left(\frac{1}{s}\right)-0.0026\right]$$

Point 4

$$f(s)=2.917\left(\frac{1}{s}\right)^3-1.403\left(\frac{1}{s}\right)^2+0.4913\left(\frac{1}{s}\right)-0.0315$$

Centrally-placed hole between double-edged notches (see Figure 7-9))

At the Notch

$$f(r_h,w)=0.2\left(\frac{r_n}{w}\right)+0.95 \qquad \text{for } \frac{r_h}{r_n}<-7\left(\frac{r_n}{w}\right)+2.3$$

$$f(r_h,w)=\left[8.4\left(\frac{r_n}{w}\right)-0.9\right]\left(\frac{r_h}{r_n}\right)+0.3 \qquad \text{for } \frac{r_h}{r_n}>-7\left(\frac{r_n}{w}\right)+2.3$$

At the Hole

$$f(r_h,w)=0.9 \qquad \text{for } \frac{r_h}{r_n}<-7.4\left(\frac{r_n}{w}\right)+2.3$$

$$f(r_h,w)=\left[7.2\left(\frac{r_n}{w}\right)-0.9\right]1.02\left(\frac{r_h}{r_n}\right)+\left(\frac{r_h}{r_n}\right)0.3 \qquad \text{for } \frac{r_h}{r_n}>-7.4\left(\frac{r_n}{w}\right)+2.3$$

Centrally-placed hole between shoulder fillets (see Figure 7-10)

At the Shoulder

$$f(r_h, r_f) = 0.99 \qquad \text{for } \frac{r_h}{r_f} < 5$$

$$f(r_h, r_f) = 0.21\left(\frac{r_h}{r_f}\right) \qquad \text{for } \frac{r_h}{r_f} > 5$$

At the Hole

$$f(r_h, r_f) = \left[0.43\left(\frac{r_h}{d}\right) - 0.015\right]\left(\frac{r_h}{r_f}\right) - \left(\frac{r_f}{d}\right) + 1$$

Hole in proximity to a single shoulder fillet (see Figure 7-11)

At the Shoulder

$$f(r_f) = 5.92\left(\frac{r_f}{d}\right)^2 - 5.64\left(\frac{r_f}{d}\right) + 1.54$$

At the Hole

$$f(r_f) = -0.17\left(\frac{r_f}{d}\right) + 0.95$$

Cross-wise bore holes (see Figure 7-12)

$$f(r_b) = 0.67\left(\frac{r_a}{r_b}\right)^{0.0812}$$

Figure 7-17. The associated multiplicative functions relating to each of the interacting geometries the features lie on a common cross-section

Features of Alternative Alignment

The tailored evaluation tools developed for each of the problems containing geometries of alternative alignment are given in Figure 7-18.

Features	Analysis technique
Central hole surrounded by eight satellite holes	Interpolation from the empirical data given in Figure 6-29 Chapter 6. Formulations for the definition of the plate boundaries are given in Figure 7-4.
Central hole surrounded by four satellite holes	Interpolation from the empirical data given in Figure 6-33 Chapter 6. Formulations for the definition of the plate boundaries are given in Figure 7-4.
Transverse hole in proximity to an L-section	Maximum stress concentrations are evaluated for each hole from the two-dimensional data of an offset hole in a finite-width plate, for plate width (w+0.5t) and hole position (p_a+0.5t)
Transverse hole in proximity to a fillet radius	Predicted maximum $K_{tg} = (0.37 r_f^{-0.485})(r_h + 1) + 2.75$

Figure 7-18. Individually tailored methodologies for those features which do not lie on a common cross-section

7.4 VALIDATION AND IMPLEMENTATION

On completion of the methodological development, the final stages of this research project were a process of thorough validation of the accuracy and flexibility of the techniques, and the implementation of the methodologies into the fatigue analysis process at BAE SYSTEMS. In this section, a brief overview is provided of these validation procedures (Section 7.4.1) and implementation processes (Section 7.4.2).

7.4.1 Validation of Methodology

Validation of the methodologies was conducted, in each case, by their application to particular geometric configurations which were not studied in the original data gathering process, and comparing the resulting stress concentration values with those generated from an equivalent finite element model. This process helped to ensure that each methodology is not simply regurgitating the original empirical stress concentration

values on which it was generated, but rather was basing the predictions on fundamental properties of the feature interaction and its geometric parameters.

For each of the interaction problems which contained features at a common cross-section, the data validation process confirmed that the methodologies developed here generated stress concentration values within 2% of those results generated numerically. For those problems involving features of alternative alignment, this validation process established a maximum 4% discrepancy between the results generated from the methodologies developed in this research and the results from the numerical analysis. All of the methodologies were designed such that, wherever possible, any error in the prediction should provide an overestimate of the maximum stress concentration rather than an underestimate.

An additional element of the methodological validation process involved an evaluation of the suitability of these techniques within a practical industrial application. This analysis was achieved through a comparison between current techniques adopted within the aerospace industry and those methods developed here for a series of real-life case studies.

In consultation with fatigue experts from BAE SYSTEMS, a case study was selected of a recent geometry of potential feature interaction encountered during the assessment of a manufacturing concession. This problem is illustrated in Figure 7-19 for the geometry of a hole (radius 2mm) placed in close proximity to a misplaced pilot hole (radius 1.2mm). The flange is loaded by in-plane endload, and the section is restrained by adjacent components such that minimal bending is observed.

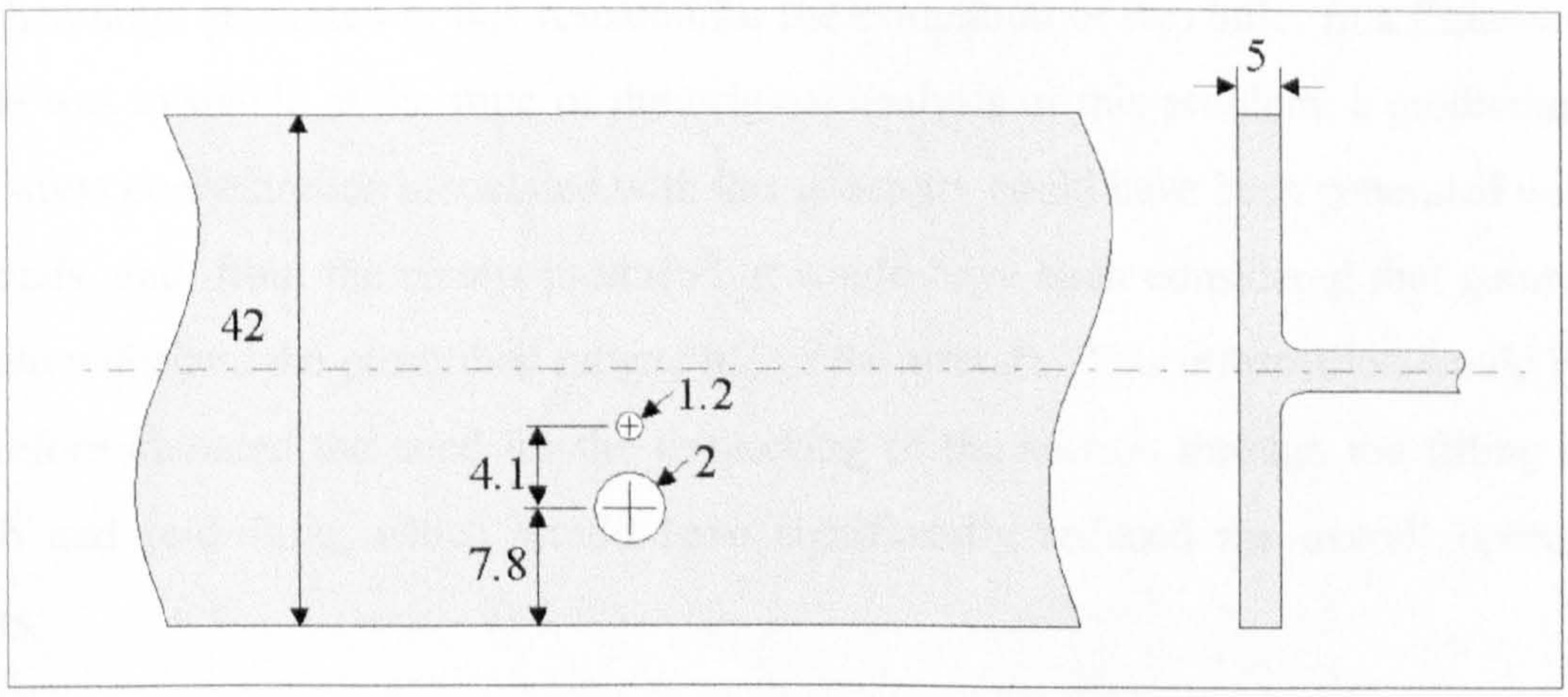

Figure 7-19. Case study example taken from a manufacturing concession of a misplaced pilot hole (all dimensions in mm)

During the original evaluation of this manufacturing concession, traditional analysis techniques were employed for the geometry using the two equations: $K_t = K_{t1}\sqrt{K_{t2}}$ (where $K_{t1}>K_{t2}$) (Equation 2-1 Chapter 2) and $K_t=K_{t1}.K_{t2}$ (Equation 2-2 Chapter 2). In each case, the individual stress concentration values associated with each hole was taken as 3, and therefore these equations generated maximum stress concentration predictions of 5.2 and 9 respectively. Given the structural application, the fatigue experts at BAE SYSTEMS considered these stress concentration values too high.

Rather than undertake time-consuming finite element analyses to confirm these figures, the entire section surrounding the feature was drilled out, a bush placed in this larger hole and a new 2mm hole re-drilled at the desired location. However, although the re-drilling operation was considered to be less costly than performing a finite element analysis of the component, this operation may have been unnecessary if a more accurate and straight-forward assessment tool could have been employed to evaluate the maximum stress concentration.

The application of the methodology for two holes in a finite-width plate (Section 7.3.1.2) to the particular geometric problem illustrated in Figure 7-19 generated a maximum stress concentration prediction of 4.50, which occurred at the smaller pilot hole on the edge closest to the 2mm hole. In addition, a finite element model was also constructed for this geometry which identified the maximum stress concentration at the same point, at a value of 4.44. The discrepancy between these two values is approximately 1.5%, with the methodology developed in this research slightly overestimating the finite element results for the equivalent geometry. If the methodology generated in this research for the evaluation of two holes in a finite-width plate was available at the time of the original analysis of this problem, a prediction of the stress concentration associated with this geometry could have been generated within seconds, and, from the results produced, it would have been considered that geometry would withstand the prescribed fatigue life of the aircraft. This information would have therefore obviated the need for the re-working of the section through the fitting of a bush and re-drilling, which would have significantly reduced the overall operation costs.

7.4.2 Implementation of Methodology

Each of the methodologies generated in this research for the stress concentration evaluation of stress-raising features in proximity is currently being implemented as standard practice within the fatigue analysis process at BAE SYSTEMS. This process involves the implementation of the methodologies within the BAE SYSTEMS Technical Standards and Procedures Manual for stress concentration evaluation (BAE SYSTEMS 2001 (2)) as well as within the knowledge-based software system SCONES (BAE SYSTEMS 2001 (1); Robinson et al. 2001). The full implementation of all of the feature interaction problems into both the Technical Standards Manuals and the SCONES system is planned for early 2002.

To date, two feature interaction problems have now been fully implemented: (i) cross-wise bore holes and (ii) geometries of four and eight satellite holes. Given in Figure 7-20 is a screen capture of the SCONES interface for the evaluation of cross-wise bore

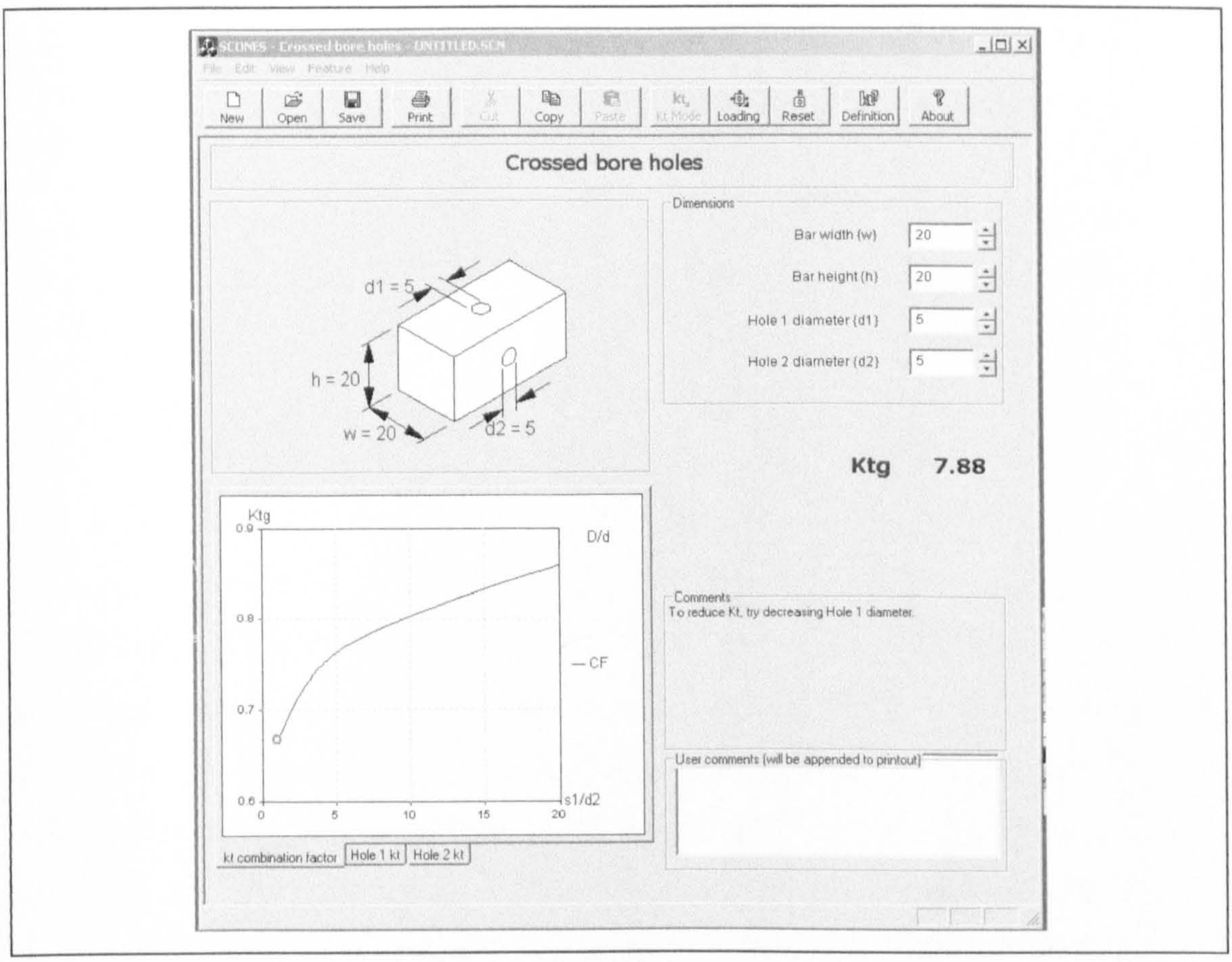

Figure 7-20. SCONES system interface for the evaluation of the feature interaction problem of cross-wise bore holes

holes. As can be seen from this figure, the user screen allows for the specification of the block dimensions and the relative sizes of each hole. Using this information, a

prediction of the overall maximum gross stress concentration is provided on the right-hand side of the screen. Through variation in the geometric parameters, the user can operate simple design optimisation for the minimisation of the component's susceptibility to fatigue.

Once fully implemented, the design tools developed in this research will not only provide a platform for design optimisation through stress concentration predictions for features in proximity, but it will also offer design advice for particular geometric configurations. For example, during the analysis of the three-dimensional geometry of a transverse hole in proximity to a fillet radius, it was established that, regardless of the relative sizes of the hole and fillet, the two feature produced no significant interacting influence if they were separated by a distance greater than $2.5r_f$. This general property is not currently known by designers, and will be incorporated within SCONES as very useful design advice during the consideration of such geometries.

CHAPTER 8

DISCUSSION, CONCLUSIONS AND FUTURE WORK

This chapter provides an overview of the work conducted during this research, drawing out particular project deliverables and contributions in the context of the overall aims and objectives. The chapter begins with a discussion of each task involved in the research programme, highlighting the important aspects of the work undertaken. An overview is then provided of the project achievements, with particular focus on the industrial and scientific contributions of the work. The final section presents a discussion of the potential for further developments in this field, and the anticipated future work tasks involved in the overall research project.

8.1 INTRODUCTION

This thesis has tackled a key issue facing fatigue analysts within aircraft design, which concerns the prediction of stress concentration factors around stress-raising features placed in proximity. A literature research and review, discussed in Chapter 2, has revealed a dearth in the knowledge of the impact of such stress-field interaction on the fatigue susceptibility of the structure, and current evaluation techniques adopted in the aerospace industry have been found to be highly inaccurate. The aims of the study, therefore, were to carry out fundamental research into the evaluation of interacting stress-raising features in aerospace structures, and develop new methodologies for the prediction of the associated stress concentration factors. The work-plan designed to achieve these objectives, outlined in Chapter 3, involved numerical solutions and experimental studies, followed by a focused programme of data analysis and interpretation. The initial stage of the research investigation involved the development

of numerical models, using the finite element method, for each of the geometric problems under consideration, as discussed in Chapter 4. This work was complemented by an experimental programme, presented in Chapter 5, comprising photoelastic analysis and automated strain gauge measurements. In Chapter 6, the results from each of these investigations were validated and drawn together for the two- and three-dimensional problems under consideration. These results were analysed through a detailed data analysis and interpretation process, as outlined in Chapter 7. Through an understanding of the trends and correlations identified in this data analysis process, a series of methodologies was developed for the evaluation of the stress concentrations associated with each of the feature interaction problems under consideration in this research. The development of these methodologies is presented in Chapter 7.

This chapter discusses the work conducted during this research and draws overall conclusions of the contribution made by this thesis in both a scientific and industrial context. This chapter also provides an overview of the potential for further developments in this field, and the anticipated future work tasks involved in the overall research project.

8.2 REVIEW OF RESEARCH OBJECTIVES

The ultimate objective of this research was to fulfil the aerospace industry's need for an accurate and flexible analysis tool for the evaluation of stress-raising features in proximity. This technique had to be suitable for implementation as standard practice within the fatigue analysis process at BAE SYSTEMS, both for the identification of potential fatigue susceptibility in manufacturing concessions, and for the operation of optimisation routines in the early stages of aerostructure design.

Within this brief, the particular aims of the research project were identified as:

- to identify the specific requirements of the aerospace industry, with respect to the evaluation of stress-raising features placed in proximity,
- to establish the current state of the art for the understanding and analysis of problems of interacting stress concentration features,
- to carry out fundamental research into a range of two- and three-dimensional problems to determine the influence of the position and orientation of multiple stress concentration features placed in proximity,

- to translate these measures into a technique suitable for incorporation within an efficient fatigue methodology process and into the knowledge-based system SCONES, so as to enhance the efficient design of fatigue sensitive structures, and
- to validate the technique through application to 'real life' design situations.

8.3 REVIEW OF PREVIOUS WORK

A comprehensive literature search and review was conducted into the general issue of stress-raising features placed in proximity. This investigation highlighted the limited work available in this field, with very few published methods of analysis.

The methods revealed from this investigation each relied on very different methodologies, ranging from theory-based solutions to crude 'rules of thumb'. A number of these methods, including two techniques currently used in the aerospace industry, were selected for evaluation and comparison. A series of quantitative comparisons was generated in order to evaluate the relative accuracy of each of the methods (as outlined in Chapter 2). These comparisons were undertaken by employing each of the methods to analyse the same standard feature interaction geometry of two equal holes in an infinite plate under tension. This standard problem is one of the few cases of feature interaction for which an analytical solution is available (Haddon 1967) and can therefore be used as a benchmark against which the accuracy and consistency of the methods can be compared for this geometry.

In general, it was concluded from this investigation that most of the existing methods available did not produce results of sufficient accuracy to be relied upon within the fatigue analysis process. In particular, an evaluation of those results generated from the methods typically adopted in the aerospace industry revealed the largest deviation, with the techniques vastly overestimating the 'actual' stress-levels present. Of the few methods for which the accuracy was of an acceptable level, the flexibility and ease of application were insufficiently beneficial to provide a workable alternative to finite element analysis. This study further highlighted the need for a new robust methodology for the analysis of interacting features which was accurate, easy to use and applicable to a wide range of geometries.

8.4 RESEARCH DEVELOPMENT

8.4.1 Identification of Problem

The initial task of any research project involves the detailed identification of the overall requirements, in order to specify and structure the project objectives. As discussed in Section 8.3, the literature search and review had highlighted the dearth of current knowledge and appropriate methodologies for the evaluation of stress-raisers in proximity. In particular, those methods currently used in the aerospace industry are highly inaccurate and therefore need to incorporate very significant safety factors which can generate inefficient and costly designs.

Through a series of consultations with fatigue experts at BAE SYSTEMS, a number of important project requirements were identified. These requirements focused on two aspects of the potential development of evaluation methodologies for problems involving interacting stress-raisers:

(i) the circumstances under which such a predictive tool would be implemented, and

(ii) the particular geometric problems involving interacting features commonly encountered during the fatigue analysis of aircraft structures.

It was established that the aerospace industry required a straightforward and accurate predictive tool, which could be used as an alternative or pre-cursor to more time-consuming techniques, such as finite element analysis. The tool would primarily be used under two distinct circumstances: (i) in the operation of design optimisation routines in the early stages of design, and (ii) for the evaluation of manufacturing concessions, in order to assess the fatigue susceptibility of a component. The evaluation tool had to be flexible and suitable for implementation both within the fatigue analysis process and in the knowledge-based software system SCONES.

Fatigue experts at BAE SYSTEMS also identified a number of two- and three-dimensional geometries involving potential feature interaction which frequently required stress concentration analysis, each subjected to tensile load. These problems are illustrated in Figure 3-1 and Figure 3-2 in Chapter 3. The specifications of these geometries were enhanced and modified by BAE SYSTEMS throughout the project, as new problems were encountered within the design office.

8.4.2 Development of a Work Programme

The next stage of the research was to develop a programme of work, designed to achieve the objectives outlined above.

It was initially envisioned that the research investigation would comprise experimental, numerical and analytical methods. In order to explore the potential application of experimental and analytical studies in this context, the author secured a six month secondment to the Engineering Mechanics and Design laboratory at the University of Toronto, funded through a Foresight Award from the Royal Academy of Engineering. This secondment provided new insights into the scientific and industrial context of this research, as well as access to experimental fatigue testing equipment. The secondment also provided the opportunity to assess the potential for the development of analytical treatments of interacting stress concentrations, using the complex potential method. These investigations established that, due to the inherent complexities in the problems under consideration, it would not be feasible to develop analytical models for these geometries. This research consequently confined the analytical considerations to the application of foregoing treatments for single features (Ling 1967; Isida 1953) and for problems involving two circular holes in an infinite plate (Meguid and Gong 1993). It was therefore established that the programme of research investigation should be focused on experimental and numerical studies, complemented by validations from appropriate analytical treatments.

On completion of the research investigations, these results would then be drawn together for validation and detailed data analysis. Based on these new understandings, methodologies for the analysis of feature interaction problems would then be generated and implemented.

The work tasks specified to achieve the overall research objectives were then finalised, and are presented in Figure 3-3 Chapter 3.

8.4.3 Numerical Investigations

The primary stage of the research investigation programme was the numerical analysis of each of the two- and three-dimensional geometries under consideration, using the commercial finite element code ANSYS. An important aspect of this work involved

ensuring the accuracy of the model representation, through the optimisation of the elements. The initial geometries investigated, therefore, were those of single geometric features and simple configurations of holes, allowing detailed comparisons to be made between these results and the solutions from foregoing analytical treatments. Using these comparisons, the modelling techniques were optimised before the analysis of more complex problems of multiple and three-dimensional features was conducted. On the request of BAE SYSTEMS, a detailed report of these modelling techniques has been documented, to be used to inform the future numerical analyses of stress concentration features within the fatigue analysis process.

8.4.4 Experimental Investigations

The second stage of the work schedule involved the validation of the numerical results through detailed photoelastic and strain gauge investigations.

The photoelastic studies generated extensive and highly accurate data for each of the two-dimensional geometries under investigation. Work was conducted using a Sharples 250mm Diameter Field Polariscope with epoxy resin models made from Araldite CT200. The models were loaded using a traditional loading mechanism called a *Whipple Tree* (see Figure 5-3 Chapter 5), and detailed measurements were taken from each model using a travelling microscope. The photoelastic analyses generated data both for the direction and magnitude of the maximum stress concentration, as well as for appropriate ligament plots of the stress concentration distribution between adjacent features.

These investigations, however, represented a substantial period in the research programme which extended the duration of the overall project. These delays were due, in part, to a number of experimental inaccuracies identified during the analysis of the single feature problems and geometries involving two holes in an infinite plate. Although recommended photoelastic procedures (Hendry 1966; Heywood 1952; Frocht 1941) were adhered to throughout the analysis of each model, the experimental results were found to deviate by up to 20% from those generated from equivalent analytical treatments. In order to identify the sources of these observed errors, collaboration was

sought both with a commercial photoelastic company[1] and the experimental stress analysis research group at AIRBUS, which maintain one of the UK's largest photoelastic facilities. A detailed programme of work was conducted to establish the source of the experimental error in the photoelastic analyses, and to refine current experimental procedures to alleviate these problems. Through this investigation, the critical feature found to be the cause of the erratic photoelastic results was the presence of high levels of time-edge effects in the models. These problems were vastly reduced as a result of increasing the temperature during the model's storage, and the adherence to a stricter time frame for the model analysis. These recommendation for modified photoelastic procedures have been documented in a technical note, which is to be submitted to *Strain* journal. Following the incorporation of these new techniques, all the results from the photoelastic investigations were found to be within 1% from the appropriate analytical solutions, and within 2% of the finite element data.

In addition to the photoelastic studies, the experimental research programme also included the strain gauge analysis of both two- and three-dimensional model geometries. These analyses were conducted at the Engineering Mechanics and Design laboratory at the University of Toronto using a Measurements Group 500 electro-hydraulic servo-controlled testing rig. The particular geometric specification for each of the models under investigation had been identified through preliminary finite element analysis. The models were machined from Al 6061 T6 and fitted with a series of fine strain gauges (gauge EA-06-031MH-120 for the measurement of localised maximum strains and strain gradients, and gauge EA-06-050SB-120 to measure the applied strains).

As discussed in Section 5.3 Chapter 5, the use of strain gauges in the analysis of highly localised regions of large strain levels can only generate approximate values over a finite area. In this application, therefore, strain gauges were used primarily for the validation of finite element results for the three-dimensional problems. The results from the strain gauge analyses were found to be consistently within 8% of those generated from finite element modelling.

---

[1] Sharples Stress Engineers, Bamber Bridge, Preston, Lancashire, UK

8.4.5 Analysis of Results

A selection of the results generated during this research for each of the six two-dimensional problems and the three three-dimensional problems was presented in Chapter 6. Comparisons between the numerical, experimental and appropriate analytical data indicated a high degree of similarity between all of the results.

A comprehensive data analysis process was then conducted to identify common trends and correlations within the investigation results. A number of issues identified during this data analysis process were found to be of particular relevance to the methodological development. This issues are discussed in brief below.

8.4.5.1 Analysis of the Maximum Stress Concentration

For each of the feature interaction problems under investigation, detailed results were generated of the magnitude, direction and position of the maximum stress concentration over a wide range of geometric configurations. These results were found to provide a good basis for the generation of empirical relationships between geometric variation in the problem configuration and the resulting maximum stress concentration. For example, correlations were identified between the maximum stress concentrations observed at the interacting geometries, and the values of the maximum stress concentration associated with each feature individually. Correlations were also identified between geometric variations in the problem configuration, and the resulting changes in the maximum stress concentration.

In addition, common trends were established for the location of the maximum stress concentration. In general, it was observed that the maximum stress concentration occurs at the feature edge, along a line perpendicular to the applied stress. This maximum stress concentration also tended to be located at the feature of smallest relative size. One particular geometric problem did not adhere to these characteristics; that of a central hole surrounded by eight satellite holes. For these geometries, it was observed that the maximum stress concentration was consistently located at one of the radial holes, irrespective of the relative sizes of the hole configuration. In addition, for certain geometries of the four satellite hole problem, this point of maximum stress concentration tended to migrate around the hole edge, as the hole separation distance was decreased. This migration of the point of maximum stress concentration was

caused by the build-up of a relatively large, highly-stressed region between the satellite holes, and resulted in a change in the direction as well as a dip in the magnitude of the maximum stress concentration.

Another point of particular interest, identified during these analyses, was that the levels of maximum stress concentration observed for the problems of interacting features were significantly lower than those that would have been predicted using the traditional analysis techniques adopted within the aerospace industry. It has been generally assumed by fatigue experts within BAE SYSTEMS that any increases in the maximum stress concentration due to the introduction or expansion of additional stress-raisers was caused by two elements: (i) an overall increase in the nominal stress concentration, and (ii) the stress-field interaction between the features. However, analysis of the data generated during this research has shown that the actual observed increases in the maximum stress concentration are actually less significant than that contributed by just one of these elements, namely that of the increase in the nominal stress. This surprising effect is due to the influence of the additional region of high stress concentration. It has been proposed in this research that, for equilibrium to be maintained, the additional peak stress generated by the secondary feature causes a reduction in the remaining nominal stress, which counteracts any increases that may have been observed from the loss in cross-sectional area. The only significant factor, therefore, resulting from the introduction of an additional feature, is that of the stress-field interaction between the stress-raisers.

Another interesting result drawn out from the analysis of the maximum stress concentration was observed in the analysis of the three dimensional problem of an L-section containing transverse holes. These results indicated that the maximum stress concentration associated with any hole on either face of the L-section remained unaffected by the presence or relative movement of an additional hole on the opposite face. It was proposed in the research that this apparent absence of stress-field interaction was due to the L-section acting as an artificial boundary.

8.4.5.2 Analysis of the Stress Concentration Distribution

For a large number of the problems investigated during this research, in addition to analysis of maximum stress concentration levels, it was also possible to generate ligament plots of the stress concentration distributions between adjacent features.

These plots were found to provide additional insights into the form and influencing factors of stress-field interactions. One finding of particular interest during this analysis was the correlations between the stress concentration decay from individual features, and the stress concentration distribution generated when those features were placed in proximity. Through detailed investigations of these correlations, an interesting trend was drawn out, relating to the decay of the stress concentration from each feature edge. It was observed that the gradient of the stress concentration decay from any feature is independent of the presence or relative size of any additional features. This finding was of particular interest as the gradient, and thereby the form, of the stress concentration distribution between interacting features could simply be determined from knowledge of the relative sizes of each of the individual features involved. This result also allowed much more straightforward comparisons to be made between the decay from the individual features and the distributions between associated interacting features.

Using the insights gained from the data analysis process, it was clear that the feature interaction problems considered in this research needed to be divided into two categories: (i) those problems for which the ligament stress concentration distribution could be used to generate correlations between the configuration geometry and the resulting stress concentration factor, and (ii) those geometries for which any prediction methodologies would simply be based on the absolute magnitude and position of the maximum stress concentration.

8.4.6 Methodological Development

The data analysis process identified two distinct categories of feature interaction problem. Essentially, these can be classified as: (i) those features that lie on a common cross-section, normal to the applied stress, and (ii) those features of alternative alignment. Further analysis of these problem categories established that two distinct approaches would be required for the generation of predictive methodologies in each case.

Detailed analysis of the empirical results generated from those features that lie on a common cross-section revealed that prediction of the maximum stress concentration generated from all such geometries is governed by a single overarching formula. As discussed in Section 7.3.1.7, this equation comprises two important elements:

(i) the product of the stress concentrations associated with each feature individually, calculated over the gross section, and

(ii) a multiplication factor dependent on the relative size of the feature associated with the point under consideration, and the distance between this point and the adjacent boundary.

The general form of this equation is governed by the following formula:

$$\textbf{Predicted } K_{tg} = K_{1\alpha}\, K_{1\beta}\, [f(s, r_\alpha)]$$

for a point (point *1*) on the edge of a feature (feature α, of radius r_α) lying at a distance, s, from a free boundary or secondary feature β.

As this generic formulation was universal to all of the problems involving features on a common cross-section considered in this research, it can be proposed that this methodology is generic in nature, and can be utilised in any geometric problem of this form. This would allow for the relatively straightforward expansion of the scope of coverage of the methodology, through the implementation of new feature interaction problems. A series of comparisons was conducted, between the results for a particular geometry using the newly developed methodology, and those generated from equivalent finite element models. In all cases investigated, these comparisons showed very little discrepancy between the results of the two techniques (<2% discrepancy). However, it must be emphasised that the methodologies developed here provided a much greater efficiency in terms of time and ease of application.

The analysis of the data generated from those features of alternative alignment revealed no overarching trends or similarities, due to the inherent differences in the geometries considered. For these problems, therefore, individually-tailored prediction techniques were developed for each geometry. The evaluation techniques ranged from the utilisation of the empirical data (for the cases of the four and eight satellite hole problems) to the simple manipulations of the geometric parameters (for the hole in proximity to a transverse fillet radius). In all cases, the resulting stress concentration values were found to be within 4% of equivalent numerical solutions for the models.

Each of the methodologies is currently being implemented as standard practice in the fatigue analysis process at BAE SYSTEMS (BAE SYSTEMS 2001 (2)). The primary application of these techniques is through the knowledge-based software system

SCONES (Robinson et al. 2001). Early assessment of this implementation has confirmed that the technique is flexible in terms of design optimisation and provides a straightforward prediction of accurate stress concentration values.

8.5 SCIENTIFIC CONTRIBUTION

This research has dealt with the unresolved scientific issue of the stress-raising influence of multiple features placed in proximity. The literature review has highlighted the limited knowledge in this field and the current dearth of rigorous and accurate evaluation methodologies.

Through this research, new insights have been gained into the manner in which two or more stress-raisers interact when placed in proximity. Understandings have been gained of the impact of the feature type, size and location on the resulting magnitude and location of the maximum stress concentration.

It has also been established that problems involving interacting stress-raisers can be considered in two distinct categories: (i) those features that lie on a common cross-section, normal to the applied stress, and (ii) those features of alternative alignment.

Through the analysis of those features that lie on a common cross-section, a generic methodology has been developed for the prediction of the associated stress concentration values. This methodology is dependent on the product of the stress concentration values associated with each feature individually, and a geometric multiplication factor, based on the relative size of the feature under consideration and its distance from the adjacent boundary. Due to the generic nature of this methodology, the determination of the appropriate multiplication factor for any new geometry would be relatively straight-forward, allowing the potential for the implementation of additional interaction problems. Validation of the prediction technique through comparison of the resulting values with appropriate finite element solutions have shown a maximum discrepancy of 2%.

The analysis of problems of alternative alignment suggested that no generic methodology could be developed for the consideration of these problems. A series of tailor-made techniques was therefore developed for the evaluation of these geometries, which were found to produce results within 4% of equivalent numerical models.

In addition to the contributions to knowledge in the field of interacting stress-raisers, this research has also proposed a number of refinements to current photoelastic procedures, which have been found to enhance significantly the experimental accuracy.

A list of publications generated during this research is provided in Appendix B.

8.6 INDUSTRIAL CONTRIBUTION

The ultimate aim of this research was to provide the aerospace industry with a rigorous design tool for the prediction of stress concentration values associated with problems of interacting features. This research has established the unsuitability of current procedures in the aerospace industry for the flexible and accurate evaluation of the influence of interacting stress-raisers. In addition, the research has highlighted the dearth of alternative predictive techniques currently available.

Through this research, methodologies have been developed for the evaluation of all commonly-occurring feature interaction problems within aircraft design. Each of these methodologies is straightforward to apply, allowing for the operation of design optimisation routines, and produces highly accurate results (within 4% of equivalent numerical and analytical models).

The methodology is currently being implemented as standard practice within BAE SYSTEMS, both through documentation in the BAE SYSTEMS Technical Standards Manual on fatigue methodology (BAE SYSTEMS 2001 (2)) and through integration within the knowledge-based system SCONES. Early testing of this methodology within the SCONES interface has established that these techniques will provide an accurate design tool which can be used for the straight-forward evaluation of a series of alternative design configurations, as well as in the assessment of manufacturing concessions.

The implementation of these methodologies will inform the design of future aircraft and provide a standard, validated approach for the fatigue optimisation of stress concentration interaction problems.

8.7 GENERAL CONCLUSIONS

This research has successfully fulfilled the overall project brief, through the development and implementation of rigorous techniques for the prediction of stress concentrations around a range of commonly-occurring problems of feature interaction within aircraft design.

More specifically, this research project has:

- identified the detailed requirements of the aerospace industry, both in terms of the scope of coverage of the methodology as well as the particular circumstances under which it would be implemented,
- conducted a thorough literature review, highlighting the lack of current knowledge in the field of interacting stress-raising features,
- undertaken fundamental research into the geometric problem of multiple stress-raisers, through the employment of numerical and experimental techniques, alongside the application of foregoing analytical solutions. This research programme has provided a number of insights into the influence of feature type, size and separation distance on the maximum stress concentration associated with problems of feature interaction,
- developed new methodologies for the evaluation of problems of feature interaction. These methodologies have been found to be highly accurate, in all cases producing results within 4% of those generated from numerical models, and
- commenced the programme of implementation of the methods in the BAE SYSTEMS Technical Standards Manual for fatigue methodology and within the knowledge-based system SCONES, which is to be adopted as standard practice for stress concentration evaluation within the company. Early testing of this methodology within the SCONES interface has established that these techniques will provide an accurate deign tool which can be used for the straightforward evaluation of a series of alternative design configurations, as well as in the assessment of manufacturing concessions.

8.8 FUTURE WORK

At present, the methodologies developed here are under implementation into the SCONES knowledge-based system (BAE SYSTEMS 2001 (1); Robinson et al. 2001), and also into the BAE SYSTEMS Technical Standards Manual for stress concentration analysis (BAE SYSTEMS 2001 (2)).

The immediate goal is the completion of this implementation process, such that these methodologies are incorporated as standard practice within BAE SYSTEMS. Based on feedback from fatigue experts within the company of the practical application and usage of these evaluation tools, the next stage of the project is to expand their scope of coverage to incorporate additional feature types and loading conditions. In particular, it has already been proposed that the evaluation of the satellite hole problems under bending and bi-axial tension would be a beneficial addition to the system.

Other potential developments to the methodology include the consideration of additional influences to the stress-field surrounding interacting features, such as residual stresses and surface treatments. It is also proposed that, in the longer term, this work will lead into a project designed to investigate the stress-raising influence of joints and the impact of joint assemblies placed in proximity.

REFERENCES

Albich, R. (1994) *Assessment of Simple Photoelastic Models in Aircraft Design*, Strain, **30**, 2, 73-74

Arjyal, B. P. (2000) *Measurement and Modelling of Stress Concentration Around a Circular Notch*, Experimental Mechanics, **40**, 3, 248-255

Babuska, I. and Andersson, B. (1997) *A Global-Local Finite Element Method for Efficient and Accurate Solution of Multi-Site Damage Problems*, FFA TN 1995-23, Stockholm

Babuska, I. and Andersson, B. (1998) *The Approximate Domain Method for Accurate Analysis of 3D Structures*, private correspondence

BAE SYSTEMS (2001 (1)) *SCONES, The Stress Concentration Evaluation System*, Technovation, **17**, 15-17, internal document

BAE SYSTEMS (2001 (2)) Technical Standards and Procedures Manual, **30**: Fatigue (10): Stress Concentrations

BAE SYSTEMS Technical Report (2000) *Comparative Study between Automated and Manual Photoelasticity on a Plate with Two Equal Diameter Holes Loaded under Uniaxial Tension*, Structures Engineering, Experimental Mechanics, Ref: PHEL/B4504/23156

Basic, S. L. (1999) *Damage Tolerance Stress Rating for an Array of Satellite Holes in a Pressurized Fuselage*, private correspondence

Bathe, K. J. (1996) *Finite Element Procedures*, Prentice Hall

Beaudet, P. and Roth, M. (1991) *Failure Analysis Case Histories of Canadian Forces Landing Gear Components*, AGARD Conference Proceedings 484, Landing Gear Design Loads

Brewster, D. (1815) *On the Effects of Simple Pressure in Producing that Species of Crystallisation which Forms Two Oppositely Opposing Polarised Images*, Philosophical Transactions of the Royal Society, 60-64

Bristow, J. W. (2000) *The Meaning of Life*, The Aeronautical Journal, 264-270

British Aerospace Defence Limited (1996) *T-45 Fatigue Methodology Guidelines*, Report Number BAE-BSS RP-T45-FAT-0044

British Aerospace Military Aircraft & Aerostructures (1997) *Fatigue Methodology Guidelines for the Hawk*, Reference Number BAE-BSS-EN-HWK-FAT-1237

Chen, K. T., Ting, K. and Yang, W. S. (2000) *Stress Analysis of Two-Dimensional Perforated Plates Using Boundary Element Alternating Method*, Computers and Structures, **75**, 515-527

Chong, K. P. and Pinter, W. J. (1984) *Stress Concentrations of Tensile Strips with Large Holes*, Computers and Structures, **19**, 4, 583-589

Coker, E. G. (1920) General Electric Review, **23**, 870

Coker, E. G. and Filon, L. N. G. (1931) *A Treatise on Photoelasticity*, Cambridge University Press, Cambridge, England, 486

Cole, A. G. and Brown, A. F. (1958) *Photoelastic Determination of Stress Concentration Factors Caused by a Single U-notch on One Side of a Plate in Tension*, Journal of the Royal Aeronautical Society, **62**, 597

Collins, J. A. (1993) *Failure of Materials in Mechanical Design*, Second Edition, John Wiley & Sons

Cooper, T. D. and Kelto, C. A. (1979) *Fatigue in Machines and Structures – Aircraft*, Fatigue and Microstructure, American Society for Metals, 29-56

Doughtie, V. L. and Vallance, A. (1964) *Design of Machine Elements*, Fourth Edition, McGraw-Hill, New York

Eccles, A. R. (1996) *Software Development of a Knowledge-Based System for Designing Against Fatigue*, MSc Thesis, University of Hull, UK

Erickson, P. E. and Riley, W. F. (1978) *Minimising Stress Concentration Around Circular Holes in Uniaxially Loaded Plates*, Experimental Mechanics, **18**, 97-100

ESDU (1964) *Guide to Stress Concentration Data*, Data Item 64001

ESDU (1967) *Geometric Stress Concentrations: Two Equal Reinforced Circular Holes in Infinite Plates*, Data Item 67023

ESDU (1969) *Elastic Stress Concentration Factors. Geometric Discontinuities in Flat Bars or Strips of Isotropic Materials*, Data Item 69020

ESDU (1975 (1)) *Design Against Fatigue: Basic Design Calculations*, Data Item 75022

ESDU (1975 (2)) *Geometric Stress Concentration Factors: Two Adjacent Un-Reinforced Circular Holes in Infinite Flat Plates*, Data Item 75007

ESDU (1985 (1)), Aeronautical Series, Fatigue Sub-Series, Fatigue Endurance Data, Stress Concentrations, **3**

ESDU (1985 (2)) *Stress Concentrations: Interaction and Stress Decay for Selected Cases*, Data Item 85045

ESDU (1994) *Three-Dimensional Elastic Stress Concentration Factors Plain or Countersunk Hole in a Wide Plate Subjected to Tension, Bending or Pin Loading*, Data Item 93030

Everett, R. A. and Elber, W. (2000) *Damage Tolerance Issues as Related to Metallic Rotorcraft Dynamic Components*, Journal of the American Helicopter Society, **45**, 1, 3-10

Filon, and Harris, F. C. (1923) *On the Diphasic Nature of Glass as Shown by Photo-elastic Observation*, Proceedings of the Royal Society, **103**, 561-571

Finch, D. V. (1997) *Widespread Fatigue – The End of Damage Tolerance?*, Aircraft Maintenance Engineers' Conference Proceedings, Royal Aeronautical Society, 5.1-5.14

Fraga, W. E. and Hewitt, R. L. (1983) *Computer Program for Solving Notch Problems using Nisitani's Body Force Method*, NRC, Laboratory Technical Report, LTR-ST-1479, National Research Council, Ottawa

Frank, W. and Faucett, T. R. (1961) *The Superposition of Stress Concentration Factors*, American Society of Mechanical Engineers, Technical Paper Number 61-SA-5

Frocht, M. M. (1935) *Factors of Stress Concentration Photoelastically Determined*, Transactions of the ASME, Applied Mechanics Section, **57**, 67-68

Frocht, M. M. (1941) *Photoelasticity*, John Wiley & Sons, New York

Gelder, M., Roberts, S., Holford, D. and Reed, S. (2000) *Fatigue and Operational Loads Monitoring of the Red Arrows*, Proceedings of the 20th Symposium on Aircraft Integrated Monitoring Systems, Garmisch-Partenkirchen, Germany

Haddon, R. A. W. (1967) *Stresses in an Infinite Plate with Two Unequal Circular Holes*, Quarterly Journal of Mechanics and Applied Mathematics, **20**, 277-291

Hendry, A.W. (1966) *Photo-Elastic Analysis*, Pergamon Press

Heywood, R. B. (1952) *Designing by Photoelasticity*, Chapman and Hall, London

Horii, H. and Nemat-Nasser, S. (1985) *Elastic Fields of Interacting Inhomogeneities*, International Journal of Solids and Structures, **21**, 7, 731-745

Howland, R. C. J. (1929) *On the Stresses in the Neighbourhood of a Circular Hole in a Strip Under Tension*, Philosophical Transactions of the Royal Society London A, **229**, 49-86

Inglis, C. E. (1913) *Stresses in a Plate Due to the Presence of Cracks and Sharp Corners*, Transactions of the Institute of Naval Architects, **55**, 1

Isida, M. (1952) *On the Bending of an Infinite Strip with an Eccentric Circular Hole*, Proceedings of the 2nd Japan National Congress of Applied Mechanics, 57-60

Isida, M. (1953) *On the Tension of an Infinite Strip with an Eccentric Circular Hole*, Transactions of the Japan Society of Mechanical Engineers, **19**, 100-106

James, T. C. (1950) *Determination of Stress Concentration Factors by the Brittle Materials Method Using Kriston*, MS Thesis, Department of Theoretical and Applied Mechanics, University of Illinois

Jindal, U. C. (1983) *Reduction of Stress Concentration Around a Hole in a Uniaxially Loaded Plate*, Journal of Strain Analysis, **18**, 2, 135-141

Joint Aviation Authorities (2000) *JAR 25.271 Damage Tolerance and Fatigue Evaluation of Structures*, JAR-25, Subpart C, Fatigue Evaluation

Juvinall, R. C. (1967) *Engineering Consideration of Stress, Strain and Strength*, McGraw-Hill

Kikukawa, M. (1962) *Factors of Stress Concentration for Notched Bars under Tension and Bending*, Proceedings of the 10th International Congress on Applied Mechanics, Elsevier, New York, 337

Kirsch, G. (1898) Verein Deutscher Ingenieure, **42**, 797

Kurajian, G. M. and Na, T. Y. (1980) *Combined Fatigue Stress Concentration Factor Determination*, Transactions of the ASME Journal of Mechanical Design, **102**, 427-731

Leven, M. M. (1963) *Epoxy Resins for Photoelastic Use*, from Photoelasticity, Proceedings of the International Symposium held at Illinois Institute of Technology, edited by Frocht, M. M., Pergamon Press

Ling, C. B. (1948) *On the Stresses in a Plate Containing Two Circular Holes*, Journal of Applied Physics, **19**

Ling, C. B. (1967) *On Stress Concentration at Semi-Circular Notch*, Transactions of the ASME, Applied Mechanics Section, **89**, 522

Mackerie, J. (1997) *Finite Element Linear and Non-linear, Static and Dynamic Analysis of Structural Elements: A Biography (1992-1995)*, Engineering Computations, **14**, 4, 347-440

Mann, J. S., Machin, A. S. and Lupson, W. F. (1984) *Improving the Life of the Mirage IIIO Wing Main Spar*, Structures Report 398, Department of Defence, Defence Science and Technology Organisation, Aeronautical Research Laboratories, Australia, ARL-STRUC-REPORT-398

Marquet, T. and Struzik, A. (1998) *Damage Tolerance Applied on Metallic Components*, European Rotorcraft Forum, 24th, Association Aeronautique et Astronautique de France, SMO8.1-SMO8.15

McDonnell Douglas Aerospace (1993) *Harrier Fatigue Design Methods Report*, Report Number: MCD 93B0023, internal report

Measurements Group (1982) *Instruction for Machining Two-Dimensional Models from PSM-5 and CR-39*, Measurement Group, Photoelastic Division, Instruction Bulletin IB-202

Measurements Group (1996) *Strain Gage Installations with M-Bond 200 Adhesive*, Measurements Group, Micro-Measurements Division, Instruction Bulletin B-127-13

Meguid, S. A. (1986) *Finite Element Analysis of Defence Hole Systems for the Reduction of Stress Concentration in a Uniaxially-Loaded Plate with Two Coaxial Holes*, Engineering Fracture Mechanics, **25**, 4, 403-413

Meguid, S. A. and Gong, S. X. (1993) *Stress Concentrations Around Interacting Circular Holes: A Comparison Between Theory and Experiments*, Engineering Fracture Mechanics, **44**, 2, 247-256

Meguid, S. A. and Shen, C. L. (1992) *On the Elastic Fields of Interacting Defence and Main Hole Systems*, International Journal of Mechanical Science, **34**, 1, 17-29

Mindlin, R. D. (1948) *Stress Distribution Around a Hole Near the Edge of a Plate Under Tension*, Proceedings of the Society of Experimental Stress Analysis, **5**, 56-68

Ministry of Defence (1999) *DEF STAN 00-970I Fatigue: Safe-Life Substantiation*, Part 1, Section 3, Leaflet 35

Mowbray, A. Q. (1953) *The Effect of Superposition of Stress Raisers on Members Subjected to Static or Repeated Loads*, Proceedings of the Society for Experimental Stress Analysis, **X**, 153-166

Muskhelishvili, N. I. (1953) *Some Basic Problems of the Mathematical Theory of Elasticity*, 3rd Revised Ed. (translated from Russian by J. R. M. Radok) P. Noordhoff Ltd., Rev. 2099

Neuber, H. and Hahn, H. G. (1966) *Stress Concentrations in Scientific Research and Engineering*, Applied Mechanics Review, **16**, 187-199

Nisitani, H. (1967) *Two-Dimensional Problems Solved Using a Digital Computer*, Journal of the Japan Society of Mechanical Engineers (in Japanese), **70**, 580, 627

North, W. E. (1965) *A Photoelastic Study of the Interaction Effect of Two Neighbouring Holes in a Plate Under Tension*, M.S. Thesis University of Pittsburgh

O'Brien, E. W. (1995) *Progress in Experimental Stress Analysis for Airbus Aircraft Design*, Strain, **31**, 9, 131-134

Oppel, G. (1937) *The Photoelastic Investigation of Three-Dimensional Stress and Strain Conditions*, N.A.C.A. Tech. Mem., **824**

Peterson, R. E. (1974) *Stress Concentration Design Factors*, John Wiley & Sons

Pilkey, W. D. (1994) *Peterson's Stress Concentration Factors*, New York, John Wiley & Sons

Pitt, S. and Jones, R. (1997) *Multiple-Site and Widespread Fatigue Damage in Aging Aircraft*, Engineering Failure Analysis, **4**, 4, 237-257

Poe, R. C. (1961) *Photoelastic Study of Stress Concentration Due to Combined Slot and Semi-Circular Notch*, M.S. Thesis University of Pittsburgh

Robinson, P. A., Graham, R. H., Gill, L., Peckover, S., Raines, M. and Swift, K. G. (2001) *An Expert System for the Determination of Stress Concentration Factors*, Proceedings of the Institution of Mechanical Engineers, **215**, Part G

Rubayi, N. A. (1984) *Minimising Stress Concentration Factors Around Multiple Holes Near the Edge of a Plate*, Proceedings of the V International Congress on Experimental Mechanics, Canada, 1984SESA, 350-357

Savin, G. N. (1961) *Stress Concentration Around Holes*, Pergamon Press, New York

Schijve, J. (2001) *Fatigue of Structures and Materials*, Kluwer Academic Publishers, Netherlands

Sharples, K. (1981) *Photoelastic Stress Analysis*, Chartered Mechanical Engineers, 42-47

Shin, C. S., Man, K. C. and Wang, C. M. (1994) *A Practical Method to Estimate the Stress Concentration of Notches*, International Journal of Fatigue, **16**, 4, 242-256

Sloan, C. S., Cowell, M. D.and Lehnhoff, T. F. (1999) *The Effect of a Large Hole on the Stress Concentration Factor of a Satellite Hole in a Tension Field*, Journal of Pressure Vessel Technology-Transactions of the ASME ,**121**, 3, 252-256

Stranart, J. C. E. (2000) *Mechanically Induced Residual Stresses: Modeling and Characterisation*, PhD Thesis, University of Toronto

Strannigan, J. S. (1964) *Variation of Edge Stress During Storage of an Epoxy Resin*, National Engineering. Lab. Report 127

Suresh, S. (1998) *Fatigue of Materials*, Cambridge University Press, Second Edition

Tafreshi, A. and Thorpe, T. E. (1995) *Numerical Analysis of Stresses in Oblique Holes in Plates Subjected to Tension and Bending*, Journal of Strain Analysis for Engineering Design, **30**, 4, 317-323

Tardy, H. L. (1929) *Méthode Practique d'Examen et de Mesure de la Birefringence des Verres d'Optique*, Rev. Opt., **8**, 59-69

Taylor, D., Bologna, P. and Knani, K. B. (2000) *Prediction of Fatigue Failure Location on a Component Using a Critical Distance Method*, International Journal of Fatigue, **22**, 735-742

Ting, K., Chen, K. T. and Yang, W. S. (1999) *Applied Alternating Method to Analyse the Stress Concentration Around Interacting Multiple Circular Holes in an Infinite Domain*, International Journal of Solids and Structures, **36**, 533-556

Trevelyan, J. (1994) *Boundary Elements for Engineers: Theory and Application*, Computational Mechanics Publications, Southampton

Trevelyan, J. and Wang, P. (2001) *Interactive Re-Analysis in Mechanical Design Evolution. Part 1. Background and Implementation*, Computers and Structures, **79**, 929-938

Trevelyan, J., Wang, P. and Walker S. K. (2001) *A Scheme for Engineering Optimisation in Mechanical Design*, Engineering Analysis with Boundary Elements, special issue on Industrial Applications, in press

Tusch, O. and Woithe, K. (2001) *A340-600 Full Scale Fatigue Test: A Further Step Forward into an Efficient Structure Qualification*, 21st Symposium International Committee on Aeronautical Fatigue (proceedings to be published)

Ukadgaonker, V. G. and Kale, P. A. (1998) *Finite Element Stress Analysis of Tubesheets Perforated by Circular Holes in Square Pitch Pattern*, Pressure Vessel Technology – Transactions of the ASME, **120**, 1, 12-16

Ukadgaonker, V. G., Avargerimath, R. R. and Koranne, S. D. (1995) *Stress Analysis of an Infinite Plate Containing Two Unequal Collinear Elliptical Holes in In-Plane Stresses at Infinity*, Indian Journal of Engineering & Materials Science, **2**, 62-79

Umezaki, E. (2000) *Application of Isotropic Points Extracted Using Computerised Photoelastic Experiment to Design Structural Elements*, The Journal of Strain Analysis, **35**, 5, 415-421

Wahl, A. M. and Beeuwkes, R. (1934) *Stress Concentrations Produced by Holes and Notches*, Transactions of the ASME, Applied Mechanics Section, **56**, 617-625

Wilson, I. H. and White, D. J. (1973) *Stress-Concentration Factors for Grooves in Plates*, Journal of Strain Analysis, **8**, 1, 43-51

Withey, P. A. (1997) *Fatigue Failure of the De Havilland Comet I*, Engineering Failure Analysis, **4**, 2, 147-154

Young, W. C. (1989) *ROARK'S Formulas for Stress and Strain*, McGraw-Hill

Zhenhuan, L., Guo, W. and Zhenbang, K. (2000) *Three-Dimensional Elastic Stress Fields Near Notches in Finite Thickness Plates*, International Journal of Solids and Structures, **37**, 7617-7631

Zienkiewicz, O. C. and Taylor, R. L. (1989) *The Finite Element Method*, McGraw-Hill

APPENDIX A

MODEL SPECIFICATIONS

This appendix contains engineering drawings for the specification of the ten photoelastic and five strain gauge analysis models produced for the analysis of feature interactions.

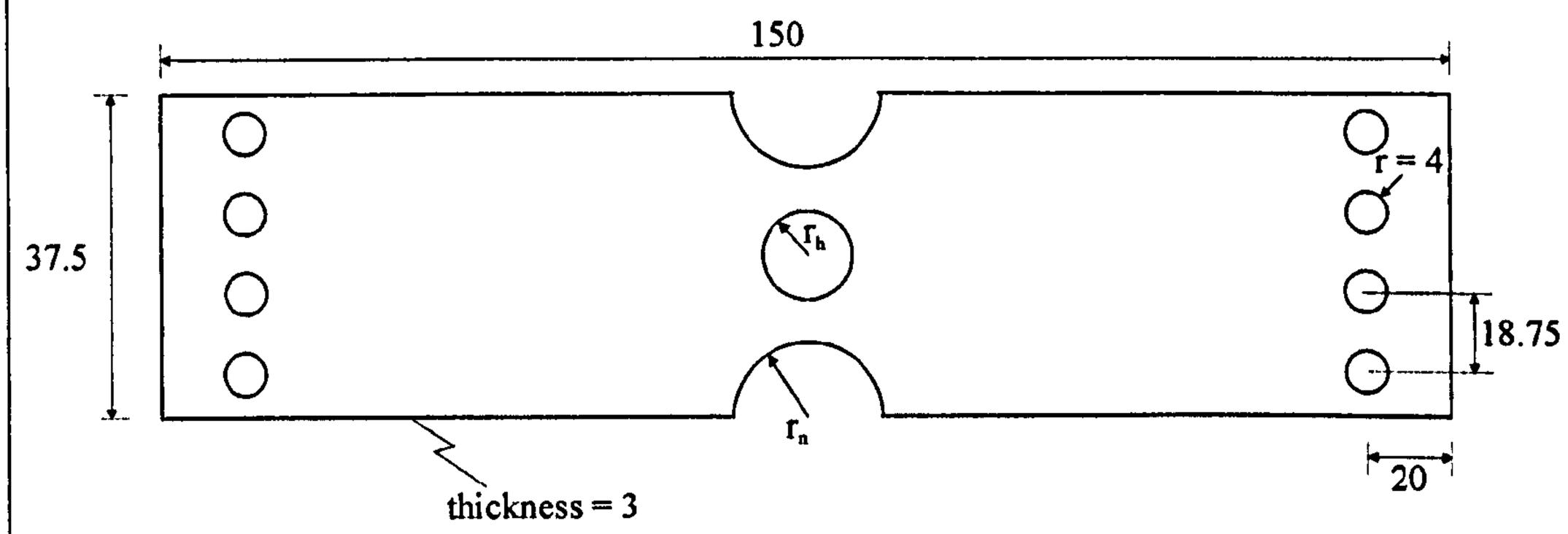

For values of r_n and r_h:	
r_n	r_h
5.625	0
5.625	2.5
5.625	3.5
5.625	4.5
5.625	5.5
5.625	6.5
7.5	0
7.5	2.5
7.5	3.5
7.5	4.5
7.5	5.5
7.5	6.5
9.375	0
9.375	2.5
9.375	3.5
9.375	4.5
9.375	5.5
9.375	6.5

Date: 9 July 1999
Scale: 2:1
Material: Epoxy resin, Araldite CT200/HT907
Model numbers: 1, 2, 3
Tolerance on all machined surfaces: 0.02
Central hole between double-edge notches
Sheet 1 of 4 All sizes in mm

Figure A-1. Specification for the production of three photoelastic models with double-edged notches containing initially no central hole, followed by the introduction of six holes of progressively larger radius

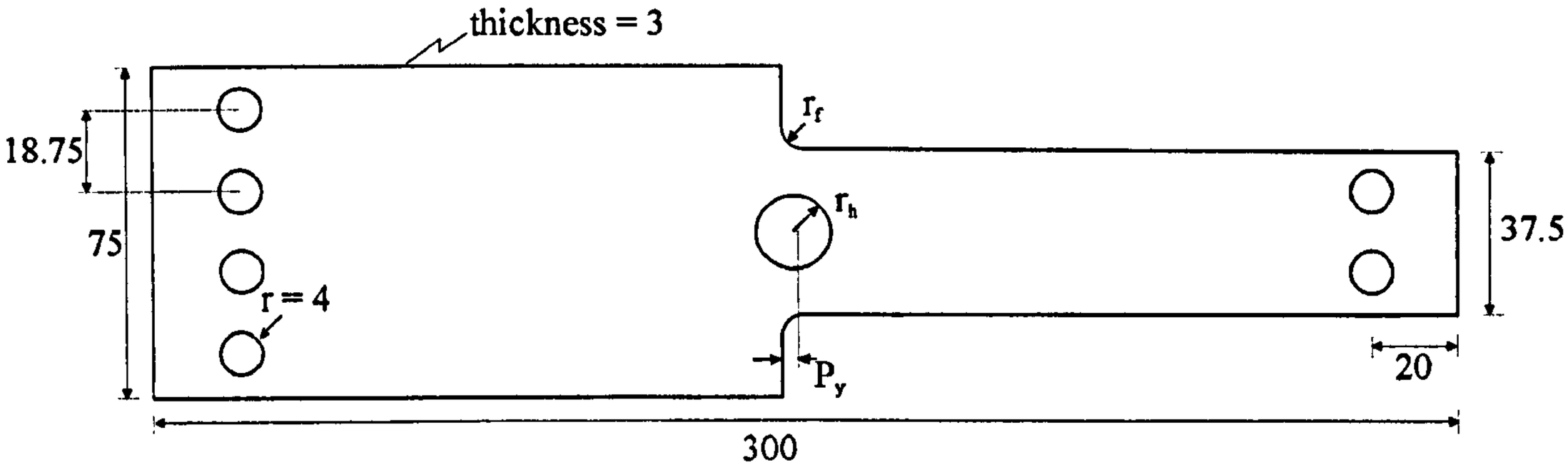

For values of r_f and r_h:	
r_f	r_h
1.5	0
1.5	2.5
1.5	5
1.5	7.5
1.5	10
1.5	12.5
4.5	0
4.5	2.5
4.5	5
4.5	7.5
4.5	10
4.5	12.5
9	0
9	2.5
9	5
9	7.5
9	10
9	12.5

Date: 9 July 1999
Scale: 2:1
Material: Epoxy resin, Araldite CT200/HT907
Model numbers: 4, 5, 6
Tolerance on all machined surfaces: 0.02
Central hole between shoulder fillets
Sheet 2 of 4 All sizes in mm

Figure A-2. Specification for the production of three photoelastic models with shoulder fillets containing initially no central hole, followed by the introduction of five holes of progressively larger radius

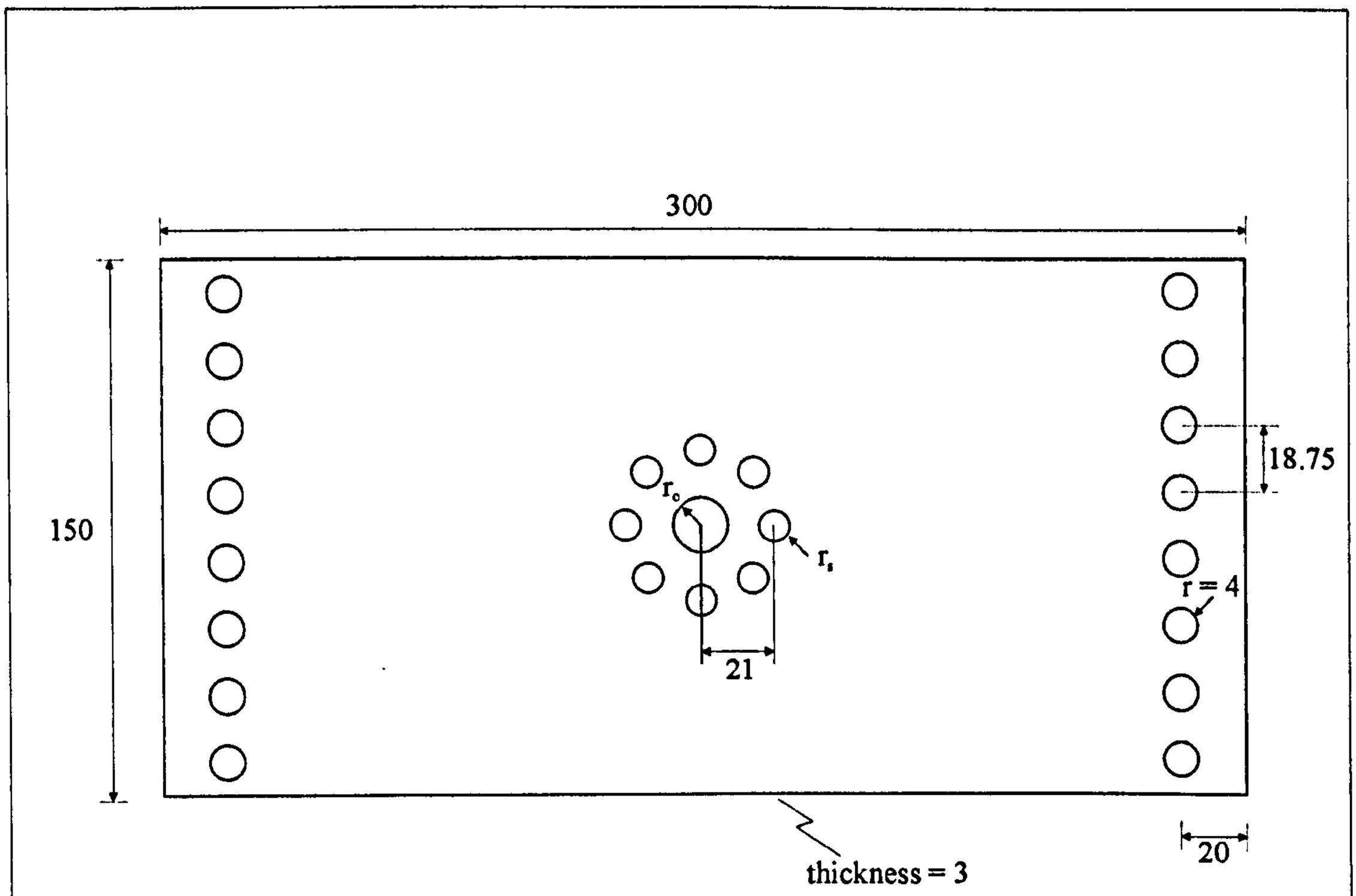

For values of r_c and r_s:

r_c	r_s
3.5	3.5 (=r_c)
4	4 (=r_c)
4.5	4.5 (=r_c)
5	5 (=r_c)
5.5	5.5 (=r_c)
6	6 (=r_c)
6.5	6.5 (=r_c)
7	7 (=r_c)
5	2.5 (=r_c/2)
6	3 (=r_c/2)
7	3.5 (=r_c/2)
8	4 (=r_c/2)
9	4.5 (=r_c/2)
10	5 (=r_c/2)
11	5.5 (=r_c/2)
12	6 (=r_c/2)

Date: 9 July 1999
Scale: 4:1
Material: Epoxy resin, Araldite CT200/HT907
Model numbers: 7, 8
Tolerance on all machined surfaces: 0.02
Central hole surrounded by eight radial holes
Sheet 3 of 4 All sizes in mm

Figure A-3. Specification for the production of two photoelastic models, one for which r_c=r_s, and one for which r_c=2r_s. The radius of each of these holes is incrementally increased, while maintaining this r_c:r_s ratio

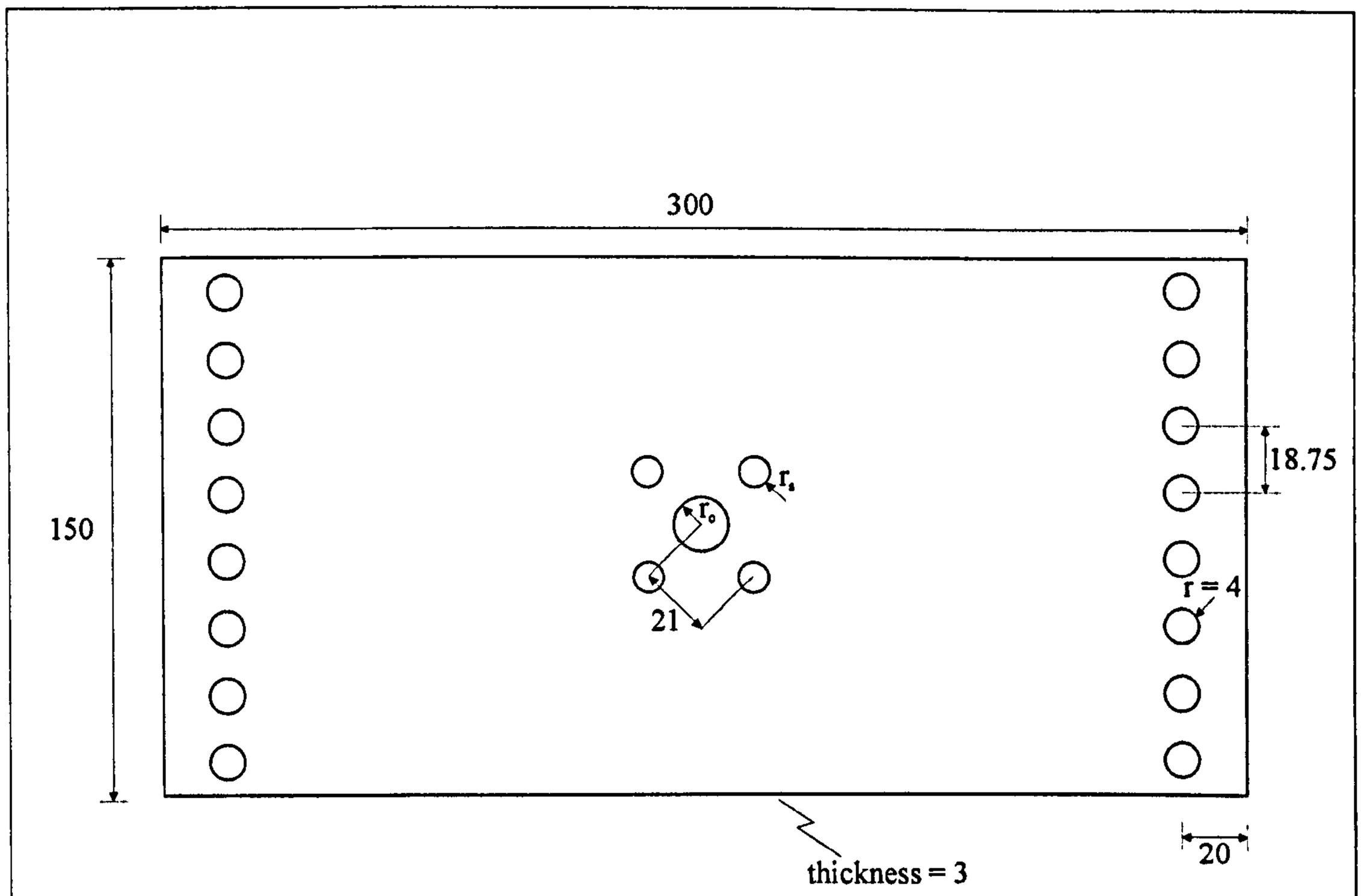

For values of r_o and r_s:	
r_o	r_s
3.5	3.5 (=r_o)
4	4 (=r_o)
4.5	4.5 (=r_o)
5	5 (=r_o)
5.5	5.5 (=r_o)
6	6 (=r_o)
6.5	6.5 (=r_o)
7	7 (=r_o)
5	2.5 (=r_o/2)
6	3 (=r_o/2)
7	3.5 (=r_o/2)
8	4 (=r_o/2)
9	4.5 (=r_o/2)
10	5 (=r_o/2)
11	5.5 (=r_o/2)
12	6 (=r_o/2)

Date: 9 July 1999
Scale: 4:1
Material: Epoxy resin, Araldite CT200/HT907
Model numbers: 9, 10
Tolerance on all machined surfaces: 0.02
Central hole surrounded by four radial holes
Sheet 4 of 4 All sizes in mm

Figure A-4. Specification for the production of two photoelastic models each containing a central hole of a different radius. Around this central hole, four radial holes are machined of five different radii

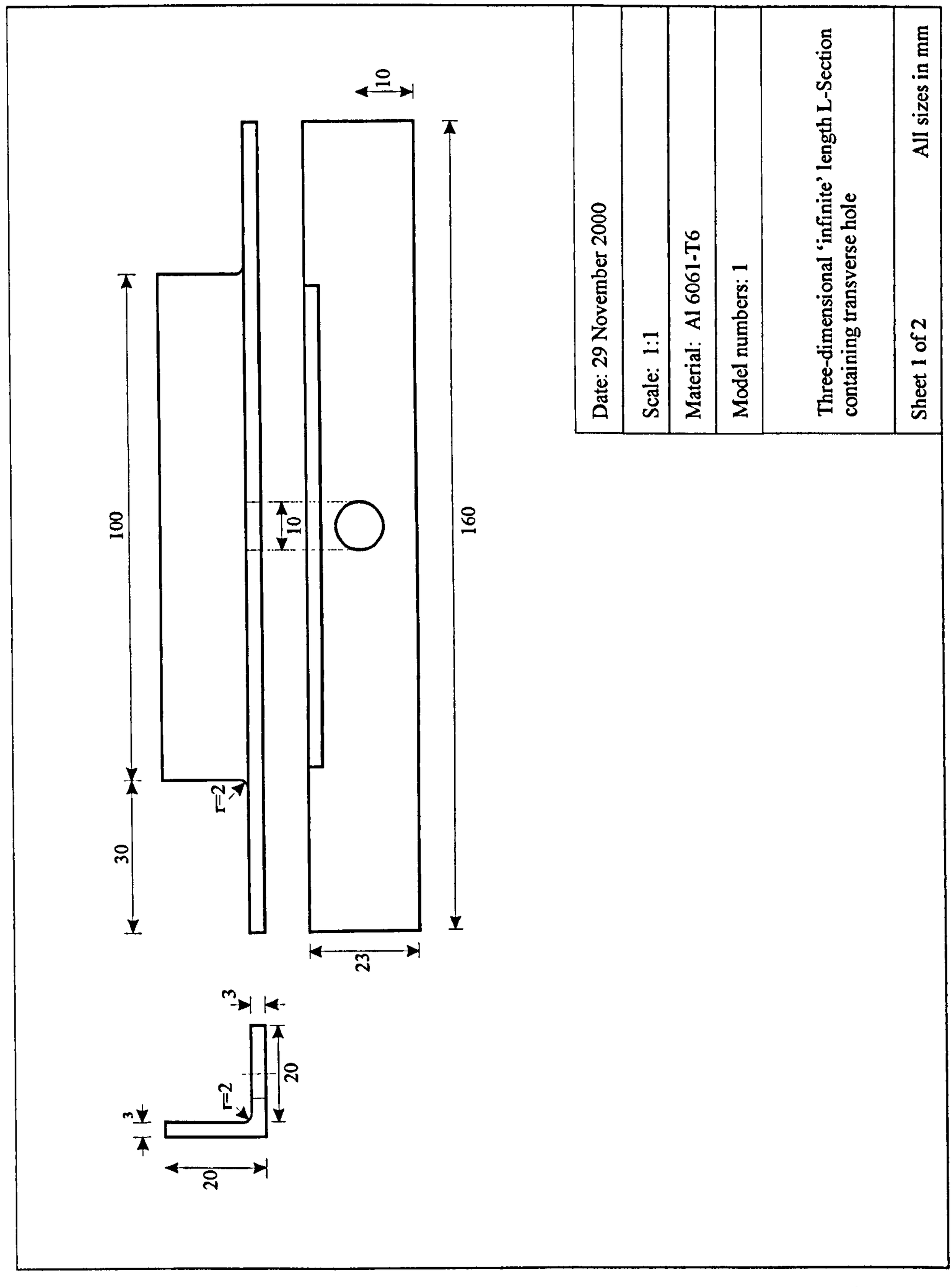

Figure A-5. Specification for the production of a three-dimensional strain gauge model of an L-section specimen containing a transverse hole

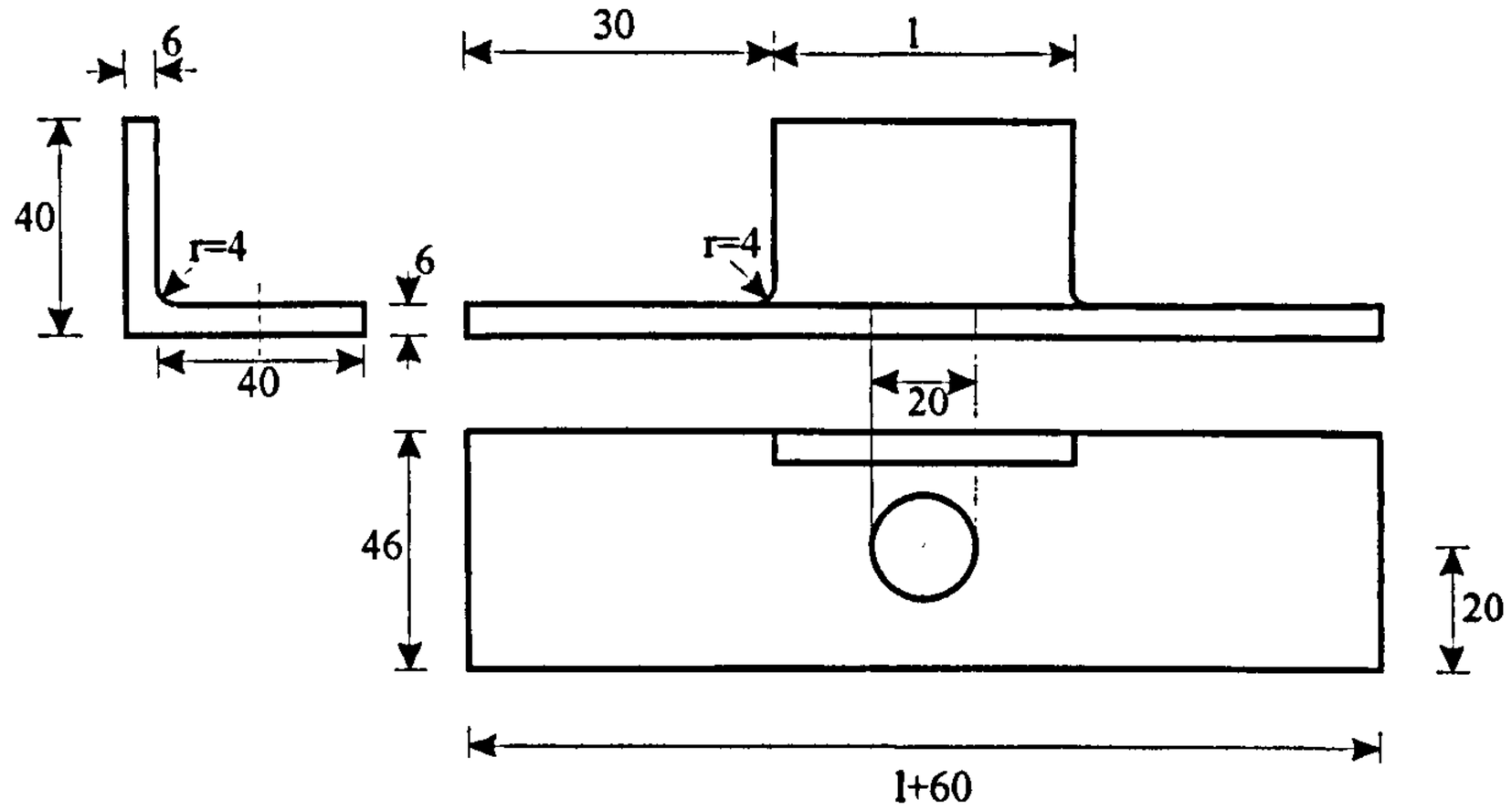

	Date: 29 November 2000
	Scale: 2:1
	Material: Al 6061-T6
	Model numbers: 2, 3
	Three-dimensional finite length L-Section containing transverse hole
For values l:	
Model 1 / l=40	Model 2 / l=80
	Sheet 2 of 2 — All sizes in mm

Figure A-6. Specification for the production of two three-dimensional strain gauge models of an L-section specimen of differing lengths (l) containing a transverse hole

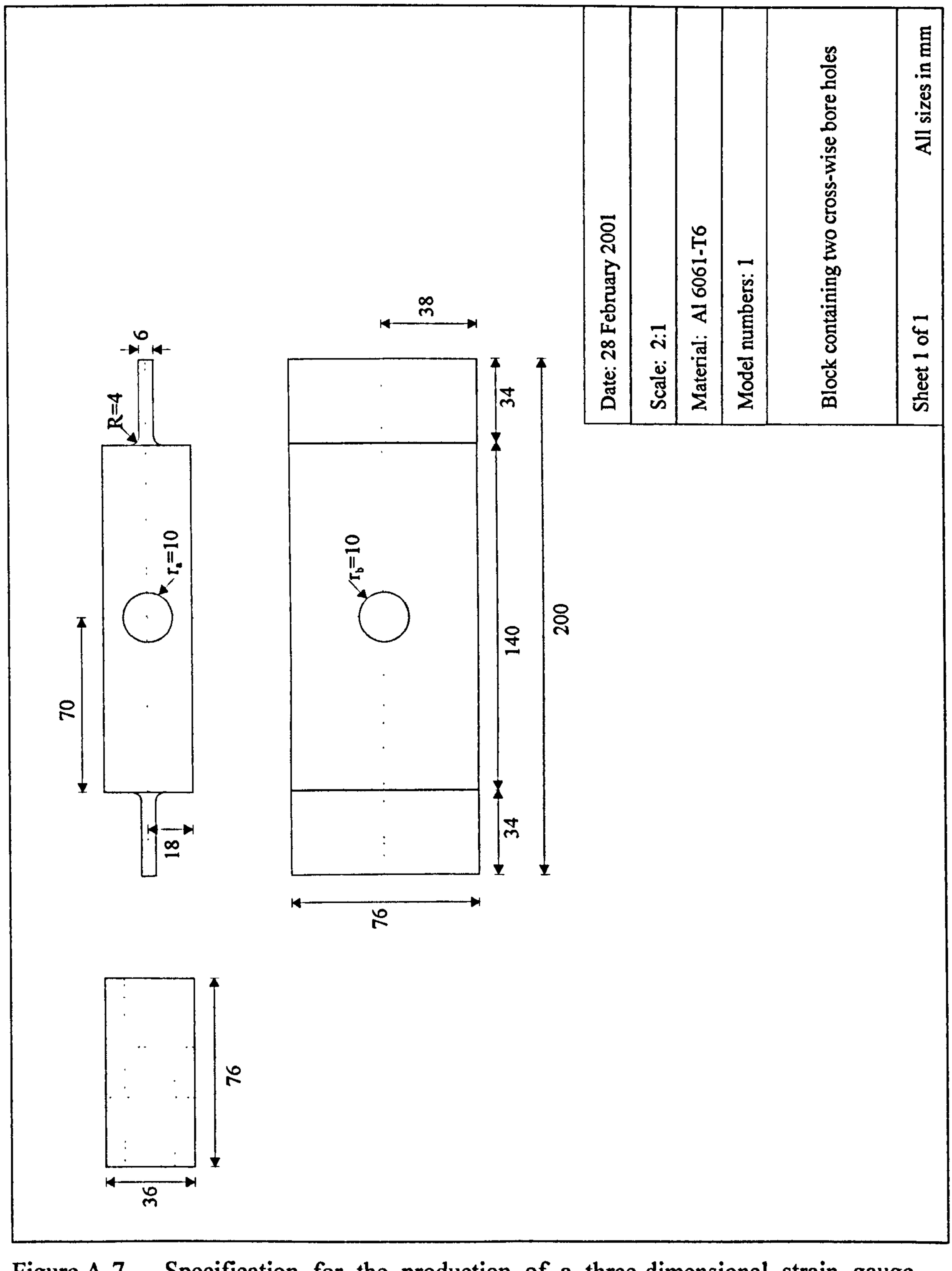

Figure A-7. Specification for the production of a three-dimensional strain gauge model of two cross-wise bore holes in a block of finite cross-section

APPENDIX B

PUBLICATIONS

(i) Refereed Papers in Primary Journals

Robinson, P. A., Graham, R. H., Gill, L., Peckover, S., Raines, M. and Swift, K. G. (2001) *An Expert System for the Determination of Stress Concentration Factors*, Proceedings of the Institution of Mechanical Engineers, **215,** *4*, 219-228

Graham, R. H., Gill, L., Raines, M. and Swift, K. G. *Evaluation of Interacting Stress-Raising Features*, to be submitted to the IMechE Journal of Strain Analysis

Graham, R. H., Gill, L., Raines, M. and Swift, K. G. *Methodologies for the Prediction of Interacting Stress-Raisers within Aircraft Design*, to be submited to the IMechE Journal of Aerospace Engineering

(ii) Contributions to Symposia and Compiled Volumes

Graham, R. H., Gill, L., Raines, M. and Swift, K. G. (2001) *A New Methodology for the Evaluation of Interacting Features in Aircraft Design*, International Conference of Aeronautical Fatigue: Design for the Digital Age, proceedings to be published

Graham, R. H., Gill, L., Raines, M. and Swift, K. G. (2000) *Advances in Designing Against Fatigue: A New Analysis Tool for Stress Concentration Evaluation in Aerostructures*, Mechanics and Materials in Design 2000, 29-31 May

Graham, R. H., Gill, L., Raines, M. and Swift, K. G. (1999) *New progress in the Evaluation of Stress Concentration Interactions in the Aerospace Industry*, International Conference of Aeronautical Fatigue: Structural Integrity for the Next Millennium, **2,** 945-956

(iii) Abstracts and Short Papers

Graham, R. H., Gill, L., Raines, M. and Swift, K. G. (1999) *Designing Against Fatigue: Evaluation of Interacting Features in Aircraft Design*, Integrity, Reliability and Failure Conference, Porto, 19-22 July

Design of Future Aircraft: Understanding Stress Interactions in Aerostructures as part of Engineering in the 21st Century: Highlights of Engineering by Younger Researchers, March 2000

The Design of Future Aircraft: Understanding Stress Interactions in Aircraft Design as part of SET'99 showcase of the best of British Science, Engineering and Technology by younger researchers, House of Commons, April 1999

Graham, R. H. (1999) *The Interaction of Stress Features in the Aerospace Industry*, Engineering Integrity Society Journal, **5**, 26-29